UNIVERSITÉ DE BOURGOGNE

DOCTORAL SCHOOL E2S

SCIENCES ET TECHNOLOGIES DE L'INFORMATION ET DE LA COMMUNICATION

P H D T H E S I S

to obtain the title of

PhD of Science

of the Université de Bourgogne

Speciality: COLOR IMAGE SCIENCE

Presented by

Jean-Baptiste THOMAS

Colorimetric characterization of displays and multi-display systems

defended on October 13^{th}, 2009

Jury :

President:	Françoise VIÉNOT	-	CRCC (Muséum national d'histoire naturelle)
Reviewer :	Sabine SÜSSTRUNK	-	LCAV2 (EPFL)
Reviewer :	Lindsay MACDONALD	-	London College of Communication
Co-director :	Pierre GOUTON	-	LE2I (Univ. de Bourgogne)
Co-director :	Jon Yngve HARDEBERG	-	Colorlab (Gjøvik Univ. College)
Advisor :	Irène FOUCHEROT	-	LE2I (Univ. de Bourgogne)

There aren't any great men. There are just great challenges that ordinary men like you and me are forced by circumstances to meet.

Admiral William Frederick Halsey Jr. (Bull)

Well I've been to the mountain and I've been in the wind,
I've been in and out of happiness.
I have dined with kings, I've been offered wings
And I've never been too impressed.

Bob Dylan

Acknowledgments

So many people to thank that I do not know who to begin with.

I would like to thank my advisoring team, Irène Foucherot, Pierre Gouton, Jon Y. Hardeberg for their good advice all along these three years, their research and human qualities, and for the freedom they gave me considering my work.

I want to thank my reviewers, Sabine Süsstrunk and Lindsay MacDonald for the time they spent on this manuscript. The quality of their review made the final thesis definitely better.

Many thanks to Françoise Viénot who accepted to join this jury a week before the viva even in the middle of her holidays.

I cannot forget to thank Philippe Colantoni, who gave me his passion of image processing and of color science. He is a really good color scientist who has never forgotten to write some lines of code after having discussed an idea. To the friend and the colleague, for the work we done together, and for what we will do in the future, thank you Philippe.

I would like to thank Alain Trémeau, for his advice throughout the last years and for the early learning of research. He should have been a part of the jury, but he had to cancel at the last moment for health reasons.

These years would have been less interesting without the whole Colorlab staff, students and permanents. It has always been good and easy to talk about either science or things of life with you guys! Thanks to the Dijon's crew as well, for their good friendship.

My girls all along these three years. I have been many times obsessed by another

thing than you. A special thought to Bara, Lucie, Gaby and especially Fanny (surtout toi!) who supported me when I was writing this manuscript. It has been great to share some pieces of my life with you, each one of you for different reasons.

I have a special thought to all the international friends I met for a (too) short time for most of them. A big hug to all my monkeys... It was a wonderfull start to an international life meeting you. A big hug to Wili and Gab too, Thomas as well, may we spend some time (and some beers) together again.

I want to thank my family, that I neglected for running around the world. My brother, mother, father, Tiago, my grandmother. All the rest of them, cousins, aunts, uncles... I hope to spend more time with you in the future. My thoughts are going to my late grandparents as well. Thanks for everything! I want also to say welcome to my other nephew who will arrive soon on earth ;)

Jean-Baptiste Thomas
Dijon
November 23, 2009

Abstract

In the context of color imaging, this thesis focuses on colorimetric characterization of displays and multi-display systems. Starting from the conventional pointwise approach we continue to some spatial analysis. We give some special attention to the duality between a professional and a consumer-oriented characterization.

In the first part of this thesis we consider pointwise display color characterization. We propose, evaluate and improve several methods to control the color in displays.

We investigate deeply the PLVC (Piecewise Linear assuming Variation in Chromaticity) model especially in comparison to the PLCC (Piecewise Linear assuming Chromaticity Constancy) model. We show that this model can be highly beneficial for LCD (Liquid Crystal Display) technology. We evaluate and improve a end-user method proposed by Bala and Braun. This method is quick and simple and does not need any measurement device other than a simple digital color camera. We confirm that this method gives significantly better results than using default gamma settings for both LCD and DLP (Digital Light Processing) projectors.

We focus on the distribution of color patches in color space for the establishment of 3D LUT (Look Up Table) models. We propose a new accurate display color characterization model based on polyharmonic spline interpolation. This model shows good results and is applied in real time for the accurate colorimetric rendering of multi-spectral images of art paintings viewed under virtual illuminants. We propose methods to build an optimized structure that permits to invert any display color characterization forward model. Several criteria linked with the grid itself or with an evaluation data set are tested. Our evaluation shows that in using our methods, we can achieve better results than with a regular equidistributed grid.

In a second part, we establish a basis for spatial color characterization via the quantitative analysis of the color shift and its spatial variation throughout the display area. We show that the spatial chromaticity shift is not negligible in some cases and that some features are spatially invariant within one display of a given technology.

Keywords: Display, multi-display system, display color characterization, display spatial color uniformity.

Résumé

Dans le contexte de l'imagerie couleur, cette thèse se focalise sur la caractérisation colorimétrique des moniteurs, vidéo-projecteurs et système multi-projecteurs. A partir de l'approche ponctuelle, nous considérons une extension pour une caractérisation spatiale.

Dans une première partie, nous considérons une approche ponctuelle. Nous proposons, évaluons et améliorons certains modèles destinés au contrôle colorimétrique des moniteurs ou vidéo-projecteurs.

Nous étudions le modèle PLVC (Piecewise Linear assuming Variation in Chromaticity), particulièrement en comparaison directe avec le PLCC (Piecewise Linear assuming Chromaticity Constancy). Nous montrons son efficacit à modliser le comportement des cristaux liquides. Nous évaluons et améliorons une méthode proposée par Bala et Braun qui est rapide et ne nécessite pas l'usage d'un appareil de mesure autre qu'un appareil photo numérique. Nous confirmons que cette méthode peut donner de meilleurs résultats que d'utiliser une correction plus classique pour les vido-projecteurs LCD (Liquid Crystal Display) et DLP (Digital Light Processing).

Nous travaillons sur la distribution des données dans les espaces colorimétriques pour la construction de 3D LUT (Look Up Table). Nous proposons un nouveau modèle de caractérisation très précis considérant une interpolation/approximation basée sur les polyharmonic splines. Ce modèle montre de bons résultats et est utilisé pour le rendu colorimétrique d'image multi-spectrales d'oeuvres d'arts sous différentes illuminations. Nous proposons également de construire une structure optimisée qui permet d'inverser n'importe quel modèle de caractérisation colorimétrique. Plusieurs critères liés à la structure de la distribution ou au comportement du modèle sur un jeu de données d'apprentissage. Notre évaluation montre que nous pouvons avoir de meilleur résultats en utilisant notre distribution que lors de l'utilisation d'une grille régulière.

Dans une seconde partie, nous établissons les bases d'une caractérisation colorimétrique spatiale à travers l'analyse quantitative de la variation spatiales des couleurs dans les vidéo-projecteurs. Nous montrons que la variation en chromaticité n'est pas nécessairement négligeable comparée à la variation en luminance, et que certaines spécificités sont spatialement invariantes pour un appareil donné et une technologie donnée.

Keywords: moniteurs, vidéo-projecteurs et système multi-projecteurs, caractérisation colorimétrique, uniformité colorimétrique spatiale.

Contents

List of Figures

Chapter 1

General Introduction

Le noir, c'est la seule couleur qui ne change pas.

Jacques Ferron

Abstract

This general introduction defines first the context of this work between physics, signal processing, image processing and colorimetry. The two main parts of this thesis are then introduced. The first concerns the point wise color characterization of displays. The second part considers spatial issues in projectors and multi-projector systems.

1.1 Context

The research presented in this thesis takes place in the context of color image science. Color imaging is at the intersection of several research fields, between color science, vision, digital image processing, and signal processing.

Before reading this document, the readers should have some prior knowledge of colorimetry, digital color images, and display technology.

Readers with limited knowledge of display technology should read Appendix A that is a brief overview of the field. Much information on display technology can also be found on the web. For projectors, the book of Matthew et al. (2008) is a great source of information. For readers with limited knowledge of colorimetry, Chapter 2 presents a short reminder about the colorimetric tools we used in this thesis. For a better and complete background on colorimetry, we recommend the classic book of Wyszecki and Stiles (2000). The Digital Color Imaging Handbook (Sharma, 2003) is also a great source of information and references.

This introduction first explains the concept of a cross-media reproduction system, color management, color device calibration and characterization. We then propose a general formulation of what a display is in this context. We explain the structure of this thesis and we finish this introduction by giving the contents and key contributions of each chapter.

1.1.1 Cross-media color reproduction

A cross-media color reproduction system can be considered to begin with the acquisition of a color scene and end up with the display of this scene by any medium. It is well known that the color acquired or reproduced by different devices for the same input is not the same. Thus, the use of a color management process is required to keep the color consistent through the entire color workflow. In a nutshell, cross-media color reproduction needs the characterization of each color device, and a color rendering algorithm, which permits to map the color gamut from one device to another.

The gamut mapping can be a global process (Morovic and Luo, 2001), or an image content dependent process (Farup et al., 2007). The color characterization is a major part, as all devices have to be color controlled.

The **calibration** process put a device in a fixed state, which will not change with time. For a color device, it consists in setting up the device. Settings can be position, brightness, contrast, and sometimes primaries and gamma, etc.

The **characterization** process can be defined as understanding and modeling the relationship between the input and the output, in order to control a device. For a digital color device, which means either to understand the relationship between a digital value

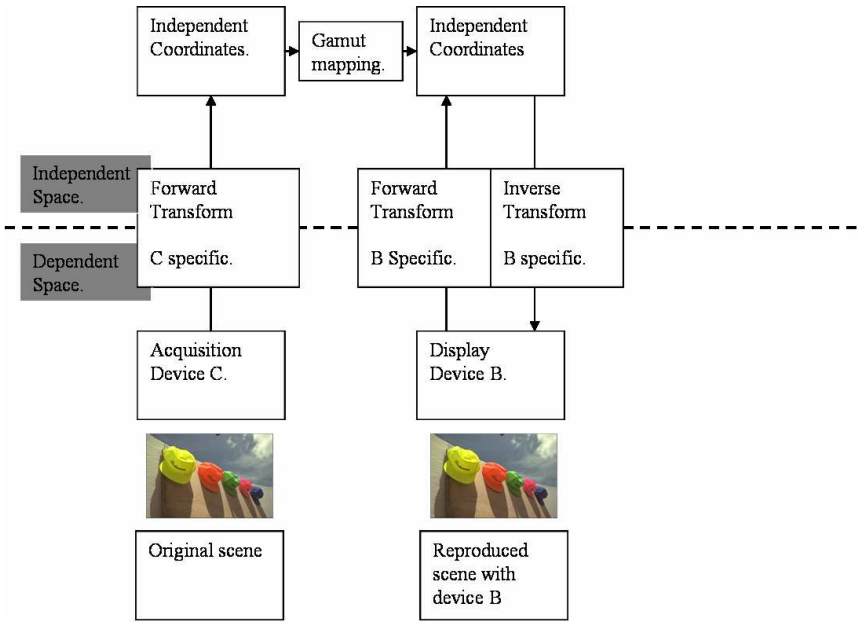

Figure 1.1: *Cross-media color reproduction from a camera to a display.*

input and a produced color for an output color device (printer, display) or, in the case of an input color device (camera), to understand the relationship between the color acquired and the digital value output.

When these steps are done, the cross-media color reproduction process preserves the color information within the color workflow such as in Figure 1.1 or Figure 1.2.

In some cases it can be useful to be able to simulate the color rendering of one device to another, such as in Figure 1.3.

Data used to set up the characterization model may be written in an ICC profile (ICC, 2004) that is read by a color management system. It is today the common and practical way to ensure a good color rendering.

1.1.2 Color displays

Display color characterization aims to understand the relationship between a digital value, input to the display, and the displayed color itself.

A display can be considered as an interface or as a function between an input signal and a displayed color, as shown in Figure 1.4.

We can consider this function and its inverse, F and F^{-1} that associate the signal and the color, such as:

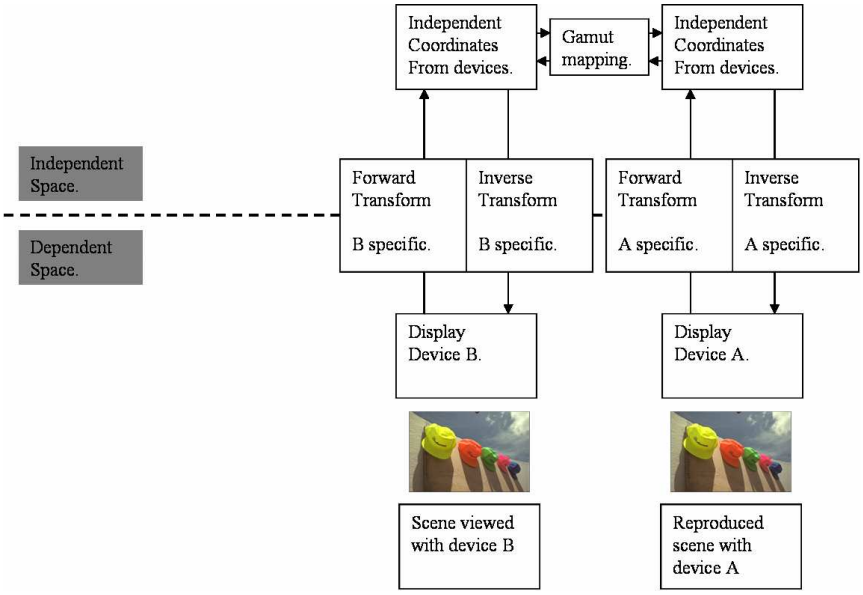

Figure 1.2: *Cross-media color reproduction from one display to another.*

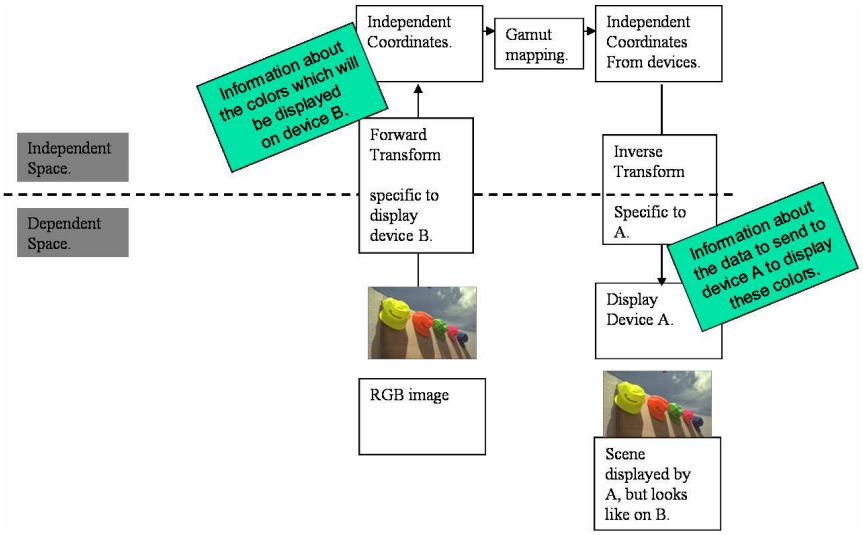

Figure 1.3: *Simulating a display with another one.*

$$F : \begin{cases} Dependent\ \ color\ \ space \longrightarrow Reference\ \ color\ \ space \\ Signal \longrightarrow Color{=}F(Signal) \end{cases} \tag{1.1}$$

$$F^{-1} : \begin{cases} Reference\ \ color\ \ space \longrightarrow Dependent\ \ color\ \ space \\ Color \longrightarrow Signal{=}F^{-1}(Color) \end{cases} \tag{1.2}$$

Figure 1.4: *A display can be considered as a function between the input signal and the displayed color.*

Equation 1.1 is called the forward transform, meanwhile Equation 1.2 is called the inverse transform.[1] This equation does not include the spatial dimension historically. However, in the case of multi-display systems, this dimension is included either partially or fully.

More precisely, this thesis aims to improve the state of the art of pointwise display color characterization while pointing out the difference between a professional color characterization that has to be as accurate as possible and a consumer characterization that aims only to preserve the intended meaning and the aesthetic of the content. Moreover it appears that when we want an accurate color characterization, or when we want to set up a multi-display system, the spatial color drift across the display cannot be disregarded. Thus this thesis also aims to improve the knowledge on the spatial behavior of displays.

1.2 Agenda

This section details the content of this thesis. It explains the structure in two parts, and gives a summary of the content and key contributions of each chapter.

Chapter 2 presents our general framework, and considers model quality evaluation. It contains a reminder of the main results of colorimetry, and justifies the choices related with the results we present afterwards.

Historically, display color characterization considers one spatial measurement location to perform any correction. It has been shown in the litterature that it can be a correct assumption for CRT monitors while applying a simple scaling factor (Brainard, 1989). Point wise color characterization is treated in the first part of this document.

However, and especially for other technologies, for projectors or for multi-display systems, the assumption of spatial uniformity can be severely challenged. The second part of this thesis considers spatial issues for the color characterization of projectors and multi-projector systems.

[1] The inverse transform is also called backward transform in some works.

1.2.1 Part I

The first part of this thesis includes Chapters 3, 4, 5, 6 and 7.

In this part, we first review the display characterization models presented in the bibliography, from physical to empirical models. We then present in detail our contribution to this state of the art. We show that the PLVC model can be highly beneficial for accurate color characterization of LCDs as compared with some other classical models. We show how a end-user characterization method can become more accurate with the help of a simple consumer camera. We present a new accurate characterization model we helped to improve with choices, discussions and evaluation. This model is used in a color rendering framework. We perform a study on data distribution for inverting any color characterization model that requires too much computation to be performed analytically in real time.

Chapter 2 presents our general framework. It introduces basic concepts of colorimetry relevant to our work. It justifies the way we evaluated our following results, discussing the choice of the method, the metric and the statistics. It presents the common experimental framework. It presents a duality between two types of display characterization methods and goals: the consumer one, which intends only to keep the meaning and aesthetic unchanged through the color workflow, and the accurate professional one, which aims to have a very high colorimetric fidelity through the color workflow.

Chapter 3 describes the state of the art of display color characterization. We have tried to be exhaustive, and to explain the features, advantages and drawbacks of the different models.

Chapter 4 considers a detailed analysis and experimental validation of the PLVC model (see 3.2.2). This work has led to publications at Gjøvik Color Imaging Symposium (Thomas, Hardeberg, Foucherot and Gouton, 2007) and in Color Research & Application (Thomas, Hardeberg, Foucherot and Gouton, 2008).

Chapter 5 concerns mainly the independent evaluation and improvement of a characterization method introduced by Bala and Braun (2006) for a simple yet accurate end-user colorimetric characterization of projection displays. We participated in this work through the supervision of a master thesis done by Espen Mikalsen at Gjøvik University College (Mikalsen, 2007). We contributed to this work considering design choices, and in the presentation and organization of the results. This work has been presented at GCIV'08 (Mikalsen et al., 2008).

Chapter 6 presents a part of the color workflow used in a new software (PCASpectralViewer) that has been developed by Philippe Colantoni, namely the color management process. I had the chance to work with him on this project mainly for improvement of the method, discussions, choices, evaluation and presentation of the results as a display and color expert. We presented our first results at the MCS'09 within the SCIA'09

conference (Colantoni and Thomas, 2009) and we are currently writing a more detailed journal paper that covers this method and its results.

Chapter 7 focuses on distribution of patches in *RGB* color space to perform a linear tetrahedral interpolation from *CIELAB* or *CIEXYZ* to *RGB*. The color of the *RGB* values may be estimated in an independent color space using any forward model. We used the PLVC model for testing this new approach. We worked on this project with Philippe Colantoni who contibuted with discussion, implementation and with his pragmatism. We used his C++ library for the implementation. Results have been presented at the EI'08 conference (Thomas, Colantoni, Hardeberg, Foucherot and Gouton, 2008*b*) and in the Journal of the Society for Information Display (Thomas, Colantoni, Hardeberg, Foucherot and Gouton, 2008*a*).

1.2.2 Part II

The second part of this thesis considers the challenging issue of spatial uniformity of displays with an emphasis on the problem faced in colorimetric uniformity in multi-displays. It includes Chapters 8 and 9.

This part considers spatial issues within projection displays. We first review the state of the art, introducing the problems and the advantages linked to the use of multi-projector systems. We then reduce the problem to its color dimension, which is colorimetric uniformity or perceived color uniformity within these displays. The second chapter in this part considers a colorimetric study of projectors along their spatial dimension. It is shown that, considering colorimetric indicators, it is not sufficient to consider only a luminance shift while correcting for intra-projector non-uniformity. We investigate the assumptions commonly used in display color characterization considering the spatial dimension.

Chapter 8 describes the state of the art of the methods to reach colorimetric uniformity in multi-projector systems. We explain the context of a multi-display system and present the problems and some methods used to reach spatial color uniformity. It is difficult to claim to be exhaustive here, since many solutions are proprietary solutions often with a dedicated hardware, however we reviewed the existing academic solutions.

Chapter 9 is an investigation and a study of the color spatial uniformity of projectors. This is the result of a balanced collaboration with Arne Magnus Bakke. Jérémie Gerhardt contributed to the second part of this work. We have presented our results at the CCIW'09 conference (Thomas and Bakke, 2009) and at the GCIS'09 conference (Bakke et al., 2009). We have submitted a journal paper to the Journal of Imaging Science and Technology.

Chapter 10 pulls together many topics discussed in this thesis. We consider the *user need* as a criterion to select a good color characterization model. We discuss the

capability of standard ICC profiles and Color management modules considering the applications of some color characterization models. We propose to build a end-user photometric spatial correction system and finally we discuss more future works that can be done to achieve good colorimetric accuracy within multi-projector displays.

Chapter 11 concludes this thesis, summarizing our contributions.

Appendix A presents briefly todays display technologies. **Appendix B** presents a uniform sampling based on an hexagonal grid. We used it to sample color spaces in different works. **Appendix C** gives the mathematical definition of the polyharmonic spline interpolation we used. **Appendix D** gives more results on PLVC model. A list of the publications related to this work is given at the end of the thesis, in **Appendix E**.

Chapter 2

Color, definitions and quality

Don't think twice, it's all right!

Bob Dylan

Abstract

This chapter provides a definition of color display device and define the colorimetric tools we used. It explains how we considered the interaction between a device, a screen and an ambient light as a combination that is consistent and explain our choices and processes considering the evaluation of a color characterization model.

2.1 Introduction

This chapter defines the colorimetric tools we used and our experimental framework. We discuss then how to evaluate the accuracy of a color characterization model, first considering a pointwise transform. Indeed, displays are mainly treated as spatially invariant functions in the litterature. The spatial color uniformity quality is often evaluated via the appreciation of the observer, or through colorimetric measurements of a uniform color patch at several locations. Chapter 9 considers the evaluation of spatial uniformity and is not considered in this Chapter.

2.2 Colorimetry

This section presents the main elements of CIE colorimetry. We describe mainly the color spaces and the standard color difference metrics we used in the thesis. We limit the presentation to colorimetry's tools, and we do not go through the detailed theory neither through color appearance.

From the main elements of colorimetry, CIE defined a system of color spaces where a 3D point is representing a color under a given set of {material, illuminant, viewing geometry}. These CIE tristimulus values, $CIEXYZ$, are the cornerstone of what is presented in this section. For more information, and a complete background, we refer the reader to Wyszecki and Stiles (2000) and CIE (2004).

2.2.1 CIE system

Colorimetry aims to specify the color of a given visual stimulus with quantitative data based on the spectral power distribution of the stimulus. It is also concerned with the specification of the difference between two stimuli. The *trichromatic generalization* states that, over a wide range of conditions, many color stimuli can be matched by additive mixture of three fixed primaries. Considering that linearity laws (symmetry, transitivity, proportionality and additivity) are added to the additive mixture, we have a strong quantitative framework.

The CIE system is based on the spectral information coming from an object (via reflectance or transmittance) weighted by the color matching functions of a standard observer. These three color matching functions represent the sensitivities of a standard observer to the different wavelengths considering a given geometry, a solid angle of viewing of 2 degrees (1931) or 10 degrees (1964). The wavelengths range considered is from 360 nm to 830 nm, defined as the visual spectrum. These three functions are considered as primaries. The CIE modified the real functions in order to ensure only

positive addition of weighted spectral power to reach most colors, considering virtual primaries X, Y, Z.

The goal of CIE colorimetry is to define some practical rules and standard for color measurement and color difference measurement.

2.2.2 Tristimulus values

These CIE tristimulus values, the most basic values in CIE colorimetry, *CIEXYZ*, are defined by:

$$\begin{aligned} X &= k \int_{\lambda} P_\lambda \bar{x}(\lambda)\, d\lambda \\ Y &= k \int_{\lambda} P_\lambda \bar{y}(\lambda)\, d\lambda \\ Z &= k \int_{\lambda} P_\lambda \bar{z}(\lambda)\, d\lambda \end{aligned} \tag{2.1}$$

where X, Y, Z denote the CIE tristimulus values, and $\bar{x}(\lambda)$, $\bar{y}(\lambda)$, $\bar{z}(\lambda)$ the CIE color matching functions. P_λ denotes the monochromatic component of wavelength λ of a given tristimulus whose spectral radiant power distribution is $\{P_\lambda d\lambda\}$. k is a normalizing factor.

From these equations, the chromaticity values can be computed, such as:

$$\begin{aligned} x &= \frac{X}{X+Y+Z} \\ y &= \frac{Y}{X+Y+Z} \end{aligned} \tag{2.2}$$

x and y being the chromaticity coordinates, that can be useful to define a color with normalized values.

The interaction object-color stimuli can be defined as $P_\lambda = R(\lambda)L(\lambda)$, $R(\lambda)$ being the spectral reflectance of the object viewed and $L(\lambda)$ the spectral characteristics of the illumination. Equation 2.1 becomes Equation 2.3:

$$\begin{aligned} X &= k \int_{\lambda} R(\lambda)L(\lambda)\bar{x}(\lambda)\, d\lambda \\ Y &= k \int_{\lambda} R(\lambda)L(\lambda)\bar{y}(\lambda)\, d\lambda \\ Z &= k \int_{\lambda} R(\lambda)L(\lambda)\bar{z}(\lambda)\, d\lambda \end{aligned} \tag{2.3}$$

where k is usually chosen as in Equation 2.4

$$k = \frac{100}{\int_{\lambda} L(\lambda)\bar{y}(\lambda)\, d\lambda} \tag{2.4}$$

In all practical situations, to compute abolute values, the integrals are replaced by sums, such as:

$$\begin{aligned} X &= \sum_{\lambda=\lambda_a}^{\lambda_b} R(\lambda)L(\lambda)\bar{x}(\lambda)\Delta\lambda \\ Y &= \sum_{\lambda=\lambda_a}^{\lambda_b} R(\lambda)L(\lambda)\bar{y}(\lambda)\Delta\lambda \\ Z &= \sum_{\lambda=\lambda_a}^{\lambda_b} R(\lambda)L(\lambda)\bar{z}(\lambda)\Delta\lambda \end{aligned} \tag{2.5}$$

the Y quantity being expressed in $cd.m^{-2}$ for analogy with photometry.

2.2.3 Pseudo-uniform color spaces and color differences

The CIE system offers practical methods to predict the perceived color difference between two colors.

CIE $L^*a^*b^*$ and CIE $L^*u^*v^*$ color spaces

These two color spaces are attempts to distribute uniformly perceived colors, linearizing the evaluation of color differences. They mimic the logarithmic eye response. The color information is related to the white stimulus, X_w, Y_w, Z_w.

CIELAB color space is defined such as:

$$\begin{aligned} L^* &= 116\left(\frac{Y}{Y_w}\right)^{\frac{1}{3}} - 16 \quad \text{if } \frac{Y}{Y_w} > 0.008856 \\ L^* &= 903.3\left(\frac{Y}{Y_w}\right) \quad \text{if } \frac{Y}{Y_w} \leq 0.008856 \\ a^* &= 500\left[f(\frac{X}{X_w}) - f(\frac{Y}{Y_w})\right] \\ b^* &= 200\left[f(\frac{Y}{Y_w}) - f(\frac{Z}{Z_w})\right] \end{aligned} \tag{2.6}$$

with f a function that associates s to $f(s)$ defined such as Equation 2.7. L^* is the perceived lightness, a^* and b^* corresponding approximately to the color opposition red-green and blue-yellow.

$$\begin{aligned} f(s) &= s^{\frac{1}{3}} \quad \text{if } s > 0.008856 \\ f(s) &= 7.787s + \frac{16}{116} \quad \text{if } s \leq 0.008856 \end{aligned} \tag{2.7}$$

CIELUV color space is defined such as:

$$\begin{aligned} L^* &= 116\left(\frac{Y}{Y_w}\right)^{\frac{1}{3}} - 16 \quad \text{if } \frac{Y}{Y_w} > 0.008856 \\ L^* &= 903.3\left(\frac{Y}{Y_w}\right) \quad \text{if } \frac{Y}{Y_w} \leq 0.008856 \\ u^* &= 13L^*\left[u' - u'_w\right] \\ v^* &= 13L^*\left[u' - u'_w\right] \end{aligned} \tag{2.8}$$

with u' and v' defined such as:

$$\begin{aligned} u' &= \frac{4X}{X + 15Y + 3Z} \\ v' &= \frac{9Y}{X + 15Y + 3Z} \end{aligned} \tag{2.9}$$

CIE $L^*a^*b^*$ and CIE $L^*u^*v^*$ color differences

Within these color spaces a perceived color difference can be expressed as the Euclidean distance such as in Equation 2.10.

$$\begin{aligned} \Delta E^*_{ab} &= \left[(\Delta L^*)^2 + (\Delta a^*)^2 + (\Delta b^*)^2\right]^{1/2} \\ \Delta E^*_{uv} &= \left[(\Delta L^*)^2 + (\Delta u^*)^2 + (\Delta v^*)^2\right]^{1/2} \end{aligned} \tag{2.10}$$

Decomposition to perceived lightness, chroma and hue

It is practical to evaluate the difference in term of Chroma, Hue or Lightness shift. Let us to consider two color stimuli Q_1 and Q_2.

The lightness being defined by the formulas above, the difference in lightness between Q_1 and Q_2 is $\Delta L^* = L^*_1 - L^*_2$.

The chroma can be calculated with:

$$\begin{aligned} C^*_{uv} &= \left[(u^*)^2 + (v^*)^2\right]^{1/2} \\ C^*_{ab} &= \left[(a^*)^2 + (b^*)^2\right]^{1/2} \end{aligned} \tag{2.11}$$

and the difference in chroma between Q_1 and Q_2 is $\Delta C^*_{ab} = C^*_{ab1} - C^*_{ab2}$, and similarly for ΔC^*_{uv}.

The hue angles h are defined by Equation 2.12

$$\begin{aligned} h_{uv} &= arctan\left(\frac{v^*}{u^*}\right) \\ h_{ab} &= arctan\left(\frac{b^*}{a^*}\right) \end{aligned} \tag{2.12}$$

expressed in degrees with the following convention:

$$\begin{array}{rl} 0 < h_{ab} < 90, & if\, a^* > 0\, and\, b^* > 0 \\ 90 < h_{ab} < 180, & if\, a^* < 0\, and\, b^* > 0 \\ 180 < h_{ab} < 270, & if\, a^* < 0\, and\, b^* < 0 \\ 270 < h_{ab} < 360, & if\, a^* > 0\, and\, b^* < 0 \end{array} \tag{2.13}$$

and similarly for h_{uv}.

Then the quantities ΔH^*_{uv} and ΔH^*_{ab} between Q_1 and Q_2 can be defined using Equation 2.14. These quantities have to be computed indirectly because of the relativity of a hue angle.

$$\begin{array}{l} \Delta H^*_{ab} = \left[(\Delta E^*_{ab})^2 - (\Delta L^*)^2 - (\Delta C^*_{ab})^2\right]^{1/2} \\ \Delta H^*_{uv} = \left[(\Delta E^*_{uv})^2 - (\Delta L^*)^2 - (\Delta C^*_{uv})^2\right]^{1/2} \end{array} \tag{2.14}$$

Other metrics

CIELAB has been shown not to be perfectly perceptually homogeneous, thus it is not really able to reach its aim of showing a Just Noticeable Difference [1] (JND) equivalent to 1 unit in the euclidean metric. The color perception can be influenced by different factors, such as the material that shows color (uniformity, texture, reflexion), the conditions of presentation (vision field, location and distance between the two colors to assess if they are equally perceived or not, the background), moreover, some psychological factors can influence the perception.

It is then possible to weight the previous model, and to introduce some parameters, such as $\Delta E' = \frac{\Delta E}{k_i S_i}$, k_i being a parameter that include some of the factors defined above, S_i being a weight.

More color difference formulas have been derived from this thought and for different purposes, such as ΔE^*_{94} (Equation 2.15) that has been defined originally for textile color differences.

$$\Delta E^*_{94} = \left[\left(\frac{\Delta L^*}{k_L S_L}\right)^2 + \left(\frac{\Delta C^*}{k_C S_C}\right)^2 + \left(\frac{\Delta H^*}{k_H S_H}\right)^2\right]^{1/2} \tag{2.15}$$

With $S_L = 1$, $S_C = 1 + 0.0045C^*$ and $S_H = 1 + 0.015C^*$. The k_i parameters are dependent of the measurement conditions. $k_L = k_C = 1$ and $k_L = 2$ for textile applications. The three parameters are set up to 1 for default use of the metric.

Other metrics (Equations 2.16 and 2.17) are trying to increase the homogeneity of the *CIELAB* color space:

[1] A JND is the smallest detectable difference between a starting and secondary level of a particular sensory stimulus, in our case two color samples.

$$\begin{aligned}\Delta E^*_{CMC} &= \left[\left(\frac{\Delta L^*}{lS_L}\right)^2 + \left(\frac{\Delta C^*}{cS_C}\right)^2 + \left(\frac{\Delta H^*}{S_H}\right)^2\right]^{1/2} \\ \Delta E^*_{BFD} &= \left[\left(\frac{\Delta L^*}{l}\right)^2 + \left(\frac{\Delta C^*}{cD_C}\right)^2 + \left(\frac{\Delta h}{D_h}\right)^2 + w\frac{\Delta C^*}{D_C}\frac{\Delta h}{D_h}\right]^{1/2}\end{aligned} \tag{2.16}$$

The last metric, ΔE^*_{00} (CIE, 2001; Luo et al., 2001) is supposed to be even more homogeneous (Equation 2.17), with a JND equivalent to approximately 1 unit everywhere in the color space. However, it shows some discontinuities as shown by Sharma et al. (2005, 2004).

$$\Delta E^*_{00} = \left[\left(\frac{\Delta L'^*}{k_L S_L}\right)^2 + \left(\frac{\Delta C'^*}{k_C S_C}\right)^2 + \left(\frac{\Delta H'^*}{k_H S_H}\right)^2 + R_T\frac{\Delta C'^*}{k_C S_C}\frac{\Delta H'^*}{k_H S_H}\right]^{1/2} \tag{2.17}$$

We refer the reader to the articles or CIE reports for the definition of the terms, defining them here would provide no benefit for the following.

This short reminder of colorimetry tools should be enough to follow the content of the thesis. For the second part of the thesis, which considers spatial issues for projection displays, we would like to recall that colorimetry has been defined for 2 and 10 degrees viewing angles and for adjacent uniform color patches.

2.3 Display characterization

2.3.1 Introduction

Color characterization of a color display device is a major issue for the accurate color rendering of a scene on a display device. We recall that it aims to define the transformation between the device digital color space, typically *RGB*, and a reference color space, describing the perceived color, based on the *CIE* standard observer, typically *CIEXYZ* or *CIELAB* (Widdel and Post, 1992). This transformation has two directions. The forward transformation aims to predict the displayed color for any set of digital values input to the device, i.e. a triplet (R, G, B). The inverse transformation provides the set of digital values to input to the display in order to display a desired color. A calibration process precedes the characterization. This step maintains the settings (gamma, contrast, brightness, correlated color temperature, etc) of the display in a given state. Before we venture deeper into the methodology applied to build a display color characterization model, we need to set some definitions and conditions.

We consider the characterization model to be set up with some knowledge about the display. This knowledge can come from the technology, the manufacturer and/or

from a set of measurements. Once a model is set up, there is a need to evaluate its performance.

This section presents our definition of a display, how we performed the experiments, and how we evaluated the performance of the models in terms of accuracy and precision.

2.3.2 Display: definition

In this thesis, we consider a display device as the combination of the display apparatus itself with the ambient light and with the screen, in the case of a projection device (Figure 2.1). Thus, if we start with the assumption that the observer is not moving, the information we want to predict is the color that the observer will see at one location of the screen at a given time.

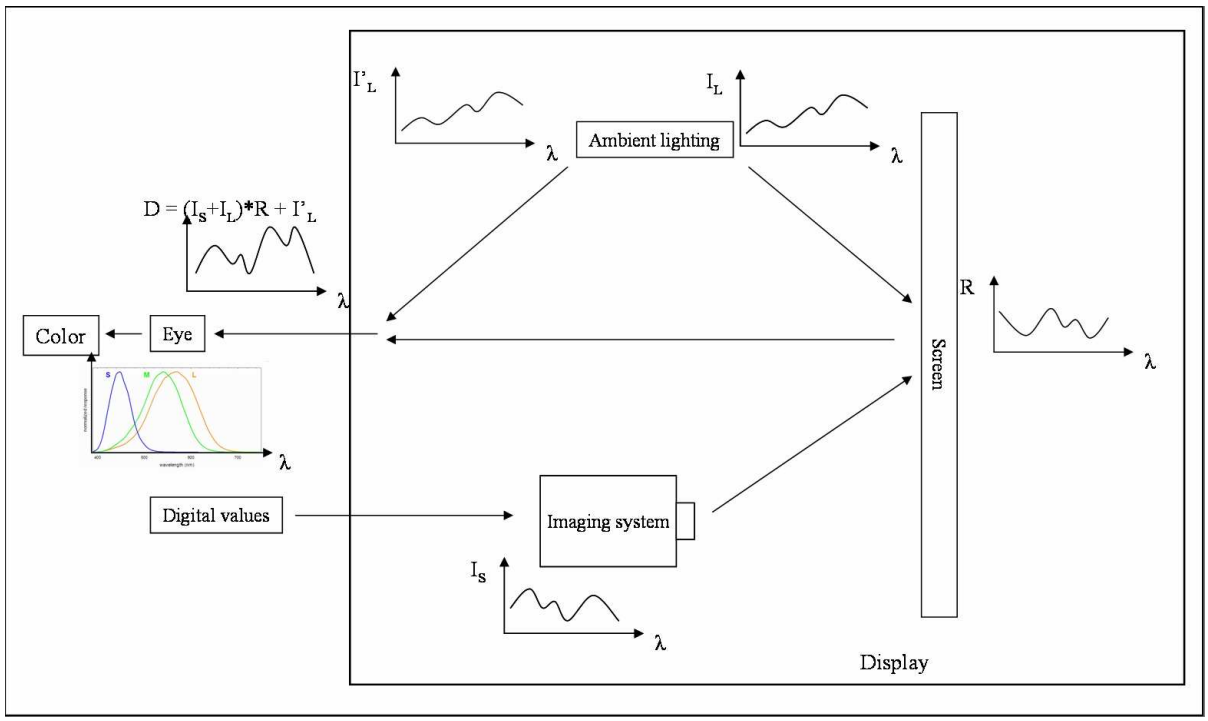

Figure 2.1: *Scheme that presents what we consider as a display device. A given input results in a displayed signal that reaches the eye and becomes a color. While considering the whole apparatus as a display, we are including implicitly the screen properties of reflectance (or transmittance) and of the ambient light, since they are included in the model.*

Using such a definition, we are including implicitly the spectral properties of the screen in the resultign signal. We can either consider the whole display as a black box and set a model only based on measurements or consider each part of it and model it physically. The first thing we suppose is that this system remains stable over time.

Let us detail the parts of this display configuration:

- The imaging system produces a visual signal. It is often based on three primaries (refer to Appendix A for more details). It often includes an optical system (mostly in projection systems), which magnifies the signal for displaying on a screen. The lenses have to be carefully chosen and corrected for aberrations (Bass et al., 2010*a*,*b*). Geometrical aberrations (Spherical, Coma, astigmatism, distortion) are due to the failure of the Gaussian approximations. Chromatic aberrations are due to the variation of the refractive index depending on the wavelength. Vignetting effect is due to the lenses. Some diffraction effects can appear as well. Most of the effects are corrected in order to create no disturbance to the visual system, however there are still some effects. The imaging system can contain a light source as well. The properties of this light source and its homogeneity influence the characteristics of the whole system.

- The screen can be either in reflectance (such as in some projection configurations) or in transmittance (such as for monitors or some projection configurations). Its spectral properties are influencing the resulting signal.

- An ambient lighting can illuminate the place and influence the resulting signal.

When the signal enters the eye, we can refer to colorimetry.

2.3.3 Experimental setup

In order to have accurate measurements, we used the CS-1000 spectroradiometer from Minolta (Accuracy: luminance: $\pm 2\%$, x: ± 0.0015, y: ± 0.001, Repeatability: Luminance: $\pm 0.1\%$, xy: 0.0002 for illuminant A). This device is supposed to be accurate enough and often serve as a reference.

In some experiments (Chapter 6) we used the X-Rite (Gretag Macbeth) Eye One Pro spectrophotometer (Repeatability: x,y: 0.002 at $5000K$, 80 cd/m^2). We used this device on this occasion to answer the constraints due to the application and to the model. The drawback is that its estimation of the dark colors can be less accurate than the estimation of brighter signals. We will see in Chapter 6 how we took that effect into account.

Considering the previous definition, in our experiments the measurement device was placed where the observer should be placed except when using the Eye One Pro (that needs to be attached to the screen). The image was displayed considering display standard settings and recommendations from the manufacturer (The geometry of the whole system for projectors was basically of the same type that the one used in (IEC:61966-3, 1999; Kwak and MacDonald, 2000), with some variations depending on

the recommandations of www.projectorcentral.com (2009)). We considered a dark surrounding (we switched off any ambient light source but the one coming from the projector/monitor or from the screen. We displayed full screen color patches. The influence of the induced flare on the measure is then not consistent with the measured color, however, it is consistent through the whole experimental process, and consistent while we measure color at different spatial locations.

A warming up time of at least one hour and fifteen minutes has been used before any measurement to reach a correct temporal stability.

2.3.4 Evaluation strategy

In order to evaluate the quality of a model, we need to define a strategy. In the following, we consider the evaluation of a model in the forward and inverse directions, the data set, the statistics and the metric we used.

Forward model evaluation

The goal is to predict the displayed color. The process is simple. We process a digital value with the model to obtain a result and compare it in a perceptually homogeneous color space with the measurement of the same input. Figure 2.2 illustrates the process.

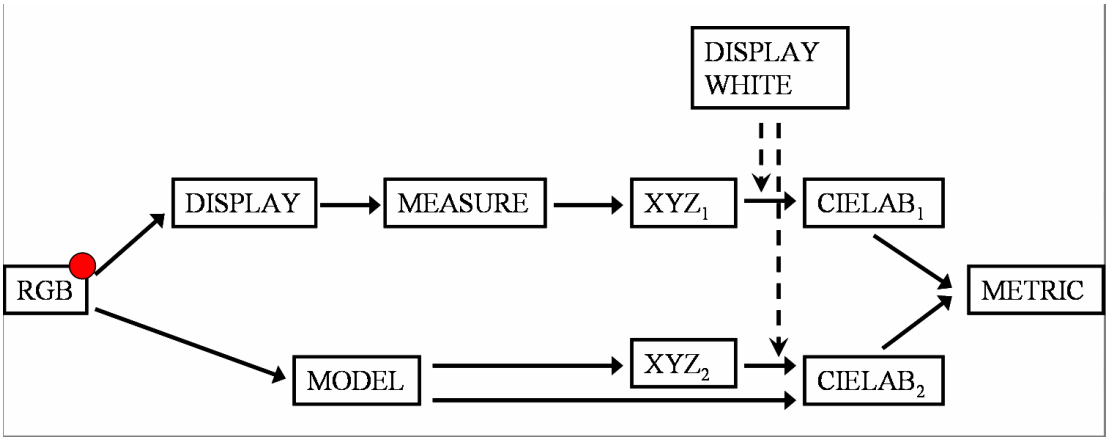

Figure 2.2: *Evaluation of a forward model scheme. A digital value is sent to the model and to the display. A value is computed and a value is measured. The difference between these values represents the error of the model.*

Inverse model evaluation

In the inverse direction, we can consider two different features to evaluate. We present the two features and the two different ways to evaluate them.

The first method evaluates the inverse model accuracy (Figure 2.3). In doing that, we consider a color that we want to display, we compute the values to send to the display, we display and measure. The difference in a perceptually homogeneous color space between the estimation and the measure show how the model fails. However, since the color has to be displayed after computation, it requires another estimation data set than the one used to estimate the accuracy of the forward model (that means three diferent data sets: one for the model establishment, one for the evaluation of the forward model and one for the evaluation of the inverse model), and we have to be sure that the colors are inside the display gamut (we do not want to introduce a bias due to gamut mapping).

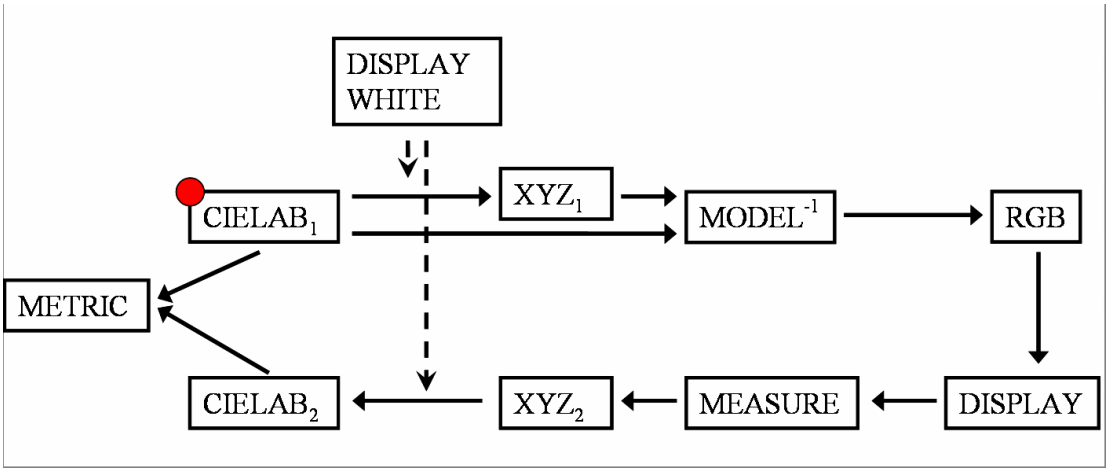

Figure 2.3: *Evaluation of a model in the inverse direction. We want to reproduce a color given in a reference color space. We compute the digital values to send to the display. This value is sent to the display, and measure. The difference between the wanted value and the measured one represents the error of the inverse model.*

The second method evaluate the model inversion. It uses a data set designed in the digital space (*RGB*). Then we can evaluate directly the error in *RGB* such as on Figure 2.4. The first advantage is that the same data set can be used for the forward and for the inverse directions. The second advantage is that we can use the same data set from device to device without taking care of a gamut mapping process. In doing that, a really bad model can be perfectly invertible. It can be considered as not relevant since it does not consider color.

We chose this second method for our experiments except for Chapter 5 where we used the first method in order to quantify the error perceptually. The choice of the second method for the other cases is justified by the fact that we wanted to evaluate the inverse model mathematically, not from a perceptual point of view. However these spaces are related via the display, and the error in *RGB* reflect the error we would have

perceived (since we consider that the display will reproduce the same color for the same input).

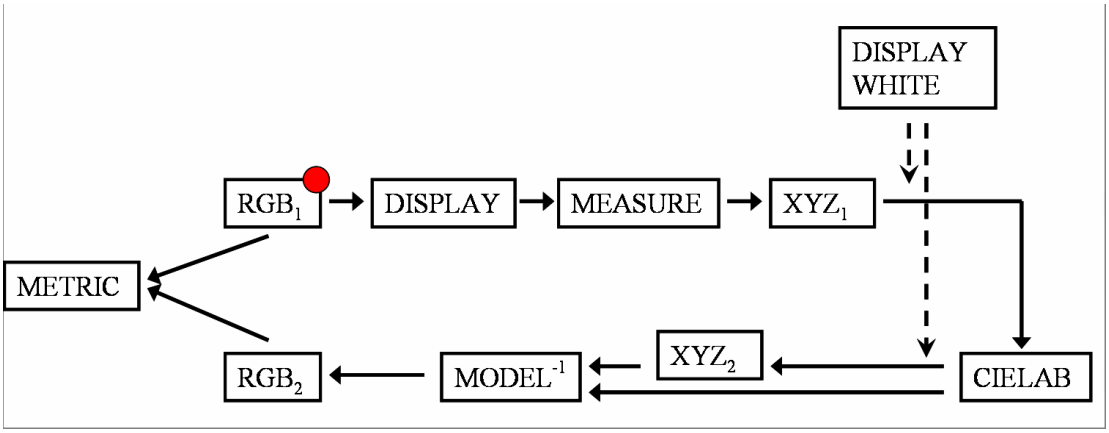

Figure 2.4: *Evaluation of a model inversion. We send a digital value to the display, we measure it and obtain a color. This color is sent through the model to obtain the digital value to send to the display to obtain it again. While computing the difference between these digital values, we obtain the error of the model inversion.*

Evaluation data set

Except in Chapter 5, we used the same data set for the evaluation all across this thesis. In Chapter 5 only the accuracy in lightness was of importance.

We designed a random data set of 100 color patches equiprobably distributed in *RGB* color space. On Figure 2.5 one can see the distribution of the data projected on *RG*, *GB* and *BR* planes. On Figure 2.6, one can see the distribution of the data set in 3D in *RGB* space.

We can notice that, the low and high digital values on the *GB* plane, the are not well represented and that in *BR* plane, the high digital values along R are not well represented. That is shown in Figure 2.6: the cyan color are not very present. In hindlight, it could have been judicious to build another data set that includes *RGB* values following some regular pattern to counterbalance this effect.

Metric choice and statistical analysis

In the previous sections, we considered a metric to compare two colors and we saw that we could have chosen between several metrics.

We chose to use the ΔE^*_{ab} metric.

First because it is the one that is still recommended by standards (even if it may change soon). Moreover most of the work about display characterization are using this

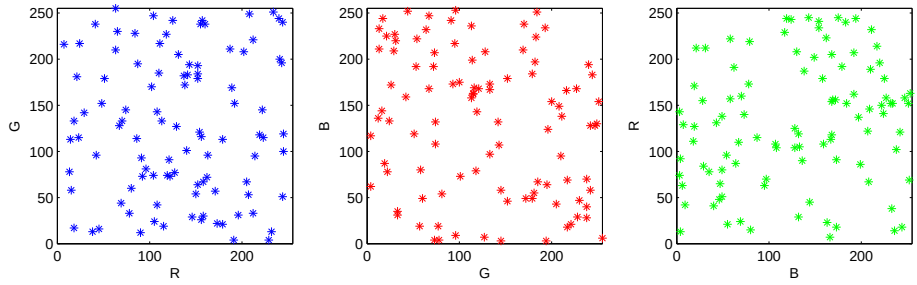

Figure 2.5: *Our evaluation data set projected on RG, GB and BR planes of the RGB color space.*

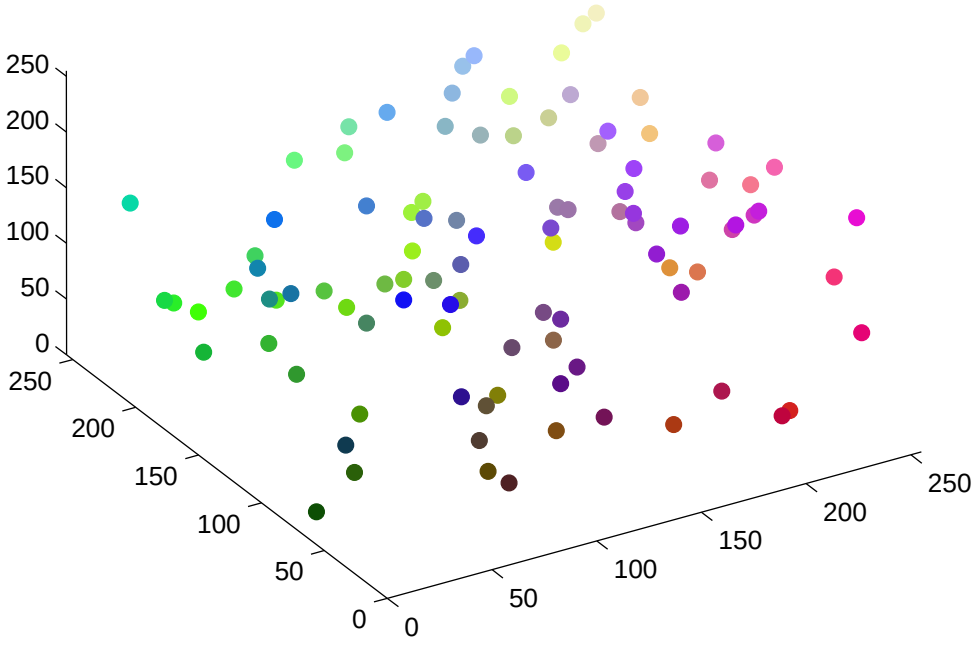

Figure 2.6: *Our evaluation data set in RGB color space. Note that the cyan part is less dense.*

metric. In some works, the ΔE^*_{94} is used. In older work, some results are presented in $u'v'$, but but most of the papers used ΔE^*_{ab} metric. It is then easier to compare our results with the ones found by others.

However, since some more recent color differences have been shown to be more perceptually homogeneous, we could have decided to use them. We did not want to use ΔE^*_{94} because the parameters are specified empirically for textile. The default ones does not make a special sense for displays as far as we know. And by extension, we would not chose all parameter based metrics unless the parameters have been designed specially for the display case.

In addition, a ΔE^*_{94} is always lower than a ΔE^*_{ab} while computing the distance between the two same colors. Considering that, we can over-estimate the errors, but it is a smaller problem than to under-estimate them.

Since we have a large data set, we can and need to perform some statistics. The two choices to have an estimation of the model accuracy are the median and the average. We chose the average since it is the indicator that is used in most papers.

The maximum error is of strong importance since it represents the worst case for the model (if we consider the evaluation data set as representative). This is as important as the overall estimation, since it can be a criterion to select a model.

The standard deviation is an important indicator. It represents the precision (repeatability + reproducibility) of the model.

It is possible to push deeper the statistical analysis, considering confidence intervals and percentile. It can be of interest, but in our opinion most of the time, the maximum error is more interesting.

2.3.5 Results analysis

Once we have an estimation of the model failure, we would be able to say how it is good or not. The best case is to have an error below the JND. Kang (1997) said on the page 167 of his book that the JND is of 1 ΔE^*_{ab} unit. Mahy et al. (1994) study assessed that the JND is of 2.3 ΔE^*_{ab} units. Considering that the *CIELAB* color space is not perfectly uniform, it is impossible to give a perfect threshold. Moreover, these thresholds have been defined for simultaneous pair comparison of uniform color patches. It may not be the best choice when comparing color imaging devices since it is seldom this case (except maybe in soft proofing).

In the case of color imaging devices, many thresholds have been used. Abrardo et al. (1996) proposed that between 0 and 1 the difference is *out of perception*, from 1 to 3 it is *very good quality*, from 3 to 6 it is *good quality*, from 6 to 10 it is *sufficient*, over 10 it is *insufficient*. Hardeberg (1999) used a different set of thresholds. To him, from 0 to 3 it is *hardly perceptible*, from 3 to 6 it is *perceptible, but acceptable*, over 6 it is *not*

acceptable. Schläpfer (1993) used a more constraining set: under 0.2 it is *not visible*, 0.2 to 1 it is *very small (JND)*, from 1 to 3 it is *small*, between 3 and 6 *medium* and over 6 it is *large*. Different other thresholds have been used with the ΔE^*_{ab} metric. For printers applications, the acceptable threshold is of 6 units (Stamm, 1981), the accepted standard deviation was of 3.63 units. Stokes et al. (1992) found a perceptibility acceptance for pictorial images of an average of 2.15 units. Catrysse et al. (1999) used a threshold of 3 units.

Gibson and Fairchild (2000) found acceptable a characterized display that has a prediction error average of 1.98 and maximum of 5.57, while the non-acceptable has at the best an average of 3.73 and a maximum of 7.63. It is fitting with Table 2.1, however, they used ΔE^*_{94}.

In this thesis we would like to propose another set of thresholds that would be an attempt to quantify the success of the color control depending on the purpose. This is only a basis for our evaluation, and does not aspire to be exact. In the following, we will distinguish between accurate professional color characterization, which purpose is to ensure a really high quality color reproduction, and a consumer color reproduction, which aims only at the preservation of the intended meaning.

Considering the professional reproduction, let us consider the following rule of thumb. We want to reach a good accuracy and in our opinion we need to consider the two indicators, the average and the maximum eror.

Let us consider the average: from 0 to 1 it is good, from 1 to 3 it is acceptable, and over 3 it is not acceptable. If now we consider the maximum, from 0 to 3 it is good, from 3 to 6 it is acceptable, over it is not acceptable. If we compare this scale with the rule of thumb used by Hardeberg (1999), it makes sense since below three it is hardly perceptible, the same if we look at Abrardo et al. (1996). If we look at the JND proposed by Kang (1997) and Mahy et al. (1994) it seems to make sense since in both case the good is under the JND. In this case we would prefer results to be good, and it may be possible to discard a couple model/display if it does not satisfy this condition. In the case of this professional reproduction, it could be better to use the maximum error to discard a couple model/display.

Considering the consumer prediction, we propose to consider that from 0 to 3 it is good, from 3 to 6 it is acceptable, and over 6 it is not acceptable. In this case we would rather accept methods that shows average results up to 6, since it should not spoiled the meaning of the reproduction. This is basically the same than he rule of thumb proposed by Hardeberg (1999), the *perceptible but acceptable* being the basic idea of preserving the intended meaning.

Table 2.1 summarizes this set of thresholds.

Table 2.1: *This table shows the set of thresholds we used to assess the quality of a color characterization model depending on the purpose.*

ΔE^*_{ab}	Professional		Consumer
	Mean ΔE^*_{ab}	Max ΔE^*_{ab}	Mean ΔE^*_{ab}
$- < 1$	good	good	good
$1 \leq - < 3$	acceptable		
$3 \leq - < 6$	not acceptable	acceptable	acceptable
$6 \leq -$		not acceptable	not acceptable

Part I

Display color characterization

Chapter 3

State of the art of display color characterization

Day after day, love turns grey
Like the skin of a dying man.
Night after night, we pretend its all right
But I have grown older and
You have grown colder and
Nothing is very much fun anymore.

Pink Floyd

Abstract

This chapter considers the state of the art of display color characterization. We focus on a bibliography that started in the early 80's with the development of personal computer displays, and that is still a current research topic, mainly because of the digitalization of cinema color flow and displays, with the generalization of home-cinema projector-based kits, and with the fast emergence of new display technologies. We describe many models that have been studied during the last 30 years.

3.1 Introduction

This state of the art considers point wise display color characterization. Indeed, displays are mainly treated as spatially invariant functions in the literature.

Color characterization of a display color device is a major issue for the accurate color rendering of a scene on a display device. It aims to define the transformation (Equation 3.1) between the device color space, typically *RGB*, and a reference color space, describing the color, based on the *CIE* standard observer, typically *CIEXYZ* or *CIELAB* (Widdel and Post, 1992).

$$CIELAB = F(RGB) \tag{3.1}$$

This transformation has two directions. The forward transformation aims to predict the displayed color for any set of digital values input to the device, i.e. a triplet (d_r, d_g, d_b). The inverse transformation provides the set of digital values to input to the display in order to display a desired color. Note that a calibration process precedes the characterization. This step aims to fix the settings (gamma, contrast, brightness, correlated color temperature, etc) of the display.

For some applications the color characterization model has to be as precise as possible. However, a compromise between the amount of experimental data required to build a model and the accuracy required by the application has to be found. Indeed, for some uses, the number of measurements has to be limited either because of the conditions of use, or because of the number of transformations that have to be set up. The latter is particularly true for projectors and for multi-display systems, where one may have to perform an accurate characterization for each display and at several positions of the display to compensate for spatial non-uniformity (Hardeberg et al., 2003). This problem will be developed in the second part of the thesis.

The first section of this chapter introduces the different models. The second section discusses the inversion of models.

3.2 Display color characterization

3.2.1 State of the art

Many color characterization methods or models exist; we can classify them in three groups. In a first one, we find the models, which tend to model physically the color response of the device. They are often based on the assumption of independence between channels and of chromaticity constancy of primaries (the chromaticity value of a primary being independent of its intensity level). Then, a combination of the primary

tristimulus at the full intensity weighted by the luminance response of the display relative to a digital input can be used to perform the colorimetric transform. The second group can be called numerical models. They are based on a training data set, which permits optimization of the parameters of a polynomial function to establish the transform. The last category consists of 3D Look Up Table (LUT) based models. Some other methods can be considered as hybrid. They can be based on a dataset and assume some physical properties of the display, such as in the work of Blondé et al. (2009), where they assume separation between chromaticity and intensity.

3D LUT models

The models in the 3D LUT group are based on the measurement of a defined number of color patches, i.e. we know the transformation between the input values (i.e. *RGB* input values to a display device) and output values (i.e. *CIEXYZ* or *CIELAB* values) measured by a colorimeter or spectrometer in a small number of color space locations (see Figure 3.1). Then this transformation is generalized to the whole space by interpolation. Studies assess that these methods can achieve accurate results (Bastani et al., 2005; Stauder et al., 2007), depending on the combination of the interpolation method used (Akima, 1970; Amidror, 2002; Bookstein, 1989; Kasson et al., 1995; Nielson et al., 1997), the number of patches measured, their distribution (Stauder et al., 2007) (some of the interpolation methods cited above cannot be used with a non-regular distribution) and on the display technology. However, to be precise enough, a lot of measurements are typically required, i.e. a $10 \times 10 \times 10$ grid of patches measured in Bastani et al. (2005). Note that such a model is technology independent since no assumptions are made about the device but that the display will always have the same response at the measurement location. Such a model needs high storage capacity and computational power to handle the 3D data. The computational power is usually not a problem since Graphic Processor Units can perform this kind of task easily today (Colantoni and Thomas, 2009). The high number of measurements needed is a greater challenge.

Numerical models

The numerical models suppose that the transform can be approximated by a set of equations, usually an n-order polynomial function. The parameters are retrieved using an n-order polynomial regression process based on measurements. The number of parameters required involves a significant number of measurements, depending on the order of the polynomial function (Green and MacDonald, 2002). The advantage of these models is that they take into account channel inter-dependence by applying cross components factors in the establishment of the function (Katoh et al., 2001*a*,*b*; Tamura et al.,

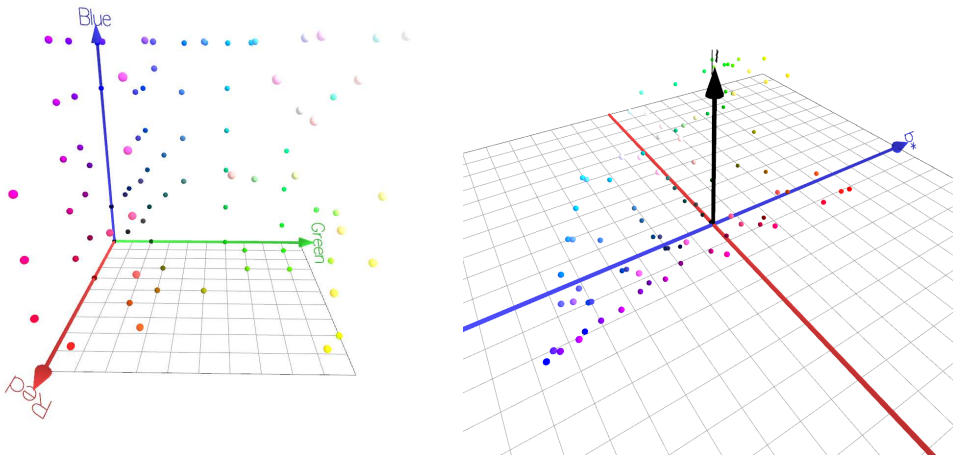

Figure 3.1: *3D lookup table for a characterization process from RGB to CIELAB.*

2003). More recently, an alternative method has been proposed by Wen and Wu (2006) who removed the three-channel crosstalk from the model, considering that the inter-channel dependence is only due to two-channel crosstalk, thus reducing the required number of measurements. They obtained results as accurate as when considering the three-channel crosstalk.

Physical models

Physical models are historically widely used for displays, since the CRT technology follows well the assumptions cited above (Berns, Gorzynski and Motta, 1993; Brainard, 1989; Cowan and Rowell, 1986). Such a model typically first aims to linearize the intensity response of the device. This can be done by establishing a model that assumes the response curve to follow a mathematical function, such as a gamma law for CRT (Berns, Gorzynski and Motta, 1993; Berns, Motta and Gorzynski, 1993; Cowan, 1983; Sharma, 2003), or a S-shaped curve for LCD (Kwak et al., 2003; Kwak and MacDonald, 2000; Yoshida and Yamamoto, 2002). Another way to linearize the intensity response curve is to generalize measurements by interpolation along the luminance for each primary (Post and Calhoun, 1989). The measurement of the luminance can be done using a photometer. Some approaches propose as well a visual response curve estimation, where the 50% luminance point for each channel is determined by the user to estimate the gamma value (Cowan, 1983). This method can be generalized to the retrieval of more luminance levels in using half toned patches (Mikalsen et al., 2008; Neumann et al., 2003). Recently, a method to retrieve the response curve of a projection display using an uncalibrated camera has been proposed by Bala and Braun (2006); Bala et al. (2007) and

extended by Mikalsen et al. (2008). Note that it has been assumed that the normalized response curve is equivalent for all the channels, and that only the gray level response curve can be retrieved. In the case of a doubt about this assumption, it is of use to retrieve the three response curves independently. Since visual luminance matching for the blue channel is a harder task, it is of use to perform an intensity matching for the red and green channel, and a chromaticity matching or gray balancing for the blue one (Klassen et al., 2005). This method should not be used with projectors since they have a large chromaticity shift with the variation of input for the pure primaries.

A model has been defined by Wyble and Rosen (2004); Wyble and Zhang (2003) for DLP projectors using a white segment in the color wheel. In their model, the characteristics of the luminance of the white channel is retrieved with regard to additive property of the display, given the four-tuplet (R, G, B, W) from an input (d_r, d_g, d_b).

The second step of these models is commonly the use of a 3×3 matrix containing primary tristimulus values at full intensity to build the colorimetric transform from luminance to an additive reference color space. The primaries can be estimated by measurement of the device channels at full intensity, using a colorimeter or a spectroradiometer, assuming their chromaticity constancy. In practice this assumption does not hold perfectly, and the model accuracy suffers from that. The major part of the non constancy of primaries can be corrected by applying a black offset correction (Jimenez Del Barco et al., 1995). Some authors tried to minimize the chromaticity non-constancy in finding the best chromaticity values of primaries (optimizing the components of the 3×3 matrix) (Day et al., 2004). Depending on the accuracy required, it is also possible to use generic primaries such as *sRGB* (Anderson et al., 1995) for some applications (Bala and Braun, 2006; Bala et al., 2007), or data supplied by the manufacturer (Cowan, 1983). However, the use of a simple 3×3 matrix for the colorimetric transform leads to inaccuracy due to the lack of channel independence and of chromaticity constancy of primaries. An alternative approach has been derived in the masking model and modified masking model, which takes into account the cross-talk between channels (Tamura et al., 2003). Furthermore, the lack of chromaticity constancy can be critical, particularly for LCD technology, which has been shown to fail this assumption (Brainard et al., 2002; Kwak and MacDonald, 2000). The Piecewise Linear assuming Variation in Chromaticity (PLVC) (Farley and Gutmann, 1980) is not subject to this effect, but has not been widely used since Post and Calhoun (1989) demonstrated that among the models they tested in that article, the PLVC and the Piecewise Linear assuming Chromaticity Constancy (PLCC) models were of equivalent accuracy for the CRT monitors they tested. The last one requiring less computation, it has been more used than the former one. These results have been confirmed in studies on CRT technology (Post and Calhoun, 1989, 2000), especially with a flare correction (Jimenez Del Barco et al., 1995; Thomas, Hardeberg, Foucherot and Gouton, 2008). On DLP technology when there is a flare cor-

rection, results can be equivalent (Thomas, Hardeberg, Foucherot and Gouton, 2008). However, the PLVC can give better results on LCDs (Thomas, Hardeberg, Foucherot and Gouton, 2007, 2008).

Other models exist, such as the 2-steps parametric model proposed by (Blondé et al., 2009). This model assumes separation between chromaticity and intensity, and is shown to be accurate, with average ΔE^*_{ab}'s around 1 or below for one DLP projector and a CRT monitor. The luminance curve is retrieved, as for other physical models, but the colorimetric transform is based on 2D interpolation in the chromaticity plane based on a set of saturated measured colors.

3.2.2 Physical models

Display color characterization models

Historically and for practical reasons, physical models have been widely used for display color characterization. Especially the gamma based models and the PLCC model. They are easily invertible, do not require a lot of measurements, require a little computer memory, and do not require high computing power so they can be used in real time. Moreover, the assumptions of channel independence and chromaticity constancy are appropriate for the CRT technology. However, these assumptions (and others such as spatial uniformity, both in luminance and in chromaticity, view angle independence, etc.) do not fit so well with some of today's display technologies. For instance the colorimetric characteristic of a part of an image in a Plasma Display is strongly dependent of what is happening in the surrounding (Choi et al., 2007) for energy economy reasons. In LC technology, which has become the leader for displays market, these common assumptions are not valid. Making such assumptions can reduce drastically the accuracy of the characterization. For instance, a review of problems faced in LC displays has been done by Yoshida and Yamamoto (2002). Within projection systems, the large amount of flare induces a critical chromaticity shift of primaries.

In the same time, computing power has become less and less of a problem. Some models not used in practice because of their complexity can now be highly beneficial for display color characterization. This section provides definitions, analysis and discussion about display color characterization models. We do not detail hybrid methods or numerical methods in this section because they show less interest for modelling purpose, and we do prefer to refer the reader to the papers cited above. The 3D LUT based method are presented in-depth in the contribution section.

In 1983, Cowan (1983) wrote what is considered to be the pioneer article in the area of physical models for display characterization. In this work, the author stated that a power function can be used, but is not the best to fit with the luminance response curve

of a CRT device. Nevertheless, the well known "gamma" model that considers a power function to approximate the luminance response curve of a CRT display is still currently widely used.

Whichever shape the model takes, the principle remains the same. First, it estimates the luminance response of the device for each channel, using a set of functions monotonically increasing such as Equation 3.2. Note that the results of these functions can also be estimated with any interpolation method, since the problem of monotonicity that can arise during the inversion process is taken into account. This step is followed by a colorimetric transform.

Response curve retrieval

We review here two types of models. The models of the first type are based on functions, the second type is the PLCC model. This model is based on linear interpolation of the luminance response curve and its accuracy has been demonstrated by Post and Calhoun (1989) who found it the best among the models they tested (except in front of the PLVC model for chromatic accuracy).

For function based model, the function used is the power function for CRT devices, which is still the most used even if it has been shown that it does not fit well LC technology (Fairchild and Wyble, 1998). It has been shown that for other technologies, there is no reason to try to fit the device response with a gamma curve, especially for LCD technology that shows a S-shape response curve in most cases (Figure 4.1) and a S-curve model can be defined (Kwak et al., 2003; Kwak and MacDonald, 2000; Yoshida and Yamamoto, 2002). However, the gamma function is still often used, mainly because it is easy to estimate the response curve with a few number of measurements, or using estimations with a visual matching pattern.

The response in luminance for a set of digital values input to the device can be expressed as follows:

$$\begin{aligned} Y_R &= f_r(D_r) \\ Y_G &= f_g(D_g) \\ Y_B &= f_b(D_b), \end{aligned} \tag{3.2}$$

where f_r, f_g and f_b are functions that give the Y_R, Y_G and Y_B contribution in luminance of each primary independently for a digital input D_r, D_g, D_b. Note that for CRT devices, after normalization of the luminance and digital value, the function can be the same for each channel. This assumption is not valid for LCD technology (Sharma, 2002), and is only a rough approximation for DLP based projection systems, as seen for instance in the work of Seime and Hardeberg (2003).

For a CRT, for the channel $h \in \{r, g, b\}$, this function can be expressed as :

$$Y_H = (a_h d_h + b_h)^{\gamma_h}, \tag{3.3}$$

where $H \in \{R, G, B\}$ is the equivalent luminance from a channel $h \in \{r, g, b\}$ for a normalized digital input d_h, with $d_h = \frac{D_h}{2^n - 1}$. D_h is the digital value input to a channel h and n is the number of bits used to encode the information for this channel. a_h is the gain and b_h is the internal offset for this channel. These parameters are estimated empirically using a regression process.

This model is called Gain-Offset-Gamma (GOG) (Berns, 1996; CIE, 1996; Katoh et al., 2001*b*). If we make the assumption that there is no internal offset and no gain, $a = 1$ and $b = 0$, it becomes the simple "gamma" model.

Note that for luminance transforms, polynomials can be fitted better in the logarithmic domain or to cube root function than in the linear domain because the eye response to signal intensity is logarithmic (Weber's law). For gamma based models, it has been shown that a second order function with two parameters such as $Log(Y_H) = b_h \times Log(d_h) + c_h \times (Log(d_h))^2$ [1] gives better results(Cowan, 1983) and that two gamma curves should be combined for a better accuracy in low luminance(Arslan et al., 2003).

For a LCD, it has been shown by Kwak et al. (2003); Kwak and MacDonald (2000) that a S-shape curve based on 4 coefficients per channel can fit well the intensity response of the display.

$$Y_H = A_h \times g_h(d_h) = A_h \times \frac{d_h^{\alpha_h}}{d_h^{\beta_h} + C_h}, \tag{3.4}$$

with the same notation as above, and with A_h, α_h, β_h and C_h parameters obtained using the least-squares method. This model is called S-curve I.

The model S-curve II considers the interaction between channels. It has been shown in (Kwak et al., 2003; Kwak and MacDonald, 2000; Yoshida and Yamamoto, 2002) that the gradient of the original S-curve function fits the importance of the interaction between channels. Then this component can be included in the model in order to take this effect into account.

$$\begin{aligned} Y_R &= A_{rr} \times g_{Y_R Y_R}(d_r) + A_{rg} \times g'_{Y_R Y_G}(d_g) + A_{rb} \times g'_{Y_R Y_B}(d_b), \\ Y_G &= A_{gr} \times g'_{Y_G Y_R}(d_r) + A_{gg} \times g_{Y_G Y_G}(d_g) + A_{gb} \times g'_{Y_G Y_B}(d_b), \\ Y_B &= A_{br} \times g'_{Y_B Y_R}(d_r) + A_{bg} \times g'_{Y_B Y_G}(d_g) + A_{bb} \times g_{Y_B Y_B}(d_b), \end{aligned} \tag{3.5}$$

where $g(d)$ and its first-order derivative $g'(d)$ are $g(d) = \frac{d^\alpha}{d^\beta + C}$ and $g'(d) = \frac{(\alpha-\beta)x^{\alpha+\beta-1} + \alpha C x^{\alpha-1}}{(x^\beta + C)^2}$.

To ensure the monotonicity of the functions for the S-curve models I and II, some constraints on the parameters have to be applied. We let the reader to refer to the discussion in the original article (Kwak et al., 2003) for that matter.

[1] Note that Post and Calhoun (1989) added a term to this equation, which became $Log(Y_H) = a + b_h \times Log(d_h) + c_h(Log(d_h))^2$.

For the PLCC model, the function f is approximated by a piecewise linear interpolation between the measurements. The approximation is valid for a large enough amount of measurements (16 measurements per channel in Post and Calhoun (1989)). This model is particularly useful when no information is available about the shape of the display luminance response curve.

Colorimetric transform

A colorimetric transform is then performed from the (Y_R, Y_G, Y_B) "linearized" luminance to the XYZ color tristimulus.

$$\begin{bmatrix} X \\ Y \\ Z \end{bmatrix} = \begin{bmatrix} X_{r,max} & X_{g,max} & X_{b,max} \\ Y_{r,max} & Y_{g,max} & Y_{b,max} \\ Z_{r,max} & Z_{g,max} & Z_{b,max} \end{bmatrix} \times \begin{bmatrix} Y_R \\ Y_G \\ Y_B \end{bmatrix} \tag{3.6}$$

where the matrix components are the tristimulus colorimetric values of each primary, measured at their maximum intensity.

Using such a matrix for the colorimetric transform supposes perfect additivity and chromaticity constancy of primaries. These assumptions have been shown to be acceptable for CRT technology (Brainard, 1989; Cowan and Rowell, 1986).

The channel inter-dependence observed in CRT technology is mainly due to an insufficient power supply and an inaccuracy of the electron beams, which meet inaccurately the phosphors (Katoh et al., 2001*a*). In LC technology, it comes from the overlapping of the spectral distribution of primaries (the color filters), and from the interferences between the capacities of two neighboring sub pixels (Seime and Hardeberg, 2003; Yoshida and Yamamoto, 2002). In DLP-DMD projection devices, there is still some overlapping between primaries and inaccuracy at the level of the DMD mirrors.

Considering the assumption of chromaticity constancy, it appears that when there is a flare (Katoh et al., 2001*a*), either a black offset (internal flare) or an ambient flare (external flare), added to the signal, the assumption of chromaticity constancy is not valid anymore. Indeed, the flare is added to the output signal and the lower the luminance level of the primaries, the more the flare is a significant fraction of the resulting stimulus. This leads to a hue shift toward the black offset chromaticity. Often the flare has a "gray" (nearly achromatic) chromaticity, thus the chromaticities of the primaries shift to a "gray" chromaticity (Figure 3.2, left part). Note that the flare "gray" chromaticity does not necessarily correspond to the achromatic point of the device (Figure 3.2). In fact, in the tested LCD devices (Figure 3.2, a, b, e, f), we can notice the same effect as in the work of Marcu et al. (2001): the black level chromaticity is bluish because of the poor filtering power of the blue filter in the low wavelength.

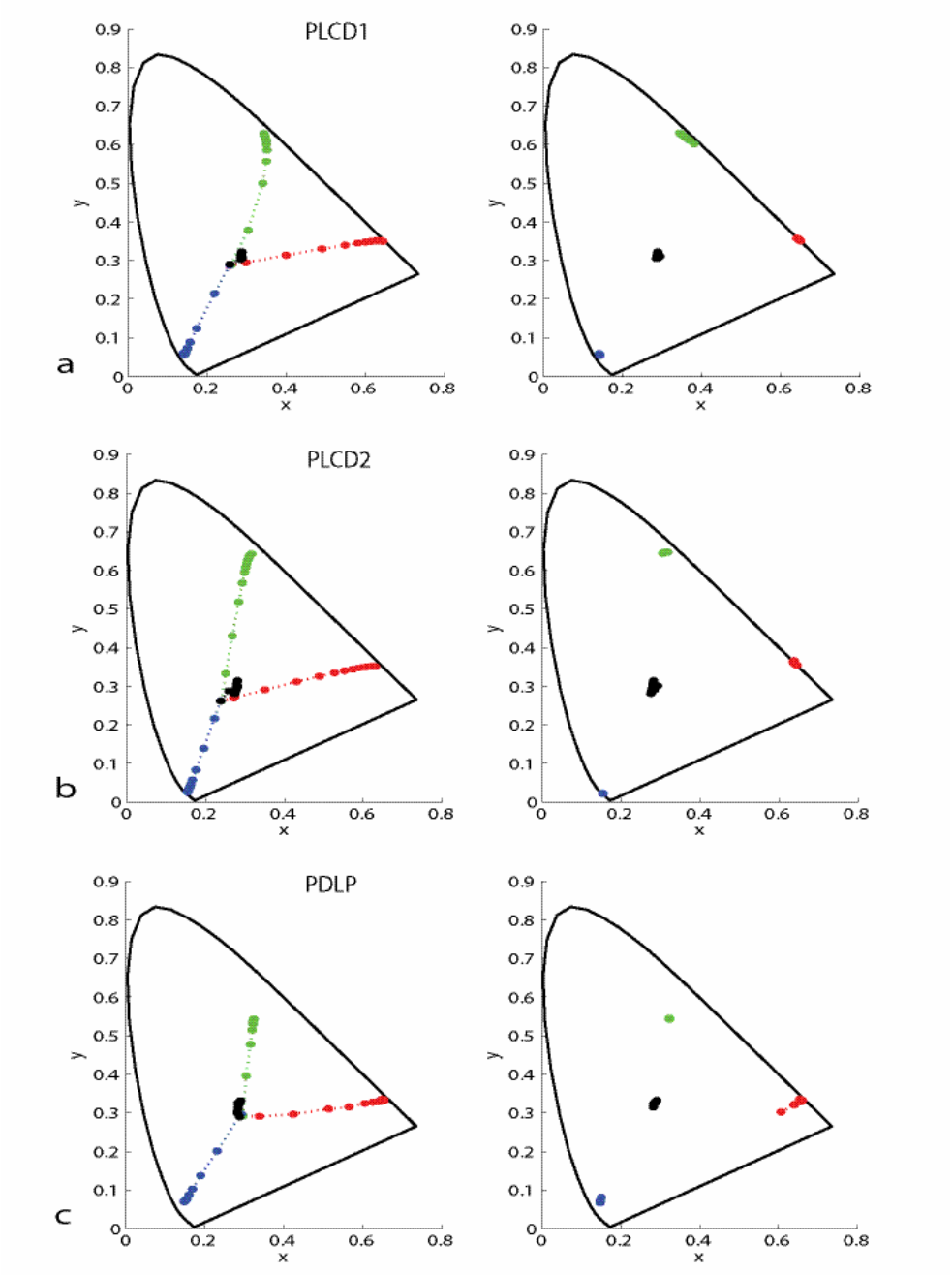

abc

Figure 3.2: *Chromaticity tracking of primaries with variation of intensity. The left part of the figure shows it without black correction. On the right, one can see the result with a black correction performed. All devices tested in our PLVC model study are shown, a-PLCD1, b-PLCD2, c-PDLP, d-MCRT, e-MLCD1, f-MLCD2. See the correspondence list in next chapter, table 4.1.*

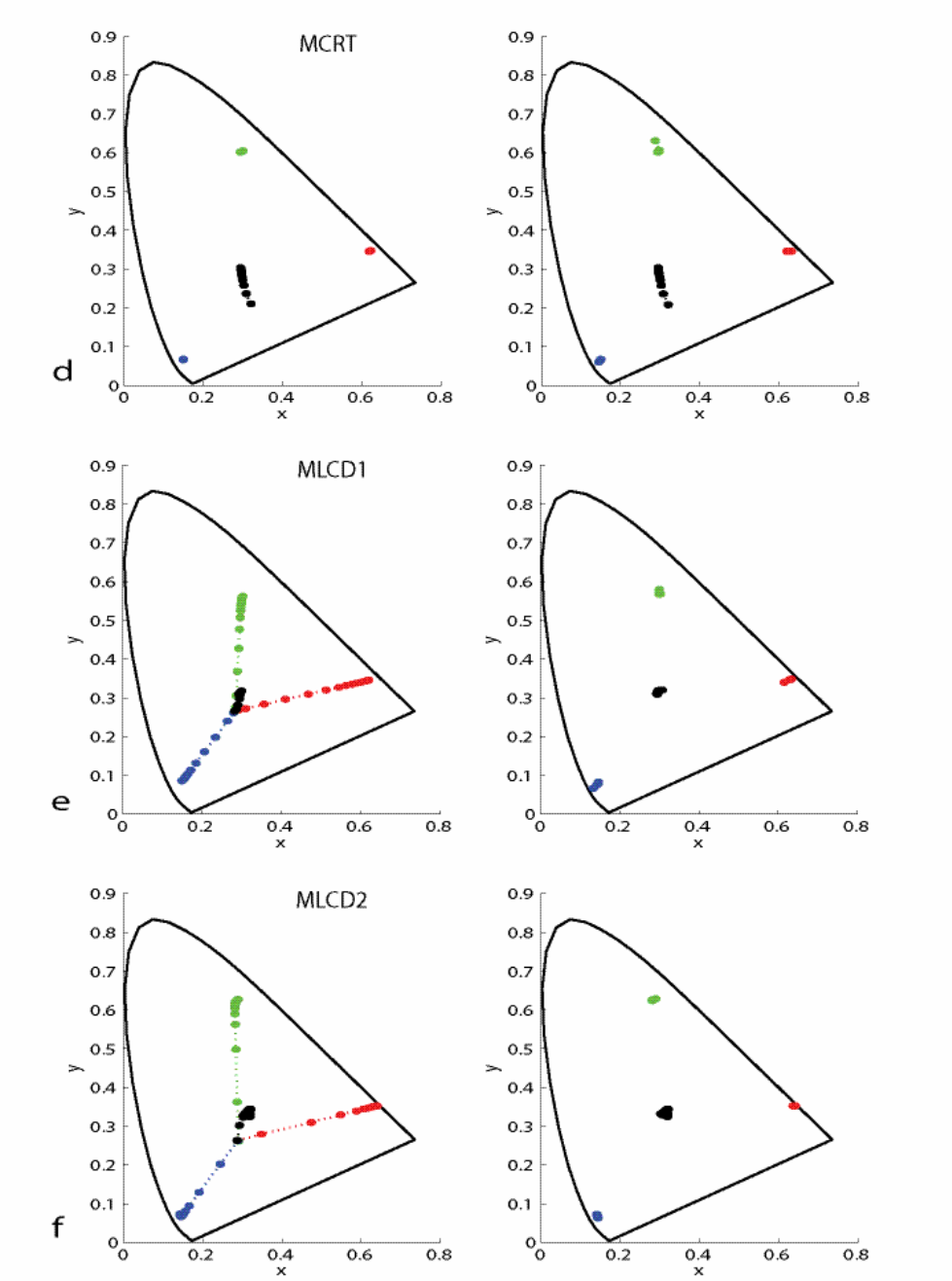

Figure 3.2: *Chromaticity tracking of primaries with variation of intensity. The left part of the figure shows it without black correction. On the right, one can see the result with a black correction performed. All devices tested in our PLVC model study are shown, a-PLCD1, b-PLCD2, c-PDLP, d-MCRT, e-MLCD1, f-MLCD2. See the correspondence list in next chapter, table 4.1.*

The flare can be taken all at once as the measured light for an input $(d_{r,k}, d_{g,k}, d_{b,k}) = (0, 0, 0)$ to the device. Then it includes ambient and internal flare.

The ambient flare comes from any light source reflecting on the display screen. If the viewing conditions do not change it remains constant, can be measured and taken into account, or can be simply removed in setting up a dark environment (note that for a projection device, there is always an amount of light that lights the room, coming from the bulb through the ventilation hole).

The internal flare, which is the major part of chromaticity inconstancy at least in CRT technology (Katoh et al., 2001*a*), is coming from the black level. In CRT technology, it has been shown that in setting the brightness to a high level, the black level increases to a non-negligible value (Katoh et al., 2001*a*). In LC technology, the panel let an amount of light passing through due to a leakage of the crystal to stop all the light. In DLP technology, an amount of light can be not absorbed by the "black absorption box", and is focused on the screen via the lens.

On Figure 3.2, one can see the chromaticity shift to the flare chromaticity with the decreasing of the input level. We have performed these measurements in a dark room, then the ambient flare is minimized, and only the black level remains. After black level subtraction, the chromaticity is more constant (Figure 3.2), and a new model can be set up in taking that into account (Hardeberg et al., 2003; Jimenez Del Barco et al., 1995; Katoh et al., 2001*a,b*).

The gamma models reviewed above have been extended in adding an offset term. Then the GOG can become a Gain-Offset-Gamma-Offset (GOGO) model (IEC:61966-3, 1999; Katoh et al., 2001*a*,*b*).

The previous equation 3.2 becomes:

$$Y_H = (a_h d_h + b_h)^{\gamma_h} + c, \tag{3.7}$$

where c is a term containing all the different flares in presence. If we consider the internal offset b_h as null, the model becomes Gain-Gamma-Offset (GGO) (IEC:61966-3, 1999).

A similar approach can be used for the PLCC model. When the black correction (Jimenez Del Barco et al., 1995) is performed, we name it PLCC* in the following. The colorimetric transform used then is the Equation 3.8 that permits to take the flare into account during the colorimetric transformation. For the S-curve models, the black offset is taken into account in the matrix formulation in the original papers.

If we consider that mathematically, the linear transform from the linearized *RGB* to *CIEXYZ* needs to associate the origin of *RGB* to the origin of *CIEXYZ* in order to respect the vectorial space property of additivity and homogeneity. Thus the original transform of the origin of *RGB* to *CIEXYZ* needs to be tranlated of $[-X_k - Y_k - Z_k]$. However, in

doing that we modify the physical reality and we need to translate the result of the transformation of $[X_k Y_k Z_k]$. We can formulate these transforms such as in Equation 3.8.

$$\begin{bmatrix} X \\ Y \\ Z \end{bmatrix} = \begin{bmatrix} X_{r,max} - X_k & X_{g,max} - X_k & X_{b,max} - X_k & X_k \\ Y_{r,max} - Y_k & Y_{g,max} - Y_k & Y_{b,max} - Y_k & Y_k \\ Z_{r,max} - Z_k & Z_{g,max} - Z_k & Z_{b,max} - Z_k & Z_k \end{bmatrix} \times \begin{bmatrix} Y_R \\ Y_G \\ Y_B \\ 1 \end{bmatrix} \tag{3.8}$$

The A_k's, $A \in \{X, Y, Z\}$, come from a black level estimation.

Such a correction permits to achieve better results. However, on the right part of Figure 3.2, one can see that even with the black subtraction, the primary chomaticities do not remain perfectly constant. On Figure 3.2, right-a, it remains a critical shift especially for the green channel.

Several explanations are involved. First, there is a technology contribution. For LC technology, the transmittance of the cells of the panel changes within the input voltage (Brainard et al., 2002; Yeh and Gu, 1999). This leads to a chromaticity shift when changing the input digital value. For different LC displays, we notice a different shift in chromaticity; this is due to the combination back-light/LC with the color filters. Since the filters transmittances are optimized taking into account the transmittance shift of the LC cells, the display can achieve good chromaticity constancy. For CRT, there are less problems due to the same phosphors properties, as well for DLP as the light and the filters remain the same.

However, even with the best device, there is still a small amount of non-constancy. This leads to a discussion about the accuracy of the measured black offset. Indeed, the measurement devices are less accurate in the low luminance. Berns et al. (2003) proposed a way to estimate the best black offset value. A way to overcome the problems linked with remaining inaccuracy for LCD devices has been presented by Day et al. (2004). It consists in the replacement of the full intensity measurement of primary chromaticitiescolorimetric values by the optimum values in the colorimetric transformation matrix. It appears that the chromaticity shift is a major issue for LCD. Sharma (2002) stated that for LCD devices the assumption of chromaticity constancy was weaker than the channel inter-dependence.

More models that linearize the transform exist. in this section we presented the ones that appeared to us as the more interesting, or the more known.

Piecewise Linear model assuming Variation in Chromaticity

Defining the Piecewise Linear model assuming Variation in Chromaticity (PLVC) in this section has many motivations. First, it is the first display color characterization model introduced in the literature as far as we know. Secondly, it is an hybrid method, consid-

ering that it is based on data measurement and assumes a small amount of hypothesis on the behavior of the display. Finally there is a section in next chapter devoted to the study of this model.

According to Post and Calhoun (1989), the first persons who have introduced the PLVC were Farley and Gutmann (1980) in 1980. Note that it preceded the well known article from Cowan (1983). Further studies have been performed afterward on CRT (Jimenez Del Barco et al., 1995; Post and Calhoun, 1989, 2000), and recently on more recent technologies (Thomas, Hardeberg, Foucherot and Gouton, 2007, 2008). This model does not consider the channel inter-dependence, but does model the chromaticity shift of the primaries. In this section, we recall the principles of this model, and some features that characterize it.

Knowing the tristimulus values of X, Y, and Z for each primary as a function of the digital input, assuming additivity, the resulting color tristimulus values can be expressed as the sum of tristimulus values for each component (i.e. primary) at the given input level. Note that in order not to add several times the black level, it is removed from all measurements used to define the model. Then, it is added to the result, to return to a correct standard observer color space (Jimenez Del Barco et al., 1995; Post and Calhoun, 2000). The model is summarized and generalized in Equation (3.9) for N primaries, and illustrated in Equation (3.10) for a three primaries *RGB* device, following an equivalent formulation as the one given by Jimenez Del Barco et al. (1995).

For an N primary device, we consider the digital input to the i^{th} primary, $d_i(m_i)$, with i an integer $\in [0, N]$, and m_i an integer limited by the resolution of the device (i.e. $m_i \in [0, 255]$ for a channel coded on 8 bits). Then, a color $XYZ(..., d_i(m_i), ...)$ can be expressed by :

$$\begin{aligned} X(..., d_i(m_i), ...) &= \textstyle\sum_{i=0, j=m_i}^{i=N-1} [X(d_i(j)) - X_k] + X_k \\ Y(..., d_i(m_i), ...) &= \textstyle\sum_{i=0, j=m_i}^{i=N-1} [Y(d_i(j)) - Y_k] + Y_k \\ Z(..., d_i(m_i), ...) &= \textstyle\sum_{i=0, j=m_i}^{i=N-1} [Z(d_i(j)) - Z_k] + Z_k \end{aligned} \tag{3.9}$$

with X_k, Y_k, Z_k the color tristimulus coming out from a $(0, ..., 0)$ input.

We illustrate this for a three primaries *RGB* device, with each channel coded on 8 bits. The digital input are $d_r(i)$, $d_g(j)$, $d_b(l)$, with i, j, l integers $\in [0, 255]$. In this case, a $XYZ(d_r(i), d_g(j), d_b(l))$ can be expressed by :

$$\begin{aligned} X(d_r(i), d_g(j), d_b(l)) &= [X(d_r(i)) - X_k] + [X(d_g(j)) - X_k] + [X(d_b(l)) - X_k] + X_k \\ Y(d_r(i), d_g(j), d_b(l)) &= [Y(d_r(i)) - Y_k] + [Y(d_g(j)) - Y_k] + [Y(d_b(l)) - Y_k] + Y_k \\ Z(d_r(i), d_g(j), d_b(l)) &= [Z(d_r(i)) - Z_k] + [Z(d_g(j)) - Z_k] + [Z(d_b(l)) - Z_k] + Z_k \end{aligned} \tag{3.10}$$

If the considered device is a *RGB* primaries device, thus the transformation between digital *RGB* values and *RGB* device's primaries is as direct as possible. The A_k, $A \in$

$\{X, Y, Z\}$ are obtained by accurate measurement of the black level. The $[A(d_i(j)) - A_k]$, are obtained by one dimensional linear interpolation with the measurement of a ramp along each primary. Note that any 1-D interpolation method can be used. In the literature, the piecewise linear interpolation is mostly used.

Studies of this model have shown good results, especially on dark and mid-luminance colors. When the colors reach higher luminance, the additivity assumption is less true for CRT technology. Then the accuracy decreases (depending on the device properties). More precisely, Post and Calhoun (1989, 2000) stated that chromaticity error is lower for the PLVC than for the PLCC in low luminance. This is due to the setting of primaries colorimetric values at maximum intensity in the PLCC. Both models show inaccuracy for high luminance colors due to channel inter-dependence. Jimenez Del Barco et al. (1995) found that for CRT technology, the higher level of brightness in the settings leads to a non-negligible amount of light for a (0,0,0) input. This light should not be added three times, and they proposed a correction for that [2]. They found that the PLVC model was more accurate in medium to high luminance colors. Inaccuracy is more important in low luminance, due to inaccuracy of measurements, and in high luminance, due to channel dependencies. Thomas, Hardeberg, Foucherot and Gouton (2008) demonstrated that this model is more accurate than usual linear models (PLCC, GOGO) for LCD technology, since it takes into account the chromaticity shift of primaries that is a key features for characterizing this type of display. More results for this model are presented in the next chapter.

3.3 Model inversion

3.3.1 State of the art

The inversion of a display color characterization model is of major importance for color reproduction since it provides the set of digital values to input to the device in order to display a desired color.

Among the models or methods used to achieve color characterization, we can distinguish two categories. The first one contains models that are practically invertible (either analytically, or in using simple 1D LUT)(Berns, Gorzynski and Motta, 1993; Berns, Motta and Gorzynski, 1993; Cowan and Rowell, 1986; Jimenez Del Barco et al., 1995; Katoh et al., 2001*a*,*b*; Post and Calhoun, 1989), such as the PLCC, the black corrected PLCC*, the GOG or GOGO models. The second category contains the models or methods, which are not practically invertible directly. and that show difficulties to be applied.

[2] Equation 3.9 and Equation 3.10 are based on the equation proposed by Jimenez Del Barco et al. (1995), and take that into account.

Models of this second category require other methods to be inverted in practice. We can list some typical problems and methods used to invert these models:

- A condition has to be verified, such as in the masking model (Tamura et al., 2003).
- A new matrix might have to be defined by regression in numerical models (Green and MacDonald, 2002; Katoh et al., 2001*a*,*b*; Wen and Wu, 2006).
- A full optimization process has to be set up for each color, such as in S-curve model II (Kwak et al., 2003; Kwak and MacDonald, 2000) in the modified masking model, (Tamura et al., 2003) or in the PLVC model (Jimenez Del Barco et al., 1995; Post and Calhoun, 1989; Thomas, Colantoni, Hardeberg, Foucherot and Gouton, 2008*a*).
- The optimization process can appear only for one step of the inversion process, as in the PLVC (Post and Calhoun, 1989) or in the S-curve I (Kwak et al., 2003; Kwak and MacDonald, 2000) models.
- Empirical methods based on 3-D LUT (lookup table) can be inverted directly (Bastani et al., 2005), using the same geometrical structure. In order to have a better accuracy, however, it is common to build another geometrical structure to yield the inverse model. For instance, it is possible to build a draft model to define a new set of color patches to be measured (Stauder et al., 2007).

The computational complexity required to invert these models makes them seldom used in practice, except the full 3-D LUT, which major drawback is that it requires a lot of measurements. However, these models do have the possibility to take into account more precisely the device color-reproduction features, such as interaction between channels or chromaticity inconstancy of the primaries. Thus, they are often more accurate than the models of the first category.

3.3.2 Practical inversion

The models that are invertible easily (Berns, Gorzynski and Motta, 1993; Berns, Motta and Gorzynski, 1993; Cowan and Rowell, 1986; Jimenez Del Barco et al., 1995; Katoh et al., 2001*a*,*b*; Post and Calhoun, 1989), such as the PLCC, the black corrected PLCC*, the GOG or GOGO models, are easily inverted since they are based on linear algebra and on simple functions. For these models it is sufficient to invert the matrix of Equation 3.6. Then we have:

$$\begin{bmatrix} Y_R \\ Y_G \\ Y_B \end{bmatrix} = \begin{bmatrix} X_{r,max} & X_{g,max} & X_{b,max} \\ Y_{r,max} & Y_{g,max} & Y_{b,max} \\ Z_{r,max} & Z_{g,max} & Z_{b,max} \end{bmatrix}^{-1} \times \begin{bmatrix} X \\ Y \\ Z \end{bmatrix} \tag{3.11}$$

Once the linearized $\{Y_R, Y_G, Y_B\}$ have been retrieved, the intensity response curve function is inverted as well to retrieve the $\{d_r, d_g, d_b\}$ digital values. This task is easy for a gamma based model or for an interpolation based one. However, for some models such as the S-curve I, an optimization process can be required (note that this response curve can be used to create a 1D LUT).

3.3.3 Indirect inversion

When the inversion becomes more difficult, it is of use to set an optimization process using the combination of the forward transform and the color difference (often the euclidean distance) in a perceptually uniform color space, such as *CIELAB*, as cost function. This generally leads to better results than usual linear models, depending on the forward model, but is computationally expensive, and can not be implemented in real time. It is then of use to set a 3-D LUT based on the forward model. Note that it does not mean that an optimization process is useless, since it can help to design a good LUT.

Such a model is defined by the number and the distribution of the color patches used in the LUT, and by the interpolation method used to generalize the model to the entire space. In this subsection, we review some basic tools and methods. We distinguish works on displays from more general works, which have been performed in this way either in a general purpose or especially for printers. We present in detail the tetrahedral structure that is often used as a basis in this case.

3-D LUT inverse models in displays are often based on the measurement of a defined number of color patches, i.e., we know the transformation between *CIELAB* and *RGB* in a small number of color-space locations. Then, this transformation is generalized to the entire color space by interpolation. Previous studies assess that these methods achieve good results for display devices (Bastani et al., 2005; Stauder et al., 2007), depending on the combination of the interpolation method used (Akima, 1970; Amidror, 2002; Bookstein, 1989; Kasson et al., 1995; Nielson et al., 1997), the number of patches measured, and on their distribution (Stauder et al., 2007) (some of the interpolation methods cited above cannot be used with a non-regular distribution). However, to be precise enough, a lot of measurements are typically required, e.g., a $10 \times 10 \times 10$ grid of patches measured in Bastani et al. (2005) paper. Note that such a model is technology independent since no assumption is made about the device, except that the display is spatially and temporaly uniform. Such a model needs high storage capacity and computational power to handle the 3-D data. The computational power is usually not a problem since graphic processor units can perform this type of task easily today. The high number of measurements needed is a greater challenge. The problem of measurement is even more restrictive for printers and many works have been carried out in using a 3-D LUT for the color characterization of these devices. Moreover, since printer devices are highly

non-linear, their colorimetric models are complex. So it has been customary in the last decade to use a 3-D complex LUT for the forward model, created by using an analytical forward model, both to reduce the amount of measurements and to perform the color space transform in a reasonable time. The first work we know about creating a LUT based on the forward model is a patent from Stokes (1997). In this work, the LUT is built to replace the analytical model in the forward direction. It is based on a regular grid designed in the printer *CMY* color space, and the same LUT is used in the inverse direction, simply in switching the domain and co-domain. Note that in displays, the forward model is usually computationally simple and that we need only to use a 3-D LUT for the inverse model. The uniform mapping of the *CMY* space leads to a non-uniform mapping in *CIELAB* space for the inverse direction, and it is common now to re-sample this space to create a new LUT. To do that, a new grid is usually designed in *CIELAB* and is inverted after gamut mapping of the points located outside the gamut of the printer. Several algorithms can be used to re-distribute the data (Chan et al., 1997; Dianat et al., 2006; Groff et al., 2000) and to fill the grid (Balasubramanian and Maltz, 1996; Shepard, 1968; Viassolo et al., 2003). Returning to displays, let us call source space the reference color-space (typically *CIELAB* or alternatively *CIEXYZ*), the domain from where we want to move, and destination space, the *RGB* color space, the co-domain, where we want to move to. If we want to build a grid, we then have two classical approaches to distribute the patches in the source space, using the forward model. One can use directly a regular distribution in *RGB* and transform it to *CIELAB* using the forward model; this approach is the same as used by (Stokes, 1997) for printers, and leads to a non-uniform mapping of the *CIELAB* space, which can lead to a lack of homogeneity of the inverse model depending on the interpolation method used (See Figure 3.3). An other approach can be to distribute the patches regularly in *CIELAB*, following a given pattern, such as an hexagonal structure (Stauder et al., 2007) or any of the methods used in printers (Chan et al., 1997; Dianat et al., 2006; Groff et al., 2000). Then, an optimization process using the forward model can be performed for each point to find the corresponding *RGB* values. The main idea of the method and the notation used in this document are the following:

- One can define a regular 3-D grid in the destination color space (*RGB*).
- This grid defines cubic voxels. Each one can be split into five tetrahedra (See Figure 3.4).
- This tetrahedral shape is preserved within the transform to the source space (either *CIEXYZ* or *CIELAB*).
- Thus, the model can be generalized to the entire space, using tetrahedral interpolation (Kasson et al., 1995). It is considered in this case that the color space has a

linear behavior within the tetrahedron (e.g. the tetrahedron is small enough).

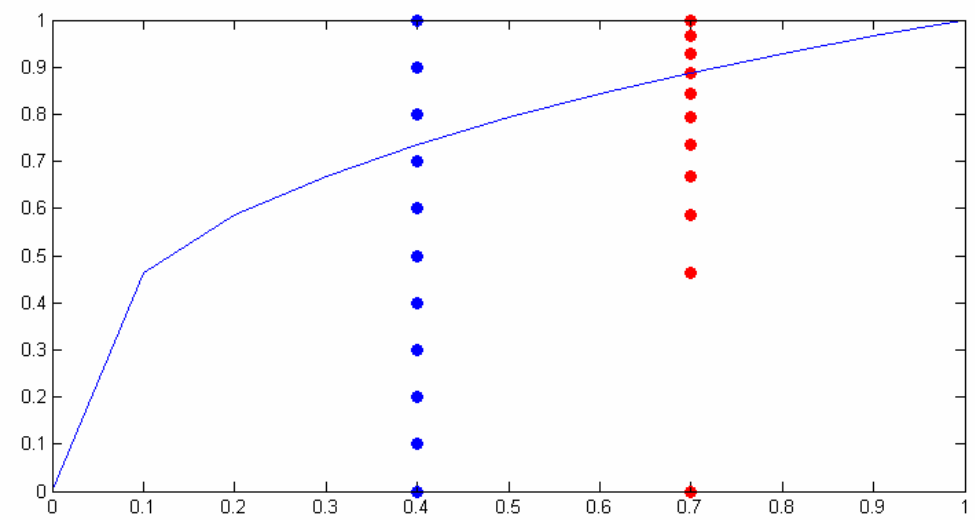

Figure 3.3: *The transform between RGB and CIELAB is not linear. Thus while using a linear interpolation based on data regularly distributed in RGB, the accuracy is not the same everywhere in the colorspace. This figure shows a plot of regularly distributed data in a linear space (blue dot) and the resulting distribution after a cubic root transform (that mimic CIELAB transform)(red dots).*

The most used way to define such a grid is to take directly a linear distribution of points on each digital d_r, d_g, and d_b axis as seeds and to fill up the rest of the destination space. A tetrahedral structure is then built with these points. The built structure is used to retrieve any *RGB* value needed to display a specific color inside the devices gamut. The more points are used to build the grid, the more the tetrahedra will be small and the interpolation accurate. In this work, we characterize such a grid by $N_{rgb} = N_r + N_g + N_b$, where N_r (resp. N_b, N_g) is the number of steps along channel R (resp. G, B). Each vertex is defined by $V_{i,j,k} = (R_i, G_j, B_k)$, where $R_i = d_i$, $G_j = d_j$, $B_k = d_k$, and d_i, d_j, d_k $\in [0, 1]$ are the possible normalized digital values, for a linear distribution. $i \in [0, N_r - 1]$, $j \in [0, N_g - 1]$, and $k \in [0, N_b - 1]$ are the indexes (integers) of the seeds of the grid along each primary.

Once this grid has been built, we define the tetrahedral structure for the interpolation following Kasson et al. (1995). Then we use the forward model to transform the structure into *CIELAB* color space. An inverse model has been built. According to the non-linearity of the *CIELAB* transform, the size of the tetrahedra is not anymore the same as it was in *RGB*. In the following section, a modification of this framework is proposed that makes this grid more homogeneous in the source color space where we perform the interpolation; this should lead to a better accuracy, following Groff et al. (2000).

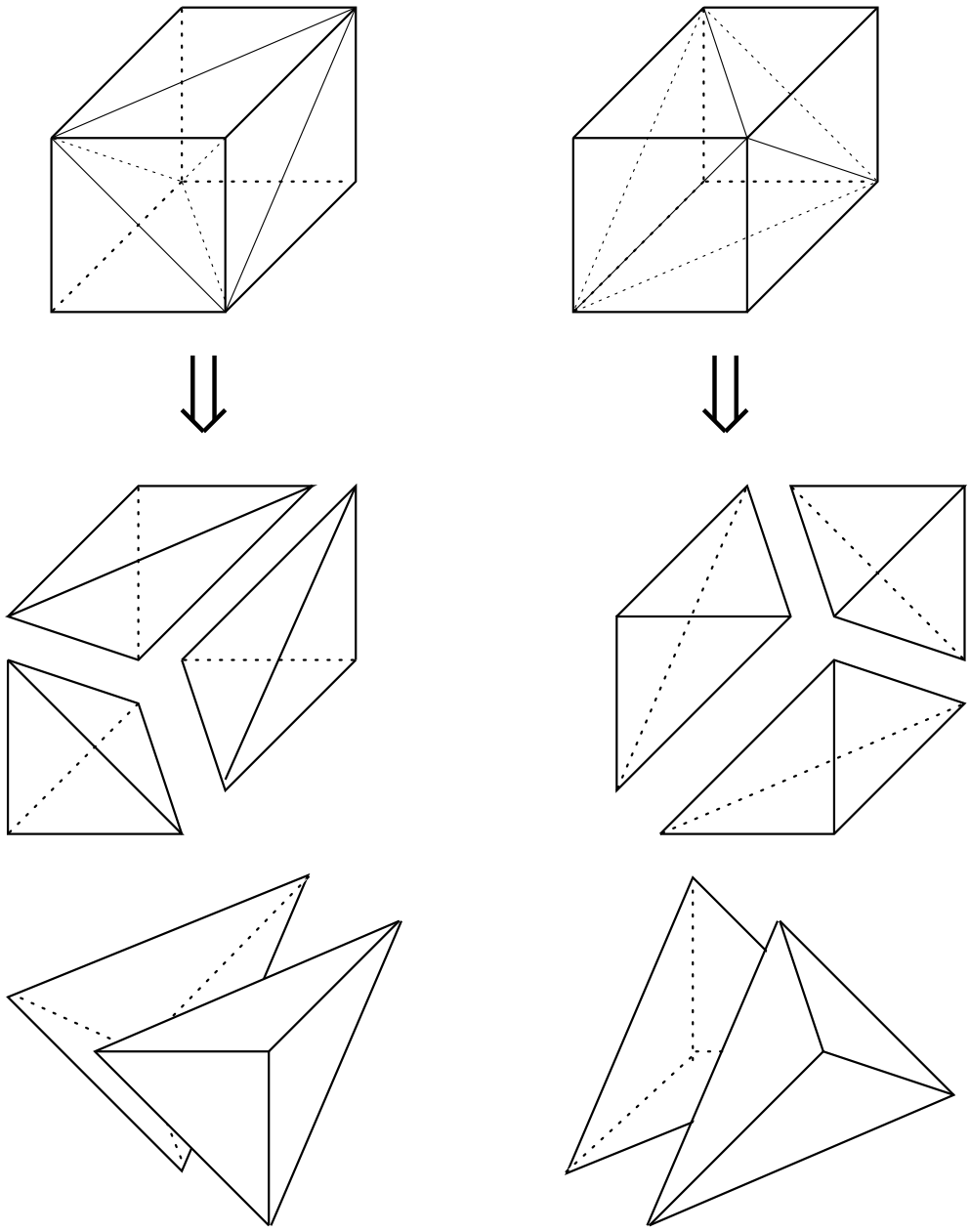

Figure 3.4: *The two ways to split a cubic voxel in 5 tetrahedra. These two methods are combined alternatively when splitting the cubic grid to guarantee that no coplanar segments are crossing.*

Let us consider the PLVC model inversion as example. This model inversion is not as straightforward as the matrix based models previously defined. For a three primaries display, according to Post and Calhoun (1989), it can be performed defining all subspaces defined by the matrices of each combinations of measured data (the intercepts have to be subtracted, and once all the contributions are known, they have to be added). One can perform an optimization process for each color (Jimenez Del Barco et al., 1995),

or define a grid in *RGB*, such as described above, which will allow us to perform the inversion using 3D interpolation. Note that Post and Calhoun have proposed to define a full LUT considering all colors. They said themselves that it is inefficient. Defining a reduced regular grid in *RGB* leads to the building of an irregular grid in *CIELAB* due to the non-linear transform. This irregular grid could lead to inaccuracy or a lack of homogeneity in interpolation, especially if it is linear. Some studies addressed this problem (Thomas, Colantoni, Hardeberg, Foucherot and Gouton, 2008*a*,*b*). They built an optimized Look Up Table, based on a customized *RGB* grid. Details are presented in chapter 7.

Chapter 4

Analysis and experimental validation of the PLVC model

Il faut toujours se réserver le droit de rire le lendemain de ses idées de la veille.

Napoléon Bonaparte

Abstract

This chapter considers the analysis and experimental validation of the PLVC model, and its comparison with other physical models. It is shown through a detailed analysis that this model can be highly beneficial for today display technologies, especially LCD.

4.1 Introduction

The PLVC model is studied with attention. It is shown that this model can be highly beneficial for today display technologies, especially LCD. The idea to study further this model came from the study of recent display characterization literature. It appears that the PLVC model is not well known. It has been studied only for CRT technology (as far as we know, and excluding our recent paper) and as the chromaticity shift of primaries is not critical for this technology, it was not necessary to use it (Post and Calhoun, 1989, 2000), especially after flare correction (Jimenez Del Barco et al., 1995). For today's display technologies such as LCD or DLP, we found no study involving the PLVC model.

A preliminary work we have done (Thomas, Hardeberg, Foucherot and Gouton, 2007) has suggested that this model can give better results than some classical matrix based methods in color prediction on liquid crystal technology, for the same amount of measurements. A more complete study has been published in Color research & application (Thomas, Hardeberg, Foucherot and Gouton, 2008).

We study the PLVC model through this chapter, providing detailed results and analysis on several display technologies, and we show that it could be beneficial to use this model particularly for LC technology. In the following, we show how this model could yield a better compromise between the accuracy, the assumptions made and its computational complexity. This study is sustained by experimental results obtained for six display devices listed in Table 4.1. The device set contains two LCD and one DLP projectors, one CRT and two LCD monitors. We compare the precision of the PLVC model with that of the PLCC, the GOGO and the black corrected PLCC* with the same amount of measurements.

In general the PLVC gives better results than the other methods tested for the same amount of measurements except for the technologies with low chromaticity shift of primaries (CRT and DLP after black correction), for which the results are similar. Following the definition of the model, the improvement depends significantly on how the chromaticity of primaries is shifting.

4.2 Experimental setup

We measured 18 color patches for each primary (each 15 digital values from 0 to 255) to build the models, thus including 3 measurements of the black level, which were averaged to limit the low luminance measurement inaccuracy. 100 random patches equiprobably distributed in *RGB* color space were measured for the evaluation. We used the spectroradiometer CS-1000 from Minolta (Accuracy: luminance: $\pm 2\%$, x: ± 0.0015, y: ± 0.001, Repeatability: Luminance: $\pm 0.1\%$, xy: 0.0002 for illuminant A). The devices

Table 4.1: *References of the tested devices.*

Related in the text as:	Device reference:
PLCD1	Panasonic PT-AX100E
PLCD2	3M-X50
PDLP	ProjectionDesign Action One
MCRT	Philips 107S monitor
MLCD1	Acer AL1721 monitor
MLCD2	DELL 1905FP monitor

were warmed up for at least one hour before any measurement, and the random patches were measured just after the ramp patches to limit the influence of the display non-repeatability. Experiments were performed in a dark room. We used the 2 degrees *CIE* observer and the white point of the display for any color space transform.

Considering the black level estimation, we did not use the method presented in the work of Berns et al. (2003) as we considered that our measurement device (a spectro-radiometer Minolta CS-1000) was precise enough, especially for projectors and LCD monitors, which show a consequent amount of black level. However we have averaged 3 measurements of the black level and increased the acquisition time of the spectroradiometer, to be sure to have a good estimation of it.

4.3 Global results

A comparison of models is provided in Table 4.3 for the tested models (PLCC, PLCC*, GOGO and PLVC) and each display. We provide the ΔE^*_{ab} error in average (mean), maximum (max), its standard deviation (std. dev.) and the 95 percentile (95 ptl) between the measured and the predicted color for our random test data set. We give also the average ΔL^*, ΔC^*_{ab} and ΔH^*_{ab} errors [1]. The values ΔE^*_{ab}, ΔL^*, ΔC^*_{ab} and ΔH^*_{ab} have been computed following the CIE 015.2004 colorimetry, technical report (CIE, 2004).

We can notice that the PLCC without black correction does not perform well when there is a major chromaticity shift of primaries. Results can be considered not acceptable for most applications. Major errors in average and impressive maximum error occurs

[1] Please note that when we say that any of ΔL^*, ΔC^*_{ab} or ΔH^*_{ab} is better, we evaluate a systematic error. These indicators are signed. A 0 average only shows that the error is distributed perfectly around the 0 error, and not that there is no error.

Table 4.2: *Results for tested displays. Errors and statistics for 100 random colors equiprobably distributed in RGB. We applied the PLCC, PLCC with black correction (PLCC*), GOGO and PLVC models. We computed ΔE^*_{ab}, ΔL^*, ΔC^*_{ab} and ΔH^*_{ab} following (CIE, 2004) between the estimated and the measured colors.*

Displays VS models VS indicators		ΔE^*_{ab} mean	ΔE^*_{ab} max	ΔE^*_{ab} std. dev.	ΔE^*_{ab} 95 ptl	ΔL^* mean	ΔC^*_{ab} mean	ΔH^*_{ab} mean
PLCD1	PLCC	6.42	19.06	4.28	18.01	-0.51	-5.27	-0.56
	PLCC*	3.93	8.28	2.15	7.27	-0.86	-2.45	-0.47
	GOGO	3.96	14.61	2.62	9.26	**-0.39**	**0.20**	-0.44
	PLVC	**1.41**	**3.56**	**0.63**	**2.58**	-0.86	-0.64	**-0.09**
PLCD2	PLCC	15.19	55.62	14.94	46.42	1.20	-7.63	-1.08
	PLCC*	1.78	2.96	0.51	2.55	**0.25**	-0.30	-0.29
	GOGO	2.86	11.41	2.30	8.67	0.32	-0.44	-0.28
	PLVC	**0.54**	**1.64**	**0.28**	**1.13**	**0.25**	**-0.03**	**-0.05**
PDLP	PLCC	1.81	8.87	1.80	7.15	0.81	-0.78	-0.41
	PLCC*	0.99	2.17	0.34	1.62	**0.61**	**0.11**	-0.14
	GOGO	5.42	21.17	3.75	12.75	-1.13	1.35	**0.07**
	PLVC	**0.85**	**2.02**	**0.33**	**1.38**	**0.61**	0.21	-0.11
MCRT	PLCC	0.92	1.91	0.39	1.62	0.52	-0.27	-0.03
	PLCC*	**0.88**	**1.87**	**0.40**	**1.59**	0.51	-0.20	**-0.02**
	GOGO	1.41	4.45	0.91	3.31	**0.06**	-0.95	-0.05
	PLVC	0.94	2.06	0.42	1.77	0.51	**-0.12**	-0.11
MLCD1	PLCC	7.26	23.90	5.80	21.12	**0.53**	-5.32	**-0.13**
	PLCC*	1.81	4.10	0.86	3.06	-0.95	-0.70	0.46
	GOGO	4.22	24.45	3.28	8.80	-0.56	0.70	0.17
	PLVC	**1.50**	**3.32**	**0.64**	**2.67**	-0.95	**-0.57**	0.52
MLCD2	PLCC	4.66	12.08	2.30	9.45	**-0.58**	-1.44	0.46
	PLCC*	4.88	9.36	2.16	7.76	-0.84	**0.41**	0.43
	GOGO	6.89	45.54	6.09	16.38	-1.39	1.01	**-0.29**
	PLVC	**2.04**	**4.55**	**0.91**	**3.78**	-0.84	1.03	0.81

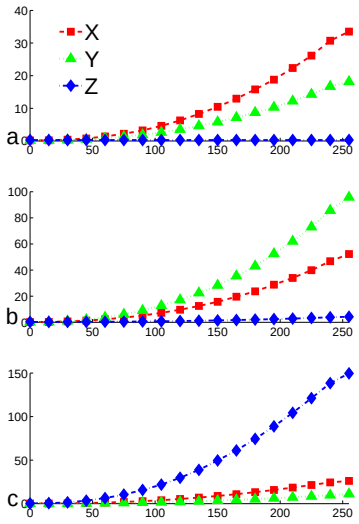

Figure 4.1: *Response curve in X, Y and Z for display PLCD1 in function of the digital input for respectively the red(a), green(b) and blue(c) channel.*

for these devices (Figure 3.2, a, b, e, f). One can see that the ΔC^*_{ab} is the main weakness. However, for the MCRT display it can be judged acceptable with an average error of $\Delta E^*_{ab} = 0.92$ as the primary chromaticities do not shift with the lightness (Figure 3.2, d). For the display PDLP, it could be judged satisfactory with an average error of $\Delta E^*_{ab} = 1.81$ as the chromaticities are remaining quite constant except for really low luminance (Figure 3.2, c and Figure 4.2).

Applying a black correction, we reduce drastically the error for almost all devices except MLCD2, even if also for this device the error in chroma is better distributed. On the right part of Figure 3.2, one can see that the major part of chromaticity inconstancy has been removed. For most applications such a model can be used, we found averaged error from 0.88 to 4.88 ΔE^*_{ab} units for our set of displays. The major improvement is in chroma. We can notice that this increases the systematic error in lightness for devices PLCD1, MLCD1 and MLCD2, while it is decreasing in PLCD2. For displays PDLP and MCRT, it remains more or less the same (the error in lightness decreases not significantly, a bit more for PDLP).

The GOGO model gives possibly acceptable results for some displays especially for MCRT, but for others it seriously fails, especially for MLCD1, MLCD2 and PDLP with average errors from around 4 to around 7 ΔE^*_{ab} units. These displays are showing a really different response curve in luminance from a gamma shape (Figure 4.2).

The PLVC model yields significantly improved model precision, compared with the

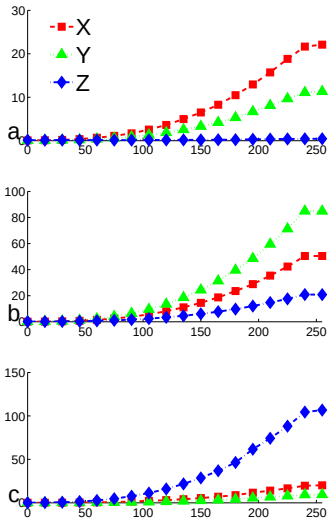

Figure 4.2: *Response curve in X, Y and Z for display PDLP in function of the digital input for respectively the red(a), green(b) and blue(c) channel.*

discussed models, for most of the tested displays. Especially for the two LCD projectors and the monitor MLCD2 where the averaged accuracy is more than doubled (Table 4.3). One can see in Figure 3.2 that for PLCD1 the chromaticity shift is still significant after black correction. This is not so obvious for the other ones. For MCRT we reduced the systematic error in chroma, but increased it in hue. For PDLP, the improvement compared with the PLCC* is not major but exists, probably due to the shift in chromaticity on the red channel (see Figure 3.2). Display MLCD1 shows only a small improvement comparing with the PLCC*.

4.4 Detailed analysis

The PLCC* and the PLVC give the best results among the tested models, and in the following, we have compared these two models in more detail. Obviously the ΔL^* are the same for these two models, as both use the same response curve along Y.

If we look at the histogram of the error distribution on Figure 4.3 and at the standard deviation in Table 4.3, we notice that using the PLVC model reduces the spreading of the error (except for the display MCRT where it remains the same).

The following deals with the results in deeper details concerning the location of errors in the device gamut. For this purpose, we used visualization of errors in *CIELAB*. We present here the projection in $a*b*$ and $L*a*$ planes (respectively Figure 4.4 and Fig-

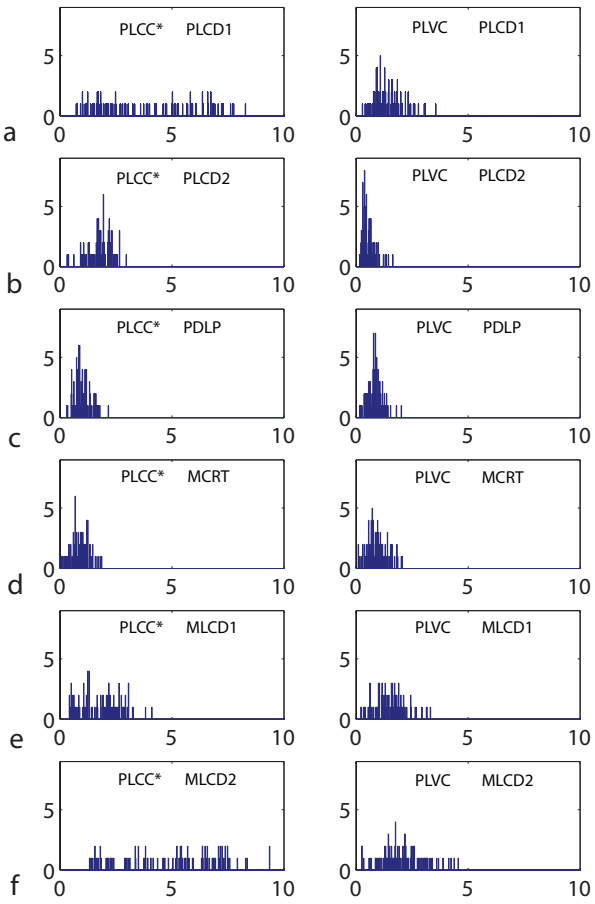

Figure 4.3: *Comparison of the model prediction error distribution in ΔE^*_{ab} between PLCC* (left) and PLVC (right). The errors are shown on the abscissa, the ordinate shows the number of test samples that is estimated with this error.*

ure 4.5 for the display PLCD1) and the projection in $L*a*$ plane for MCRT (Figure 4.6) and MLCD2 (Figure 4.7), to illustrate our analysis and because they can be considered representative of the general results found, under some restrictions. The full set of visualizations for all displays is in appendix D.

One can see on the $a*b*$ plane in Figure 4.4 that the main improvement obtained with the PLVC model follows roughly the direction of the line from $(-a*, +b*)$ to $(+a*, -b*)$. This effect can be seen more or less strong on every tested LCD devices especially in the bluish area. That means that a correction in chroma has been performed for the bluish area, and mainly in hue for the reddish and cyan area. A small similar effect can be seen

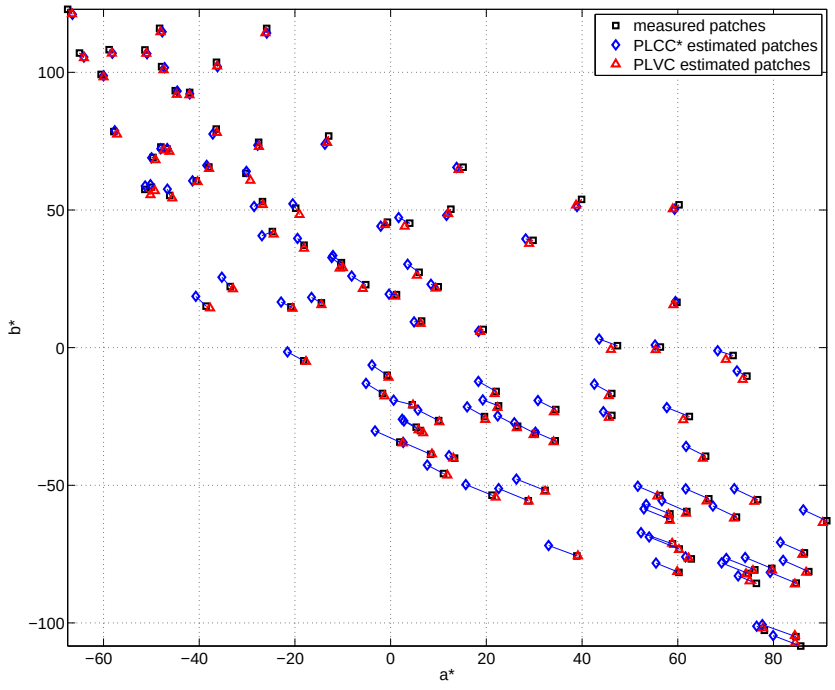

Figure 4.4: *PLCD1: visualization of errors for the testing data set projected on the $a*b*$ plane.*

in the not saturated blue of PDLP. Nothing is noticeable for MCRT in $a*b*$ plane, as the chromaticity of primaries is constant.

About the error location in $a*b*$ plane of the PLVC model, it is difficult to find a systematic type of error as they are really small in the $a*b*$ plane. Examining Figure 4.4, one could say that the remaining error is localized in the red area. However, nothing similar has been noticed for the other displays, and it is not representative.

For the display PLCD2, no noticeable error remains in $a*b*$ plane. For PDLP we can notice some errors in the purple and in the desaturated greenish/yellowish area. For MCRT, some errors remain in the half plane defined by positive $b*$ values. For MLCD1, they are located in the bluish to reddish area (and a little bit in the yellow). For MLCD2, an amount of error remains everywhere. The location of errors appears to be different for different displays, and to conclude we can say that the results in chroma/hue depend on the display.

If we now look at the luminance factor, in display PLCD1 (see Figure 4.5), PDLP, MLCD1 and MCRT we can notice the same thing as in the previous studies: from low

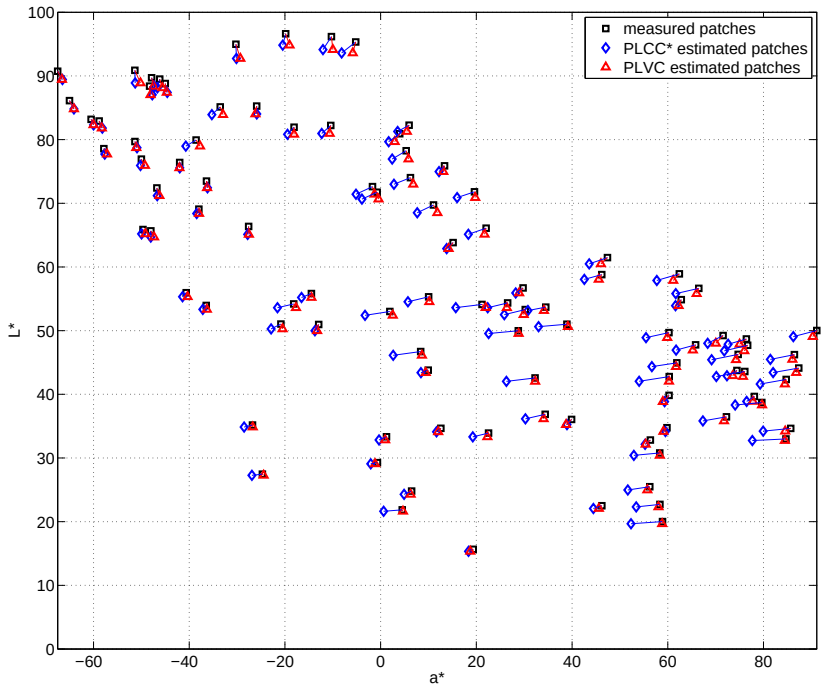

Figure 4.5: *PLCD1: visualization of errors for the testing data set projected on the $a * L*$ plane.*

to medium luminance, the accuracy is good. The results are worse when the luminance is high. PLCD2 shows really small luminance shift. MLCD2 shows a stronger luminance shift in the medium level (Figure 4.7). Note that for PDLP and MCRT displays, the measured luminance is lower than the estimated one when there is a difference (Figure 4.6), while the opposite occurs for the other devices.

These differences in behavior could be explained by the inter-dependence between channels. MLCD2 luminance shift follows the shape of the derivative of an S-shape curve, as shown by Yoshida and Yamamoto (Yoshida and Yamamoto, 2002). The LCD projectors tested were 3-LCD ones, therefore the interaction between channels due to coupling capacitive should not appear, at least for uniform color patches, since they are physically independent. The over-estimation of the luminance in MCRT is probably due to a lack of power supply when the maximum intensity is required. For pure colors, we did not notice any non-monotonicity in the response curve, but the gray response curve is below the sum of the pure color response curve. The same remark can be done for PDLP, but we can observe the saturation of the response curves at the higher input values (see Figure 4.2).

In summary, the error in luminance is strongly dependent on the interaction be-

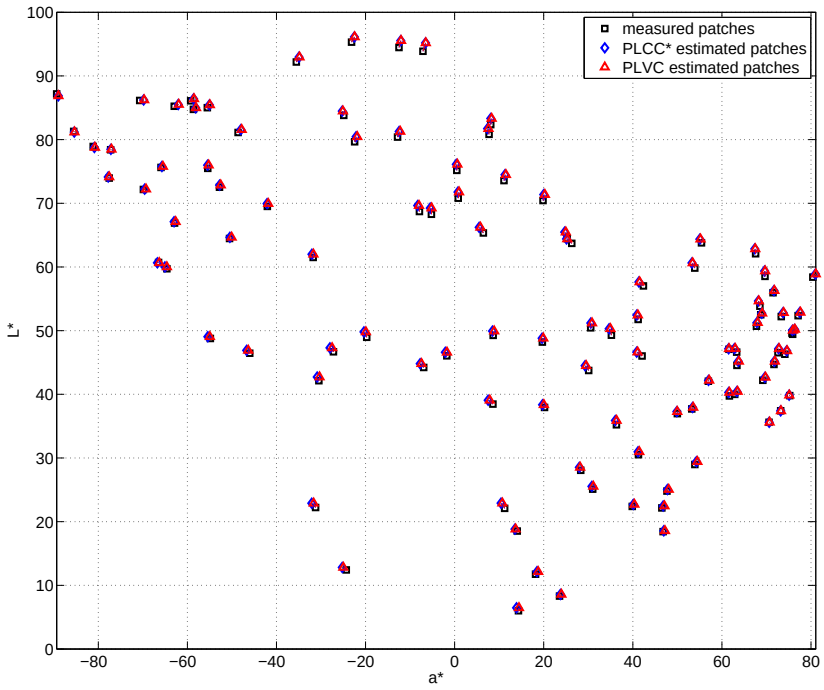

Figure 4.6: *MCRT: visualization of errors for the testing data set projected on the $a*L*$ plane.*

tween channels, which is indeed the weakness of the PLVC model. This seems to be not critical for the display tested, as we achieve good results in using the PLVC or PLCC models. Looking at the $a*b*$ plane, the PLVC model increases significantly the accuracy in chroma and hue for LCD technology.

4.5 Conclusion and further work

In this section, we presented results on the PLVC display color characterization model. We achieved the same conclusion on CRT technology as the previous published studies of this model, and we extended this conclusion to the DLP tested projector: the PLCC is performing well, as long as a black correction is carried out, with equivalent results. For our DLP projector, the averaged ΔE^*_{ab} is of 0.99 using the PLCC* against 0.85 using the PLVC. For our CRT monitor, the averaged error is of 0.88 using the PLCC* against 0.94 using the PLVC. Furthermore we have shown, through our experiments, the efficiency of the PLVC model for LCD technology. On three out of six of the tested displays we reduced significantly the error by using PLVC instead of PLCC*. On these devices, we

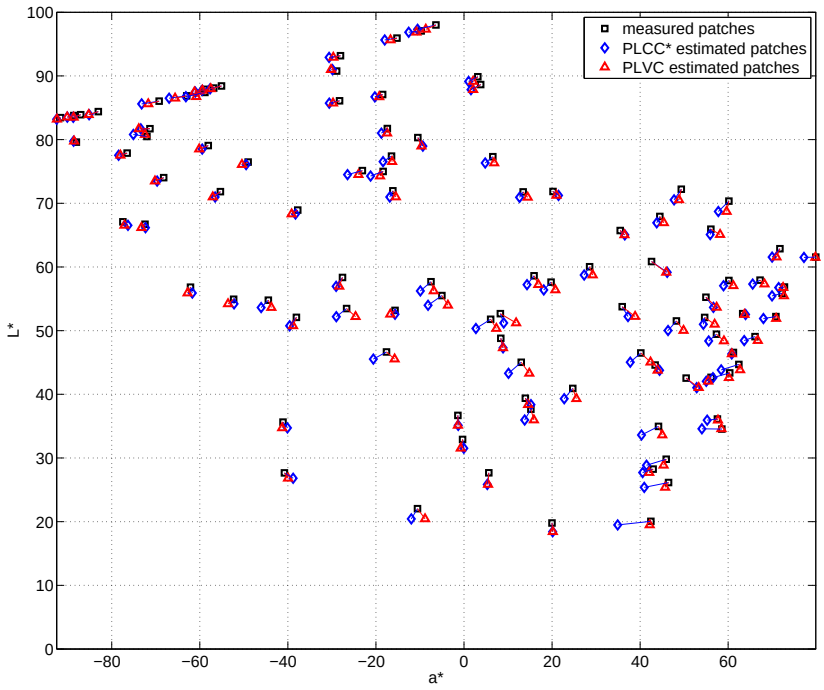

Figure 4.7: *MLCD2: visualization of errors for the testing data set projected on the* $a*L*$ *plane.*

obtained average ΔE^*_{ab} of 3.93, 1.78 and 4.88 with the PLCC* model, and 1.41, 0.54 and 2.04 with the PLVC model.

Looking at these results, and comparing with the thresholds we defined, we can say that:

- None of these models show an accuracy that can be used for a professional accurate characterization independently of the technology. However, the PLCC*, the PLVC and possibly the GOGO for CRT could be used for accurate characterization.

- The PLCC won't be accurate enough for a consumer characterization in any display that shows a consequent black level, and by extension in the presence of an ambient light.

- the GOGO model will be possibly used for a professional for a CRT monitor.

- the PLCC* gives a good compromise for a consumer characterization. For a professional us however, when it is on LCD technology, the result is not guaranteed to be accurate enough.

- The PLVC surely gives results good enough for a consumer use, however, the professional use is strongly dependent of the device.

Considering any of these model, a consumer or professional use is possible only when an *acceptable* accuracy is reached. That means there is a need to test them on a display before to decide to use them.

A straightforward further experiment of this work could be to evaluate results on multi-primary displays using Equation 3.9. Indeed, in order to increase the size of the display's gamut, one could use N primaries. Several systems have been defined for this purpose; see for example the work of Ajito et al (Ajito et al., 2000). The problem is that one needs to isolate each channel to measure their response curves. As we usually do not know the transformation used by the manufacturer, this can be a tough task. A solution has been proposed for 4 primaries DLP (R,G,B and white segments) by Wyble and Rosen (2004); Wyble and Zhang (2003). In their model, the characteristics of the luminance of the white channel is retrieved with regard to additive property of the display, given the four-tuplet (R, G, B, W) from an input (d_r, d_g, d_b). An idea could be to retrieve as well the X and Z components of the white channel using the same method. We would be able then to apply the PLVC model. For more primaries, this can be less obvious. In such cases, major problems can arise to perform the model inversion, which becomes far more difficult than the problems addressed in previous studies (Jimenez Del Barco et al., 1995; Post and Calhoun, 1989; Thomas, Colantoni, Hardeberg, Foucherot and Gouton, 2008*a*,*b*), as it is a projection from a 3-dimensional space into a N-dimensional one. However one could use some work that has been done in this direction (Ajito et al., 2001).

Chapter 5

Camera-based end-user approach

It's easier to resist at the beginning than at the end.

Leonardo Da Vinci

Abstract

This chapter considers a camera-based, end-user method. An approach to retrieve the response curve of a projector using a simple consumer camera is evaluated and updated. It is confirmed that this approach gives better results than others and equivalent end-user approaches.

5.1 Introduction

Nowadays, in common use of projectors, there is a lack of color accuracy that often leads to a loss of visual appeal in the presented material, and also in many cases to a loss of intended meaning. The major cause is that the model set up requires an expensive and/or not easy to move measurement device. We describe and evaluate here a method that only requires a end-user consumer camera to retrieve the response curve of a projector.

This work concerns mainly the independent evaluation and improvement of a method introduceded by Bala and Braun (2006); Bala et al. (2007) for an accurate, end-user, colorimetric characterization of projection displays. We refer the reader to the original paper for more explanations about the method.

We first recall the original method, showing the advantages and drawbacks. We then present our set-up and experimental results.

5.2 Context and methodology

The Bala method introduced in (Bala and Braun, 2006; Bala et al., 2007) aims to achieve a good calibration for projection displays using no equipment other than an uncalibrated consumer digital camera that anyone could have at home. This removes the need for any radiometric or colorimetric measurements in the calibration process. It can be assumed that the system primaries are *sRGB* (Anderson et al., 1995). Similarly, data provided by the manufacurer may be used if available. This method is to put together with the other visual calibration methods.

Their proposal is to calibrate the camera relatively to the display, using the following information:

- The 50% luminance point of the projector (Bala and Braun, 2006; Bala et al., 2007; Sharma, 2003), estimated visually using a matching pattern.
- The maximum normalized luminance considered at 1 and the true black at 0.
- The black level of the projector considered at 2% of the maximum luminance (Bala and Braun, 2006; Bala et al., 2007) (for a dim environment).

This information is used to estimate the camera response curve, using spline interpolation. Based on this estimation, the camera can replace a more sophisticated photometric measurement device and can be used to estimate the projector's tone response curve, by taking a picture of a pattern displayed on the screen. the flow is summerized

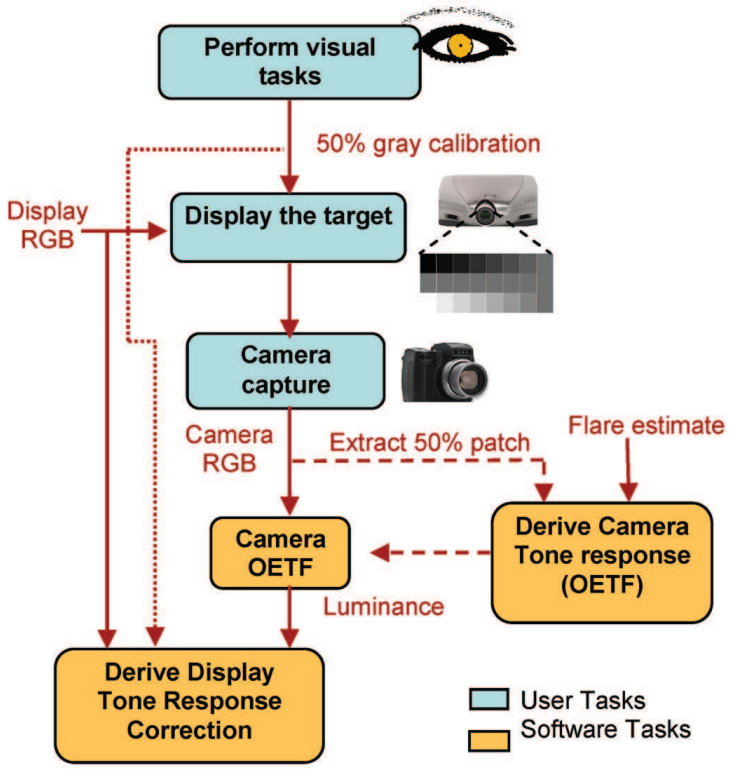

Figure 5.1: *Summary of the flow proposed by Bala and Braun. First, the mid-grey level is evaluated by the user. A pattern is generated, and captured by a camera. The mid-grey level, projector's black level, projector's full intensity and real black are used to evaluate the camera response curve. The pattern is used to retrieve the projector's response curve, considering the camera as a relative photometer. Image from (Mikalsen, 2007)*

in Figure 5.1. We invite the reader to read (Bala and Braun, 2006; Bala et al., 2007) in order to get all details.

In this section, we want to identify strengths and weaknesses of the approach. Moreover, we propose to enhance the original method as follows:

- The original method assumes that the normalized gray level response curve is the same as the normalized curves for each primary. We propose to separate the estimations of the three primary color channels response curves through duplication of the calibration procedure per channel.

- The original method uses only one patch at 50% luminance for visual luminance matching. We propose to increase the number of visually determined luminance levels from one to three by adding targets for 25% and 75% luminance to the original 50% level, obtained by a halftoning like process, similarly to the full visual calibration proposed in (Neumann et al., 2003).

5.3 Experimental setup and results

The Bala method and its proposed enhancements were implemented and tested with two different digital cameras: the Nikon D200 DSLR and the Fujifilm Finepix S7000 compact type camera, and two different projectors with different technologies: a Panasonic AX-PT100E LCD and a Projectiondesign Action one DLP. All experiments were done with default hardware settings and no gamma correction performed by image source computer.

Throughout the experimentation with the Bala method (Mikalsen, 2007; Mikalsen et al., 2008) it became apparent that the method can be accurate enough for some applications, but performances are largely dependent on three main factors:

- The estimation of the camera's response curve is based on four points. Two of these are the absolute black point and the projector's black point which are close together. The proximity of these points strongly influences the shape of the interpolation function. We have concluded that we need to have an accurate estimation of the projector's black level when using this method (see Figure 5.2). We propose no solution yet for an estimation of this parameter without an accurate measurement device. This is a major weakness in the approach as it moves away from the initial chain of thought on replacing expensive color and luminance measurement equipment with the digital camera. We do not put aside the fact that for other interpolation methods it could work well with a generic black level. However, we wonder how increasing the number of visual patterns (in low luminance), while simply removing the projector black point to estimate the camera response curve, can lead to better results.

- Secondly, the observer's precision in the visual matching task will determine a known data for the estimation of the camera response curve. This will have significant influence on the estimation of camera tone response. This is the weakness of every visual calibration method. Note that the visual estimation of the 50% luminance for the blue channel is a harder task for the human visual system compared to the higher wavelengths of red and green. Furthermore, a "gray balancing" (Klassen et al., 2005) method can not be used as the projectors are used to show a large chromaticity shift with the variation of input for the pure primaries.

- The third factor is the camera's capability to differentiate between projected luminances in the calibration pattern. If it lacks accuracy when recreating on-screen luminance differences it will not give the information needed to estimate projector tone response. When testing the method, it appeared that the FujiFilm camera had severe problems with capturing suitable images for this method. The captured

images seemed to be either saturated in brighter areas or the darker patches were indistinguishable from each other, and the resulting estimated curves were not representative. Major efforts were put into experimentation with camera settings without achieving better images. As a consequence, the camera was not found suitable to be used with this method; hence no further results from this camera will be reported. This problem might be avoid in using simple HDR techniques, but the method would suffer of a loss of its simplicity.

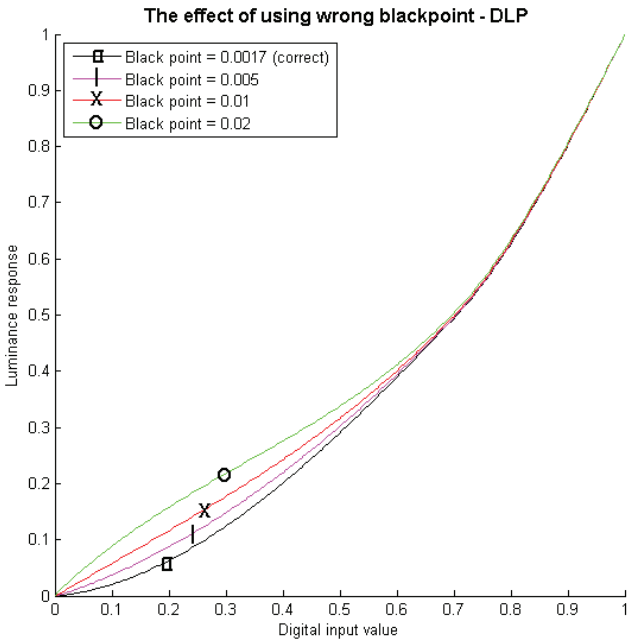

Figure 5.2: *Camera response estimation using different black levels. Giving a wrong black point makes the estimation to vary strongly for the luminance below the 50% of the projector.*

Although such critical factors were identified, the method shows good results, mostly less than 3 ΔL^* units were found for our evaluation data set (Table 5.1). These results are presented for a dark environment. The ΔL^* is computed from the measured response curve and the estimated one, for a full ramp (256 values) of gray level patches or for each independent channel. Note that Bala et al worked in dim environment. In such a case, it is possible that the estimation of 2% luminance for the black level is better. To be fair in our comparison, and to present comparable results, all the methods presented used the same level of black, which is the black level of the projector measured with a spectroradiometer Minolta CS-1000. The ΔL^* has been computed for two luminances L_1 and L_2 as $\Delta L^* = \sqrt{(L_1 - L_2)^2}$.

Figure 5.3 shows the estimated tone reproduction curve for the Projectiondesign DLP projector using the original method. Here an average ΔL^* luminance difference

Table 5.1: *Average ΔL^* between the real projector response curve and the estimated one (the 256 possible values were measured and estimated), depending on the method used.*

Method	**Projector**	ΔL^*	ΔL^* **Red**	ΔL^* **Green**	ΔL^* **Blue**	***RGB*** **average** ΔL^*
Original	LCD	3.47	-	-	-	-
3 matched luminance	LCD	2.14	-	-	-	-
Original	DLP	1.64	-	-	-	-
3 matched luminance	DLP	0.59	-	-	-	-
Separate Channel match w/ 1 lum. match	LCD	-	1.83	3.03	2.51	2.46
Separate Channel match w/ 3 lum. match	LCD	-	1.48	2.30	1.92	1.90
Separate Channel match w/ 1 lum. match	DLP	-	1.90	1.05	2.96	1.97
Separate Channel match w/ 3 lum. match	DLP	-	1.89	0.96	2.01	1.62

of 1.64 from the projectors measured response was achieved. Figure 5.4 shows results when using the extended method with three visually matched luminance levels instead of one. This shows an even closer match to the measured response with an averaged ΔL^* difference of only 0.59. With the LCD projection device, we obtained 3.47 ΔL^* for the original method to 1.90 using both improvements (calibration of each primary, with 3 visual patches). Figures 5.5 and 5.6 are showing the estimated tone response curve for the LCD for respectively the original and the extended method using three visually matched luminance levels. One can notice the same thing that for the previous display: we reduced the average error to 2.14.

It appears that the independent estimation of the blue channel response curve for the both projectors shows a ΔL^* of 2.52 and 2.96 for one luminance match and of 1.92 and 2.01 for three luminance matches. It is supposed to be the worst case as the visual system is better to distinguish luminance changing in long wavelengths than in short ones. Using three luminance matching points, we improve the estimation of the blue channel response curve while, for the red channel, this does not change the result very much. Doing this for the DLP projector green channel, we do not improve the estimation

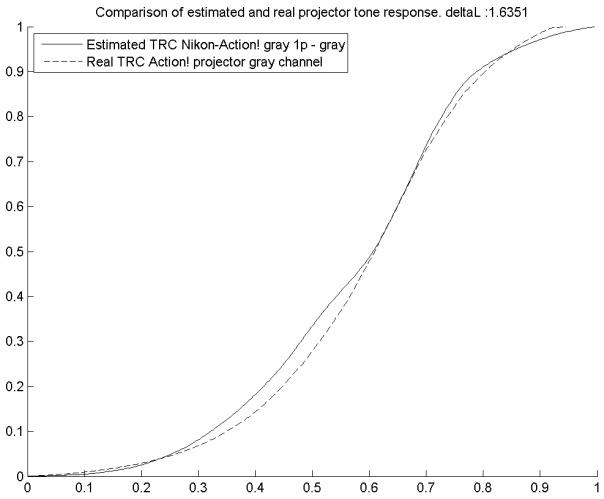

Figure 5.3: *Normalized luminance gray level response curve estimation for the original method (plain line) versus the measured one (dashed line) for the DLP projector, function of the input digital value.*

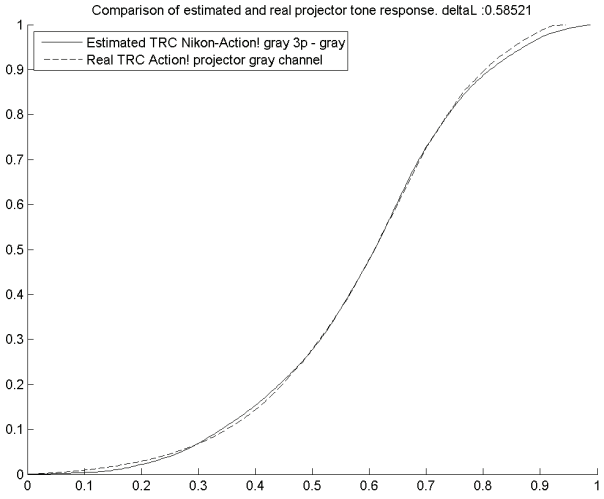

Figure 5.4: *Normalized luminance gray level response curve estimation for the three luminance match method (plain line) versus the measured one (dashed line) for the DLP projector, function of the input digital value.*

quality. However, the LCD projector shows a large error of matching for this channel, and using three points is beneficial for its estimation. Note that this error in matching luminance for the green channel, over the error on the blue one, is surprising. It is possible that the bad match in luminance is induced by a strong chromaticity shift on

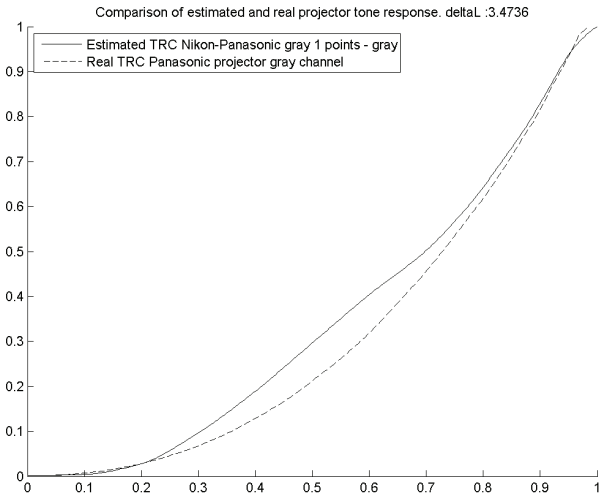

Figure 5.5: *Normalized luminance gray level response curve estimation for the original method (plain line) versus the measured one (dashed line) for the LCD projector, function of the input digital value.*

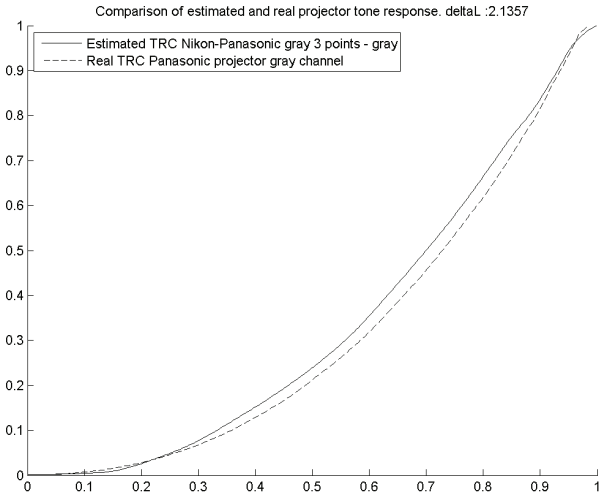

Figure 5.6: *Normalized luminance gray level response curve estimation for the three luminance match method (plain line) versus the measured one (dashed line) for the LCD projector, function of the input digital value.*

the green channel.

When using an inverse characterization model, in the case of color reproduction, the results of the forward model are confirmed. Table 5.2 shows numeric results for the inverse test with our two projectors. This table also shows results obtained when using

the standard PC gamma correction of 2.2. We used a 16 grayscale set of patches. Here we can see that the widely used default gamma correction does not give satisfactory results when comparing to the proposed methods. Figures 5.7 and 5.8 show plots of corrected output respectively according to a standard 2.2 gamma correction and to the enhanced Bala method. It is obvious that for this display the 2.2 gamma correction does not work efficiently. However, the Bala's method achieves a good result compared with a 2.2 gamma.

Table 5.2: *ΔL^* for different methods for an inverse model test built up on a set of 16 grayscale luminance patches.*

Method	**Device**	**Mean** ΔL^*	**Max** ΔL^*	**std. dev.**
Original (Bala)	DLP	2.30	6.21	2.00
3 matched luminance (using half toned patches)	DLP	0.60	1.39	0.50
Separate Channel match w/ 1 lum. match	DLP	0.90	2.77	0.82
Separate Channel match w/ 3 lum. match	DLP	0.87	1.78	0.65
Gamma 2.2	DLP	10.53	25.68	9.52
Original (Bala)	LCD	4.13	9.14	3.02
3 matched luminance (using half toned patches)	LCD	3.35	5.70	1.82
Separate Channel match w/ 1 lum. match	LCD	3.11	6.21	2.10
Separate Channel match w/ 3 lum. match	LCD	3.04	5.68	1.85
Gamma 2.2	LCD	4.32	9.31	3.03

5.4 Conclusion and further work

In this section, we have verified that the model proposed by Bala yields significantly better color reproduction than using default gamma settings for both the LCD and DLP projectors. It is a quick and simple approach, which does not require any accurate mea-

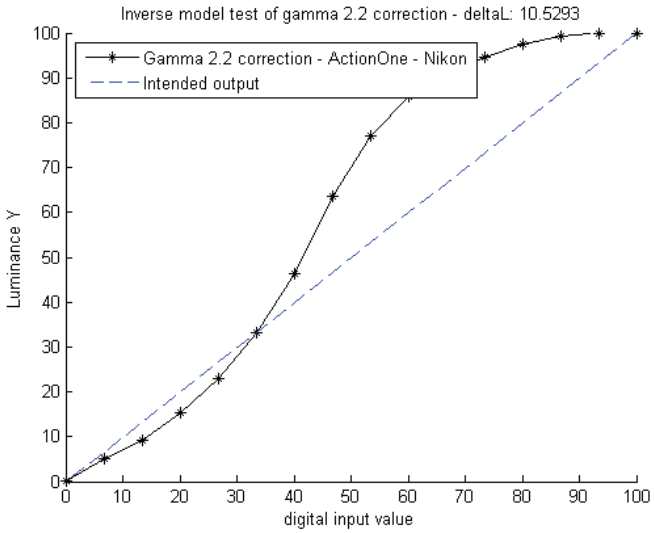

Figure 5.7: *"Linearized" values using a 2.2 gamma inverse model. The dashed line is the ideal line.*

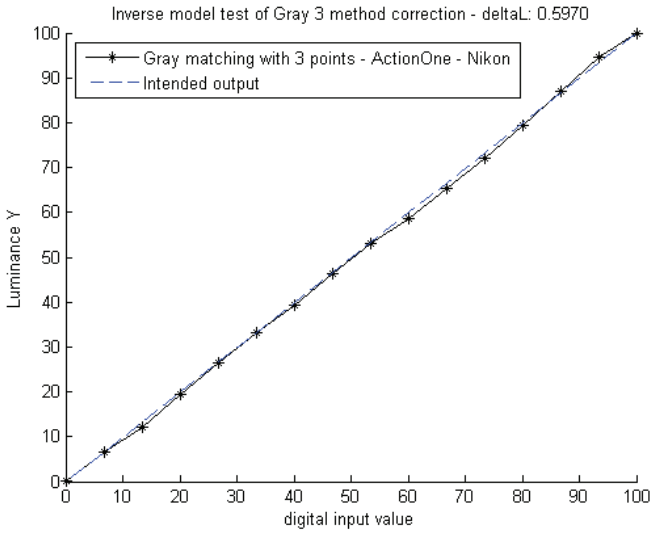

Figure 5.8: *"Linearized" values using an enhanced Bala's inverse model. The dashed line is the ideal line.*

surement device. The proposed extensions add little complexity yet provide a good improvement of the results. We would prefer to add more matching patterns rather than to calibrate each channel independently, at least as long as the normalized response curves are similar by channel, -which is not obvious for LCD-, in order to keep a good time/accuracy gain.

This method aims only to provide a consumer characterization. And it manages to do that. If we look at Bala et al results, none of the other similar methods are able to

provide the wanted result. Looking at our results, it is possible to use the original Bala's method to characterize DLP projectors. It can be necessary to augment the method with an independent evaluation of each primaries response for LCDs.

We still have to find a solution to perform a better estimation of the projector black level in order to permit the model to give its best. Some approaches could be tried, such as using other type of interpolation method less dependent on this point, using more visual matching point in low luminance and removing the black offset point, or finding a visual method to evaluate the percentage of flare.

Moreover, it would be possible to extend this method to spatial non-uniformity correction. That is discussed in Chapter 10.

Chapter 6

Accurate polyharmonic splines method

You can go elsewhere when you're someone else.

Bob Dylan

Abstract

This chapter proposes a polyharmonic splines 3D interpolation display color characterization model. The novelty introduced concerns the distribution of patches to measure, and the degree of freedom on the kernel and smoothing factor choice for the interpolation. This distribution increases noticeably the accuracy of the model. The inverse model is based on a tetrahedral interpolation, using a grid designed in RGB. We illustrate the use of this model in a practical case, which consists in real time color rendering of multi-spectral images under virtual illuminants.

6.1 Introduction

An accurate and original display color characterization model based on harmonic splines is explained in detail and evaluated. This method gives accurate results on most existing technologies. The original model is based on a patent or series of patents registered by Thomson (Colantoni et al., 2005; Stauder et al., 2006, 2007). The model we describe here uses the same principles and interpolation method -polyharmonic splines- that they do, but we used an iterative system to have a better distributed interpolation data set than the one used in the patents. Moreover, a larger degree of freedom (choice of kernel for the interpolation function, destination color space) is used in the model set up, and only the best combination is selected. This characterization method is used in a color rendering software that the Centre de Recherche et de Restoration des musées de France (C2RMF) (French Museum Research and Restoration Center) uses for art painting analysis. The entire application has been developed by Philippe Colantoni. As constraints, we wanted the display color characterization model to be as accurate as possible on any type of display and we wanted the color correction to be in real time (no pre-processing). Moreover, we wanted the model establishment to be short enough to be used in practice (not to exceed the time of a coffee break).

The model we present here is based on the generalization of measurements at some positions in the color space. It is an empirical method, which does not consider any assumptions based on display technology. The forward direction (*RGB* to *CIELAB*), is based on polyharmonic splines interpolation, a subset of Radial Basis Functions (RBF), on an optimal set of measured patches. The backward model (*CIELAB* to *RGB*) is based on tetrahedral interpolation. An overview of this model is shown in Figure 6.1.

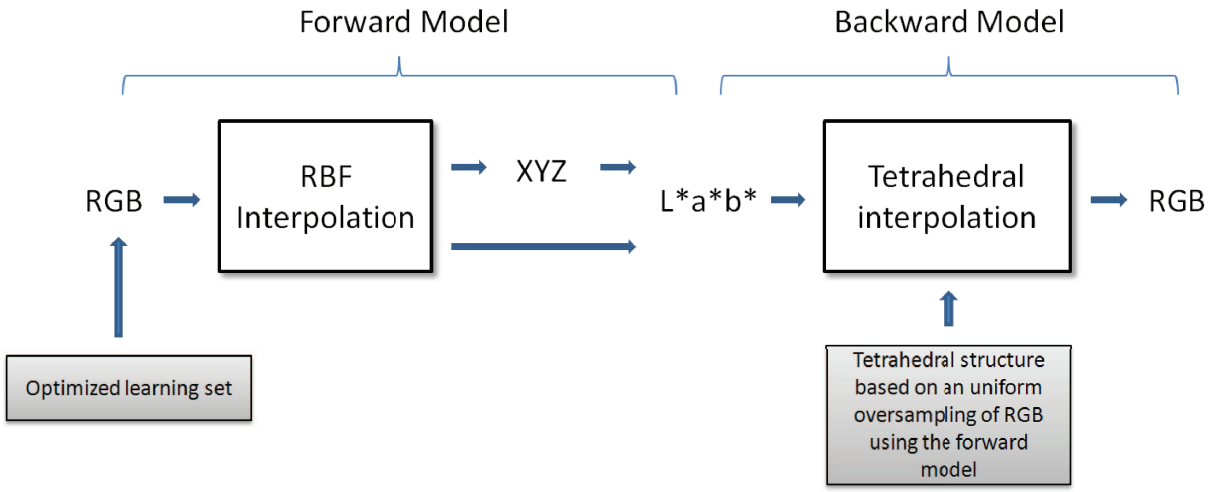

Figure 6.1: *Overview of the polyharmonic splines display color characterization model.*

First we present the details of the accurate display color characterization method and its evaluation. Then we describe its application on multispectral images of art paintings and its GPU implementation for real time rendering.

6.2 Forward model

Traditionally a characterization model (or forward model) is based on an interpolation or an approximation method. We found that RBF interpolation was the best model for our purpose.

6.2.1 Polyharmonic spline

Polyharmonic splines are a subset of RBF that can be used for interpolate or to approximate (Carr et al., 2001) arbitrarily distributed data.

In color imaging, beside of this method and its previous version, we only know the use of Thin Plate Splines (TPS) for printers colorimetric characterization (Sharma and Shaw, 2006). TPS are a subset of polyharmonic splines (bi-harmonic splines). Sharma and Shaw (2006) recalled the mathematical framework and presented some applications and results for printers characterization. They shown that using TPS, they achieved a better result than in using local polynomial regression. They shown that in using a smoothing factor, error in measurement impact can be avoided at the expense of the computational cost that optimize this parameter (see Figure 6.2). However, they did not study data distribution influence (but they said that the data distribution can improve the accuracy in their conclusion) neither the use of other kernels for interpolation.

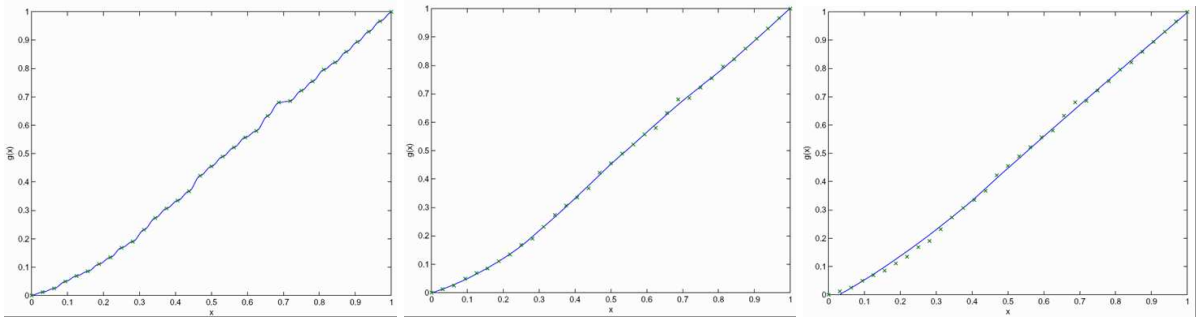

Figure 6.2: *Influence of increasing the smoothing factor on 1D TPS (bi-harmonic kernel). On the left, it is an interpolation (no smoothing factor). On the middle and on the right, the smoothing factor has been increased, it is an approximation. Figure from Sharma and Shaw (2006) presentation at EUSIPCO.*

The definition we used of the 3D polyharmonic splines interpolation/approximation is given in Appendix C.

In our work we used a set of 4 real functions as possible kernels, the biharmonic ($\phi(x) = x$), triharmonic ($\phi(x) = x^3$), thin-plate spline 1 ($\phi(x) = x^2 log(x)$) and thin-plate spline 2 ($\phi(x) = x^2 log(x^2)$), with x the distance from the origin. The use of a given basis function depends on the display device, which is characterized, and gives some freedom to the model.

6.2.2 Color space target

Our forward model uses *CIELAB* as default target (*CIELAB* is a target well adapted for the gamut clipping that we use). This does not imply that we have to use this space as target for the RBF interpolation. In fact we considered two choices. We can use either *CIELAB*, which seems to be the most logical target, or *CIEXYZ* associated with a *CIEXYZ* to *CIELAB* color transformation. The use of different color spaces as target gives us another degree of freedom.

6.2.3 Smoothing factor choice

Once the kernel and the color space target are fixed, the smoothing factor, included in the RBF interpolation model used here (Appendix C), is the only parameter that can be used to change the properties of the transformation. With a zero value, the model is a pure interpolation. With a different smoothing factor, the model becomes an approximation. This is an important feature because it helps us to deal with the measurement problems due to the display temporal stability and to the repeatability of the measurement device.

6.3 Optimized learning data set

In order to increase the reliability of the model, we introduce a new way to determine the learning data set for the polyharmonic splines interpolation (e.g. the set of color patches measured on the screen). We found that our interpolation model was most efficient when the learning data set used to initialize the interpolation was regularly distributed in our destination color space (*CIELAB*). This new method is based on a regular 3D sampling of *CIELAB* color space combined with a forward - inverse refinement process after the selection of each patch. This algorithm allows us to find the optimal set of RGB colors to measure.

This technique needs to select incrementally the RGB color patches that will be integrated into the learning database. For this reason it has been integrated into a custom software tool able to drive a spectrophotometer. This software also measures a set of

100 random test patches equiprobably distributed in *RGB* used in order to determine the accuracy of the model.

6.3.1 Iterative selection of patches

In the work of Stauder et al. (2007), the selection of the patches, in order to build the forward model, is based on an iterative process that considers the whole model. The algorithm presented in the patent considers one iteration by default. First, the original set of patches is measured, and a temporary inverse model is built up. Using this temporary model, the actual forward model is based on measured patches well distributed in the destination space. Well distributed means that the patches are as equidistant as possible in the destination color space, i.e. *CIELAB* in the patent. The distribution we used in our algorithm is the same that is used in the patent. It is based on a 3D hexagonal grid in *CIELAB* that is described in the following. Stauder et al. (2007) stated that as many iteration as wanted can be used at the expense of a new measurement series at each iteration.

The approach we used in our model is different. We consider that the cost of measurement time does not fit with the reality of an application. [1] We then do not want to measure more than a second data set. However, the establishment and evaluation of a model is fast even on CPU. Our forward model is then based on a refinement of the model after each measurement, starting from the more bright point, ending with the darker. Between each measurement, a new model is set-up, and the *RGB* value (position) of the patches that have not been measured yet is re-evaluated, using a new and more accurate temporary model at each iteration. At the end, the forward model is as precise as possible considering a given number of patches. The choice to describe the grid from higher to lower luminance is defended by the fact that the measurement device is more accurate in higher luminance. Following this choice, we build up a more homogeneous model, since the lower accuracy of the measurement device is compensated by a better estimation of the patch to measure. This way of distribution constraints the use of this model to displays since there is a need to re-evaluate the next patch value to measure after each measurement. For instance, it would be too much time and money consuming to build such a model for a printer, even more for a camera.

[1] The number of measurements for accurate display color characterization is a major problem (such as for printers) that is debated in the last articles in the literature, such as (Blondé et al., 2009) or (Thomas, Colantoni, Hardeberg, Foucherot and Gouton, 2008*a*,*b*).

6.4 Inverse model using tetrahedral interpolation

The forward model defines the relationship between the device "color space" and the CIE system of color measurement. We present in this section the inversion of this transform. Our problem is to find the corresponding *RGB* values (for a display device previously characterized), of *CIELAB* values computed by the GPU from the multispectral image and the chosen illuminant.

This inverse model could use the same interpolation methods previously presented but we used a new and more accurate method (Colantoni et al., 2005). This new method uses the fact that, if our forward model is very accurate, then it is associated with an optimal patch database (see 6.3). Basically, we use a hybrid method; a tetrahedral interpolation associated with an over-sampling of the *RGB* cube (see Figure 6.3). We have chosen the tetrahedral interpolation method because of its geometrical aspect (this method is associated with our gamut clipping algorithm).

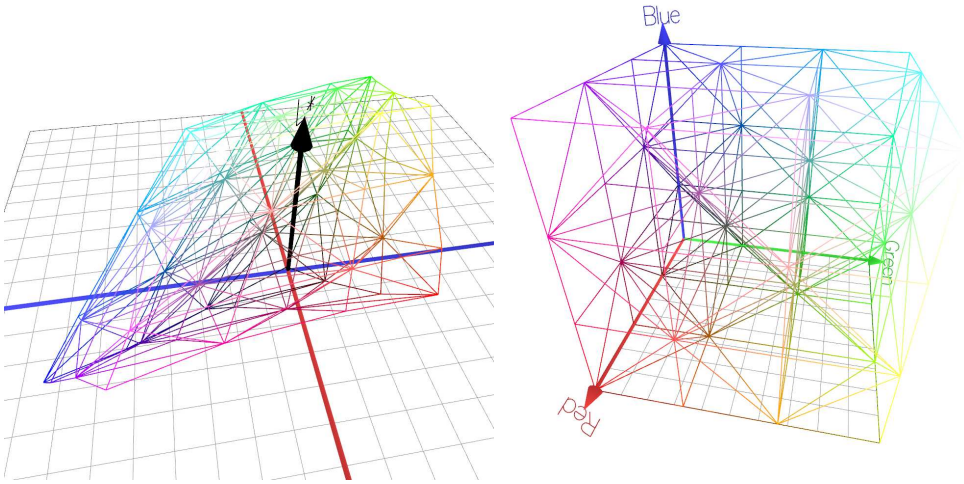

Figure 6.3: *Tetrahedral structure in CIELAB and the correponding structure in RGB.*

We build the initial tetrahedral structure using an uniform over sampling of the *RGB* cube ($n \times n \times n$ samples). This over sampling process uses the forward model to compute the corresponding structure in the *CIELAB* color space. Once this structure is built, we can compute, for an unknown C_{Lab} color, the associated C_{RGB} color in two steps: First, the tetrahedron that encloses the point C_{Lab} to be interpolated should be found (the scattered point set is tetrahedrized); and then, an interpolation scheme is used within each tetrahedron. More precisely, the color value C of the point is interpolated from the color values C_i of the tetrahedron vertices. A linear interpolation within a tetrahedron can be performed as follows:

$$C = \sum_{i=0}^{3} w_i C_i$$

The weights can be calculated by $w_i = \frac{V_i}{V}$ with V the volume of the tetrahedron and V_i the volume of the sub-tetrahedron according to:

$$V_i = \frac{1}{6}(P_i - P)[(P_{i+1} - P)(P_{i+2} - P)]; i = 0, ..., 3$$

where P_i are the vertices of the tetrahedron and the indices are taken modulo 4.

The over-sampling used is not based on the same number of points for each axis of *RGB* such as in explained in Chapter 7. It is computed according to the shape of the display device gamut in the *CIELAB* color space. Note that this concept differs from the work of Stauder et al (Stauder et al., 2007) that uses a regular grid in *RGB*, such as presented by Stokes (1997). We found that an equivalent to $36 \times 36 \times 36$ samples (46656 points) was a good choice. Using such a tight structure linearizes locally our model, which becomes perfectly compatible with the use of a tetrahedral interpolation. The selection of the number of patches along each axis is done using a brute force approach, such as used in (Thomas, Colantoni, Hardeberg, Foucherot and Gouton, 2008*a*).

6.5 Results

We want to find the best inverse model, which allows us to determine with a maximum of accuracy the *RGB* values for a computed *CIEXYZ*. In order to complete this task we must define an accuracy criterion. We chose to multiply the average ΔE_{76} by the standard deviation (STD) of ΔE_{76} of the set of 100 patches evaluated with a forward model. This criterion makes sense because the inverse model is built up on the forward model.

6.5.1 Measurement considerations

Before we expose our results we should talk about color measurement. Two main factors will influence these measurements:

- The stability of the display device: a display device is linked to a power supply and a light source (for LCD, video projector, etc) or an electron gun (for Cathode Ray Tube, SED, FED, etc) or plasma cells. We cannot expect these elements to be perfectly stable (especially with non professional equipments). The result is a color rendering unstability.

Table 6.1: *Global repeatability measurement*

display device	ΔE Mean	Mean(ΔE STD)	ΔE Max
SB2070 - CRT Mitsubishi	0.234267	0.159998	1.55088
HP2408w - LCD Hewlett-Packard	1.93712	1.35595	10.8971

Table 6.2: *Repeatability between two consecutive measurements*

display device	ΔE	ΔE Max
SB2070 - CRT Mitsubishi	0.102522	0.547393
HP2408w - LCD Hewlett-Packard	0.183674	0.664864

- The measurement device gives values with a tolerance. In the case of a colorimeter this tolerance depends on different factors: the technology used; the brightness of the color, etc.

We need to know the combined influence of these two factors. In order to quantify it, we made the following experiment for each display device tested: we send and measure 64 color patches ($4 \times 4 \times 4$ uniformaly sampled patches) 30 times (20 minutes measurement).

We computed for each color patch the ΔE mean, max and the standard deviation. Table 6.1 exposes the mean of these values for the 64 patches during all the measurements. Table 6.2 exposes the result (ΔE mean and max) between two consecutives measurements (25th and 26th measurements)

Whatever the model used during the calibration process, it will integrate this measurement error. We can also be confronted to relatively unstable display, even on a short period of time (with the HP2408w LDC display). This kind of display cannot provide reliable colors.

6.5.2 Optimal model

The selection of the optimal parameters can be done using a brute force method. We compute for each kernel (ie. biharmonic, triharmonic, thin-plate spline 1, thin-plate spline 2), each color space target (*CIELAB*, *CIEXYZ*) and several smoothing factors (0, 1e-005, 0.0001, 0.0005, 0.001, 0.005, 0.01, 0.05, 0.1) the values of this criterion and we select the minimum.

For example the following Tables 6.3 and 6.4 show the report obtained for a SB2070 Mitsubishi DiamondPro with a triharmonic kernel for *CIELAB* (Table 6.3) and *CIEXYZ* (Table 6.4) as color space target (using a learning data set of 216 patches):

Table 6.3: *Part of the report obtained in order to evaluate the best model parameters. The presented results are considering CIELAB as target color space, and a triharmonic kernel for a CRT monitor SB2070 Mitsubishi DiamondPro.*

smoothing factor	0	0.0001	0.001	0.01	0.1
ΔE Mean	0.379	0.393	0.376	0.386	0.739
ΔE STD	0.226	0.218	0.201	0.224	0.502
ΔE Max	1.374	1.327	1.132	1.363	2.671
ΔE 95%	0.882	0.848	0.856	0.828	1.769
ΔRGB Mean	0.00396	0.00459	0.00438	0.00421	0.00826
ΔRGB STD	0.00252	0.00323	0.00316	0.00296	0.00728
ΔRGB Max	0.01567	0.02071	0.01768	0.01554	0.05859
ΔRGB 95%	0.00886	0.01167	0.01162	0.01051	0.01975

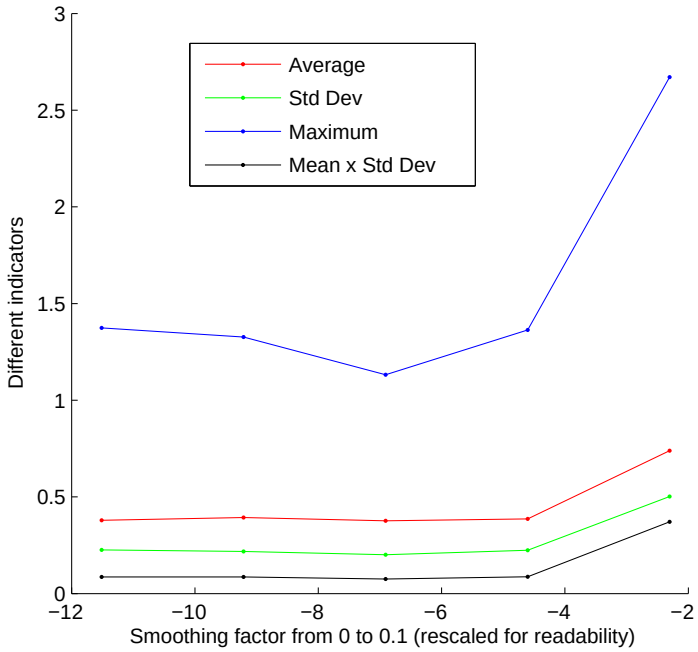

Figure 6.4: *Influence of the smoothing factor choice on different indicators based on Table 6.3.*

On Figures 6.4 and 6.5 we can see the influence of the smoothing factor choice on different indicators. We can notice that when the smoothing factor is superior to 0 there is a minimum where the model shows the best results.

According to our criterion, the best kernel is the triharmonic with a smoothing factor of 0.01 and *CIEXYZ* as target.

Table 6.4: *Part of the report obtained in order to evaluate the best model parameters. The presented results are considering CIEXYZ as target color space, and a triharmonic kernel for a CRT monitor SB2070 Mitsubishi DiamondPro.*

smoothing factor	0	0.0001	0.001	0.01	0.1
ΔE Mean	0.495	0.639	0.539	0.332	0.616
ΔE STD	0.293	0.424	0.360	0.179	0.691
ΔE Max	1.991	2.931	2.548	1.075	4.537
ΔE 95%	1.000	1.427	1.383	0.7021	1.751
ΔRGB Mean	0.00674	0.00905	0.00720	0.00332	0.00552
ΔRGB STD	0.00542	0.00740	0.00553	0.00220	0.00610
ΔRGB Max	0.02984	0.03954	0.03141	0.01438	0.04036
ΔRGB 95%	0.01545	0.02081	0.01642	0.00597	0.01907

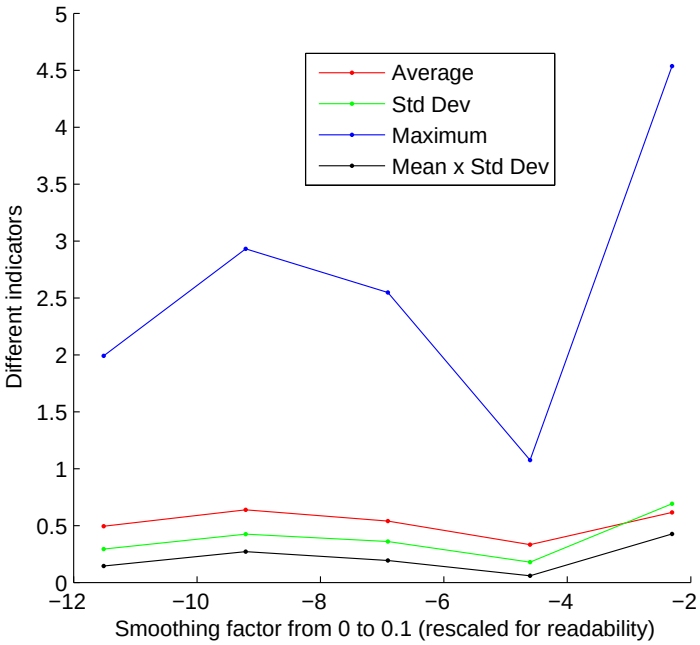

Figure 6.5: *Influence of the smoothing factor choice on different indicators based on Table 6.4.*

The measurement process took about 5 minutes and the optimization process took 2 minutes (with a 4 cores processor). We reached our goal, which was to provide an optimal model in a reasonable time.

Our different experiments showed that a 216 patches learning set was a good compromise (equivalent to a $6 \times 6 \times 6$ sampling of the *RGB* cube). A smaller data set gives

Table 6.5: *Accuracy of the model established with 216 patches in forward and inverse directions for a LCD Wide Gamut display (HP2408w). The distribution of the patches improves the model accuracy.*

	Forward model		Inverse model	
	ΔE Mean	ΔE Max	ΔRGB Mean	ΔRGB Max
Optimized	1.057	4.985	0.01504	0.1257
Uniform	1.313	9.017	0.01730	0.1168

Table 6.6: *Accuracy of the model established with 216 patches in forward and inverse directions for a CRT display (Mitsubishi SB2070). The distribution of the patches improves the model accuracy.*

	Forward model		Inverse model	
	ΔE Mean	ΔE Max	ΔRGB Mean	ΔRGB Max
Optimized	0.332	1.075	0.00311	0.01267
Uniform	0.435	1.613	0.00446	0.01332

us a degraded accuracy, a bigger gives us similar results because we are facing the measurement problems introduced previously.

6.5.3 Optimized learning data set

Table 6.5 and Table 6.6 show the results obtained with our model for two displays of different technologies. These tables show how the optimized learning data set can produce better results with the same number of patches. The improvement is not significant for a end user applications, but for specific ones it may be critical.

6.5.4 Results for different displays

Table 6.7 presents different results obtained for 3 other displays (2 LCD and 1 CRT).

Considering the thresholds presented in Chapter 2, we can see here that our model gives very accurate results on a wide range of displays.

Table 6.7: *Accuracy of the model established with 216 patches in forward and inverse directions for three other displays. The model performs well on all monitors.*

	Forward model		Inverse model	
	ΔE Mean	ΔE Max	ΔRGB Mean	ΔRGB Max
EIZO CG301W (LCD)	0.783	1.906	0.00573	0.01385
Sensy 24KAL (LCD)	0.956	2.734	0.01308	0.06051
DiamondPlus 230 (CRT)	0.458	2.151	0.00909	0.06380

6.6 Application to multispectral images of art paintings

6.6.1 Project background

The CRISATEL European Project (Ribés et al., 2005) opened the possibility to the C2RMF of acquiring multispectral images through a convenient framework. They are now able to scan in one shot a much larger surface than before (resolution of 12000×20000) in 13 different bands of wavelengths from ultraviolet to near infrared, covering all the visible spectrum. The multispectral analysis of paintings, via a very complex image processing pipeline, allows them to investigate a painting in ways that were totally unknown until now (Colantoni et al., 2007). Manipulating these images is not easy considering the amount of data (about 4GB by image). One can either use a pre-computation process, which will produce even bigger files, or compute everything on the fly. The second method is complex to implement because it requires an optimized (cache friendly) representation of data and a large amount of computations. This second point is not anymore a problem if we use parallel processors like graphic processor units (GPU) for the computation. For the data, a traditional multi-resolution tiled representation of an uncorrelated version of the original multispectral image is used. The computational capabilities of GPU have been used for other applications such as numerical computations and simulations (www.gpgpu.org, 2009). The work of Colantoni et al. (2003) demonstrated that a graphic card can be suitable for color image processing and multispectral image processing.

This application aims to produce an accurate color rendering of multispectral images of paintings on a display, considering a given illuminant. The workflow is summarized in Figure 6.6.

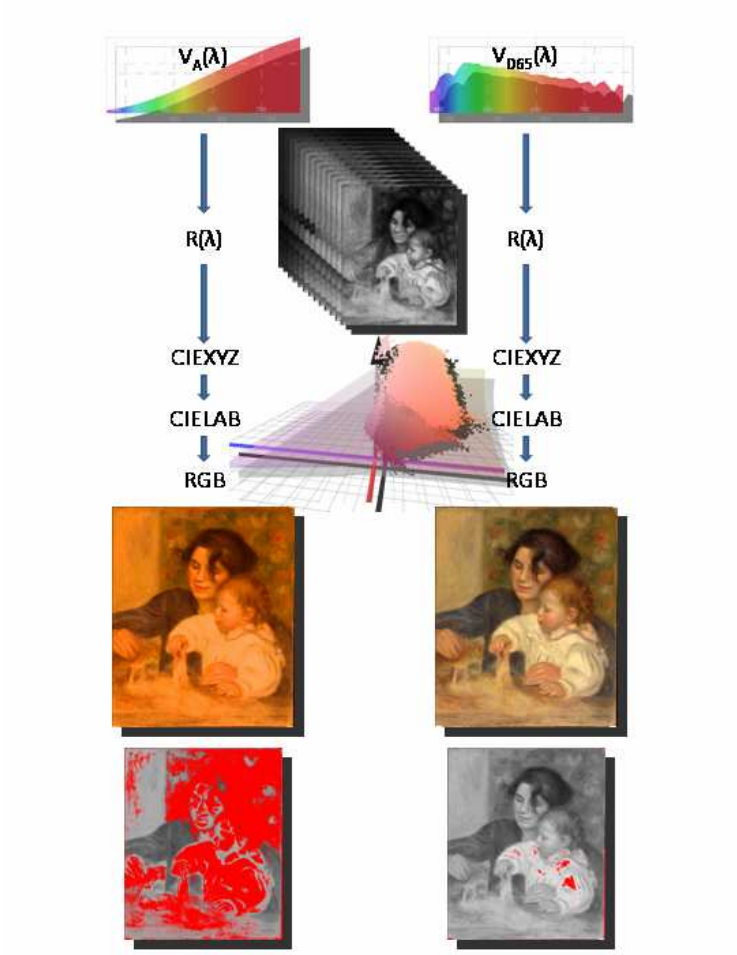

Figure 6.6: *Color rendering workflow for two different illuminants. The last images show the clipped colors in red. The display used can render this painting inside gamut for a D65 illuminant. However half of the colors present in the image are outside the display's gamut if we consider a A illuminant.*

6.6.2 Input color data

The CRISATEL project produces 13 planes multispectral images, which correspond to the following wavelengths: 400, 440, 480, 520, 560, 600, 640, 680, 720, 760, 800, 900 and 1000nm. Only the 10 first planes interact with the visible part of the light. Considering this, we can estimate the corresponding *CIEXYZ* tri-stimulus values for each pixel of the source image using Equation 6.1:

$$\begin{cases} X = \sum_{\lambda=400}^{\lambda=760} x(\lambda)R(\lambda)L(\lambda) \\ Y = \sum_{\lambda=400}^{\lambda=760} y(\lambda)R(\lambda)L(\lambda) \\ Z = \sum_{\lambda=400}^{\lambda=760} z(\lambda)R(\lambda)L(\lambda) \end{cases} \tag{6.1}$$

where $R(\lambda)$ is the reflectance spectrum and $L(\lambda)$ is the light spectrum (the illuminant).

Using a GPU implementation of this formula we can compute in real-time the *CIEXYZ* and the corresponding *CIELAB* values for each pixel of the original multispectral image with a virtual illuminant provided by the user (CIE standard or custom illuminants).

If we want to provide a correct color representation of these computed *CIEXYZ* values, we must apply a color management process, based on the color characterization of the display device used, in our color flow. We then have to find the *RGB* values to input to the display in order to produce the same color stimuli than the retrieved *CIEXYZ* values represent; or at least the closest color stimuli according to the display limits.

6.6.3 Gamut mapping

A gamut mapping[2] (GM) pre-processing step is applied to the *CIEXYZ* values computed from the multispectral image (cf section 6.6.2), such as $XYZ' = GM(XYZ)$ or $LAB' = GM(XYZ)$. The choice of the GM algorithm depends on the purpose.

For instance, in our application, to ensure an accurate colorimetric rendering, considering *CIELAB* color space, and low computational requirements, we use a geometrical gamut clipping method. This method is based on the pre-computed tetrahedral structure (generated in our inverse model) and more especially on the surface of this geometrical structure (see figure 6.3).

The clipped color is defined by the intersection of the gamut boundaries and the segment between a target point and the input color. The target point used here is an achromatic *CIELAB* color with a luminance of 50. A different gamut mapping algorithm could be used depending on the purpose, but the choice is reduced here considering the need of real time rendering.

6.6.4 GPU-based implementation

This color management method is based on a conversion process that will compute for *CIEXYZ* values the corresponding *RGB* values.

It is possible to implement the presented algorithm with a specific GPU language, like CUDA, but the software will only works with CUDA compatible GPU (nVIDIA^{TM} G80, G90 and GT200). The goal was to have a working application on a large number of GPU (*AMD* and nVIDIA^{TM} GPUs), for this reason we chose to implement a classical method using a 3D lookup table.

[2]The aim of gamut mapping is to ensure a good correspondence of overall color appearance between the original and the reproduction by compensating for the mismatch in the size, shape and location between the original and reproduction gamuts.

During an initialization process we build a three dimensional *RGBA* floating point texture, which covers the *CIELAB* color space. The alpha channel of the *RGBA* values saves the distance between the initial *CIELAB* value and *CIELAB* value obtained after the gamut mapping process. If this value is 0, the *CIELAB* color is in the gamut of the display, otherwise, this color is out gamut and we are displaying the closest color according to our gamut mapping process. This allows us to access and/or display in real time the color errors due to the screen inability to display every visible colors.

Finally the complete color pipeline includes: a reflectance to *CIEXYZ* conversion (considering an illuminant given by the user) then a *CIEXYZ* to *CIELAB* conversion (using the white of the screen as reference) and our color management process based on the 3D lookup table associated with a tri-linear interpolation process.

6.7 Conclusion and further work

We proposed a new color display characterization model that consists in an optimal combination of measured samples and interpolation settings. We presented a part of a large multispectral application used at the C2RMF. It has been shown that it is possible to implement an accurate color management process even for a real time color reconstruction. We showed a color management process based only on colorimetric consideration. The next step is to introduce a color appearance model in the color flow. The use of such color appearance model, built up on our accurate color management process, would allows the C2RMF to do color accurate virtual exhibitions of painting.

This method aims to provide a professional accurate color characterization. We can see that it does that on all tested displays. This method is fully automatic and could be used for consumer characterization as well. However, it requires a large number of measurements and a color framework based on GPU to be performed in real time.

Chapter 7

Geometrical model inversion

Je vais apprendre demain à me tenir sur les mains
J'irai pas très vite bien sûr mais je n'userai plus de chaussures.
Je verrai le monde de bas en haut c'est peut-être plus rigolo.
Je n'y perdrai rien par surcroît:
Il est pas drôle à l'endroit.

Jean Boyer

Abstract

This chapter proposes a method for the inversion of characterization models using 3D LUTs. We focus on patches distribution in RGB to perform a linear tetrahedral interpolation from CIELAB or alternatively CIEXYZ to RGB. We used the PLVC model as forward model to create this LUT and to present quantitative results.

7.1 Introduction

A method to distribute patches in a reference color space for geometrical model inversion is proposed and evaluated. It is shown that the relative accuracy gain may be not negligible. The motivation and background of this work can be found in Chapter 3.3.3. The results given in this section are based on the PLVC model that is used as testing model. However any forward model can be used. In the former section, we designed an inverse model based on a grid in *RGB* that leads non-uniform interpolation error, because of the non-linearity of the transform from *RGB* to *CIELAB*. The goal of this section is to present a new method to distribute patches in the destination space, i.e. *RGB* for yielding the inverse function of a characterization model.

7.2 Method proposed

Beginning with a regular grid in the destination space, our goal is to transform this regular cubic structure into a rectangular one, in order to make it more uniform or better in the source space. We propose to approximate an homogeneous grid in the source space using only a few number of parameters. Note that this approach resembles, but differs from the existing methods in the way that we do not modify the grid in the source space but directly and firstly in the destination space. This leads to some differences:

- First, no gamut mapping is required to map the points that rise up outside the gamut during the creation of a grid in the source space.
- Secondly, the grid is taken in its globality and we will not reach a perfect uniformity in the source space, only a rough approximation of it, depending on the function we use. We suppose that it should be enough to increase the accuracy.
- Thirdly, the order between data is preserved, which leads to an easier indexation of the tetrahedra.

In order to build a more uniform grid in the source color space, we propose to assume that:

- The number of steps has not necessarily to be the same along each primaries in the destination space, then $N_r \neq N_g \neq N_b$.
- The steps have not to be regularly spaced along a primary in the destination space, but they can be defined such as $R_i = f_r(d_i), G_j = f_g(d_j), B_k = f_b(d_k)$, considering $f \in \{f_r, f_g, f_b\}$, a monotonically increasing function from $\mathcal{R}$ to $\mathcal{R}$:

$$f : \begin{cases} [0,1] \longrightarrow [0,1] \\ d \longrightarrow f(d) \end{cases} \tag{7.1}$$

.

f could be any simple function, either a power function with one constant parameter or an S-shaped curve function with one to three constant parameters. Let us say that this function has M parameters, then the number of parameters used to set-up the distribution of the grid points is $P = 3 \times M$.

We make the hypothesis that if we can find the good function f, and the good number of steps, different for each primaries, the structure defined by the 3-D grid will become more homogeneous in the source space and will allow us to have a better inversion map. By extension, we assess that if we can build a *better* grid in the source space, the inversion will become better. The purpose of the next section is to define what a better grid is.

7.2.1 Estimation of the grid quality

A better grid can be defined in various ways. The straightforward way to assume that a grid is better is to assume that it is more regular in the source space, then some geometrical indicators should be used as cost functions to estimate the function f. It could also be a structure well designed for a given application, then an evaluation data set could be required. For a given number of steps along each channel, we have P values to optimize. The optimization process enables us to re-distribute the steps in the destination space, so we adapt the tetrahedral structure in the source space. We propose below three criteria as cost functions. One is directly linked with the geometrical structure of the grid. Others are linked to the result of the inverse model for an evaluation set of patches.

Criterion defined by the geometrical properties of the structure:

The first type of cost functions we consider contains the functions directly characterizing the geometry of the grid. We chose to use an indicator that aims to ensure the tetrahedra to have the same shape. The one we have used is the variance of the length of the tetrahedron's edges of the geometrical structure in the source space. If we minimize this function, the tetrahedron of the grid will have more or less the same shape. It is also possible to aim at the maximization of the volume of the tetrahedra, or the surface of each face. In this case, we need to use two combined indicators: the maximization of the volume/surface and the minimization of their variance. We decided that minimizing the standard deviation of edges length was more simple for the same result. Using this

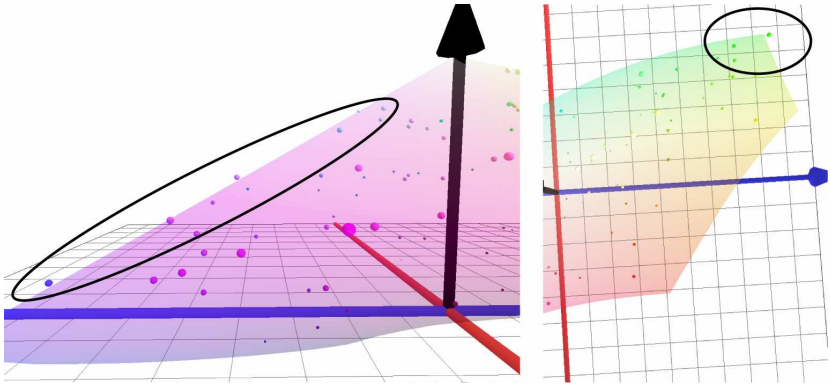

Figure 7.1: *The gamut generated with the PLVC forward model does not correspond exactly with the device gamut. Then some colors inside the true device gamut have to be mapped inside the geometrical structure to be transformed into RGB values. On these figures, one can see that some measured colors defined by some RGB values does not belong to the gamut defined by the forward model.*

criterion, we want to reduce the heterogeneity of the interpolation error throughout the space, and so to minimize the error of the model. We call this criterion *Edges* in the following.

Criteria linked with an evaluation data set:

The cost functions of the second type affect the structure indirectly. We used an evaluation data set and tried to minimize either the maximum error or the average error of the model for this data set. The evaluation data were 100 measured patches equiprobably distributed in the destination space. We call the two criteria *Mean* and *Max* in the following.

A remark has to be done first about the choice of the evaluation data set. As the data are distributed in the destination space, they are not well distributed in the source space. That means that, depending on the indicator, these data are not the best to try to homogenize the grid in the source space. If the goal is to homogenize the grid in the source space, then the data set has to be equiprobably distributed in this space. However, minimizing the feature for an evaluation data set optimizes the grid for instance for a special type of images or for a sequence of a movie for one given device.

A second important thing to notice here is that even if the color of the training (or evaluation) data set belongs to the gamut of the device, since they are defined in RGB, it is not obvious that it belongs to the gamut defined by the forward model (see Figure 7.1). Indeed, due to some forward models failure, some colors could be out of the grid; thus, a gamut mapping process is required. For instance, if the forward model

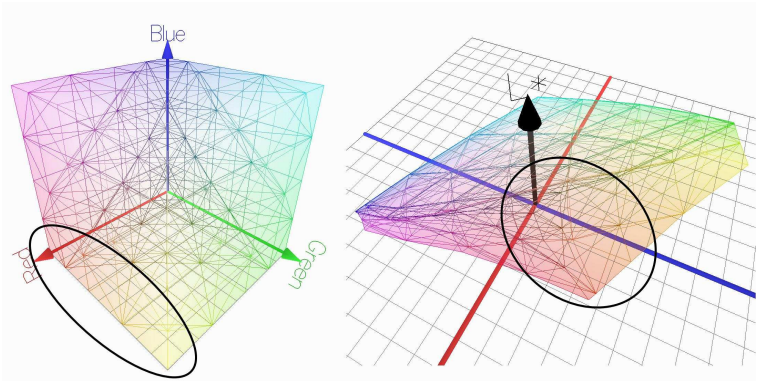

Figure 7.2: *Tetrahedral structure based on a regular grid,* $N_{rgb} = 15$ *and* $\alpha = 1.23, \beta = 1.27, \gamma = 1$ *obtained for the criterion Mean in RGB (left) and its transform in CIELAB (right).*

does not take into account interaction between channels, some colors could have more (or less) luminance than the forward model can predict and then be outside of the grid. In one of our study (Thomas, Colantoni, Hardeberg, Foucherot and Gouton, 2008*b*), we noticed that the optimization algorithm was trying to refine the grid around these colors. For some displays, a critical maximum error was coming from the mapping of a color from the evaluation data set. This effect appears especially for the *Max* criterion.

Since the model and the features seem not to be directly related with a derivable function, we chose a numerical optimization method. We used the globalized Nelder-Mead simplex downhill algorithm (Gill et al., 1982). This fits well with our problem, and we can use it easily with P variables to optimize. Let us notice that $criterion = G(p)$ is the function to minimize, with p a vector of dimension P. To give an example: Let us consider $N_{rgb} = 15$, $N_r = N_g = N_b = 5$. In minimizing the aforementioned functions, we can retrieve the best parameters α, β, γ of a power function, respectively, for each channel R, G, B, which will allow to define our definitive structure (p = [α, β, γ]). In Figure 7.2, the cost function *Mean* has been used, and the results obtained are a mean error of 4.13% and a maximum error of 18.83% in RGB, for a testing data set of 100 patches, while the original regular grid with the same number of patches gives a mean error of 4.50% and a maximum error of 20.79%.

7.2.2 Distribution of the grid seed

In this section, we first discuss the functions we used to modify the distribution of the grid seeds along the R, G, and B axis, with an equal number of data for each axis. We then discuss the number of points that should be used along each axis, considering that these numbers could be different. We separated these steps in two different algorithms to see the influence of each of these. Both are then combined in a practical case in

Section 7.3.3.

Static changing of the grid morphology:

To redistribute the grid seeds along each channel, we used either a simple power function or an S-shaped curve. For both cases, we have fixed the condition $N_r = N_g = N_b$, in order to limit the number of parameters and for modeling purpose. Let us investigate on the criteria used to find the function parameters and on the value of N_{rgb}.

- Power function: the grid seeds are expressed as $R_i = d_i^{\alpha}$, $G_j = d_j^{\beta}$, $B_k = d_k^{\gamma}$. As our digital values are normalized, the power function follows the requirements defined in Equation 7.1. There are three parameters to optimize.

- S-shaped curve function: the grid seeds are expressed as:

$$\begin{aligned} &if\ d_i < 0.5,\ R_i = \frac{(2d_i)^{\alpha}}{2},\ else\ R_i = 1 - \frac{[2(1-d_i)]^{\alpha}}{2}, \\ &if\ d_j < 0.5,\ G_j = \frac{(2d_j)^{\beta}}{2},\ else\ G_j = 1 - \frac{[2(1-d_j)]^{\beta}}{2}, \\ &if\ d_k < 0.5,\ B_k = \frac{(2d_k)^{\gamma}}{2},\ else\ B_k = 1 - \frac{[2(1-d_k)]^{\gamma}}{2}, \end{aligned} \tag{7.2}$$

  such that the curve stays inside $[0, 1]$. There are as well three parameters to optimize. Note that we chose a simple expression for the sigmoid, in order to have only one parameter for each channel to optimize. This reduces the freedom of the function, but makes the method easier to explain and understand.

Let us illustrate the method. Using a power function, the grid is defined by N_{rgb} and by the optimization of α, β, γ values. Figure 7.2 illustrates this construction for $N_{rgb} = 15$, i.e. $N_r = N_g = N_b = 5$. Using the criterion *Mean* , we found $\alpha = 1.23$, $\beta = 1.27$, $\gamma = 1$.

Spreading of the grid seeds:

An equal number of steps along each R, G, and B channel is not sufficient a priori to reach the homogeneity in *CIELAB*, even if they are not distributed linearly. Thus, we propose a second way to build the geometrical structure, which consists in distributing the steps along each channel in the best way whithout the condition $N_r = N_g = N_b$. We used a brute force approach for this task. Given a number of points, we tried the possibilities sequentially such as $N_{rgb} = N_r + N_g + N_b$ and we selected the best combination, considering the chosen cost function. To study the effect independently of the previous proposition, we distributed in a first time the steps regularly along each channel.

7.3 Results

We have defined two ways to build a geometrical structure considering a given criterion. One is based on the static changing of the morphology of the grid in the destination space. The other focuses on the number of steps along each axis in the destination space. In this section, we present the results obtained for each method developed to study the influence of both distributions. We study these methods relatively to the total number of steps used to build the grid. We then present a practical case where the two methods are combined to build the best geometrical structure considering the distribution of the points in the destination space for a given number of points and for a given criterion. In order to analyze the results, we have chosen the PLVC as forward model that assumes independence between channels, but takes into account the chromaticity shift of primaries. In this work, the $[A(d_i(j)) \in Ak]$, were obtained using Akima spline interpolation (Akima, 1970) with the measurement of a ramp along each primary. Note that any 1-D interpolation can be used. Practically, we used a bounding box centered on the color we wanted to display to determine the tetrahedron it belongs to. Then a linear tetrahedral interpolation is performed (Kasson et al., 1995), such as in the previous section. In the case of a point out of the grid, i.e., out of gamut, we performed a simple clipping toward the 50% luminance. Since our data set is defined in RGB, the gamut clipping happens only when the forward model fails. We show and discuss results obtained for the inversion of the PLVC model. We tested the algorithms on three displays, a tri-LCD projector 3M-X50 (PLCD), a CRT monitor Philips 107s (MCRT), and a LCD monitor DELL 1905FP (MLCD). The measurements of the color patches were taken using the spectroradiometer CS-1000 from Minolta.

7.3.1 Static changing of the grid morphology

This part discusses results of the first method proposed in Section 7.2.2. We consider an equal number of steps along each primary, and we distribute them using a function, which parameters were found using an optimization process. In Figure 7.3, one can see the evolution of the accuracy of the model in function of the number of steps used. All combinations between the functions and the criteria used are presented. The reference is the regular grid.

In general, it is hard to say that one criterion combined with one type of function performs much better than the other possibilities. The criterion *Edges* does not seem to give really good results neither in average nor in maximum error except for the CRT display when it is combined with the S-shaped curve. It is possible that this is the result of the testing data set, which was equiprobably spreaded in RGB. For PLCD (Figure 7.3, a), criteria based on a training data set gives equal or better results than the regular grid,

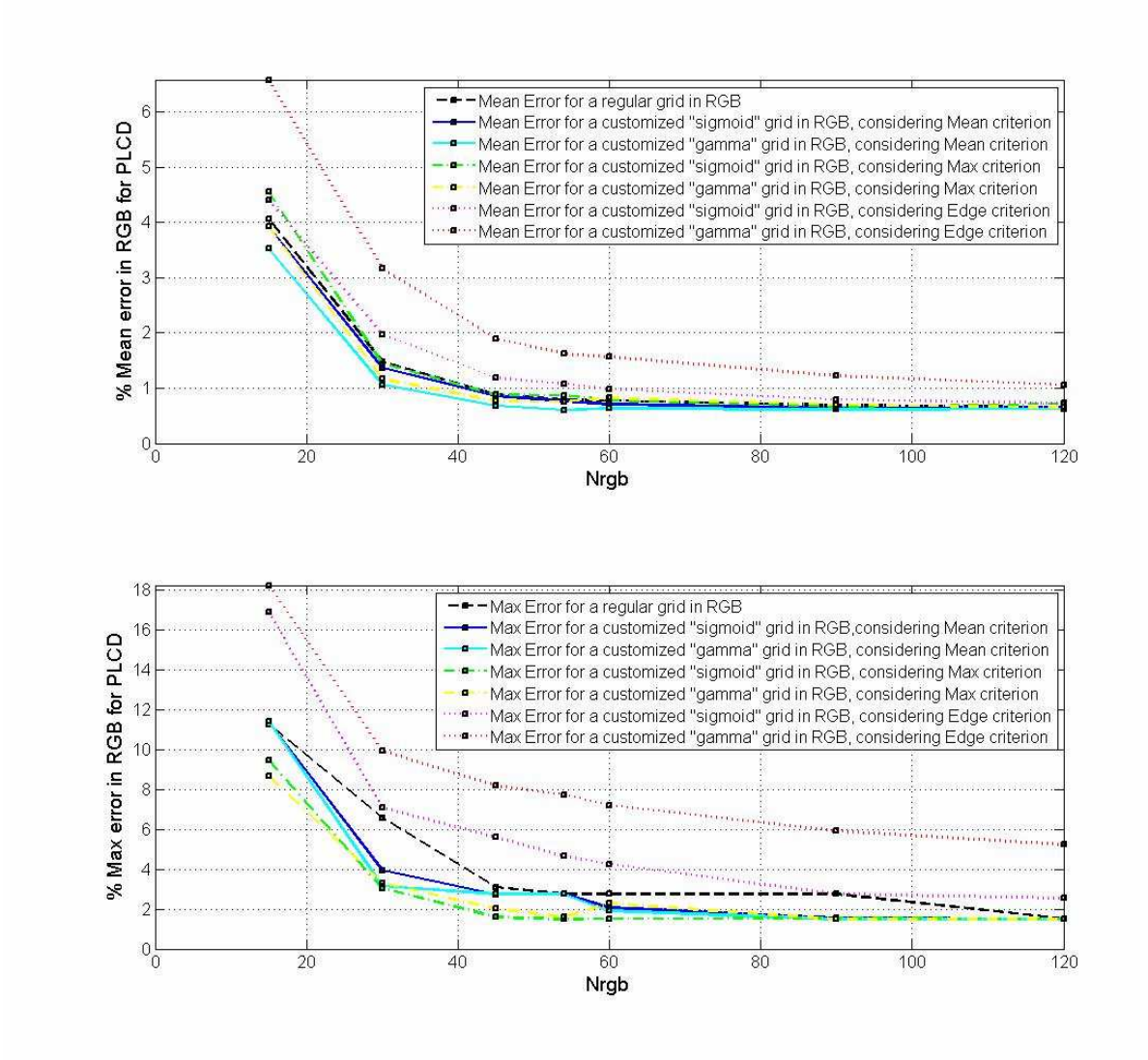

a

Figure 7.3: *Results obtained with the geometrical model in function of the total number of steps used. The three cost-function Mean, Max, and Edges and the two functions proposed were used on the three displays: (a) PLCD, (b) MLCD, and (c) MCRT. The mean error in percentage in RGB is shown on the upper part of each figure, the maximum error is shown on the bottom. One can see that the sigmoid function with the Mean criterion performs generally better than the others for both the maximum and the mean error.*

generally following the cost function used. However, one can see that the combination of the criterion *Max* and a power function gives a good compromise in both the average and maximum error for this display. This combination performs better than a regular grid. The difference is major for a reduced grid; for instance, with $N_{rgb} = 30$, the regular grid gives an average error of about 1.5%, the *Edges* criterion an error of 2% to over 3%

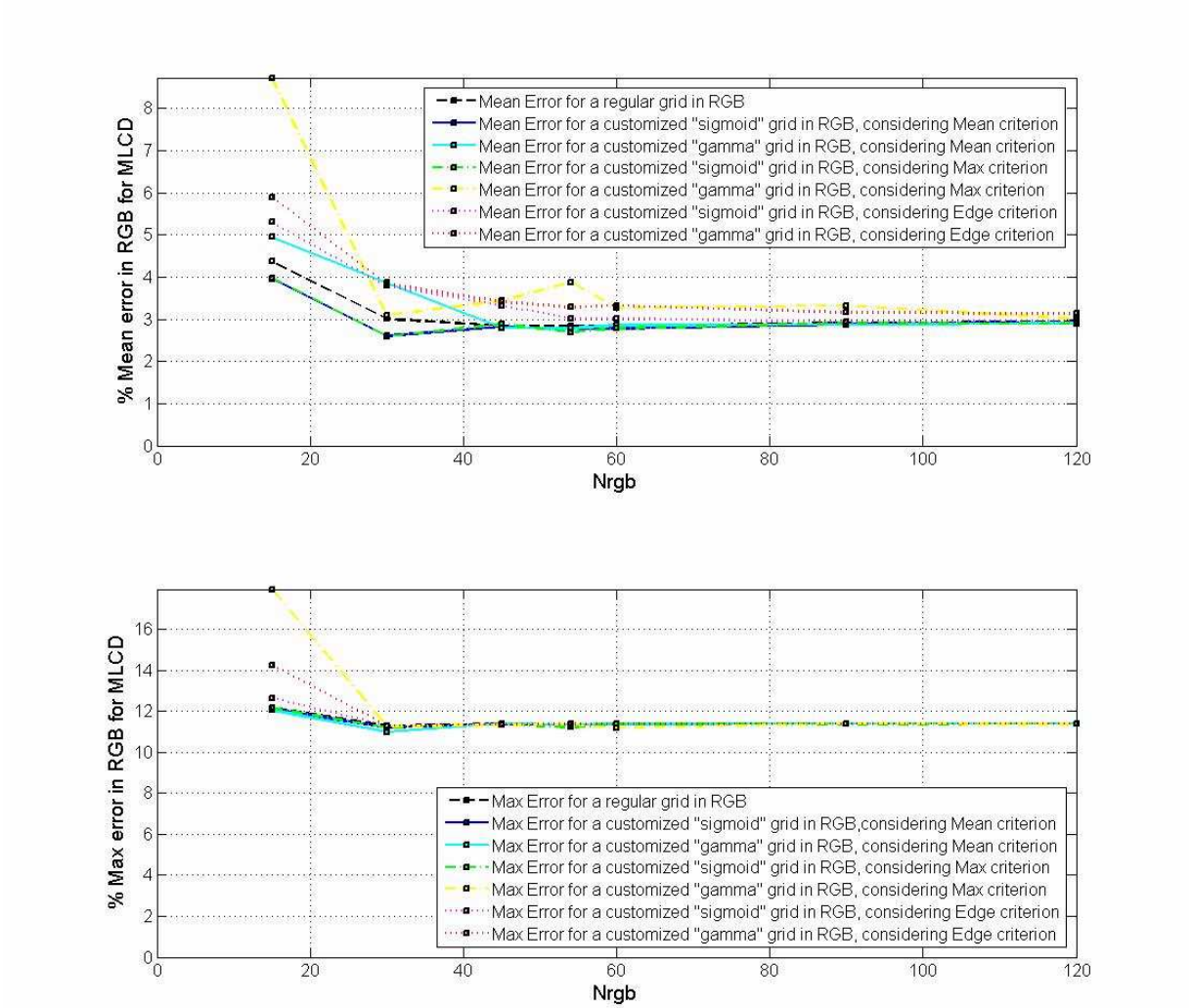

b

Figure 7.3: *Results obtained with the geometrical model in function of the total number of steps used. The three cost-function Mean, Max, and Edges and the two functions proposed were used on the three displays: (a) PLCD, (b) MLCD, and (c) MCRT. The mean error in percentage in RGB is shown on the upper part of each figure, the maximum error is shown on the bottom. One can see that the sigmoid function with the Mean criterion performs generally better than the others for both the maximum and the mean error.*

depending on the function used, while all the other methods with the *Mean* and the *Max* criteria give an average error of 1-1.5%. If we look at the maximum error for the same N_{rgb}, the regular grid gives an error over 6.5%, the refinement of the grid using the training data set gives an error of 3-4%. That means that we reduced the maximum error by a factor of two for this case. The criterion *Edges* gives a maximum error higher than

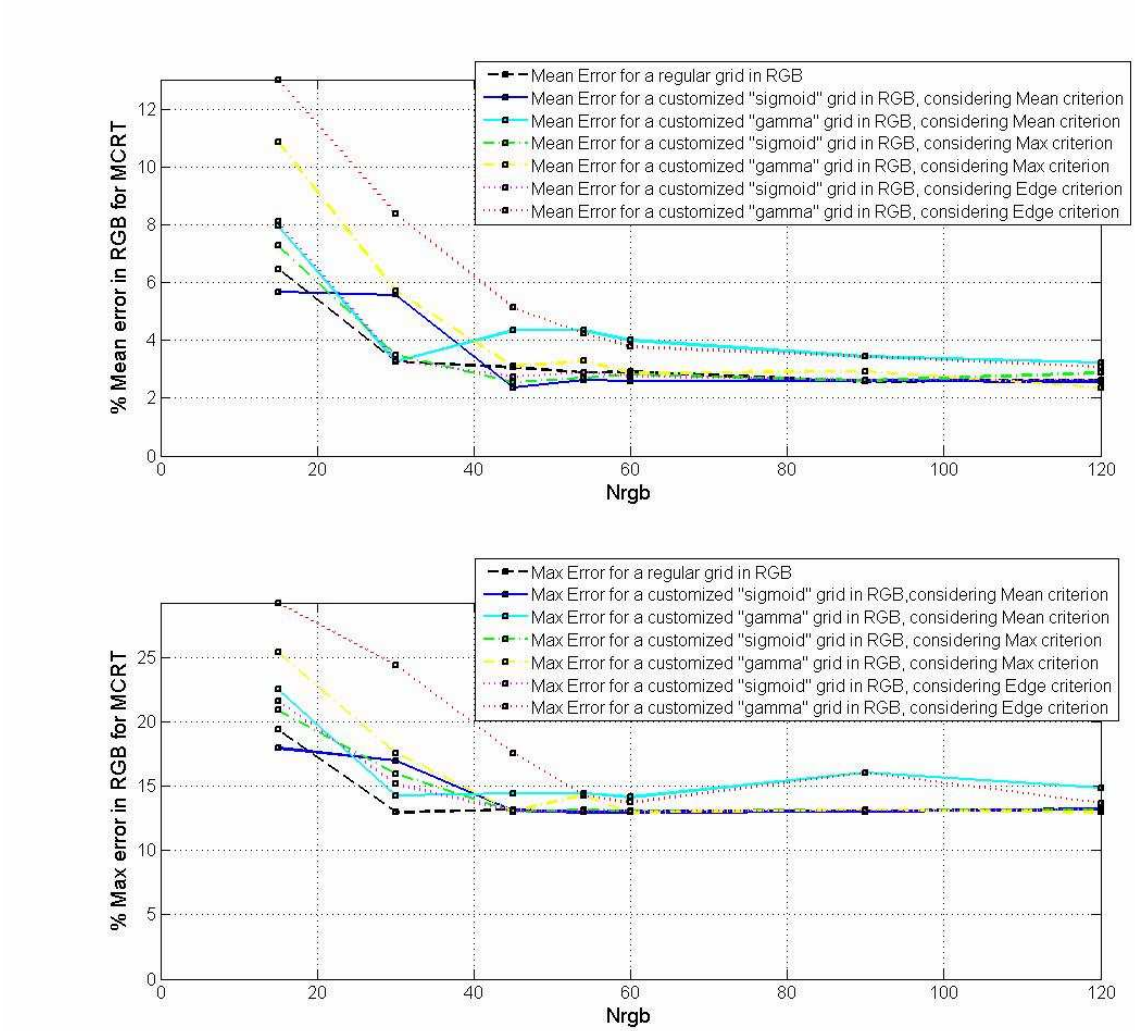

c

Figure 7.3: *Results obtained with the geometrical model in function of the total number of steps used. The three cost-function Mean, Max, and Edges and the two functions proposed were used on the three displays: (a) PLCD, (b) MLCD, and (c) MCRT. The mean error in percentage in RGB is shown on the upper part of each figure, the maximum error is shown on the bottom. One can see that the sigmoid function with the Mean criterion performs generally better than the others for both the maximum and the mean error.*

the error of the regular grid. For MLCD (Figure 7.3, b), we notice the fast convergence of the maximum error for all methods (the regular grid included). This is possibly due to the gamut mapping due to the failure of the forward model. For this device and $N_{rgb} = 30$, we notice that the sigmoid used gives better results than the regular grid (from around 3-2.6%) whatever the *Max* or *Mean* criterion we used. MCRT (Figure 7.3,

c) shows that, on this device, the regular grid gives better results than the others and that *Edges* criterion seems to perform well on it, combined with a S-curve. However, if we look at the results for $N_{rgb} = 45$, the sigmoid combined with the criteria based on the training data set gives better results, reducing the error from 3% to 2.4 and 2.5%. When the number of points increases, all methods seem to converge. All are going towards the same accuracy. Note that the *Edges* criterion combined with a power-shaped curve converge more slowly than the other for PLCD. Looking at these data, we can not say in general: *this criterion and this function is the best combination for any display*. In particular, for a given amount of steps, a difference appears, but nothing that can be generalized.

The algorithm can fall into local minima for the *Mean* and more often for the *Max* criterion, depending on the seeds given for the optimization. However, the *Edges* criterion is very stable despite a not so good general result. The fall into local minima explains the shape of the curves that are not, in many cases, monotonically decreasing with increasing N_{rgb}.

7.3.2 Spreading of the grid seeds

This subsection discusses results obtained with the second method proposed in Section 7.2.2. Considering the total number of steps, we distributed them along each channel such that the cost function is minimized. However we do not discard this criterion, because it can be valuable for other displays or other evaluation data sets.

Looking at Figure 7.4, it appears that the *Mean* criterion performs slightly better than the *Max*, since the convergence of the maximum error is fast.

However, for PLCD (Figure 7.4,a), the average error remains quite similar for the three methods used and, a better compromise provided by the *Mean* criterion, the *Max* criterion permits a slight reduction in the maximum error (from twice to once if we look at a grid of $N_{rgb} = 60$, comparing it with the regular grid). For MLCD and MCRT (Figure 7.4, b and c), the maximum error converges fast, and the *Max* criterion seems to be weak. Looking at the results for the *Mean* criterion, one can say that it follows the regular grid for MLCD. However, it decreases the average error for a midsized grid of $N_{rgb} = 45$ with MCRT from 3.2 to 2.7%.

7.3.3 A practical case

In this section, we propose to evaluate a practical case, combining both approaches previously defined. We fixed a number of steps $N_{rgb} = 90$ that appears to us to be a good compromise between the size of the structure and the optimization facilities: smaller, it is a loss of accuracy for nothing, bigger, there will be no interest in optimizing it; then a regular grid should be enough compared with the cost of the optimization. We retrieve

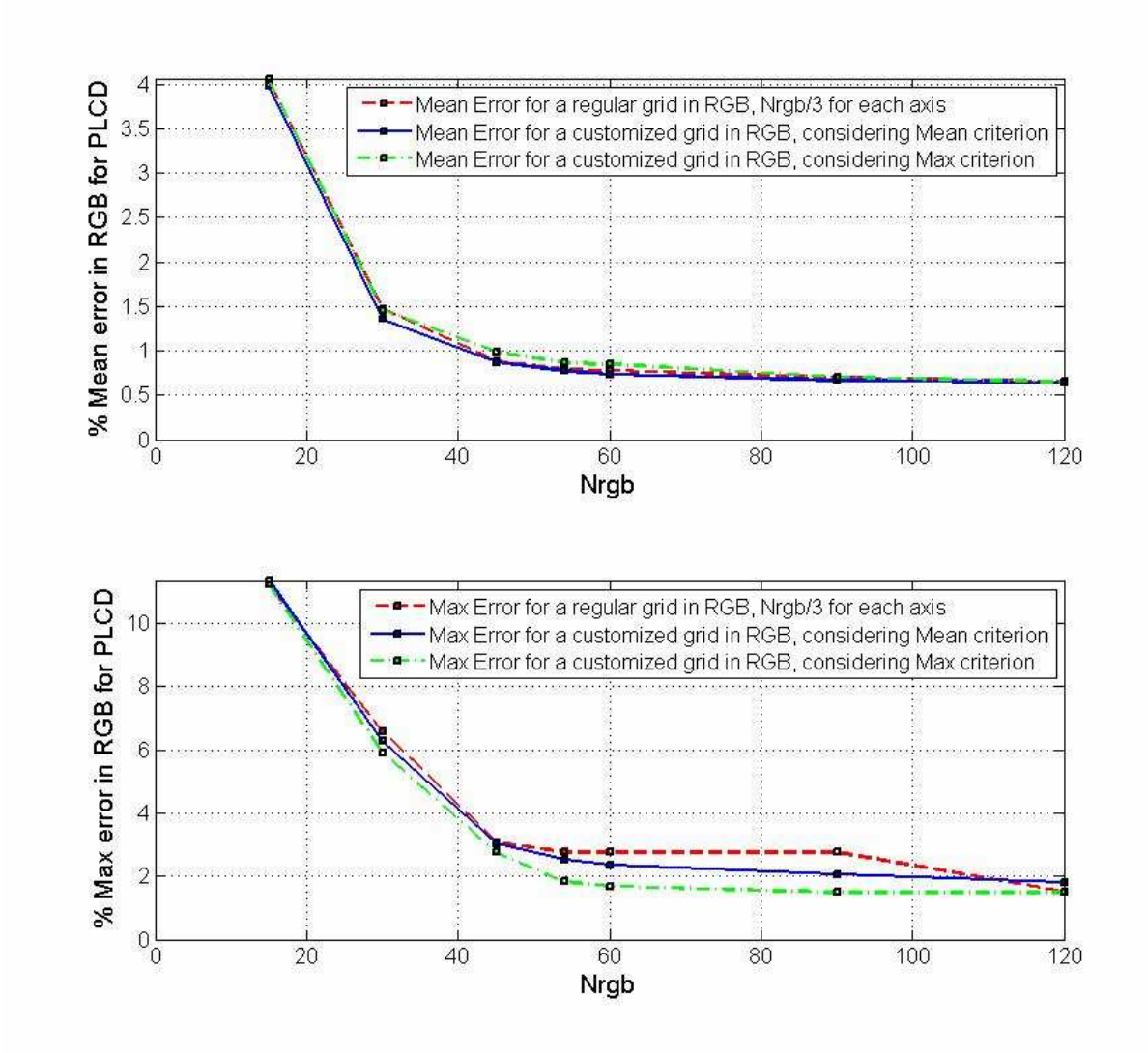

a

Figure 7.4: *Results obtained with the geometrical model in function of the number of steps used for the three displays: (a) PLCD, (b) MLCD, and (c) MCRT tested. The two cost functions Mean and Max were used to find the best number of steps along each channel. The mean error in percentage in RGB is shown on the upper part of the figure, the maximum error is shown on the bottom.*

the best function to define each axis of the destination space, considering the different criteria. We have chosen to select the best one with regard to the mean error estimation, but it is also possible to consider that the maximum error is more important, depending on the application. We keep both the power and the sigmoid functions. We then look for the best spreading of steps along channels, still with regard to the mean error of the model. The result gives us the optimized geometrical structure for this given number of

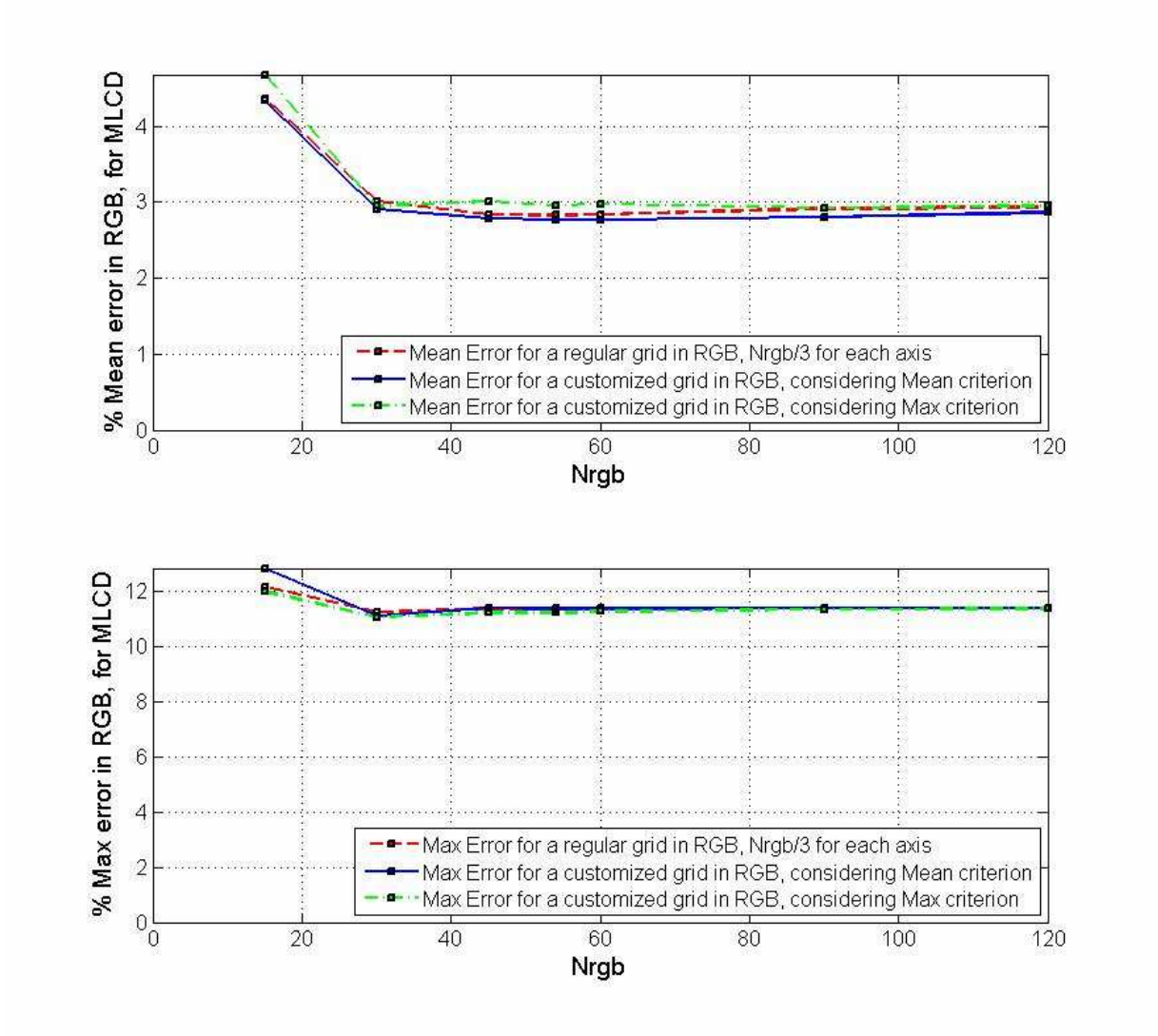

b

Figure 7.4: *Results obtained with the geometrical model in function of the number of steps used for the three displays: (a) PLCD, (b) MLCD, and (c) MCRT tested. The two cost functions Mean and Max were used to find the best number of steps along each channel. The mean error in percentage in RGB is shown on the upper part of the figure, the maximum error is shown on the bottom.*

points and for the display considered. We compare it with the regular grid, which is still our reference. Results of the inverse model estimation are presented in Table 7.1. This table shows that simply using the same amount of steps for each channel and a power or a sigmoid function to distribute them could be pretty efficient and could be the best solution for some displays, such as the MLCD where it is the best grid.

In this case, we reduce the error by 0.28%, which is relatively a gain of accuracy of

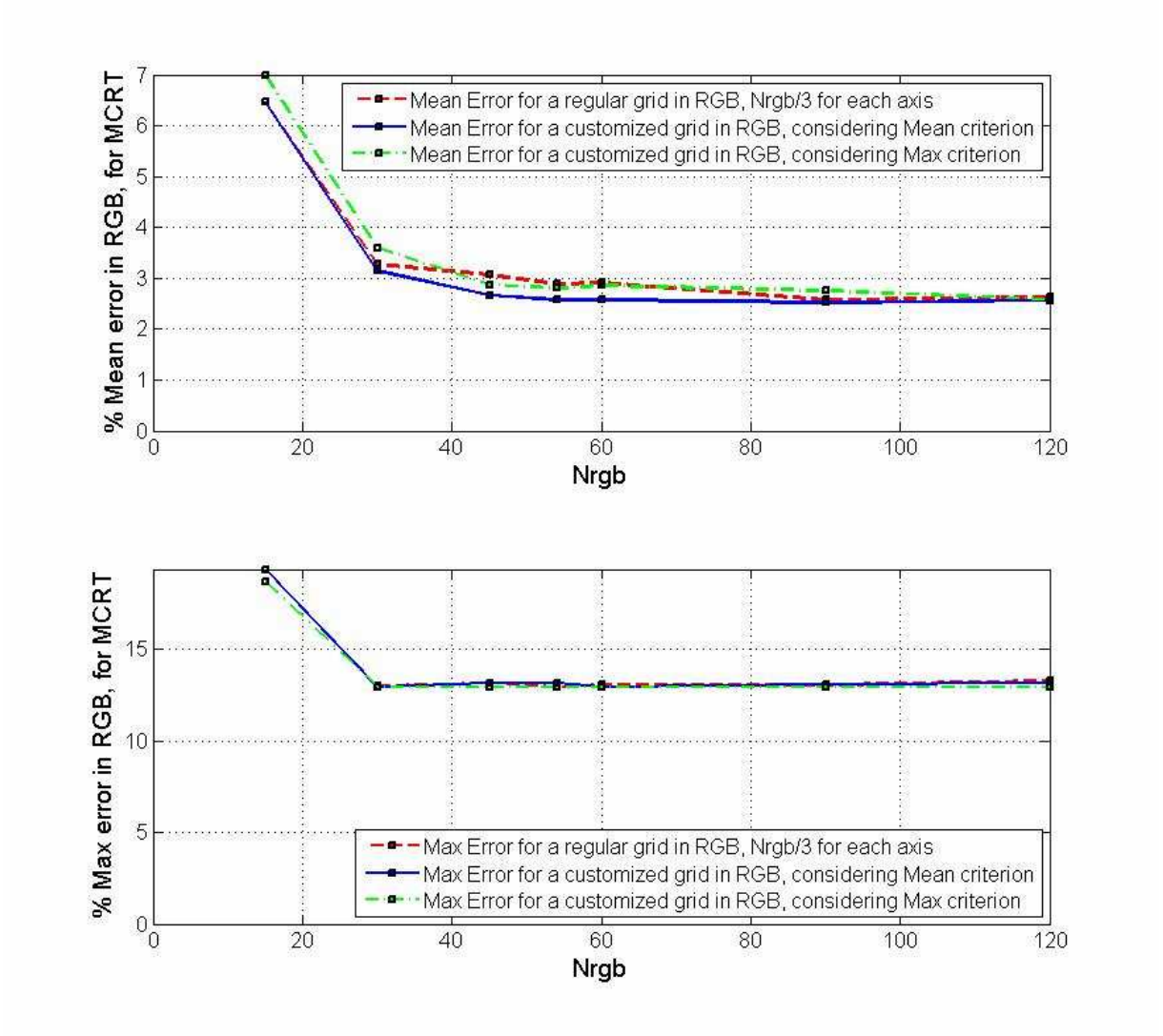

c

Figure 7.4: *Results obtained with the geometrical model in function of the number of steps used for the three displays: (a) PLCD, (b) MLCD, and (c) MCRT tested. The two cost functions Mean and Max were used to find the best number of steps along each channel. The mean error in percentage in RGB is shown on the upper part of the figure, the maximum error is shown on the bottom.*

almost 10%. Some accuracy can be won in spreading the steps after having applied the function, such as for the PLCD and MCRT. For the first one, we go from 0.69% with a regular grid to 0.66% using a power to 0.59% in spreading the steps, which is a relative improvement of around 15.5%. Note that for this display, before spreading, the best function to step the points is the sigmoid with an error of 0.64%, but after spreading the best result is given by the power function. In other words, the best function should not

Table 7.1: *A practical case, given $N_{rgb} = 90$, considering the criterion Mean and the different functions, we find the best grid for minimizing the average error for the three displays studied.*

% Error in RGB	Regular Grid		Gamma		Sigmoid		Linear +Spreading		Gamma +Spreading		Sigmoid +Spreading	
$N_{rgb} = 90$	Mean	Max	Mean	Max	Mean	Max	Mean	Max	Mean	Max	Mean	Max
PLCD	0.69	2.76	0.66	2.76	0.64	1.53	0.66	2.06	**0.59**	**1.22**	0.62	1.44
MLCD	2.91	11.40	2.87	11.40	**2.63**	**11.14**	2.81	11.41	2.86	11.41	**2.63**	**11.14**
MCRT	2.58	13.03	2.54	13.07	2.59	13.07	2.53	13.07	**2.50**	**13.00**	2.57	13.15

be chosen at the first step of the algorithm. For MCRT, we go from 2.58 to 2.54 using a power-shaped function to 2.50 in spreading the steps, showing a relative gain of 3%. The same analysis can be performed for the maximum error. In our data, the smaller maximum error found is when we use the same method, but it is not obvious that this will happen all the time. For instance, looking at MCRT with a sigmoid function and a spreading, the errors Mean and Maximum are 2.57 and 13.15, albeit the results for the linear distribution are 2.58 and 13.05. To summarize, with the displays we studied, we found a better LUT than the regular one in all the cases with a different gain in accuracy. We do not put aside that the regular grid can be the best one for a given display. In Table 7.2, we show the spreading of the steps along each axis.

Table 7.2: *Spreading of the grid seeds along each channel for the practical case studied.*

Seeds distribution	Linear +Spreading			Gamma +Spreading			Sigmoid +Spreading		
$N_{rgb} = 90$	N_r	N_g	N_b	N_r	N_g	N_b	N_r	N_g	N_b
PLCD	24	34	33	19	47	24	19	43	28
MLCD	49	21	20	40	31	19	30	30	30
MCRT	39	21	30	36	32	22	34	37	19

For the PLCD, it seems that the green channel requires a more accurate discretization than the two others, but looking at the other displays, this can not be generalized. It appears that in using a linear distribution or a power shaped one, the spreading takes quite the same shape, with different strengths. While in using a sigmoid, the spreading is totally different. Note that for the MLCD, the best spreading scheme is the equibal-

anced one. In general, it seems that no spreading scheme can be recommended a priori. To conclude with the obtained results, no a priori function or spreading scheme can be recommended. It has to be device dependent. Furthermore, it seems that it is not technology dependent, since the two LCDs show different behavior (but one is a projector, the other a monitor, so no hasty judgement should be taken). It appears that the best of the grids defined with our methods should be selected with a test, and actually this is what we do to assess their quality.

7.4 Conclusion and further work

We proposed some methods to build an optimized geometrical structure in order to invert any display color-characterization forward model. We used several criteria linked with the grid itself or with an evaluation data set. We focused on how to distribute the steps on the destination space axis in order to have the better grid in the source space, both in using a power or a sigmoid function and in spreading the steps in a non-uniform way along the axis. We studied a practical case, considering a forward model, a number of steps, and a feature to optimize for three displays. The results obtained with the proposed methods in the practical case are all better than the regular grid, and the relative gain in accuracy is not negligible, from 3% in the worst case to up to 15.5% in the best case.

This method first aims to increase the accuracy of the model inversion. It is firstly defined for a professional use. Depending on the criterion used, it may be of use for a consumer characterization. Indeed, if the criterion is not based on a training data set, the number of measurement or evaluation can remain low. However if it is based on a training data set, then the number of measurement can be a problem for some consumer methods.

Some further work could be done concerning the criteria used, especially for the ones related to the grid features, and on the training data set. Moreover, since the function used to distribute the steps on the axis could have more parameters, we are thinking about the function of higher order (monotonically increasing) or simply a more-complex S-shaped curve (such as in Equation 3.4). We also do believe that this method to build and select the optimized structure to invert the colorimetric model can be applied to any output color device, such as printers, perhaps with other functions.

Part II

Spatial issues for projection systems

Chapter 8

State of the art of color uniformity in multi-display systems

Ce que je cherche avant tout, c'est la grandeur : ce qui est grand est toujours beau.

Napoléon Bonaparte

Abstract

This chapter considers a bibliography that rose up at the end of the 90's. It considers the problem of achieving a large format display with high resolution and accurate color rendering, using multiple smaller display units. Much effort has been carried out to deal with geometric alignment but only a few works deal with colorimetric accuracy. We focus on the problem of spatial color uniformity and we explain existing models and methods, analyzing their strengths and weaknesses.

8.1 Introduction

This chapter introduces the high resolution, large scale display problematic. Why do we need such a display in an affordable solution? What are the features, advantages and drawbacks of the existing solutions? We describe many works that have been done on display color spatial uniformity. Some of these works consider one display, most of them consider the more general case of multi-display systems.

Napoléon Bonaparte said that he was *looking for what is big, because what is big is always beautiful*. In an intuitive way, we can then understand the interest of the idea of multi-display systems. This kind of display is potentially as large, as high resolution as one wants. In another word, a multi-display is as big as the user wants it to be. This intuitive way is confirmed by a user need: "I want to have a big display for designing a new car, where we could see it in real size." "I want to play a virtual game in real immersion." "I need to train my soldiers in a simulated virtual environment." "I would like to look at this flow of particles in real time with a high resolution, which will help me to understand." "My company wants to increase the developer productivity, providing them with several displays or with a large scale one.", etc.

The oldest multi-projector system that we have ever seen is at Mahaugen Museum in Lillehammer, Norway. This system is still working now and can be considered as archaique. It is displaying pictures one by one in an auditorium, summarizing Norwegian history. This system is made up of a 3×3 matrix of analog slide projection systems. These displays are combined 3 by 3 to display an image based on a row of three projectors. During the time the first image is explained by a voice, the next row is preparing the next image to be displayed.

Multi-displays systems have evolved fast with the need and applications are ranging from design, to scientific visualization, through entertainment and flight simulation. Three main applications are usually considered in the literature: immersive reality (originally for military applications and flight simulation), scientific visualization and collaborative working environment (Raskar et al., 1998; Santos et al., 2007; Wallace et al., 2005). Although the main problem was originally geometrical registration, the next issue, to make the user feel like there is only one single display, is color spatial uniformity. That will guarantee the seamlessness of the display. Of course, color is not *The solution*, and if the goal is to immerse the user inside a virtual *real world*, many considerations have to follow, such as sound, smell, touch, etc.

Lantz (2007) made the distinction between small, medium and large scale displays. He is stating that the last category has been developed with regard to commercial interest and is mostly invested in proprietary technology. That has reduced the accessibility to research community. However, it seems that now, companies and researchers are meeting with the expansion of this kind of display, for the evolution from flat screens

to spherical, for the need of immersion, and with the increasing capabilities of standard computer hardware and software (graphic cards, computer clusters, etc). There is a need of a convenient and accurate way to deal with the technical challenges of such a display.

For many applications with this kind of display, immersion is aimed. Immersion can happen when the projection surface covers a significant part of the viewing field. Some effects can break this, such as bezel effect, which is due to the physical border of tiled monitors on a displayed image. Many other applications are broken by the bezel effect, especially applications that requires cognition.

How to have a large seamless image and without bezel effect? One can use a small screen just in front of his eyes, using a head mounted screen. This is a valid solution, but it is single user, which does not fit with a collaborative environment. One can use a single projector, with a wide angle lens, which will create a wide image, but a low resolution is resulting. Aiming at one projector with a better resolution would typically increase the cost of the system significantly. At the end, tiling projectors seems to be the best way, independently of the application, considering the relatively low price and the size and resolution that are limited only by the number of projectors used. However, that leads to many technical problems to solve.

The following list shows some examples of commercial devices and of academic projects related to the use of multi-projector systems.

Example of prices and features The projection display market evolves really fast, the price goes down as fast as the technology evolves. The list below shows how the price went down in a short time, and how it is cheaper to use several projectors to get high resolution than just one:

- In 1997, the Lawrence Livermore projector wall was built using 15 projectors DLV-1280 Electrohome each with a resolution of 1280×1024, a contrast of 100:1 with 1000 ANSI Lumen. The price of one projector was $29000.

- In 2009, the model Optoma HD80 has a better resolution 1920×1080 resolution, a better contrast of 10000:1, 1200 ANSI Lumen. This model costs *only* $2500.

- To compare with a high resolution model of the same year, the Sony 4K has a high resolution of 4096×2160, a good contrast of 2500:1, 11000 ANSI Lumen. However, its weight is 120KG, and its cost is $150000.

- If the former projector (equivalent resolution) was built with 9 (3×3) projectors Optoma HD80, its cost would be $22500.

- If the former projector (equivalent resolution) was built with twelve (4×3) projectors Sony VPL-AW 15, 1280×720 resolution, 12000:1 contrast, 1300 ANSI Lumen, $ 1300 each, it would be $15600.

The resolution cost can be reduced a lot. The given prices have to be augmented considering a computer cluster and some graphics hardware. But the total cost will remain significantly lower than the $150000 of the Sony 4K. The brightness and contrast of such a system would be less than the individual brightness and contrast of each projector used, because of photometric adjustment. However, we cannot say a priori if such a system would be better than the Sony 4K with regard to these features.

Example of projects Many projects have been running or are running to face the technical issues of using several tiled projectors. Many companies and researchers are working on that. According to Lantz (Lantz, 2007),there was about 275 large scale display theaters worldwide in 2007. This number has already increased.

For instance (this list of examples is not exhaustive):

- Cave, University of Calgary, sun Microsystems (4 flat projection wall), for immersive reality, 2D and 3D visualization.

- Scalable display wall at Princeton University (24 projectors), for research purpose on seamless imaging, parallel rendering, camera-based tracking and so on.

- Large walls at University of California Irvine and San Diego (70 projectors).

- Pixelflex, University of North Carolina at Chapel Hill (8 projectors) and Sandia National Laboratories/California (6 projectors).

- LightTwist project, University of Montreal, for artistic purposes. They aim at keeping the simplest arrangement as possible, using just one camera for geometrical alignment and photometric adjustment (fish eye lens or catadioptric) -work as long as one camera can see most of the surface-.

A couple of books deals exclusively with the technological problems of multi-display systems (Bimber and Raskar, 2005; Majumder and Brown, 2007).

Technical problems include:

- Color uniformity; we will consider this problem on next section.

- Geometry registration and alignment. At the beginning, the camera were typically supposed to be calibrated or the walls had to be marked to establish the transform between the screen, the projectors and the camera(s). Now, the most recent researches consist in using uncalibrated cameras to correct for the geometry. See for example (Chen and Johnson, 2001; Chen et al., 2002; Draréni et al., 2009; Hereld et al., 2003).
- Screen properties. In order to reach a better contrast ratio for the whole system, it can be of use to limit the number of inter-reflections in using low reflectivity or gray screens (Rudd et al., 2008; Skolnick and Callahan, 1994).
- Scalability. Adding or removing easily one or several projector(s) is a technical challenge (Bhasker et al., 2006; Chen and Johnson, 2001; Chen et al., 2002).
- But also: Parallel rendering (The capabilities of GPGPU helped a lot to design real time rendering applications), synchronization and so on.

Much work have been carried out and are still going on considering all the technical challenges linked with multi-displays. In the following, we will only consider the spatial uniformity of an image considering accurate color rendering, with emphasis on spatial uniformity or perceived spatial uniformity. We present as well the contrast evaluation problem within displays that are using a curved concave screen.

8.2 Color in multi-display systems

The color characterization of a large scale display or a multi-display system is a more general case of point-wise display color characterization that includes the spatial dimension. Indeed, compared to point-wise color characterization, simplifications are seldom valid, mainly because of the configuration or because of the high number of displays.

This section reviews the attempts that have been made to achieve spatial color uniformity in multi-display systems. Many approaches and their combinations have been investigated in the literature for solving this problem. Most of them consider objective uniformity. We introduce one work that considers perceived spatial uniformity.

We first describe and classify the problems, considering intra-display differences, inter-display differences, and overlapping areas of multi-projector systems. We then expose many solutions that can be found in the literature.

8.2.1 Classification of problems

In a multi-projector system, we can distinguish between different effects that break the spatial uniformity of the display. These effects can be classified in:

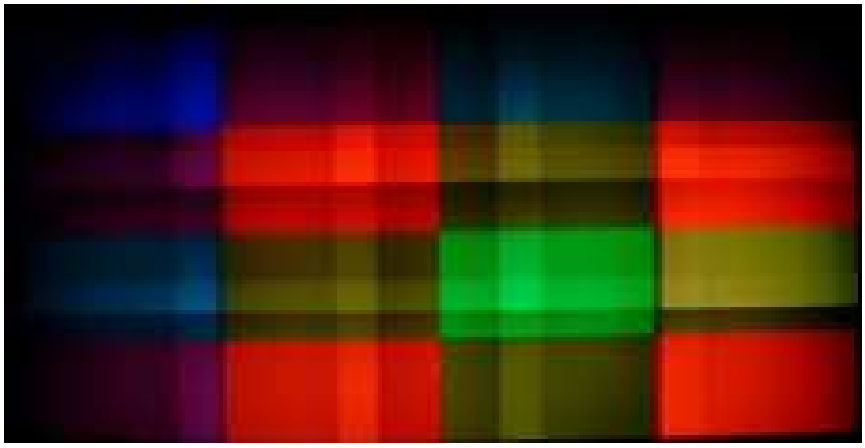

Figure 8.1: *Example of a multi-projector system with no correction except geometry. We can see distinctly the three kind of non-uniformity, inter-projector, intra-projector and overlapping area. From Majumder and Gopi (2005).*

- Intra-projector differences, which considers non-uniformity within a single projector.
- Inter-projector differences, which considers differences between two projectors.
- Moreover, in some cases, some areas can result of the overlapping between 2 to N, through 4 projectors.

Figure 8.1 shows a multi-projection display with no colorimetric or intensity correction.

Intra-projector

Looking at many studies that consider one projector (Kwak and MacDonald, 2000; Majumder and Stevens, 2004; Seime and Hardeberg, 2003; Thomas and Bakke, 2009), we can observe that the color is not uniform spatially within one projector. Although we demonstrated in (Thomas and Bakke, 2009) (more details in next chapter) that the chromaticity non-uniformity should not be neglected in some cases, in the literature of the past decade, it has been mainly considered that the intensity was the main cause of spatial color non-uniformity within one projector. This non-uniformity is mainly coming from the fact that the imaging device is decoupled from the screen itself. There is then either a lens effect, or the geometrical arrangement between the projector and the screen that influences this parameter.

Different solutions have been proposed in order to have a photometric uniformity. Many solutions consider the use of a camera to set up a luminance attenuation map, based either on a mathematical model (Majumder and Stevens, 2002, 2005) or on a LUT

(Pagani and Stricker, 2006, 2007), to correct for the uniformity. Using an objective luminance correction from the maximum black offset and the minimum of the maximum intensity reduces the dynamic range drastically.

Inter-projector

If one projector is color uniform, what can we say of the difference between projectors? The literature shows two different approaches for that[1]:

- A luminance attenuation map, considering that all displays from the same model and manufacturer show a similar gamut.
- A common gamut has to be found, which is the intersection of all projectors's gamuts involved in the image, such as in the work of Bern and Eppstein (2003) or Pagani and Stricker (2006, 2007).

Overlapping

When two or more projectors are covering the same surface of the screen, their intensities are summed up at these locations. In this case, there is a need to attenuate the contribution of each projector.

Furthermore, some fixed parameters influence the color rendering, such as screen properties, ambient light, etc.

8.2.2 Solutions: A skeletal lamping

This section performs a skeletal lamping [2] of multi-projection systems color uniformity solutions in the sense that it aims to list and explain many solutions that appear in academic bibliography. This title comes from the fact that these solutions are mainly based on the combination of several solutions to smaller problems. These *subsolutions* are combined in a skeleton to build a given correction method. Many of the existing

[1]Different optical systems can lead to different projector behavior, such as the modulation transfer function. This non-uniformity is more related to the resolution uniformity than to the color itself, so we do not consider it as a critical factor for the color problem.

[2]*Skeletal Lamping* is the title of the ninth studio album by Athens, Georgia-based band "of Montreal". Kevin Barnes (band leader) said about the title: "*This record is my attempt to bring all of my puzzling, contradicting, disturbing, humorous, ..., fantasies, ruminations and observations to the surface, so that I can better dissect and understand their reason for being in my head. Hence the title, Skeletal Lamping. Lamping is the name of a hunting technique where hunters go into the forest at night, flood an area in light, then shoot or capture the animals as they panic and run from their hiding places.*". That reminds us the state of the art of multi-display systems. Most solutions are considering a series of small corrections that are combined to form the skeleton of a complete method.

solutions are implemented in proprietary hardwares, and it is difficult to expose here all the *methods* they use.

Manual manipulation of controls

As said in the title, this method consists in modifying manually the projectors settings, such as contrast, intensity, white balance, keystone correction and so on. This method would not give good results since it ignores most of the problems defined above. However, it can be a good pre-processing, in order to optimize the capabilities of the final system.

Same bulb solution

Some authors consider that the inter-projector non-uniformities are only due to the differences in the bulbs used. Pailthorpe et al. (2001) proposed to use the same bulb for all projectors. This method is supposed to permit to have a common intensity shape for each projector across the whole system. However, this solution does not deal with the problem of intra-projector differences or of overlapping areas. In addition, nothing guarantee the bulb to age following exactly the same scheme.

Common gamut matching method

This method has been studied by Stone (2002, 2001) and Wallace et al. (2003) in 3D, but as well by Pagani and Stricker (2006, 2007). This method aims at finding the common gamut between all projectors used in the system. Taken as it is, it neglects intra-projector non-uniformities, and the overlapping area. One of the main drawbacks is the requirement of an accurate color measurement device, and the amount of measurements required of each projector to accurately determine the gamut volume. Once this information is acquired, there is a need of computing the common volume. This task can be hard if there is a complex gamut boundary descriptor. Bern and Eppstein (2003) proposes an algorithm in $O(n^3)$ that considers parallelipipedic gamuts in *CIEXYZ*. An approximation of the common gamut can be computed in O(n), such as in (Pagani and Stricker, 2006, 2007). If one considers that chromaticity does not vary a lot between two projectors of the same manufacturer and same model, it is possible to map only the luminance to the common range (Majumder, 2005; Majumder and Stevens, 2002, 2004, 2005). Note that most of the approximations made to simplify the common gamut finding are considering more the luminance than the color itself.

The resulting common gamut can typically be found to be too small, so it could be useful to use more than three primaries by display, in coupling two projectors with

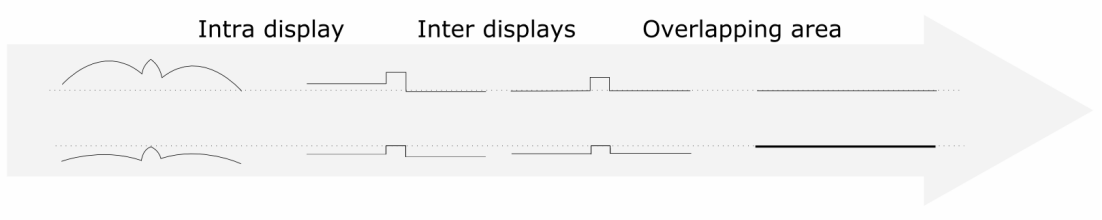

Figure 8.2: *Example of how to reach intensity spatial uniformity. This scheme details the steps considering each problem. Note that the dynamic range is really reduced at the end of the process. Note as well that in Majumder et al studies, they considered no black level. We added it in this scheme to show a more complete diagram. The uniformity is then less good in dark colors. However, in their papers Majumder et al stated that, considering the high frequency of an image, there is almost no visible artifact. They do not provide quantitative values.*

different primaries (Yamaguchi et al., 2004), or in using a 6-color wheel in DLP. To increase the luminance, it could be interesting to use a DLP projector with a fourth white segment in the color wheel (See Appendix A).

Intensity manipulation

These methods aim to provide the display system with a uniform spatial intensity. Any of the intra-projector, inter-projector or overlapping areas can be corrected.

In the work of Majumder and Stevens (2002, 2004), an intensity matching method is developed. This is an objective correction, which considers all three cases explained above. This method is illustrated in Figure 8.2. Note that Majumder et al did not consider any projector black offset (at the inverse of the Figure 8.2), no chromaticity variation along projectors, and the same normalized response curve for each channel along the multi-projector system.

The main drawbacks of such a method are:

- The minimum of luminance is kept in the available range. That reduces severely the dynamic range, and the image contrast suffers from that.
- Not taking the black offset into account leads to non-uniformity in dark colors, but also to inaccuracy in color rendering. Indeed, as explained in Part I of the thesis, there is a strong need to evaluate the black level when aiming at an accurate color rendering.
- The response of a channel is spatially invariant -after scaling- in the system. However, Bakke et al. (2009) demonstrated that this assumption can be valid for the DLP projectors, but only a rough approximation for the LCDs. This hypothesis

has to be verified before to use it. The misuses of this approximation can lead to so-called color blotches, as noticed by Majumder and Gopi (2005).

- This method considers the same chromaticity throughout the system. However, it is only valid in inter-projectors, considering the same brand, same model, and approximately the same time of use. Thomas and Bakke (2009) found that there was a gamut mismatch of only 2.75% between two projectors of the same brand, same model. However, this assumption seems to be not valid for intra-projector considerations, such as demonstrated in (Thomas and Bakke, 2009).

Edge blending

The edge blending aims to smoothen the overlapping areas between projectors. Just this method applied on a system typically considers all other differences as negligible. There are three methods proposed in the literature:

- Optical mask (Chen and Johnson, 2001): This method modifies the signal (optical or analog) near the border to create a virtual mask for the fusion of images
- Aperture mask (Li et al., 2000): This uses physical masks on the path of the light next to the border of the images.
- Software blending (Raskar et al., 1998): Uses a function to attenuate the luminance at the border. This function can be either linear or a cosine.

The two first solutions limit the accuracy of the blending. The second is limited by the accuracy of the geometrical registration.

Hybrid method

Pagani and Stricker (2006, 2007) presented an hybrid method. The method consists in first considering the luminance non-uniformity of each display using a LUT established with a camera. Then a common gamut is found, considering a common white, a common black offset, and the chromaticities of three primaries for a given number of luminances. The correction is done applying a gamut compression from the image gamut to the common multi-projector system gamut (going to xyY CIE color space) considering that the image has been acquired with a virtual camera showing the same common range of distinguishable colors as the common gamut shows. Then the color characterization forward transform of each projector (a 3*4 matrix method that considers the black offset) is applied to get the correct triplet to send to each projector. This method gives good results (they presented a ΔE^*_{ab} color difference between two projector primaries to the common gamut primaries from 0.26 to 1.22, 0.1 and 0.74 for the projectors whites

and of 2.09 and 1.21 for blacks), however it "cuts" a large portion of the gamut (original ΔE^*_{ab} color differences between native primaries and common primaries are major, from 3.48 to 62.12, with an average of 25.6 -black and white included-). This effect should be less impressive while using projectors of same brands, same ages and same settings although they do not precise the model of the two projectors they used. In addition, this model considers that the intra-projector difference is only due to a luminance shift.

Spatial color characterization

Hardeberg et al. (2003) proposed a spatial color characterization for one projector, using a colorimetric camera augmented with a spectroradiometer. Their idea was to sample the display, and to build up a color characterization model for each surface element. The display they tested was showing a ΔE^*_{ab} variation of 5.27 in average and of 24.5 as a maximum between 2 locations across the display for primaries images. After their correction, it was showing an average of 2.59 and a maximum of 7.68 ΔE^*_{ab} units. This method takes into account the intra-projector shift in chromaticity, and the black level. However, this method requires an expensive equipment.

Perceived uniformity, intensity smoothing method

If the dynamic range is too much reduced for a given application, and if there is no need of accurate color rendering in colorimetric terms, then it can be considered enough to have a perceived uniformity. Majumder (2005); Majumder and Stevens (2005) proposed a solution based on the fact that the difference between two areas of an image showing the same intensity does not necessarily have to be zero. If it respects the limits of the human visual system, it can be enough to optimize the content, considering that no difference should be **seen**, whatever a measurement device measures. In this case, more of the range of each display can be used depending on the content of the image. Their approach is based on the brightness contrast sensitivity function.

Figure 8.3: *The threshold contrast sensitivity function of the human eye. On the left the data from the plot in the left have been replotted to show sensitivity to absolute brightness differences (image from Valois and Valois (1990)).*

Contrast threshold function defines the minimum contrast required to detect a sinusoidal waveform of a particular mean and spatial frequency. Contrast sensitivity function (CSF) is a reciprocal of the contrast threshold function (Figure 8.3). the threshold CSF is plotted against absolute brightness differences (Figure 8.3). This shows that at very high spatial frequencies, sensitivity to absolute brightness differences roughly converge to the same curve, but for most of the frequency spectrum, the sensitivity to ab-

solute brightness differences increases as intensity decreases (this can also be described by the Weber Law).

8.3 Contrast problem in multi-projection systems

Aside of the color uniformity problem of a simple case, things start to be more complicated when the screen is convex curved and when therefore some inter-reflections happen. That happens when the light from the projector is reflected several times at different locations of the screen before reaching the observer. A common solution is to reduce the reflectivity of the screens (Rudd et al., 2008; Skolnick and Callahan, 1994) to reduce this effect.

However, since there is less light that is reflected and since the black level is usually increased because of overlapping areas, the contrast is severly reduced with this approach. Contrast is usually specified as the ratio between maximum (white) light output and minimum (black) light output.

The color can also be changed with inter-reflection. We do not know any prior research that considers specifically this problem. But before attempting to reach this level, it seems that there is a need in the industry to agree upon methods to evaluate contrast of display systems. In this section, we would like to address this problem.

There are a numerous ways to measure contrast within a display system:

- Sequential (dynamic), single projector contrast. This measurement assumes only a single projector, and measures the difference in luminance between a full white image, and a full black image. Projector manufacturers often use this measurement for marketing purposes. The contrast measure is typically increased by using iris functions, lamp dimming etc. to maximize white and minimize black. Typical contrast ratios claimed range from 1000:1 up to more than 10000:1.

- Checkerboard (static), single projector contrast. ANSI specifies a technique where a checkerboard pattern is projected on a flat screen, and the difference between black squares and white squares is measured. Typical contrast ratios claimed by manufacturers range from 100:1 to 500:1.

- System-level, multi-projector contrast. All projectors in a multi-projector system are turned on, each displaying a checkerboard test pattern. The difference between black squares and white squares is measured. In practical systems, contrast ratios observed range from 5:1 to 10:1 for large spherical dome systems, up to more than 100:1 for flat screen or near flat screen systems.

The huge difference in measured values from the second point to the third one is mainly due to inter-reflections between different parts of the screen.

Many companies that design multi-projector systems, large scale displays, immersive virtual reality systems, etc., have a software to help them to design their product. They need to include in this model a trustable measure of contrast. It appears that contrast evaluation is a great challenge for companies, considering that they have to select the best combination of screen reflectivity, intensity, and so on to be sure that the customer will achieve the desired contrast. If they do not have a model reasonably accurate, they have to over-estimate the quality of the material needed. The result is an over-cost for them.

Chapter 9

Spatial non-uniformity evaluation, quantitative approach

All colors are the friends of their neighbors and the lovers of their opposites.

Marc Chagall

Abstract

In this chapter, we investigate and study the color spatial uniformity of projectors. A common assumption in previous works is to consider that only the luminance is varying along the spatial dimensions. We show that the chromaticity plays a significant role in the spatial color shift, and should not be disregarded, depending on the application. We base our conclusions on the measurements obtained from three projectors. First, two methods are used to analyze the spatial properties of the projectors, a conventional approach, and a new one that considers 3D gamut differences. The results show that the color gamut difference between two spatial coordinates within the same display can be larger than the difference observed between two projectors. In a second part, we focus on the evaluation of assumptions commonly made in projector color characterization. We investigate if these assumptions are still valid along the spatial dimensions. Features studied include normalized response curve, chromaticity constancy of primaries, and channel independence. Some features seem to vary noticeably spatially, such as the normalized response curve. Some others appear to be quite invariant, such as the channel independence.

9.1 Introduction

This chapter presents a study of color spatial non-uniformity within a projection display. In many studies only a photometric correction is used within one projector, and it is shown as being an issue in some works, such as in (Majumder and Gopi, 2005).

Color spatial uniformity for projection displays has been studied (Kwak and MacDonald, 2000; Seime and Hardeberg, 2003). However, it is often considered that only the luminance is of importance, and in most applications only this aspect is corrected for. The chromaticity shift is often considered as negligible. Moreover, the analysis of the color shift along the spatial dimensions is mainly supported by either incomplete or qualitative results.

This work presents a quantitative analysis of projector spatial non-uniformity. We based our study on two aspects.

We first define our experiment. We then analyze our measurements. A conventional 2D approach is used, which considers the analysis of a projected full intensity patch. Then, we use a global comparison of the gamuts at different spatial locations to evaluate the color non-uniformity. The second part focuses on the evaluation of assumptions commonly made in projector color characterization. We investigate if these assumptions are still valid along the spatial dimension.

9.1.1 Background and motivation

A projection system displaying an image on a screen shows some color spatial non-uniformities. These non-uniformities can come from the system properties, such as lens alignment, but also simply from the position of the projection system relatively to the screen. Since the early analyses of CRT displays, it has been widely considered that only the luminance was changing along the spatial dimensions (Brainard, 1989; Brainard et al., 2002). This is still the assumption made by many researchers when modeling newer displays, and they maintain that the chromaticity shift is negligible compared with the change of luminance. In this work, we demonstrate that the chromaticity shift can not be disregarded, especially for some modern projection system applications, such as tiled projection systems, and for color research and experiments linked with the human visual system.

Despite of the studies or tentative works that have started to examine the color shift along the spatial dimensions (IEC:61966-6, 1998; Kwak and MacDonald, 2000; Seime and Hardeberg, 2003), it is still common to consider that the color varies only in luminance along the spatial dimensions of a display. Many proposed correction algorithms only use a luminance attenuation map , such as in (Brainard, 1989) for CRT monitors, and in (Majumder and Stevens, 2002) for projectors or multi-projector system correc-

tions.

In all their study of multi-projector systems, Majumder et al. assessed that the spatial chromaticity shift is negligible compared to the luminance shift. However, looking at the figures presented in (Majumder and Stevens, 2004), the gamut shows a severe shift, which at first seems to be comparable to the difference observed from one display to a completely different one.

While Majumder et al. looked at the projector gamuts in chromaticity diagrams, Bakke et al. (2006) recently proposed a method for computing the difference between two gamuts in a 3-D color space. They suggested that a method using discretized representations of the gamuts can be used to compute the relative gamut mismatch between two gamut boundaries. First, a binary voxel structure is created for each gamut. The value of each grid position is determined using the following method. If the position is within the gamut, the value is set to one, otherwise it is set to zero. Determining the differences between two gamuts can then be simplified to counting the voxels where the values of the two gamut representations are different, and multiplying this count with the volume of the cube represented by a single discretized position. The resulting number can be divided by the volume of the reference gamut, giving the relative gamut mismatch.

Beside of this aspect and to complete our study of color non-uniformity, we are interested in the behavior of some of the characteristics involved in color characterization models related with the spatial dimensions. Many works have been done in order to characterize the color of projection displays (i.e. model the relationship between the displayed color and a given input). These models make different assumptions about the devices in order to establish the most simple and as fast as possible model. They are usually based on preexisting knowledge about the technologies utilized in the displays, or determined by empirically investigating the output of the devices. These assumptions are mainly: spatial color uniformity (or only a luminance shift), temporal stability, chromaticity constancy of primaries, independence between channels, gamma or s-shape intensity response curve, etc.

Problems arise when a model is used without verifying whether these assumptions are true for a specific display device. Many of these assumptions have been shown to be reasonably correct for a CRT monitors (Berns, Gorzynski and Motta, 1993; Brainard, 1989; Cowan and Rowell, 1986; Sharma, 2002). Some studies have investigated LCD monitors (Sharma, 2002; Yoshida and Yamamoto, 2002), and a few studies have performed verification of these hypothesis on projectors (Bastani et al., 2005; Kwak et al., 2003; Kwak and MacDonald, 2000; Seime and Hardeberg, 2002, 2003). With the exception of Bastani et al. (2005), these studies investigate mostly projector features as defined by the IEC draft (IEC:61966-6, 1998). Here, we extend previous works by analyzing the characteristics of several projection displays along the spatial dimensions. We focus on

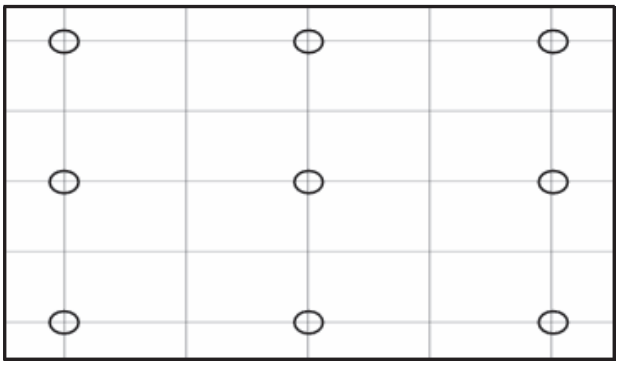

Figure 9.1: *Locations of the measurements on the screen. The circled intersections are the ones used for the reduced number of measurements.*

checking the validity of the most common assumptions.

9.2 Experimental setup

We performed our investigation on three displays, two LCD projectors of the same model and manufacturer (Sony VPL-AW 15), and one DLP projector (Projection Design Action One). They are named LCD1, LCD2 and DLP in the following. All the displays were used with the default settings. In order to have accurate measurements, we used the CS-1000 spectroradiometer from Minolta (Accuracy: luminance: $\pm 2\%$, x: ± 0.0015, y: ± 0.001, Repeatability: Luminance: $\pm 0.1\%$, xy: 0.0002 for illuminant A). The measurements were done in a dark surrounding, so that no light is involved except that from the display. A warming up time of at least one hour and fifteen minutes has been used before any measurement to reach a correct temporal stability. The geometry of the whole system was basically of the same type that the one used in (Kwak and MacDonald, 2000).

In our first experiment, we used the same kind of approach as the one described in the IEC draft (IEC:61966-6, 1998) and in the work of Kwak and MacDonald (2000). We measured only a full intensity white image (RGB=[255,255,255]) at 5×5 locations regularly distributed over the display area (Figure 9.1), having positioned the measurement device in front of the screen at the observer's position.

In addition to this approach, we were interested in looking at the differences in the gamut volume of the projectors, and at some features of the projectors along the spatial dimensions. We chose to limit the measurement process to 9 spatial positions among the set of 25, because of the time needed to complete the measurements (Figure 9.1). At these positions, we measured each ramp of primaries and grey, as well as the entire RGB cube surface with a sampling of 5×5, considering that the surface of the *RGB* cube is also the gamut boundary in an independent color space.

Bakke et al. (2006) showed that the gamut boundary descriptor algorithm (modified convex hull) suggested by Balasubramanian and Dalal (1997) performs well on most data sets when the preprocessing step is applied with the γ parameter equal to 0.2. We have therefore utilized this method to find our gamut boundaries. In order to perform the gamut evaluation, we used the ICC3D framework (Farup et al., 2002).

A part of our evaluation is performed in the CIELAB color space. We encountered a challenging issue in using this space, since it is based on pointwise colorimetry and since we are looking at a spatial display. In the past studies we know, the luminance was supposed to be at its highest value in the center of the display and the observer was supposed to look at the center first. The measurement of a white patch at the center was used as the reference white. This follows the recommendation of the IEC draft (IEC:61966-6, 1998). However, considering the position of the display or the alignment of the lens, the highest luminance point can be severely shifted from the center. That can happen for instance when the projector is made to be used in an office and to project the image on a wall for presentation, such as the DLP projector we tested. We decided to use the brightest point of the white image displayed as reference white. This choice has some advantages in our case. If we consider the geometry of the system and the lens alignment, choosing the reference white at the brightest point is more in accordance with the physical properties of the device. Since we base our experiment on colorimetry, and we do not attempt to take more human factors into consideration, we have chosen to use this as our reference white.

In the following, we refer to the measurement of the brightest white of a projector as the *global reference white* , while the *local reference white* is the white measured at each location.

9.2.1 Temporal stability

In order to ensure that our measurements at different locations were significant compared with the normal drift of the equipment, we performed a temporal stability check of the projectors we used. We started by performing an evaluation close to the one proposed in the IEC draft (IEC:61966-6, 1998). We measured a white full screen patch (full intensity) at regular intervals of 12 minutes, for about 700 minutes (11h40min). The Y, x and y coordinates are plotted for projectors DLP and LCD2 in Figure 9.2. LCD1 is considered to show the same behavior than LCD2. We used another range for x and y than the one proposed in the IEC draft since we could not see any information while plotting between 0.25 and 0.35 chromaticity diagram unit.

It appears that the LCD projector is really stable after one hour warming up, and before approximately 7 hours of use. The DLP projector however vary in intensity from 106 to 118 $cd.m^{-2}$ in a regular way. The chromaticity values are following the same

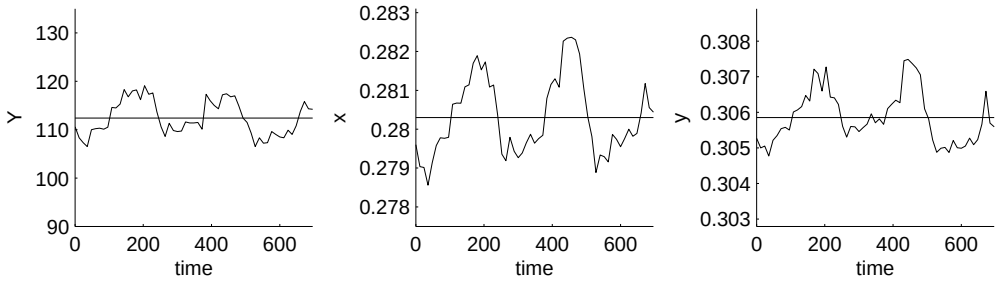

Y, x and y versus time in minutes for display DLP

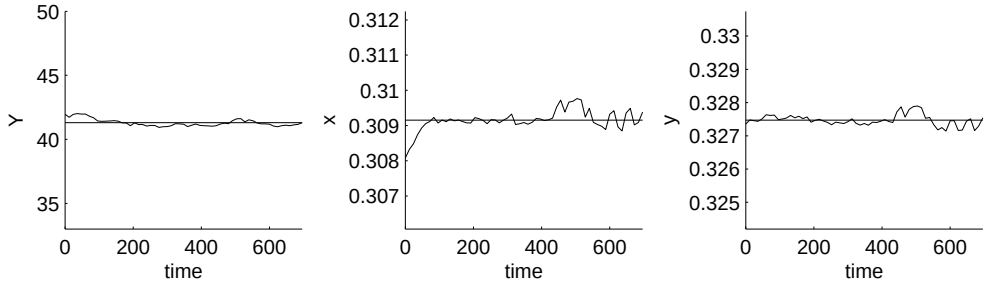

Y, x and y versus time in minutes for display LCD2

Figure 9.2: *Visualizations of the temporal shift for the DLP and one of the LCD tested projectors. The ordinate boundaries of these graphs correspond to the 20% error around the mean for Y and the 1% around the mean for x and y. One can notice that the DLP is less stable than the LCD. However, both devices appear to be stable enough to be used in normal applications. We can notice that for the LCD projector, there is an optimal time between the warming up time and a overheat time.*

Table 9.1: *Temporal stability estimation*

	DLP						LCD2				
	R	G	B	W	All		R	G	B	W	All
ΔE^*_{ab} Mean	1.29	1.21	0.78	1.17	1.11		0.60	0.33	0.58	0.22	0.43
ΔE^*_{ab} Max	2.79	2.73	1.64	2.41	2.79		4.74	1.32	1.83	0.64	4.74
ΔE^*_{ab} STD DEV	0.72	0.66	0.37	0.56	X		0.86	0.25	0.46	0.11	X

pattern.

To complete this evaluation, and to have a better idea of the global temporal stability in normal use, we measured the primaries and the graylevel at full intensity every 12 minutes for the same time, and computed the difference with the average in *CIELAB* for each color after one hour warming up. Results are presented in Table 9.1.

These results confirm what is shown by the graphs. The LCD is really stable in average (0.22 to 0.60 ΔE^*_{ab} units, depending on the primary), and the DLP is slightly less stable in average, but show a maximum shift below 3 ΔE^*_{ab} units around the average in almost 12 hours, that is good. However, there is a large maximum shift of the red channel for the LCD of 4.74 ΔE^*_{ab} units, that appears at about 8 hours and 10 minutes after switching on.

In overall, the stability of these devices is good (all are showing less than 1% variation in x and y chromaticity direction, less than 5% in luminance) for normal use, and they should be stable enough for our experiment.

9.3 Analysis of the spatial non-uniformity

In this section we present and discuss the results we obtained, first with the conventional evaluation, secondly with the 3D gamut comparison approach.

9.3.1 Conventional evaluation

By displaying the white patch and measuring the projected color at each position, we get an overview of the global behavior of the display. In Figure 9.3, we can see the lightness shift along the spatial dimensions in the left part of the figure.

This visualization is based on the measurements at 25 locations. The white surround comes from the fact that we have no information on this part of the displayed area, while we can interpolate the data inside this rectangle. We can see that the brightest point is not necessarily in the center of the screen. The color shift is illustrated in the right part of this figure. We can see the same effect as the one described in (Kwak and MacDonald, 2000), a shift in the color around the center of the lens displayed on the screen (i.e., the brightest point). The LCDs projectors show a shift from green/cyan to blue/red as a general behavior from the top left corner to the bottom right. The DLP shows a shift to the blue from the top to the bottom. The causes of this shift can be found in the literature (Matthew et al., 2008), and are probably mainly due to lens alignment and chromatic abberation.

The results of the quantitative analysis are presented in Tables 9.2 and 9.3. The first shows the ΔL^* and ΔC^* relative to the brightest point. The second shows the ΔE^*_{ab}.

The largest ΔE^*_{ab} observed are 11.64, 10.17 and 21.71 for LCD1, LCD2 and DLP respectively. The differences are definitively over the just noticeable difference from a colorimetric point of view.

For the LCDs, we noticed a maximum lightness shift of 11.27 ΔE^*_{ab} units in the bottom left corner for LCD1, and of 9.66 units in the bottom right corner for LCD2. The

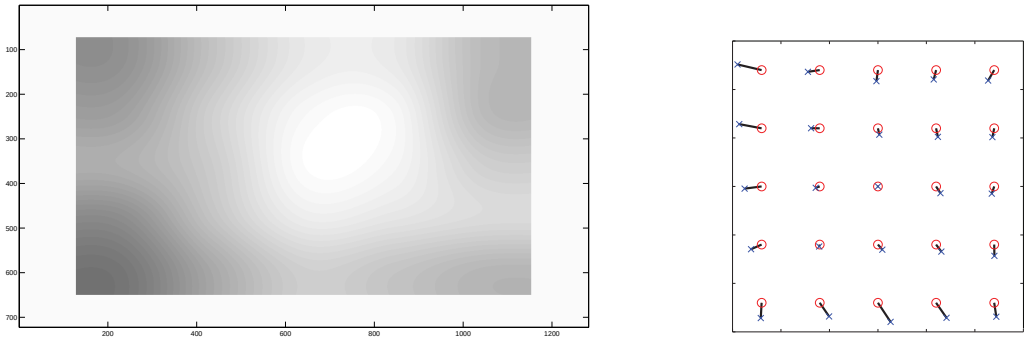

Lightness, chroma and hue shift for display LCD1

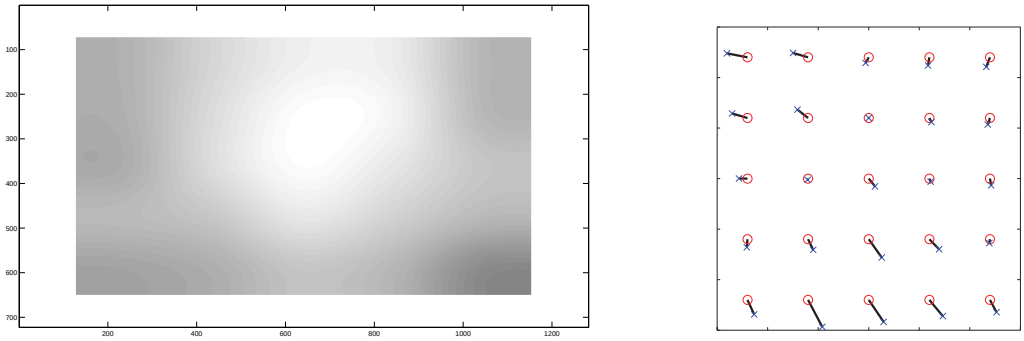

Lightness, chroma and hue shift for display LCD2

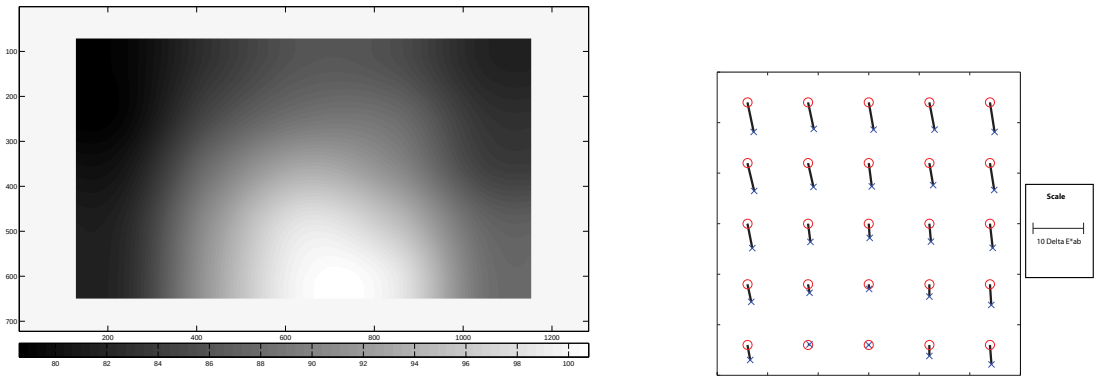

Lightness, chroma and hue shift for display DLP

Figure 9.3: *Visualization of the color shift throughout the display. On the left, we show a visualization of the lightness shift. The maximum lightness is 100 (white), the minimum (black) is around 79. On the right, hue and chroma shift are plotted relatively to their spatial position. The position of the circles (red) is the reference, the crosses (blue) indicate the measured value. The angle of the segment represents the hue shift, and the norm the chroma shift in the (a^*,b^*) plane. The reference on the right shows a difference of 10 units.*

Table 9.2: *Relative shift in lightness and chroma at 25 locations for the three tested displays.*

Shift in lightness							Shift in Chroma					
LCD1												
ΔL^*	1	2	3	4	5		ΔC^*	1	2	3	4	5
1	-8.92	-4.85	-1.61	-1.60	-5.55		1	5.09	2.46	2.29	1.99	2.49
2	-7.66	-3.72	-0.37	-0.36	-5.55		2	4.68	1.78	1.36	1.81	1.97
3	-6.42	-4.09	0.00	-0.58	-3.74		3	3.53	0.87	0.00	1.65	1.56
4	-9.29	-4.77	-1.29	-1.91	-2.81		4	2.37	0.40	1.39	1.80	2.31
5	-11.27	-7.02	-3.78	-4.64	-5.84		5	3.16	3.41	4.73	3.77	1.91
LCD2												
ΔL^*	1	2	3	4	5		ΔC^*	1	2	3	4	5
1	-6.49	-3.43	-1.14	-1.53	-6.09		1	4.13	3.09	1.26	1.63	2.03
2	-6.63	-2.93	0.00	-0.90	-5.96		2	3.17	2.68	0.00	0.92	1.38
3	-6.90	-2.85	-0.11	-2.00	-4.78		3	1.67	0.24	1.97	0.66	1.35
4	-5.71	-4.68	-1.94	-3.79	-5.89		4	1.60	2.32	4.44	2.77	0.78
5	-7.59	-6.75	-4.82	-6.09	-9.66		5	3.18	6.03	5.25	4.18	2.76
DLP												
ΔL^*	1	2	3	4	5		ΔC^*	1	2	3	4	5
1	-20.88	-16.72	-13.84	-14.40	-18.14		1	5.97	5.37	5.47	5.47	5.92
2	-20.90	-14.79	-11.49	-11.83	-16.80		2	5.68	4.85	4.65	4.44	5.40
3	-19.39	-11.46	-6.63	-9.29	-15.60		3	4.94	3.62	2.81	3.56	4.81
4	-18.06	-8.61	-1.68	-4.87	-12.63		4	3.53	1.70	0.92	2.41	4.09
5	-17.77	-7.62	0.00	-1.21	-11.58		5	3.01	0.31	0.00	2.18	3.85

corresponding chroma shifts are respectively of 3.16 and 2.76. The maximum chroma shifts for these displays are 5.09 in the upper left corner for LCD1 and 6.03 at the bottom left for LCD2, with associated lightness shifts of 8.92 and 6.75. The DLP projector shows a maximum lightness shift of 20.90 units in the upper left part of the displayed area, and 5.68 units in chroma at the same position. The maximum chroma shift is of 5.97 units in the upper left corner for 20.88 units in lightness.

In some locations we can clearly see that the lightness variation is smaller than or equivalent to the chromaticity shift, such as below the center for LCD2, which shows a ΔL^* of 1.94 and a ΔC^* of 4.44 compared to the reference location. When we consider

Table 9.3: *Relative shift in CIELAB unit at 25 locations for the three tested displays.*

Shift in CIELAB unit					
LCD1					
ΔE^*_{ab}	1	2	3	4	5
1	9.26	5.24	2.80	2.93	7.53
2	7.89	4.14	1.41	1.81	7.26
3	6.61	4.41	0.00	1.05	5.14
4	9.57	5.10	1.89	1.95	3.68
5	11.64	7.97	6.05	5.75	6.64
LCD2					
ΔE^*_{ab}	1	2	3	4	5
1	6.80	3.80	1.70	3.45	7.36
2	6.77	3.07	0.00	2.82	6.75
3	7.03	2.92	1.97	2.02	5.07
4	5.76	5.44	4.84	4.44	6.11
5	8.07	7.94	7.13	8.57	10.17
DLP					
ΔE^*_{ab}	1	2	3	4	5
1	21.71	17.60	14.88	15.36	19.09
2	21.58	15.45	12.40	12.78	17.73
3	19.97	12.00	7.20	9.97	16.36
4	18.52	8.94	1.92	5.16	13.11
5	18.18	7.92	0.00	1.25	11.97

the hue shift, which is shown in Figure 9.3 on the right, the chromaticity difference from a spatial coordinate to another can easily be larger than the lightness shift, and the hypothesis, which considers the color shift as negligible, can be disputed.

9.3.2 3D gamut evaluation

The reference gamut for each projector was constructed from the measurement data of the position with the highest luminance value. Table 9.4 contains the percentage of gamut mismatch for each position compared with this reference.

As we can see, the gamut at some locations can be as much as 52% smaller than

Table 9.4: *Relative gamut mismatch for each position compared with the gamut of the position with the highest luminance. The gamuts are calculated using the global white point as well as the local white point for each of the 9 selected locations.*

Gamut mismatch, global white point					Gamut mismatch, local white point			
LCD1								
%	1	3	5		%	1	3	5
1	27.23	4.90	17.08		1	9.57	3.30	5.72
3	23.92	0.00	16.15		3	7.49	0.00	5.53
5	32.66	9.48	13.50		5	7.90	2.07	4.09
LCD2								
%	1	3	5		%	1	3	5
1	24.84	5.83	19.75		1	9.42	2.48	4.46
3	20.18	0.00	18.79		3	6.00	0.00	2.40
5	29.75	11.01	20.82		5	5.98	1.98	2.48
DLP								
%	1	3	5		%	1	3	5
1	52.36	38.02	41.06		1	8.51	6.86	6.91
3	47.73	18.29	36.28		3	7.96	3.92	6.38
5	43.22	0.00	26.93		5	6.62	0.00	4.87

the reference, which is illustrated in Figures 9.4a and 9.4c. The luminance shift is responsible for a large part of this difference. Compensating for the luminance shift by using the local white point for calculating CIELAB values still leaves a significant maximum gamut mismatch of 8.51%, 9.42% and 9.57% for the three projectors. Figures 9.4b and 9.4d show the gamuts computed using the local white point.

This mismatch in relative volume is comparable to the error introduced when using a strictly convex hull to represent the gamut of an arbitrarily chosen device, and is greater than many inter-device gamut differences. In our experiment, the gamut mismatch between the two LCD projectors (at the reference position) is 2.75%, giving an intra-device difference 3.43 times larger than the inter-device difference.

The DLP shows large differences in gamut depending on the spatial location, similar to what we showed in our analysis of lightness. Compared with the two LCDs, a larger part of the differences can be explained by the luminance shift. The remaining gamut mismatch volume mainly consists of the volume that is contained within the ref-

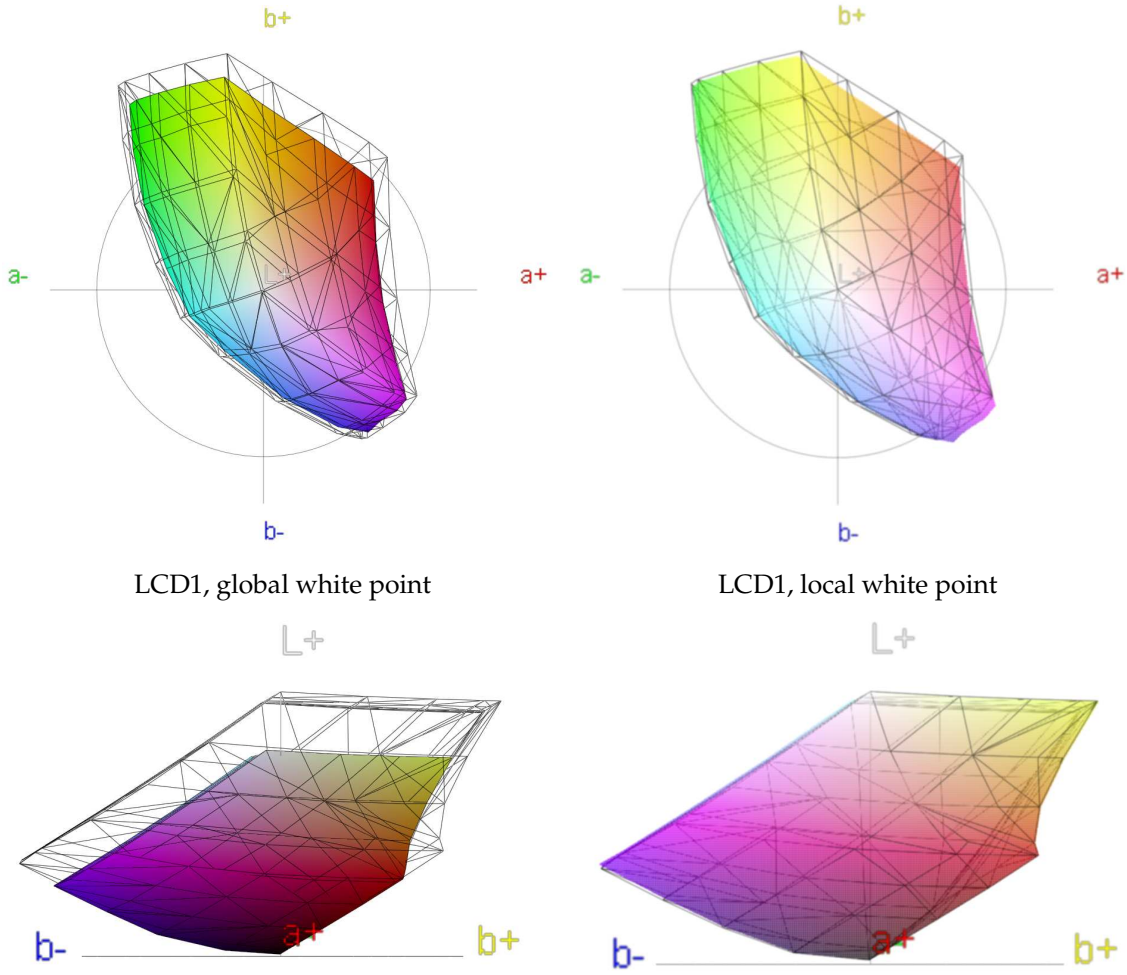

LCD1, global white point

LCD1, local white point

DLP, global white point

DLP, local white point

Figure 9.4: *The gamut boundaries for two of the projectors at the position with the highest luminance (wireframe) compared with the gamut of the top left corner (solid and wireframe). CIELAB measurement values were computed relatively to the global white point for and , while 9.4 and 9.4 utilizes the white point of each location.*

erence and is not a part of the gamut of the other spatial locations, which is illustrated in Figure 9.5. This means that there are effects in addition to the luminance shift, which contribute to the reduction of the gamuts.

9.3.3 Discussion

Based on our analysis of these results, there appears to be sufficient evidences to claim that the chromaticity shift has to be taken into account in some cases. Some applications might not be affected, while some might suffer seriously from this fact. It appears

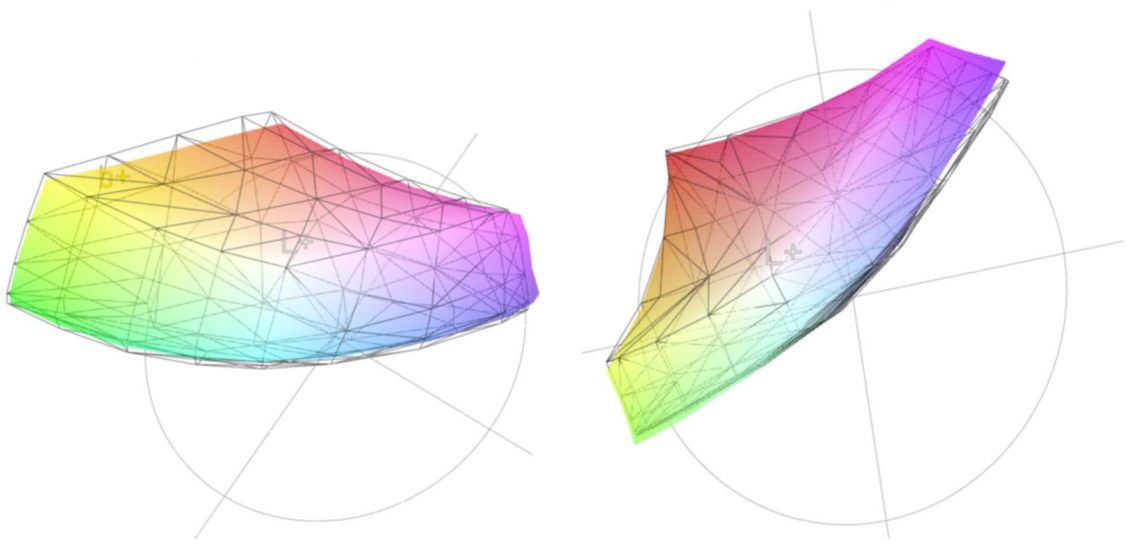

LCD1 DLP

Figure 9.5: *While using the white point of each location reduces the difference between the gamuts by compensating for the luminance shift, we still see some differences between the gamuts.*

important for us to compensate for this problem in at least two situations: While performing psychophysical experiments for color science purpose with a projector, and while tiling projectors together to build a multi-projector system.

Related to the choice we made in our experiment by using the brightest white point as a reference, we found that the gamut of the position with the largest luminance results in the largest estimated gamut volume. It is then a logical choice to use this as the basis for the reference gamut.

Considering the case of a multi-projector system, since the chroma shifts in two opposite hue directions from the center of the lens, the area around the overlapping edges will show two really different colors. Note that even though the computed chrominance shift is major (we observed some ΔC^* of about 6 from a position to another and greater differences can be found between extreme positions), if we consider the spatial content of an image, it is not certain that the chrominance shift will break the perceived uniformity.

Similarly, the reduction in gamut volume of up to 52% when using the global white point does not appear to be indicative of the perceived color capability of the projectors. However, using the local white point seems to underestimate the real difference. This is endorsed by the conventional approach. When we look at the full intensity white patch, the perceived difference does not seem to be as large as the measured one.

In order to make a model, which fits our perceived color appearance, we need to consider more psychovisual features, such as the color adaptation at the local and at the

global level, cognition and physiology.

9.4 Common assumptions in color characterization of projectors: A spatial point of view

In this section we present and discuss the common assumptions used in display color characterization. We analyze the normalized response curves of the displays, the chromaticity constancy of primaries, and the independence between channels. We use a method described by Bastani et al. (2005) in order to analyze the cross-channel interaction of the displays. By keeping the input of two channels at either full or no intensity, and varying the input of the third channel, the amount of channel interaction can be found.

9.4.1 Normalized response curves

A common assumption in display characterization is to consider the normalized response curve of each channel to have the same shape. By extension, each channel may have the same shape as the graylevel response curve. In many common methods this assumption can reduce the number of intensity measurements or evaluations that have to be taken or done. This assumption has been shown to be valid for CRT monitors but not for LCDs (Sharma, 2002). For projectors, if we look at the works of Seime and Hardeberg (2002, 2003) or of Kwak and MacDonald (2000), the LCD projector does not appear to fulfill this assumption, however the DLP in (Seime and Hardeberg, 2002, 2003) seems to show approximately equivalent normalized response curves for each channel. Let us note that in (Kwak et al., 2003), one LCD projector they tested seems to fit the hypothesis. However, no quantitative data is given in these studies to assess this. The purpose of this section is to evaluate this with quantitative data, and to extend the investigation to the spatial dimensions.

In Figure 9.6 we show the response curve of a normalized graylevel intensity ramp at the reference location of the DLP we tested, and a normalized sRGB response curve sampled as the first curve. The sRGB response curve being the one used by default in many cases, we used it as a reference.

We propose a simple method to give an indicator of similarity that consists in the absolute difference between the integrals (i.e. the surface between both curves). We multiplied the surface found by 1000 to avoid too small numbers. We compared the sRGB and the response curve of our three projectors and found a δ of 4.31, 4.29 and 5.26 for LCD1, LCD2 and DLP. That enables us to relate the following results to something known.

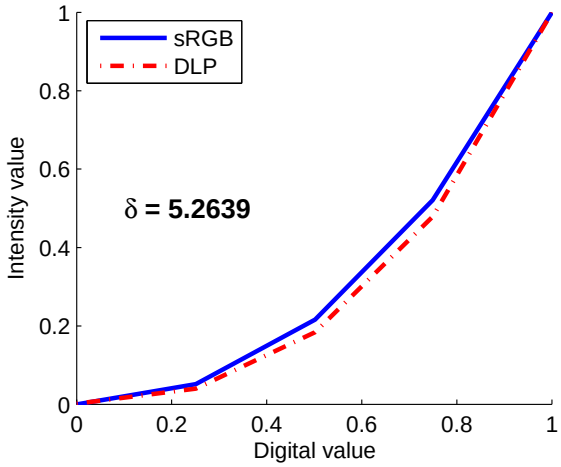

Figure 9.6: *Normalized response curve of the DLP projector compared with the normalized sRGB response curve. The indicator δ is the surface between both curves $\times$ 1000.*

Based on this indicator, we perform three experiments. First we compute the average and maximum mismatch δ_{mean} between the intensity response curve of each channel and the gray level response curve at each position. If there is no mismatch it can be enough to measure only the gray level response curve at each spatial location. Results are reported in Table 9.5.

We observe that the centers of the displays are among the locations with the largest shift between curves for each display. If we relate these numbers with the one found between the gray level reference curve and the sRGB curve, it is possible to consider normalized response curves equivalent at each location whatever the channel for *sRGB accuracy*. However, the mismatch does not appear to be negligible for many colorimetric accurate applications.

Our second experiment consists in computing the mismatch between each primary at different locations, and the same primary at the reference location. If there is no mismatch, we could consider that measuring the response curves at one random location is enough for each primary. Results are reported in Table 9.6.

It seems to be a valid assumption for DLPs. However, for the LCDs it is approximately as different as supposing the display to be sRGB (that can be an adequate hypothesis depending on the accuracy one wants to reach).

Our last experiment testing this assumption is to compare response curves at all locations and for all channels with the reference location gray level normalized response curve (as it can be measured in some cases for applying a classic physical color characterization model). If there is no mismatch, it is enough to measure only one ramp at a given location.

We found an average mismatch of 2.13, 2.48 and 1.10, and a maximum of 6.29, 8.30

Table 9.5: *Mismatch between the intensity response curves of each channel and the gray level curve, depending on the location on the screen. The maximum and average mismatches are reported.*

Average mismatch					Maximum mismatch			
LCD1								
	1	3	5			1	3	5
1	0.96	2.59	2.61		1	2.63	3.88	4.54
3	1.15	3.00	2.43		3	2.57	4.85	3.71
5	2.01	2.64	1.87		5	2.87	3.69	3.42
LCD2								
	1	3	5			1	3	5
1	1.21	2.01	2.24		1	2.05	3.30	3.68
3	1.29	2.15	1.72		3	2.76	3.30	3.01
5	2.05	1.53	1.31		5	3.31	3.27	3.14
DLP								
	1	3	5			1	3	5
1	1.43	1.24	0.98		1	3.44	3.16	1.46
3	1.34	2.05	1.01		3	2.49	4.03	2.64
5	2.62	1.37	0.84		5	4.38	2.82	1.68

and 3.85 for LCD1, LCD2 and DLP.

In average, the difference is not as large as the difference compared with an sRGB curve, especially for the DLP. However, the maximum error found in LCDs shows that for this technology (or at least for these projectors) one can introduce a critical error through this approximation.

More analysis should be performed, especially to find a just noticeable difference. As a first conclusion, we would not use this assumption for projectors for accurate color rendering. However, it seems that within DLP technology, one can consider the normalized response curve of a given channel as invariant along the spatial dimension. If a *sRGB accuracy* is enough for a given application, then it seems that measuring only one ramp for one projector could be a feasible compromise.

Table 9.6: *Mismatch at each location, between channels for each primary and the channel response curve at the reference location. The graylevel response curve mismatch is shown as well.*

Average mismatch					Maximum mismatch			
LCD1								
Red	Green	Blue	Gray		Red	Green	Blue	Gray
3.02	1.49	1.26	1.71		5.15	3.71	3.40	3.87
LCD2								
Red	Green	Blue	Gray		Red	Green	Blue	Gray
1.94	2.36	2.02	2.38		3.85	5.50	3.43	4.99
DLP								
Red	Green	Blue	Gray		Red	Green	Blue	Gray
0.48	0.24	0.97	0.57		1.83	0.80	1.67	0.95

9.4.2 Chromaticity constancy

The assumption of chromaticity constancy is important in many physical display color characterization models while performing the colorimetric transform. In this section, we want to see if the behavior of the chromaticity of primaries changes with the spatial location.

Figure 9.9, 9.7 and 9.8 illustrates the chromaticity values of the ramps of red, green and blue for each projector and at different locations. In these figures the offset is shown to be spatially variant. We can observe a slight shift between primaies. The LCDs show less uniformity along the green channel, though the DLP shows less uniformity along the red channel, and has one locaiton that is severly shifted from the others. An interesting fact to notice is that the offset is strongly inhomogeneous along with the spatial dimension.

9.4.3 Channel independence

An assumption made by several models is that of channel independence, e.g., that the output of a gray ramp is equal to the sum of the three R, G, and B ramps. For each projector, we have plotted the measured gray ramp and compared it with the computed sum of the individual ramps, see Figure 9.10.

The lack of additivity we can observe in Figure 9.10 is due to the existence of channel interaction. Bastani et al. (2005) suggested that the amount of interaction for a channel

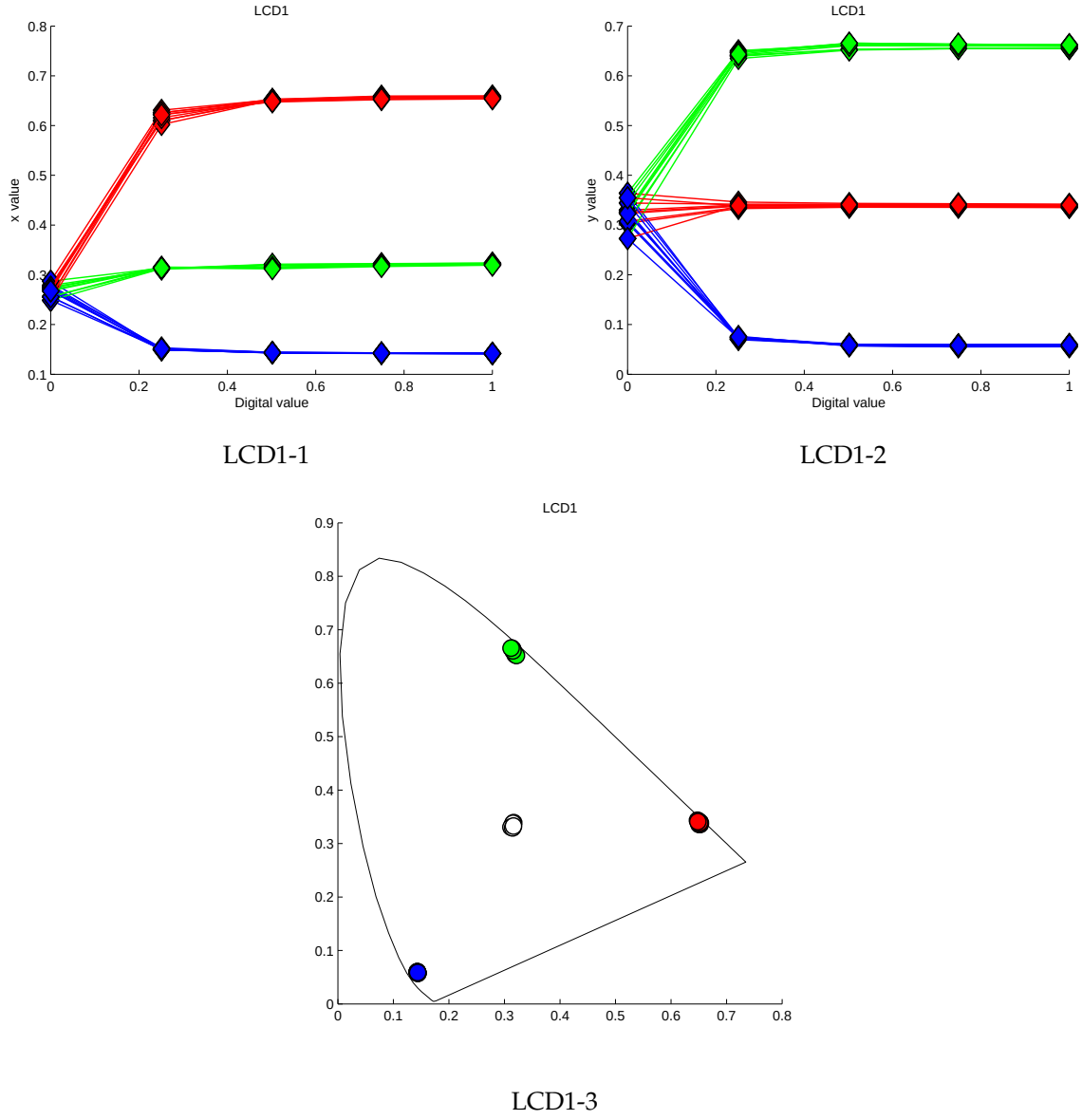

LCD1-1 LCD1-2

LCD1-3

Figure 9.7: *Illustration of the chromaticity constancy for the projector LCD1 at different locations, in (a) the x values from different locations are plotted in function of the digital input, in (b) the y values from different locations are plotted in function of the digital input, and in (c) the primaries of the digital locaitons are plotted for a digital input of 0.5 (128 on 255).*

at a given intensity can be calculated using the formula in Eq. (9.1), where $L(r, g, b)$ represents the luminance that is measured for a specified RGB input. a and b are constant values for two of the channels, while v is the varying input of the third channel. Eq. (9.1) defines the interaction for the red channel. The interaction for the other channels are found in a similar manner. We preferred this method to the more complete, but more complex method proposed in the IEC draft (IEC:61966-6, 1998) for visualization

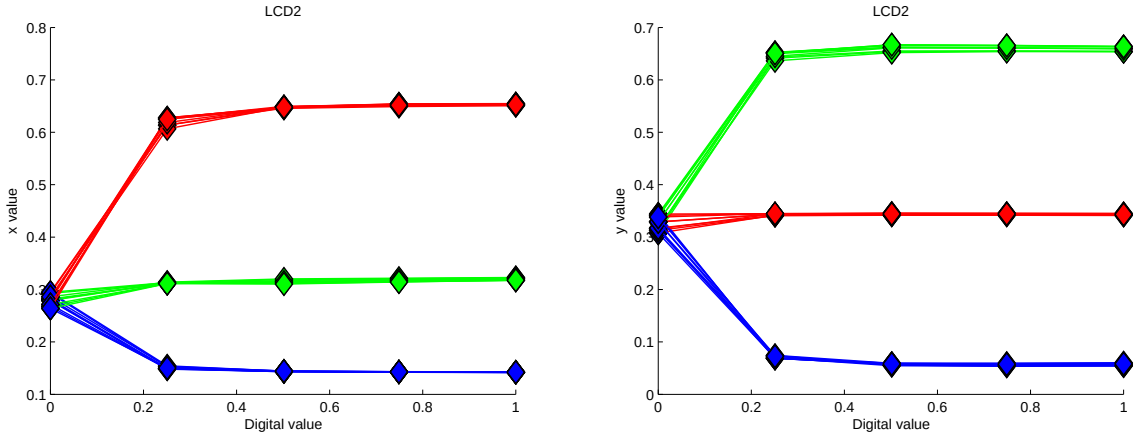

LCD2-1 LCD2-2

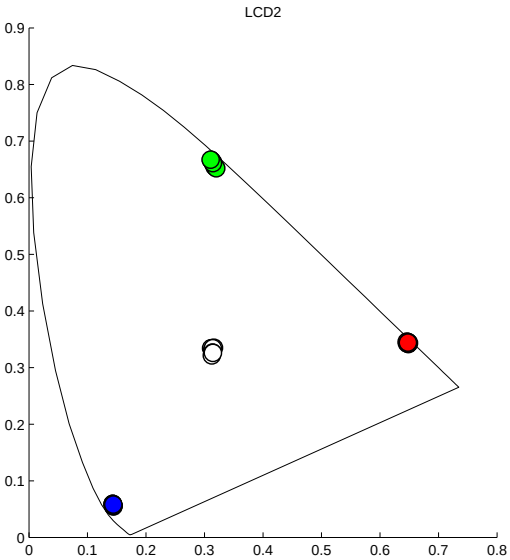

LCD2-3

Figure 9.8: *Illustration of the chromaticity constancy for the projector LCD2 at different locations, in (a) the x values from different locations are plotted in function of the digital input, in (b) the y values from different locations are plotted in function of the digital input, and in (c) the primaries of the digital locaitons are plotted for a digital input of 0.5 (128 on 255). it is almost the same behavior as LCD1.*

purpose.

$$CI_{RED}(v,a,b) = \frac{(L(v,a,b) - L(0,a,b)) - (L(v,0,0) - L(0,0,0))}{L(255,255,255) - L(0,0,0)} \tag{9.1}$$

Figure 9.11 shows the interaction between the channels for the three projectors. We

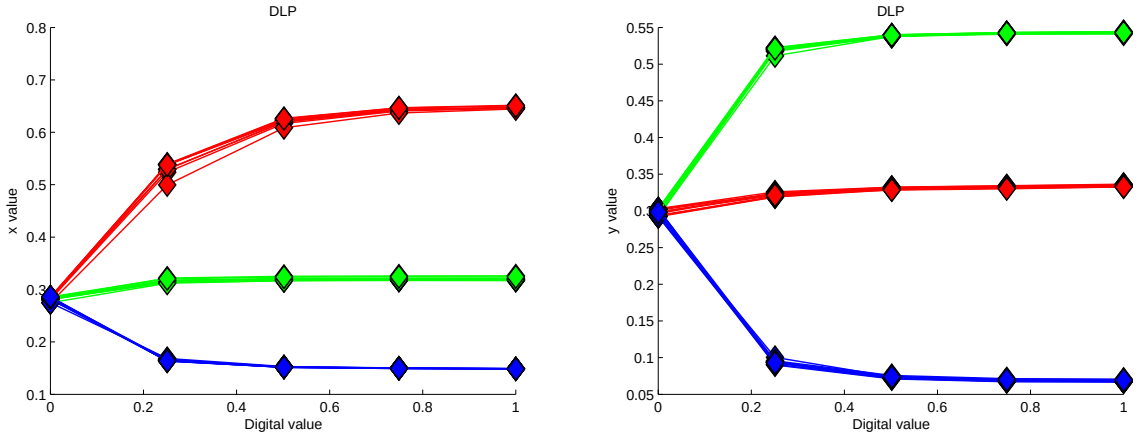

DLP-1 DLP-2

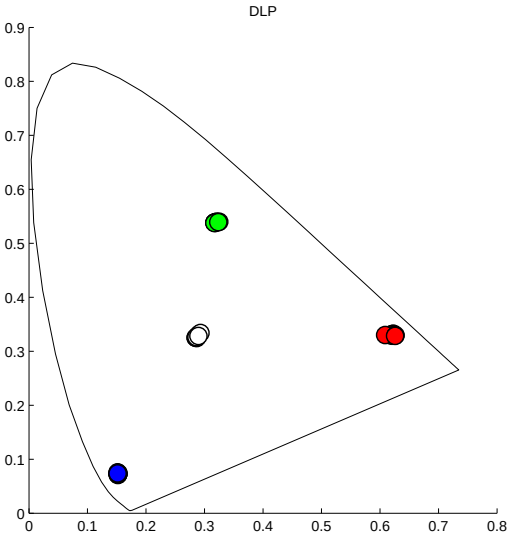

DLP-3

Figure 9.9: *Illustration of the chromaticity constancy for the projector DLP at different locations, in (a) the x values from different locations are plotted in function of the digital input, in (b) the y values from different locations are plotted in function of the digital input, and in (c) the primaries of the digital locaitons are plotted for a digital input of 0.5 (128 on 255). The red channel shows more non-uniformity.*

can clearly see that the LCDs have much more interaction than the DLP. The LCDs feature quite similar interaction characteristics, which is unsurprising given that they are of the same manufacturer and model.

The spatial effect on the interaction is shown in Figure 9.12 for LCD1 and DLP. We noticed more interaction in the corners of the image in DLP technology. That could be

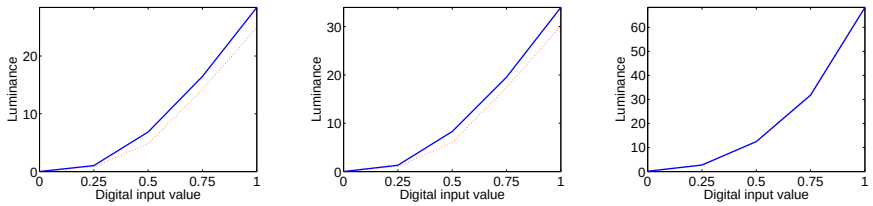

Figure 9.10: *The luminance of the gray ramp (solid line) compared with the sum of the individual ramps (dashed line) for the three projectors.*

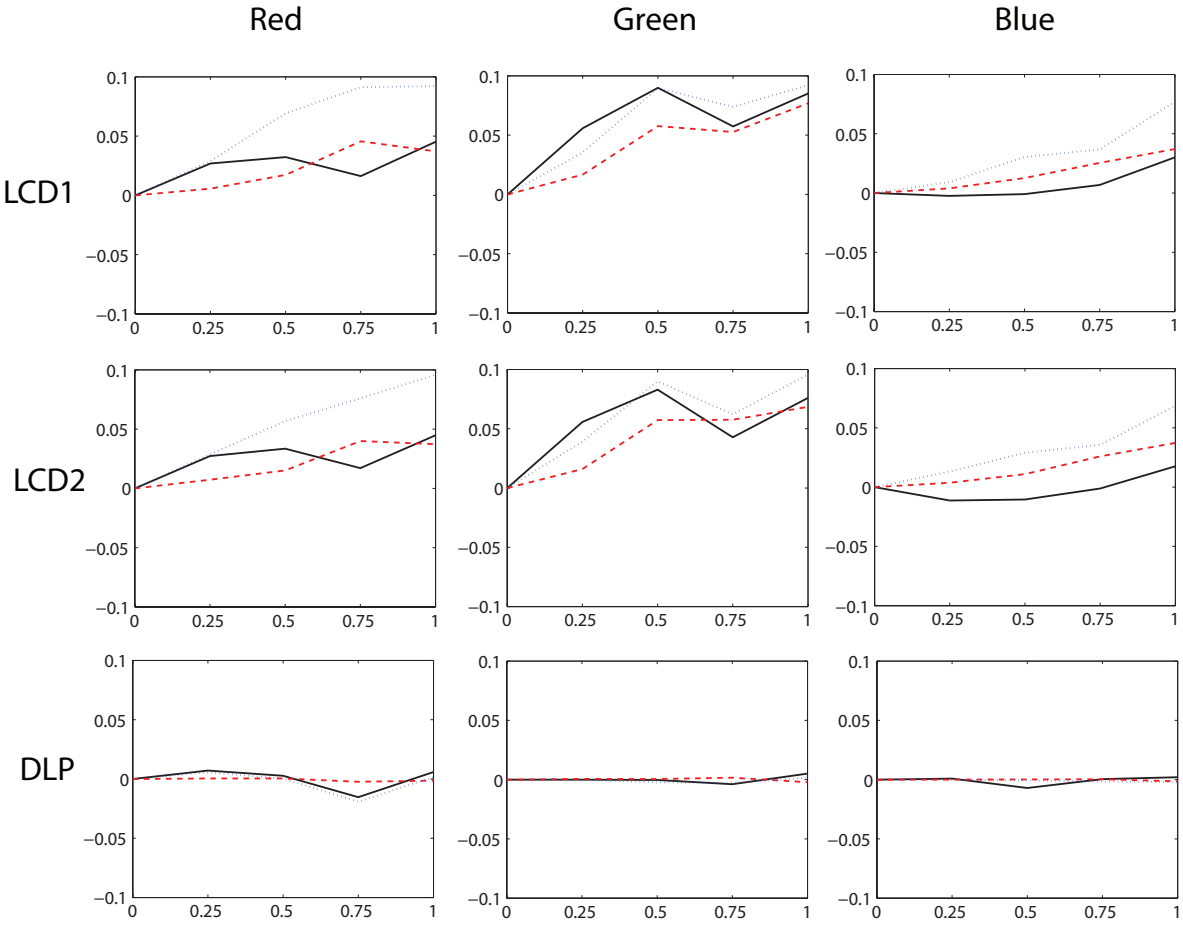

Figure 9.11: *Channel interaction for three displays. The horizontal axis represents the input value of the denoted channel, while the vertical axis represents the calculated interaction value. The solid black line is the interaction found when the two other channels are kept at maximum input value, while the dashed and the dotted lines are when the a or b, respectively, is set to 0 when computing the interaction metric.*

due either to the motion of the color wheel that is less synchronized with the micro-mirrors motion at the corner or to some lens diffraction effect.

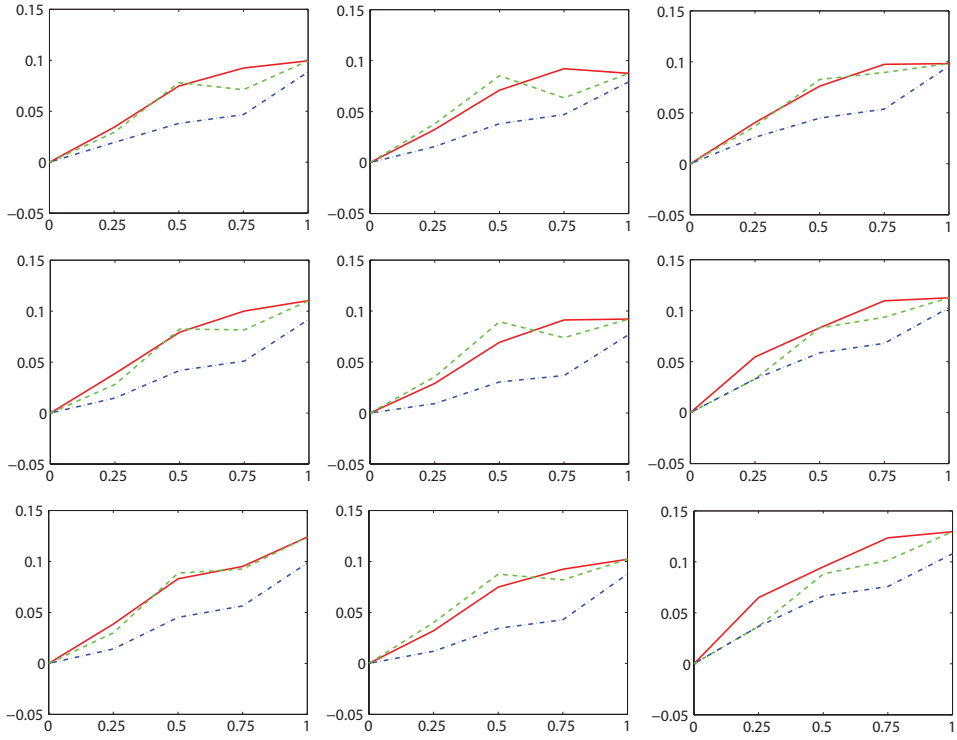

LCD1

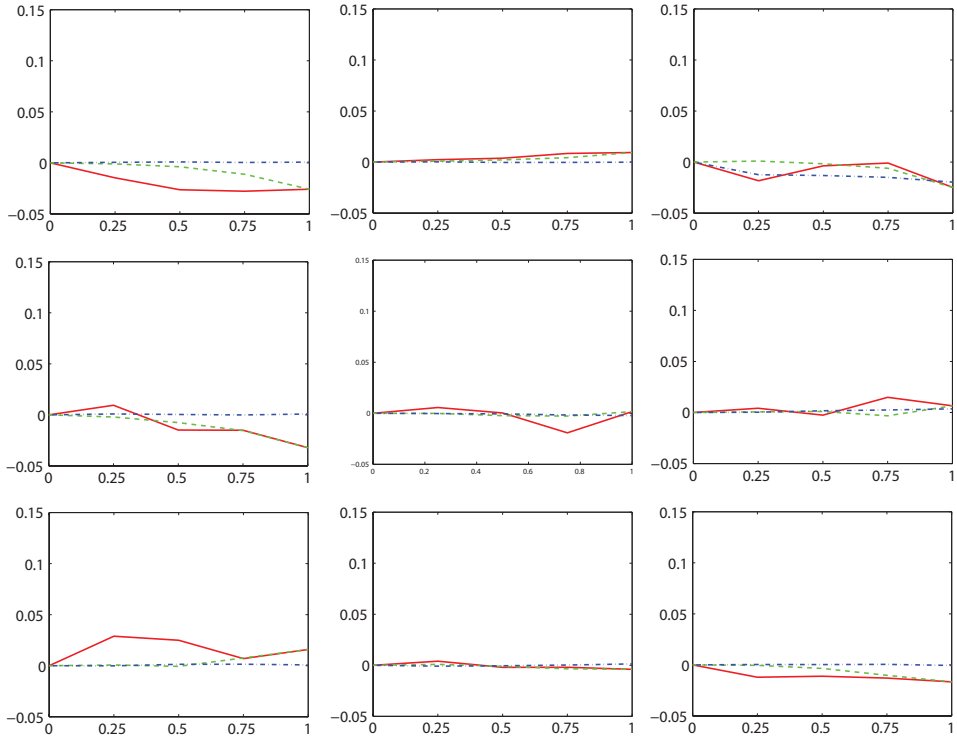

DLP

Figure 9.12: *Spatial channel interaction for two of the projectors, where each graph represents the interaction at the corresponding spatial location. The combination of a and b that gives the highest interaction is chosen for each channel.*

9.4.4 Discussion

To summarize, we can say that the normalized response curves vary enough with the spatial location to influence strongly the accuracy of the characterization, except for the tested DLP, where the spatial normalized response curve seems to be consistent by channel. We confirm previous studies, which found that LCDs projectors have a high degree of channel interaction, and their channel additivity is bad. However, DLP technology shows more independence, and a good additivity. The study of the chromaticity constancy shows as well better performances for the DLP. Considering the spatial effect, there is some differences between spatial locations in channel interaction, but not that much. We can say that the independence between channels remains quite invariant along the spatial dimensions.

Further works are needed to quantify the consequence of this non-uniformities on color characterization. In other word, how the differences measured are influencing the color control in term of perceived difference.

To construct a spatial color characterization model, performing measurements at many spatial locations on the displayed area might be required. However, the number of measurements could be reduced depending on the display characteristics. For instance, considering the DLP we tested, it could be enough to evaluate each channel normalized response curve at one location. Or, considering the interaction between channels stable along the spatial dimensions, it could be enough to take some model's parameters at one location.

9.5 Conclusion and further work

We have shown that the measured chromaticity shift along the spatial dimension of a projector is important, and that considering only the luminance to be non-uniform can be a critical mistake in some applications. Through the analysis of features, we have shown that most of the color shift, not induced by the lens system, was coming from the spatial differences in response curve in LCD projectors, and from a spatial variation of the channel interaction for DLP technology. These features will be of major interest for designing a spatial color characterization model for projectors.

However, considering the image content, it is reasonable to think that the perceived uniformity would not be broken in many cases. Further experiments could be done in this direction to find what can be considered as perceived spatial uniformity.

Further work includes performing a more in-depth statistical analysis of the results, and testing more projectors to improve the significance of the experiment. As a straightforward continuation of this work, we think it could be of great interest to utilize a spatial-gamut mapping algorithm using a spatially varying gamut in multi-projector

systems.

Chapter 10

General discussion

No time to choose when the truth must die,
No time to lose or say goodbye,
No time to prepare for the victim that's there,
No time to suffer or blink
And no time to think.

Bob Dylan

Abstract

This chapter puts together many topics discussed in this thesis. From a practical use of the algorithms designed, to some proposals of the further works that can be developed based on the work we have done.

10.1 Introduction

In this thesis, we have reviewed, analyzed and evaluated different methods to perform pointwise color characterization for accurate color rendering on displays. We have been through issues about spatial uniformity within projection systems. Here we present thoughts considering the choice of the method for a given application. We discuss the use of ICC profiles and standard CMMs and their limits considering spatial display color characterization. We draw a scheme for a projector end-user spatial color characterization, and we discuss the use of spatial-gamut mapping as a solution for multi-display spatial color uniformity.

10.2 Accurate professional models or end-user consumer models: a problem-dependent topic

Like any image processing technique, a display color characterization model has to be chosen considering the needs and the constraints. Here the need is mainly the expected level of accuracy. The constraints depend mainly on two things: the time and the measurement. The time, because you may need to minimize the time of establishment of a model, or its application to an image. The measurement because you may need to have a special device with you to establish the model. The constraint of money is distributed on the time, the software and hardware cost, particularly the measurement device.

However in the display case, the combination need VS constraint seems to be in agreement. Let us expose two situations:

- The person who needs an accurate color characterization (such as a designer): has often a color measurement device available, is working in a more or less controlled environment, and does not mind to spend 15-20 minutes to calibrate his/her monitor. This person could typically use the method we proposed in Section 6.1, coupled with the refinement of the grid for model inversion that is presented in Section 7.1 or any other accurate color characterization method available to him/her.

- The person who wants to display some pictures in a wedding party using a projector in an uncontrolled environment does not need a really accurate color rendering. That is fortunate, because he/she does not have any measurement device, does not have much time to perform a calibration (even taking the time to properly warm up the projector will probably not be possible in this situation). However, this person needs the colors not to betray the meaning she/he intends. in this case, a fast end-user characterization should be precise enough. This person might use a visual calibration, or even better, a visual/camera based calibration such as the

one we present in Chapter 5. This method should be coupled to a user-friendly software for making it easy and fast.

We see then that the constraints and the need are not necessarily in the opposite direction.

In any cases, there is a need to use one model to ensure the color content to be respected. In many cases, there is a need of a *universal* way that can be understood and applied by most of the softwares or systems. Such as an ICC profile.

10.3 On the use of ICC profiles and CMMs

The International Color Consortium aimed to define a standard for profile format. The following is some remarks considering the ICC.1:2004-08 (ICC, 2004) and correspond to the ISO 15076-1 standard. They did a great work, and many characterization models can be embedded and used successfully within such a standard file. However, mainly (on our opinion) because they decided to be independent of the CMM (Color Management Module), there are some cases where they show some limits. The CMM handles all computations that are needed to change from a color space to another. The purpose of this section is to discuss some of the good points and some of the limits putting together the content of some of the previous chapters, the consequences of embedding them in a ICC profile, and the use of a standard CMM. These are only some basic straightforward limitations, or lacks of optimization.

10.3.1 Limits considering the characterization method

If one wants to use optimally the methods we proposed in Chapter 6 and in Chapter 7, there might be a need to use a home made custom made color management module. Why? Because the data used, the interpolation method and so on can face limits either considering ICC profil format or CMM limitations.

There are four points we want to discuss here:

- While building an CLUT ICC profile, there is a need to have linear spaces between data. Even if there is the possibility to apply a function along each dimension, such as what we do in Chapter 7, and another function after the output from the LUT, in some cases it can be not enough, especially for a custom distribution of data. For instance, while designing the grid in *RGB* for the inverse transform, we do not have a well regular grid in the Profile connection space (PCS).

- The same number of data does not need to be used on each dimension while designing a LUT profile (Table 36 of ICC (2004)). That fits well for instance with the

inverse models we used in Chapter 6 and 7 where we used an optimized number different along each axis.

- Although there is no restriction considering the size of the file, there will be some problems to find an element with the increasing LUT size. The problem comes mainly because it is computed by the CPU within a CMM. In our work, we used a 3D texture, and the interpolation is easily handled by the GPU in real time for a large LUT (up to an equivalent of a $50 \times 50 \times 50$ LUT in practice).

- There is no tag for setting the interpolation method that has to be used and that can be a critical issue if the profil is design for a given interpolation method, such as a RBF 3D interpolation, while the CMM uses a linear interpolation.

10.3.2 Limits due to spatial issues

For our purpose in the part II of this thesis, which means correcting a spatial non-uniformity within a display, ICC will not be sufficient as well as all CMMs that we are aware of.

However, it can be quite simple to set a photometric spatial correction to embed in a profile. A simple way would be to be able to add some tag in a *spatial ICC profile*. This tag would relate to a shading table based either on measurement or on some a priori knowledge on the display.

There is still a lot of work to do at the research level to be able to implement a practical solution for a full spatial color characterization, so it is a bit early to discuss about that.

Although there is a possibility to use several displays on one computer, there are many reports of problems in using a different profile for each of these. CMMs could be updated for this purpose. If there is an overlapping area, then there is no possibility of adjustement via any CMM we have seen. There could be some possibilites to deal with that if first CMMs and ICC would include a shading table to correct for spatial non-uniformity, before to have something better.

10.4 Spatial photometric projector non-uniformity end-user camera-based correction

In using the method presented in Chapter 5, since there is a camera, we have the potential of a relative spatial photometer. We designed a method that may permit us to

correct for photometric spatial non-uniformity. We still need to finish to implement and to test this algorithm.

There are two possibilities to perform such a correction, either in considering simply a shading table ignoring that the black level is not negligible, or in setting a range from the maximum black offset to the minimum *white* and to map all values inside this range, such as shown in Figure 8.2.

For this purpose, the camera has to be corrected for its vignetting effect. This can be done in a end-user way, following the method presented in (Mansouri et al., 2005), which considers the median of several acquisitions of (a sheet of paper as) a flat field surface to estimate a spatial correction to remove the vignetting effect and some blotches or spots that can be on the lenses.

Then in using the method presented in Chapter 5, the camera response curve can be estimated and, shooting a correct pattern, the correction can be established.

10.5 Spatial color uniformity

This section discusses some ideas for dealing with the problem of color uniformity within a projector system.

10.5.1 Spatial colorimetric characterization

The first thing to say considering a spatial colorimetric model is that we are limited by the number of measurements that is practically possible to take. We can consider different approaches to get data in a reasonable time:

- Considering a end user, we can consider the use of a camera, some visual processes, data from the manufacturer, etc.
- Considering a professional use, which is still the most common case, some spatial colorimeters can be use, or a point-wise spectroradiometer augmented with a high quality camera.
- Some approaches aimed to use a camera built in the projector, however, manufacturers found this procedure too expensive since there is the need of a camera of quality to be able to perform measurement.

In any case, there is a need to build a display spatial color characterization model (there is the need in projector systems, but also in LCD monitors where the uniformity is known to be bad). The only attempt we know is Hardeberg et al. (2003) work. They achieved good results (see Section 8.2.2).

From the Chapter 9, we know that some features will remain invariant all along the spatial dimension of the display. That will help us to know what kind of model to use and to find what kind of measurements are required to perform to reach the needed accuracy.

At the end, there is still the need of defining standards and implementing them into softwares to handle this kind of data.

10.5.2 Perceptual approach for non-uniformity and image dependent processing

The attempt done by Majumder (2005); Majumder and Stevens (2005) gives good looking results (there is no quantitative ones), but is half satisfying for us since it deals only with intensity smoothing, and the color blotches remain. Moreover, it can not be satisfying in all cases since it considers human visual system limitations through threshold contrast sensitivity function. The neighborhood to consider in term of pixel should depend then on the distance of the viewer. For collaborative environment application that can be a limit. However, it should be possible to perform such a correction considering color. A possibility to model such a correction can be to consider a *spatial-gamut mapping* (a gamut that vary spatially along the projector). Even if there is still the problem of acquiring data, it seems to be a possibility to have smooth transition between all display areas.

In order to make a model, which fits our perceived color appearance, we need to consider more psychovisual features, such as the color adaptation at the local and at the global level, cognition and physiology.

Moreover if we consider the image content, it is reasonable to think that the perceived uniformity would not be broken in many cases. Further experiments should be done in this direction to find what can be considered as perceived spatial uniformity.

Chapter 11

General conclusion

Le caméléon n'a la couleur du caméléon que lorsqu'il est posé sur un autre caméléon.

François Cavanna

Abstract

This chapter concludes this thesis. We recall the main results of this work in the context of display color characterization.

We proposed and evaluated many pointwise display characterization models, from an end-user consumer method that does not require any expensive color measurement device to a 3D LUT model based on polyharmonic splines interpolation that requires automatic and accurate measurements. The conclusion is that the user need should be taken into consideration.

We then established a basis for spatial color characterization via the quantitative analysis of the color shift and its spatial variation throughout the display area. We found that the spatial chromaticity shift is not negligible in some cases, and that some features are spatially invariant within one display of a given technology. The conclusion is that in some cases a spatial color characterization is required.

In this research area there are still remaining challenges in several directions. First, there is a need for spatial models based on colorimetry, and some frameworks and standards to apply them in practice. Secondly, there is a need for a better understanding of spatial color perception in order to design models that are using displays at their maximum capacity considering the limits of the human visual system.

Thus, being able to manage display's colors permits to work between applied color imaging and fundamental color vision.

11.1 Summary

In the context of color imaging, this thesis focused on colorimetric characterization of displays and multi-display systems. We defined a duality in the need for consumer or professional use. From the pointwise approach we shifted to some spatial considerations.

We considered in the first part of this thesis point wise display color characterization. We proposed, evaluated and improved several methods to control the color in displays.

Among the models tested, we investigated deeply the PLVC model especially in comparison to the PLCC model. We have shown that for CRT and DLP technologies, the PLCC model was performing well, as long as a black correction was carried out. The results were found equivalent to the PLVC, in accordance with previously published results. However, we have shown that we can reduce significantly the characterization error by using PLVC instead of PLCC on LCD technology. This experiment can be pushed forward to multi-primary displays.

We confirmed that the end-user method proposed by Bala and Braun was giving significantly better results than using default gamma settings for both LCD and DLP projectors. We proposed an improved method by increasing the number of visual matching patterns and in performing the estimation of each primary response curve independently. This adds a little complexity but provides better results. This method is quick and simple and does not need any measurement device other than a simple digital color camera. There is still a challenging issue in the visual estimation of the projector black offset. Moreover, there is probably some ways to extend this method to a spatial color characterization model.

We worked on the distribution of color patches in color space for the establishment of 3D LUT models. We proposed a new accurate forward model based on polyharmonic splines and we demonstrated that it is possible to perform an accurate real time colorimetric rendering. The accuracy of such a model is strongly influenced by the distribution of measured samples, and an iterative process to select these patches coupled with an automatic measurement process improves the characterization result. We applied this method to color rendering of multispectral images of art paintings with accurate results, and the next work would be to include a color appearance model to ensure high quality color rendering for virtual exhibition of paintings.

Considering the distribution of samples, we proposed some methods to build an optimized structure that permits to invert any display color characterization forward model. We used several criteria linked with the grid itself or with an evaluation data set. The practical case we evaluated showed that we can achieve better results than with a regular equidistributed grid. Some further work could be done concerning the

optimization criteria used and the training data set. We do believe that this method to build and select the optimized structure to invert the colorimetric model can be applied to any output color device, such as printers, perhaps with other functions.

In the second part, we analyzed the spatial behavior of projection displays.

In our investigation, we performed a quantitative analysis of the color shift throughout the display area. We have shown that the measured chromaticity shift along the spatial dimension of a projector is quite large, and that considering only the luminance to be spatially non-uniform can be a critical mistake in some applications. Through the analysis of features, we have shown that most of the color shift, not induced by the lens system, was coming from the spatial differences in response curve in LCD projectors, and from a spatial variation of the channel interaction for DLP technology. These features will be of major interest for designing a spatial color characterization model for projectors.

However, considering the image content, it is reasonable to think that the perceived uniformity would not be broken in many cases. Further experiments could be done in this direction to find what can be considered as perceived spatial uniformity.

11.2 Closing

The choice of a display color characterization model depends not only on the display technology in question, but also on the user needs. There is a clear difference between a high-end professional characterization that aims to be as colorimetrically accurate as possible, and a consumer-type characterization that has the less ambitious goals of preserving the meaning and the aesthetic content of the displayed content. We have evaluated a wide range of models, and the results presented in this thesis can help to decide which model should be used for a given application and a given display.

The color spatial non-uniformity of projection displays can be a critical issue in some cases. Vision researchers who are performing display-based psychophysical experiments, and imaging engineers who are designing multi-display systems should definitively consider correcting for this non-uniformity.

To conclude, the results presented in this thesis aim to help controlling color in displays. This can help color scientists and engineers in two directions. First, one can design higher performance displays that take into account the capabilities and limits of the human visual system to maximize their capabilities. Secondly, one can design psychophysical experiments to help to understand the human visual system limitations and behavior. Indeed, far beyond this work, understanding how humans perceive color

images and how they interact with them may be a key element to better understand mankind.

Bibliography

Abrardo, A., Cappellini, V., Cappellini, M. and MECOCCI, A. (1996), Art-works colour calibration using the vasari scanner, *in* 'Color Imaging Conference', IS&T - The Society for Imaging Science and Technology, pp. 94–97.

Ajito, T., Obi, T., Yamaguchi, M. and Ohyama, N. (2000), Expanded color gamut reproduced by six-primary projection display, *in* M. H. Wu, ed., 'Proc. SPIE Vol. 3954, p. 130-137, Projection Displays 2000: Sixth in a Series, Ming H. Wu; Ed.', Vol. 3954 of *Presented at the Society of Photo-Optical Instrumentation Engineers (SPIE) Conference*, pp. 130–137.

Ajito, T., Ohsawa, K., Obi, T., Yamaguchi, M. and Ohyama, N. (2001), "Color conversion for multiprimary display using matrix switching", *Optical Review* , Vol. 8, pp. 191–197.

Akima, H. (1970), "A new method of interpolation and smooth curve fitting based on local procedures", *Journal of the Association for Computing Machinery* , Vol. 17, pp. 589–602.

Amidror, I. (2002), "Scattered data interpolation methods for electronic imaging systems: a survey", *Journal of Electronic Imaging* , Vol. 11, SPIE, pp. 157–176.

Anderson, M., Motta, R., Chandrasekar, S. and Stokes, M. (1995), Proposal for a standard default color space for the internet: srgb, *in* 'Fourth Color Imaging Conference', IS&T/SID, pp. 238–245. Scottsdale, Arizona, USA.

Arsenault, A., Puzzo, D., Manners, I. and Ozin, G. (2007), "Photonic-crystal full-colour displays", *Nature Photonic* , Vol. 1, Nat Photon, pp. 468 – 472.

Arslan, O., Pizlo, Z. and Allebach, J. P. (2003), CRT calibration techniques for better accuracy including low-luminance colors, *in* R. Eschbach and G. G. Marcu, eds, 'Color Imaging IX: Processing, Hardcopy, and Applications. Edited by Eschbach, Reiner; Marcu, Gabriel G. Proceedings of the SPIE, Volume 5293, pp. 286-297 (2003).', Vol. 5293 of *Presented at the Society of Photo-Optical Instrumentation Engineers (SPIE) Conference*, pp. 286–297.

Bakke, A. M., Hardeberg, J. Y. and Farup, I. (2006), Evaluation of gamut boundary descriptors, *in* 'CIC06', pp. 50–55.

Bakke, A. M., Thomas, J.-B. and Gerhardt, J. (2009), Common assumptions in color characterization of projectors, *in* G. Simone, ed., 'Proc. of Gjøvik Color Imaging Symposium', Vol. 4 of *Proc. of Gjøvik Color Imaging Symposium*, pp. 45–53.

Bala, R. and Braun, K. (2006), A camera-based method for calibrating projection color displays, *in* 'Fourteenth Color Imaging Conference', IS&T/SID, pp. 148–152. Scottsdale, Arizona, USA.

Bala, R., Klassen, R. V. and Braun, K. M. (2007), "Efficient and simple methods for display tone-response characterization", *Journal of the Society for Information Display* , Vol. 15, SID, pp. 947–957.

Balasubramanian, R. and Dalal, E. (1997), A method for quantifying the color gamut of an output device, *in* 'Color Imaging: Device-Independent Color, Color Hard Copy, and Graphic Arts II', Vol. 3018 of *Proc. SPIE*, San Jose, CA.

Balasubramanian, R. and Maltz, M. S. (1996), Refinement of printer transformations using weighted regression, *in* J. Bares, ed., 'Society of Photo-Optical Instrumentation Engineers (SPIE) Conference Series', Vol. 2658 of *Society of Photo-Optical Instrumentation Engineers (SPIE) Conference Series*, pp. 334–340.

Bass, M., DeCusatis, C., Enoch, J., Lakshminarayanan, V., Li, G., Macdonald, C., Mahajan, V. and Van Stryland, E. (2010*a*), *Handbook of Optics, Third Edition Volume I: Geometrical and Physical Optics, Polarized Light, Components and Instruments(set)*, McGraw-Hill, Inc., New York, NY, USA.

Bass, M., DeCusatis, C., Enoch, J., Lakshminarayanan, V., Li, G., Macdonald, C., Mahajan, V. and Van Stryland, E. (2010*b*), *Handbook of Optics, Third Edition Volume II: Design, Fabrication and Testing, Sources and Detectors, Radiometry and Photometry*, McGraw-Hill, Inc., New York, NY, USA.

Bastani, B., Cressman, B. and Funt, B. (2005), "Calibrated color mapping between LCD and CRT displays: A case study", *Color Research & Application* , Vol. 30, pp. 438–447.

Bern, M. and Eppstein, D. (2003), Optimized color gamuts for tiled displays, *in* 'SCG '03: Proceedings of the nineteenth annual symposium on Computational geometry', ACM, New York, NY, USA, pp. 274–281.

Berns, R. (1996), "Methods for characterizing CRT displays", *Displays* , Vol. 16, Elsevier Science B.V., Amsterdam, pp. 173–182.

Berns, R. S., Fernandez, S. R. and Taplin, L. (2003), "Estimating black-level emissions of computer-controlled displays", *Color Research & Application* , Vol. 28, Wiley, pp. 379–383.

Berns, R. S., Gorzynski, M. E. and Motta, R. J. (1993), "CRT colorimetry. part II: Metrology", *Color Research & Application* , Vol. 18, Wiley, pp. 315–325.

Berns, R. S., Motta, R. J. and Gorzynski, M. E. (1993), "CRT colorimetry. part I: Metrology", *Color Research & Application* , Vol. 18, Wiley, p. 299314.

Bhasker, E. S., Sinha, P. and Majumder, A. (2006), "Asynchronous distributed calibration for scalable and reconfigurable multi-projector displays", *IEEE Trans. Vis. Comput. Graph.* , Vol. 12, pp. 1101–1108.

Bimber, O. and Raskar, R. (2005), *Spatial Augmented Reality: Merging Real and Virtual Worlds*, A. K. Peters, Ltd., Natick, MA, USA.

Blondé, L., Stauder, J. and Lee, B. (2009), "Inverse display characterization: A two-step parametric model for digital displays", *Journal of the Society for Information Display* , Vol. 17, SID, pp. 13–21.

Bookstein, F. (1989), "Principal warps: Thin-plate splines and the decomposition of deformations", *IEEE Transactions on Pattern Analysis and Machine Intelligence* , Vol. 11, IEEE Computer Society, Los Alamitos, CA, USA, pp. 567–585.

Brainard, D. H. (1989), "Calibration of a computer-controlled color monitor", *Color Research & Application* , Vol. 14, Wiley, New-York, pp. 23–34.

Brainard, D. H., Pelli, D. and Robson, T. (2002), *Display characterization, Encyclopedia of Imaging Science and Technology*, Wiley, New-York.

Carr, J. C., Beatson, R. K., Cherrie, J. B., Mitchell, T. J., Fright, W. R., McCallum, B. C. and Evans, T. R. (2001), Reconstruction and representation of 3d objects with radial basis functions, *in* 'SIGGRAPH '01: Proceedings of the 28th annual conference on Computer graphics and interactive techniques', ACM, New York, NY, USA, pp. 67–76.

Catrysse, P. B., Wandell, B. A., *a, P. B. C., W, B. A., B, E. and Gamal, A. E. (1999), Comparative analysis of color architectures for image sensors, *in* N. Sampat and T. Yeh, eds, 'proc. SPIE', Vol. 3650, proc. SPIE, pp. 26–35.

Chan, J. Z., Allebach, J. P. and Bouman, C. A. (1997), "Sequential linear interpolation of multidimensional functions", *IEEE Transactions on Image Processing* , Vol. 6, pp. 1231–1245.

Chen, C.-J. and Johnson, M. J. (2001), Fundamentals of scalable high-resolution seamlessly tiled projection system, *in* M. H. Wu, ed., 'Projection Displays VII', Vol. 4294, SPIE, pp. 67–74.

Chen, H., Sukthankar, R., Wallace, G. and Li, K. (2002), Scalable alignment of large-format multiprojector displays using camera homography trees, *in* 'VIS '02: Proceedings of the conference on Visualization '02', IEEE Computer Society, Washington, DC, USA, pp. 339–346.

Choi, S. Y., Luo, M. R., Rhodes, P. A., Heo, E. G. and Choi, I. S. (2007), "Colorimetric characterization model for plasma display panel", *Journal of Imaging Science and Technology* , Vol. 51, pp. 337–347.

CIE (1996), *The relationship between Digital and Colorimetric Data for Computer-Controlled CRT displays*, CIE, Publ 122.

CIE (2001), *142-2001, Improvement to industrial colour-difference evaluation*, Commission Internationale de l'Eclairage.

CIE (2004), *015:2004, Colorimetry, 3rd edition*, Commission Internationale de l'Eclairage.

Colantoni, P., Boukala, N. and Rugna, J. D. (2003), Fast and accurate color images processing using 3d graphics cards, *in* 'VMV', pp. 383–390.

Colantoni, P. F., Stauder, J. F. and Blonde, L. F. (2005), 'Device and method for characterizing a colour device'.

Colantoni, P., Pitzalis, D., Pillay, R. and Aitken, G. (2007), Gpu spectral viewer: analysing paintings from a colorimetric perspective, *in* 'The 8th International Symposium on Virtual Reality, Archaeology and Cultural Heritage', Brighton, United Kingdom.

Colantoni, P. and Thomas, J.-B. (2009), A color management process for real time color reconstruction of multispectral images, *in* A.-B. Salberg, J. Y. Hardeberg and R. Jenssen, eds, 'Lecture Notes in Computer Science', Vol. 5575 of *16th Scandinavian Conference, SCIA*, pp. xx–xx.

Cowan, W. B. (1983), "An inexpensive scheme for calibration of a colour monitor in terms of CIE standard coordinates", *SIGGRAPH Comput. Graph.* , Vol. 17, ACM, New York, NY, USA, pp. 315–321.

Cowan, W. and Rowell, N. (1986), "On the gun independency and phosphor constancy of color video monitor", *Color Research & Application* , Vol. 11, pp. S34–S38.

Day, E. A., Taplin, L. and Berns, R. S. (2004), "Colorimetric characterization of a computer-controlled liquid crystal display", *Color Research & Application* , Vol. 29, pp. 365–373.

Dianat, S., Mestha, L. and Mathew, A. (2006), "Dynamic optimization algorithm for generating inverse printer map with reduced measurements", *Acoustics, Speech and Signal Processing, 2006. ICASSP 2006 Proceedings. 2006 IEEE International Conference on* , Vol. 3, pp. III–III.

Draréni, J., Roy, S. and Sturm, P. (2009), Geometric video projector auto-calibration, *in* 'Proceedings of the IEEE International Workshop on Projector-Camera Systems, Miami, Florida'.

Elliott, C., Credelle, T. and Higgins, M. (2005), "Adding a white subpixel", *Information Display Magazine* , Society for information display.

Fairchild, M. and Wyble, D. (1998), "Colorimetric characterization of the Apple Studio display (flat panel LCD)", *Munsell Color Science Laboratory Technical Report* .

Farley, W. W. and Gutmann, J. C. (1980), "Digital image processing systems and an approach to the display of colors of specified chrominance", *Technical report HFL-80-2/ONR-80, Virginia Polytechnic Institute and State University, Blacksburg, VA* , Virginia Polytechnic Institute and State University, Blacksburg, VA.

Farup, I., Gatta, C. and Rizzi, A. (2007), "A multiscale framework for spatial gamut mapping", *Image Processing, IEEE Transactions on* , Vol. 16, pp. 2423–2435.

Farup, I., Hardeberg, J. Y., Bakke, A. M., Kopperud, S. and Rindal, A. (2002), Visualization and interactive manipulation of color gamuts, *in* 'CIC02', pp. 250–255.

Gauss, C. F. (1801), *Disquisitiones arithmeticae*, Apud G. Fleischer, Leipzig (reprinted New-York: Springer-Verlag, 1986).

Gibson, J. E. and Fairchild, M. D. (2000), "Colorimetric characterization of three com- puter displays (LCD and CRT)", *Munsell Color Science Laboratory Technical Report* .

Gill, P. E., Murray, W. and Wright, M. H. (1982), *Practical Optimization*, Academic Press.

Green, P. and MacDonald, L., eds (2002), *Color engineering*, Wiley, Chichester, U.K.

Groff, R. E., Koditschek, D. E. and Khargonekar, P. P. (2000), Piecewise linear homeomorphisms: The scalar case., *in* 'IJCNN (3)', pp. 259–264.

Hales, T. C. (1998), 'An overview of the kepler conjecture'.

Hardeberg, J. (1999), Acquisition and reproduction of colour images: colorimetric and multispectral approaches, Th?se de doctorat, ?cole Nationale Sup?rieure des T?l?communications, ENST, Paris, France.

Hardeberg, J. Y., Seime, L. and Skogstad, T. (2003), Colorimetric characterization of projection displays using a digital colorimetric camera, *in* M. H. Wu, ed., 'proc. SPIE', Vol. 5002, proc. SPIE, pp. 51–61.

Hereld, M., Judson, I. R. and Stevens, R. (2003), Dottytoto: a measurement engine for aligning multiprojector display systems, *in* M. H. Wu, ed., 'Projection Displays IX', Vol. 5002, SPIE, pp. 73–86.

ICC (2004), 'Specification icc.1.2004-10'.

IEC:61966-3 (1999), *Color measurement and management in multimedia systems and equipment, part 3: Equipment using CRT displays*, IEC.

IEC:61966-6 (1998), *Color measurement and management in multimedia systems and equipment, part 3: Equipment used for digital image projection, committee Draft*, IEC.

Jimenez Del Barco, L., Daz, J. A., Jimenez, J. R. and Rubino, M. (1995), "Considerations on the calibration of color displays assuming constant channel chromaticity", *Color Research & Application* , Vol. 20, pp. 377–387.

Kang, H. R., ed. (1997), *Color technology for electronic imaging devices*, SPIE Press.

Kasson, L. M., Nin, S. I., Plouffe, W. and Hafner, J. L. (1995), "Performing color space conversions with three-dimensional linear interpolation", *J. of Electronic Imaging* , Vol. 4(3), pp. 226–250.

Katoh, N., Deguchi, T. and Berns, R. (2001*a*), "An accurate characterization of CRT monitor (i) verification of past studies and clarifications of gamma", *Optical Review* , Vol. 8, The Optical Society of Japan, co-published with Springer-Verlag GmbH, pp. 305–314.

Katoh, N., Deguchi, T. and Berns, R. (2001*b*), "An accurate characterization of CRT monitor (II) proposal for an extension to CIE method and its verification", *Optical Review* , Vol. 8, The Optical Society of Japan, co-published with Springer-Verlag GmbH, pp. 397–408.

Kepler, J. (1611), "The six-cornered snowflake", *Monograph* .

Klassen, R., Bala, R. and Klassen, N. (2005), Visually determining gamma for softcopy display, *in* 'Procedeedings of the thirteen's Color Imaging Conference', IS&T/SID, pp. 234–238.

Kwak, Y., Li, C. and MacDonald, L. (2003), "Controling color of liquid-crystal displays", *Journal of the Society for Information Display* , Vol. 11, SID, pp. 341–348.

Kwak, Y. and MacDonald, L. (2000), "Characterisation of a desktop LCD projector", *Displays* , Vol. 21, Elsevier, pp. 179–194.

Lantz, E. (2007), A survey of large-scale immersive displays, *in* 'EDT '07: Proceedings of the 2007 workshop on Emerging displays technologies', ACM, New York, NY, USA, p. 1.

Li, K., Chen, H., Chen, Y., Clark, D. W., Cook, P., Damianakis, S., Essl, G., Finkelstein, A., Funkhouser, T., Housel, T., Klein, A., Liu, Z., Praun, E., Samanta, R., Shedd, B., Singh, J. P., Tzanetakis, G. and Zheng, J. (2000), "Building and using a scalable display wall system", *IEEE Computer Graphics and Applications* , Vol. 20, IEEE Computer Society, Los Alamitos, CA, USA, pp. 29–37.

Luo, M. R., Cui, G. and Rigg, B. (2001), "The development of the cie 2000 colour-difference formula: Ciede2000", *Color Research & Application* , Vol. 26, Wiley Periodicals, Inc., pp. 340–350.

Mahy, M., Eycken, L. V. V. and Oosterlinck, A. (1994), "Evaluation of uniform color spaces developed after the adoption of cielab and cieluv", *Color Research & Application* , Vol. 19, Wiley Periodicals, Inc., pp. 105–121.

Majumder, A. (2005), Contrast enhancement of multi-displays using human contrast sensitivity, *in* 'CVPR '05: Proceedings of the 2005 IEEE Computer Society Conference on Computer Vision and Pattern Recognition (CVPR'05) - Volume 2', IEEE Computer Society, Washington, DC, USA, pp. 377–382.

Majumder, A. and Brown, M. S. (2007), *Practical Multi-projector Display Design*, A. K. Peters, Ltd., Natick, MA, USA.

Majumder, A. and Gopi, M. (2005), "Modeling color properties of tiled displays", *Comput. Graph. Forum* , Vol. 24, pp. 149–163.

Majumder, A. and Stevens, R. (2002), Lam: Luminance attenuation map for photometric uniformity in projection based displays, *in* 'Proceedings of ACM Virtual Reality and Software Technology', Press, pp. 147–154.

Majumder, A. and Stevens, R. (2004), "Color nonuniformity in projection-based displays: Analysis and solutions", *IEEE Transactions on Visualization and Computer Graphics* , Vol. 10, IEEE Computer Society, Los Alamitos, CA, USA, pp. 177–188.

Majumder, A. and Stevens, R. (2005), "Perceptual photometric seamlessness in projection-based tiled displays", *ACM Trans. Graph.* , Vol. 24, ACM, New York, NY, USA, pp. 118–139.

Mansouri, A., Marzani, F. and Gouton, P. (2005), "Development of a protocol for ccd calibration: application to a multispectral imaging system", *International Journal of Robotics and Automation, Special Issue on Color Image Processing and Analysis for Machine Vision* , Vol. 20, Acta Press, pp. 94–100.

Marcu, G. G., Chen, W., Chen, K., Graffagnino, P. and Andrade, O. (2001), Color characterization issues for TFTLCD displays, *in* R. Eschbach and G. G. Marcu, eds, 'Proc. SPIE', Vol. 4663, Proc. SPIE, pp. 187–198.

Matthew, M., Brennesholtz, S. and Stupp, E. H. (2008), *Projection Displays*, 2 edn, Wiley Publishing.

Mikalsen, E. B. (2007), "Verification and extention of a camera based calibration method for projection displays.", *Master Thesis, Master of media technology* , Gjøvik University College, Colorlab.

Mikalsen, E. B., Hardeberg, J. Y. and Thomas, J.-B. (2008), Verification and extension of a camera-based end-user calibration method for projection displays, *in* 'CGIV', pp. 575–579.

Morovic, L. and Luo, M. R. (2001), "The fundamentals of gamut mapping: A survey", *Journal of Imaging Science and Technology* , Vol. 45, pp. 283–290.

Neumann, A., Artusi, A., Zotti, G., Neumann, L. and Purgathofer, W. (2003), Interactive perception based model for characterization of display device, *in* 'Color Imaging IX: Processing, Hardcopy, and Applications IX', Vol. 5293, SPIE Proc., pp. 232–241.

Nielson, G. M., Hagen, H. and Müller, H., eds (1997), *Scientific Visualization, Overviews, Methodologies, and Techniques*, IEEE Computer Society.

Pagani, A. and Stricker, D. (2006), Photometric and chromatic calibration for multi-projector tiled displays, *in* 'Fourteenth Color Imaging Conference', IS&T/SID, pp. 291–296. Scottsdale, Arizona, USA.

Pagani, A. and Stricker, D. (2007), "Spatially uniform colors for projectors and tiled displays", *Journal of the Society for Information Display* , Vol. 15, SID, pp. 679–689.

Pailthorpe, B., Bordes, N., Bleha, W., Reinsch, S. and Moreland, J. (2001), High resolution display with uniform illumination, *in* 'Proc. Asia Display', pp. 1295–1298.

Post, D. L. and Calhoun, C. S. (1989), "An evaluation of methods for producing desired colors on CRT monitors", *Color Research & Application* , Vol. 14, pp. 172–186.

Post, D. L. and Calhoun, C. S. (2000), "Further evaluation of methods for producing desired colors on CRT monitors", *Color Research & Application* , Vol. 25, pp. 90–104.

Raskar, R., Welch, G., Cutts, M., Lake, A., Stesin, L. and Fuchs, H. (1998), The office of the future: A unified approach to image-based modeling and spatially immersive displays, *in* 'Proceedings of SIGGRAPH 98', Computer Graphics Proceedings, Annual Conference Series, pp. 179–188.

Ribés, A., Schmitt, F., Pillay, R. and Lahanier, C. (2005), "Calibration and spectral reconstruction for crisatel: an art painting multispectral acquisition system", *Journal of Imaging Science and Technology* , Vol. 49, pp. 563–573.

Rudd, M. J., Dunn, P. M. and Gemmer, E. C. (2008), "P-237: Measurement of the picture contrast enhancement of gray projection screens", *SID Symposium Digest of Technical Papers* , Vol. 39, SID, pp. 2093–2094.

Santos, P., Stork, A., Gierlinger, T., Pagani, A., Arajo, B., Jota, R., Bruno, L., Jorge, J. A., Pereira, J. M., Witzel, M., Conti, G., de Amicis, R., Barandarian, I., Paloc, C., Hafner, M. and McIntyre, D. (2007), Improve: Advanced displays and interaction techniques for collaborative design review., *in* R. Shumaker, ed., 'HCI (14)', Vol. 4563 of *Lecture Notes in Computer Science*, Springer, pp. 376–385.

Schläpfer, K. (1993), Farbmetrik in der reproduktionstechnik und im mehrfarbendruck, *in* S. G. Schweiz, ed., '2. Auflage UGRA'.

Seime, L. and Hardeberg, J. Y. (2002), Characterisation of lcd and dlp projection displays, *in* 'Color Imaging Conference', IS&T - The Society for Imaging Science and Technology, pp. 277–282.

Seime, L. and Hardeberg, J. Y. (2003), "Colorimetric characterization of LCD and DLP projection displays", *Journal of the Society for Information Display* , Vol. 11, SID, pp. 349–358.

Selbrede, M. and Yost, B. (2006), Time multiplexed optical shutter (tmos) display technology for avionics platforms, Vol. 6225 of *Proc. SPIE*, p. 62251B.

Sharma, G. (2002), "LCDs versus CRTs: Color-calibration and gamut considerations", *Proc. IEEE* , Vol. 90, pp. 605–622. special issue on Flat Panel Display Technologies.

Sharma, G. (2003), *Digital Color Imaging Handbook*, CRC Press.

Sharma, G. and Shaw, M. Q. (2006), Thin-plate splines for printer data interpolation, *in* 'Proc. "European Signal Proc. Conf."'. [CDROM].

Sharma, G., Wu, W. and Dalal, E. N. (2005), "The ciede2000 color-difference formula: Implementation notes, supplementary test data, and mathematical observations", *Color Research & Application* , Vol. 30, Wiley Periodicals, Inc., pp. 21–30.

Sharma, G., Wu, W., Dalal, E. N. and Celik, M. U. (2004), Mathematical discontinuities in ciede2000 color difference computations, *in* 'Color Imaging Conference', IS&T - The Society for Imaging Science and Technology, pp. 334–339.

Shepard, D. (1968), A two-dimensional interpolation function for irregularly-spaced data, *in* 'Proceedings of the 1968 23rd ACM national conference', ACM, New York, NY, USA, pp. 517–524.

Skolnick, L. P. and Callahan, J. W. (1994), "Luminance calculation on a spherical projection surface with varying screen gain characteristics", *Image VII Conference Proceedings* , pp. 23–32.

Stamm, S. (1981), An investigation of color tolerance, *in* 'TAGA Proceedings', TAGA Proceedings, pp. 156–173.

Stauder, J. F., Colatoni, P. F. and Blonde, L. F. (2006), 'Device and method for characterizing a colour device'.

Stauder, J., Thollot, J., Colantoni, P. and Tremeau, A. (2007), 'Device, system and method for characterizing a colour device', European Patent WO/2007/116077.

Stokes, M., Fairchild, M. D. and Berns, R. S. (1992), "Precision requirements for digital color reproduction", *ACM Trans. Graph.* , Vol. 11, ACM, New York, NY, USA, pp. 406–422.

Stokes, Michael (Cupertino, C. (1997), 'Method and system for analytic generation of multi-dimensional color lookup tables'.

Stone, M. (2002), *Field Guide to Digital Color*, A. K. Peters, Ltd., Natick, MA, USA.

Stone, M. C. (2001), "Color and brightness appearance issues in tiled displays", *IEEE Comput. Graph. Appl.* , Vol. 21, IEEE Computer Society Press, Los Alamitos, CA, USA, pp. 58–66.

Tamura, N., Tsumura, N. and Miyake, Y. (2003), "Masking model for accurate colorimetric characterization of LCD", *Journal of the Society for Information Display* , Vol. 11, SID, pp. 333–339.

Thomas, J.-B. (2006), "Tatouage d'image couleur, en vue de l'insertion d'une palette de couleurs caractéeristiques des couleurs d'une image", *Master Thesis* , Universit Jean Monnet, LIGIV.

Thomas, J.-B. and Bakke, A. M. (2009), A colorimetric study of spatial uniformity in projection displays, *in* 'Lecture Notes in Computer Science', number 5646 *in* 'Lecture Notes in Computer Science', Springer, pp. 160–169.

Thomas, J.-B., Chareyron, G. and Trémeau, A. (2007), "Image watermarking based on a color quantization process", *Multimedia Content Access: Algorithms and Systems* , Vol. 6506, SPIE, p. 650603.

Thomas, J.-B., Colantoni, P., Hardeberg, J. Y., Foucherot, I. and Gouton, P. (2008*a*), "A geometrical approach for inverting display color-characterization models", *Journal of the Society for Information Display* , Vol. 16, SID, pp. 1021–1031.

Thomas, J.-B., Colantoni, P., Hardeberg, J. Y., Foucherot, I. and Gouton, P. (2008*b*), An inverse display color characterization model based on an optimized geometrical structure, *in* R. Eschbach, G. G. Marcu and S. Tominaga, eds, 'proc. SPIE', Vol. 6807, SPIE, pp. 68070A–1–12.

Thomas, J.-B., Hardeberg, J. Y., Foucherot, I. and Gouton, P. (2007), Additivity based LC display color characterization, *in* J. Y. Hardeberg, P. Nussbaum and I. Farup, eds, 'Proc. of Gjøvik Color Imaging Symposium', Vol. 3 of *Proc. of Gjøvik Color Imaging Symposium*, pp. 50–55.

Thomas, J.-B., Hardeberg, J. Y., Foucherot, I. and Gouton, P. (2008), "The plvc color characterization model revisited", *Color Research & Application* , Vol. 33, Wiley Periodicals, Inc., pp. 449–460.

Thomas, J.-B. and Trémeau, A. (2007), A gamut preserving color image quantization, *in* 'ICIAPW '07: Proceedings of the 14th International Conference of Image Analysis and Processing - Workshops', IEEE Computer Society, Washington, DC, USA, pp. 221–226.

Tóth, F. (1960/61), "On the stability of a circle packing", *Ann. Univ. Sci. Budapestinensis, Sect. Math.* , Vol. 3-4, pp. 63–66.

Viassolo, D. E., Dianat, S. A., Mestha, L. K. and Wang, Y. R. (2003), "Practical algorithm for the inversion of an experimental input-output color map for color correction", *Optical Engineering* , Vol. 42, SPIE, pp. 625–631.

Wallace, G., Anshus, O. J., Bi, P., Chen, H., Chen, Y., Clark, D., Cook, P., Finkelstein, A., Funkhouser, T., Gupta, A., Hibbs, M., Li, K., Liu, Z., Samanta, R., Sukthankar, R. and Troyanskaya, O. (2005), "Tools and applications for large-scale display walls", *IEEE Comput. Graph. Appl.* , Vol. 25, IEEE Computer Society Press, Los Alamitos, CA, USA, pp. 24–33.

Wallace, G., Chen, H. and Li, K. (2003), Color gamut matching for tiled display walls, *in* 'EGVE '03: Proceedings of the workshop on Virtual environments 2003', ACM, New York, NY, USA, pp. 293–302.

Wen, S. and Wu, R. (2006), "Two-primary crosstalk model for characterizing liquid crystal displays", *Color Research & Application* , Vol. 31, pp. 102–108.

Widdel, H. and Post, D. L., eds (1992), *Color in Electronic Displays*, Plenum Press.

www.gpgpu.org (2009), 'www.gpgpu.org'.
URL: *http://www.gpgpu.org*

www.projectorcentral.com (2009), 'www.projectorcentral.com'.
URL: *http://www.projectorcentral.com*

Wyble, D. R. and Rosen, M. R. (2004), Color management of dlp projectors, *in* 'Proceedings of the twelfth Color Imaging Conference', IS&T - The Society for Imaging Science and Technology, pp. 228–232.

Wyble, D. R. and Zhang, H. (2003), Colorimetric characterization model for dlp projectors, *in* 'Procedeedings of the eleventh Color Imaging Conference', IS&T - The Society for Imaging Science and Technology, pp. 346–350.

Wyszecki, G. and Stiles, W. S. (2000), *Color Science: Concepts and Methods, Quantitative Data and Formulae (Wiley Series in Pure and Applied Optics)*, 2 edn, Wiley-Interscience.

Yamaguchi, M., Mitsui, M., Ishikawa, R., Haneishi, H. and Ohyama, N. (2004), "Real-time video reproduction using six-band hdtv camera and six-primary display", *IS&T/SID's CIC12* .

Yeh, P. and Gu, C. (1999), *Optics of Liquid Crystal Display*, Wiley, New-York.

Yoshida, Y. and Yamamoto, Y. (2002), Color calibration of LCDs, *in* 'Tenth Color Imaging Conference', IS&T - The Society for Imaging Science and Technology, pp. 305–311. Scottsdale, Arizona, USA.

Appendices

Appendix A

Display technologies

Abstract

This appendix covers display technology. It gives some information considering color reproduction and the technology being behind the screen. We present the main technologies, and how the color is created.

A.1 Foreword

This appendix is based on a lecture given to the master Media Technology at the Gjøvik University College. The sources are coming mainly form the web, from discussions, presentations and from some articles. It has no pretension of exhaustivity, especially because the display market is evolving very fast, and because it is not the purpose of this thesis. However it will help the reader to understand the core of the thesis. Hopefully the reader will enjoy to have some more information about display technology. The reader familiar with display technologies can either skip it, or pass fast over it.

A.2 Introduction

A.2.1 Display device

To start with displays, we took randomly four definitions of *display* from different places:

- A display device, or information display, is a device for visual or tactile presentation of images acquired, stored or transmitted in various forms. Inside this category are analog or digital electronic displays, projectors, mechanical types, braille displays, idiot lights, segment displays.
- A display device is a computer output surface, and projecting mechanism that shows an image to the computer user. Usually, the display is considered including the screen or the projection surface, and the display that produces the information on the screen.
- A display device is a CRT, flat panel LCD, plasma, aerial imaging, projector or other electronic device that is at the end point of a (digital, color) system, presenting the content.

- An electronic display is a device or system, which converts electronic signal information representing video, graphics and/or text to a viewable image of this information.

Whatever the definition, the common point is that we got the idea of visualizing some information through a medium.

We will limit our study to digital color displays, which means that the information is originally a digital set of values and the output is a spatial arrangement of colors.

In such a system, the information takes different shapes. Before the display, there can be a natural or analog scene, digital values from the camera, adobe RGB values, etc. Within the display the information is changing as well since it is often an analog signal that has to be input to a display, then the digital value has to be converted into a voltage. That is less true with LCD, Plasma or OLED displays coupled with DVI or HDMI standards. After the display, the information may change considering the environment, the geometrical situation of the observer, etc.

A.2.2 Features

We can draw a list of features that are of importance for a display.

For the normal users, the important features can be: Brightness (luminance), contrast (white/black), viewable size (diagonal, active display area), dot pitch (the distance between the centers of two adjacent pixels), resolution or native resolution (horizontal and vertical size expressed in pixels, which is useless for CRT), response time (minimum time necessary to change a pixel color or brightness), viewing angle, aspect ratio (4:3, 16:9, 16:10).

A high level user might want to have more information, such as: additivity properties (is the color displayed the sum of the 3 independent channels ?), gamut size and shape (the gamut being the set of colors that a display can reproduce, and/or the volume covered by these colors inside a color space), response curve (relation between the voltage/digital input and the intensity of the light output, gamma), black level (amount of light output when we want to display nothing), primary constancy (is the chromaticity of each channel consistent versus the input ?), calibration facilities (brightness, contrast, white point, customable LUT), characterization (relationship between the RGB input and the color displayed)

A.2.3 color reproduction

Most part of displays is based on the additive mixture of primaries. That means that a color C is a weighted sum of N primaries, such as in Equation A.1:

$$C = \alpha_1.P_1 + \alpha_2.P_2 + \alpha_3.P_3 + \alpha_4.P_4 + ... + \alpha_N.P_N \tag{A.1}$$

In many cases for a color display, there are three primaries [1], with dominant wavelength around the red green and blue (the so-called RGB primaries). Then Equation A.1 can become

[1] Although there is more and more a white channel to increase the overall luminance of the display, or more than 3 primaries to increase the gamut size.

Equation A.2:

$$C = \alpha_1.R + \alpha_2.G + \alpha_3.B \tag{A.2}$$

A.2.4 Types of displays

We can distinguish between three main types of displays:

- Virtual displays are forming the image to focus directly on the retina, they are single user projection displays, and are using the same technology.
- Direct view displays that produce the image on the surface being viewed. They are usually designed for a single user or a small number (monitors).
- Projection display creates the image on an auxiliary surface that is physically separated from the image generating component. They are usually well fitted for group viewing.

A.2.5 Image generation

We can have two kinds of system to generate an image. A display can be emissive, such as CRT, OLED, laser or plasma. On another hand, it can be based on a light modulating device, such as LCD or micro-electronical device (DLP).

A projection system can be rear projection (the light is coming from the other side of the screen relatively to the user -transmittance-) or front projection (the light come from the same side and is reflected on the screen).

A.3 Current technologies and systems

Among the technologies presented thereafter, we count CRT, LCD, Plasma, LED, LCOS, TMOS, Laser, DLP, Analog cinema projection device, Stereo-vision displays and so on.

A.3.1 Monitors

We will review major monitor technologies.

Cathod Ray Tube (CRT)

It exists since 1879 and is probably the most known technology both by users and scientists. Electrons are emitted by an electron gun, and go to hit a phosphorescent material, which transforms the energy in light.

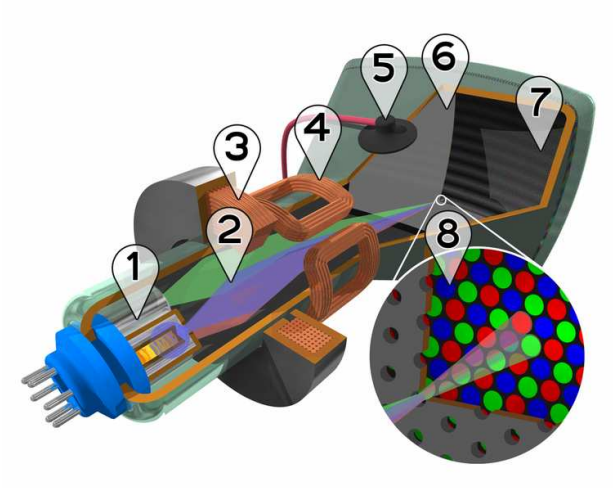

Figure A.1: *Illustration of the CRT display. 1-Electron gun. 2-Electron beam. 3-Focusing coils. 4-Deflection coils. 5-Anode connection. 6-Mask for separating beams. 7 and 8-Phosphor coated on the inner side of the screen. From http://upload.wikimedia.org/wikipedia/commons/thumb/9/9b/CRT_color_enhanced.png/750px-CRT_color_enhanced.png.*

Technology details Electrons are coming from the cathode, and take there celerity with the high voltage in the anode (difference of potential between both). Electrons are focused and deflected using a magnetic or electrostatic field. The beam arrives then on the anode that is covered by a phosphorescent material (for instance rare earth). The arriving energy excites materials electrons, and light is emitted when these electrons loose this energy. The chemical properties of the phosphors define the spectrum of the light emitted (color). The last part is a perforated piece of metal (shadow mask) that is aligned in such a way that only the red dots can be hurt by the red beam (same for the blue and green). Controlling the intensity of the beam, the wanted color is emitted. The mix between primaries is based on spatial assimilation. See Figure A.1.

Color and image Originally, the electron gun did just draw a line between two points (vector); there was no aliasing or pixelization. However it was limited to display a shapes outline. Now, the gun scans the whole screen along a defined path. In varying the intensity applied along the path, an image is created because of temporal assimilation. To reduce the flickering effect that can rise up with this kind of assimilation, it is of use to interlace 2 images. The first image describes the odd lines, then the even ones are described.

Color information is controlled by the power given to each gun (R,G,B). Note that the relationship between the input voltage and the emitted light is not linear but follow a gamma law.

Advantages and drawbacks Advantages include the low cost production (matured technology), color fidelity (well known technology), color management systems has been originally designed for it, gamut size. This technology allows the perception of true black (or almost, because of a low black level), works well at multiple resolution, displays full motion video better when comparing with LCD (high refresh rate). The angle of view does not influence so much the perception of colors.

However, there is a sharpness problem when too much power is applied to the fluorescent panel. That is due to the uncollimated electron beam. This technology is known for its radiation emission, larger size, heavy weight. It expends a lot of energy and throws off heat.

A compromise has to be found for the refresh rate. A low refresh rate leads to a flicker effect due to the desactivation of phosphors between two passages of the electron beam. Instead of that, a high refresh rate leads to a leak of sharpness due to the over-excitation of phosphors.

Although it seems this is the end of CRT, this technology still shows the best color rendering available. LED based technologies may definitely overcome CRT.

Liquid crystal display (LCD)

It is the technology that has replaced CRT displays. It has grown up since the 80's. A backlight is used as light source, and some filters based on liquid crystals are controlling the amount of light that is going out.

Technology details Two polarizers, which polarization directions show an angle of 90 (most part of time) on each side of a "sandwich" compounded by two layers of glass are the base. The layers of glass surround some liquid crystals in nematic state (between solid crystal and liquid). The molecules are distributed without order, but in average parallel, i.e. with an orientation direction as in a crystal. Around the crystals, polymer layers take the molecules fixed when no power is applied, and play the role of electrodes. The LC panel is passive (it does not emit any light).

The light comes from the backlight; it is polarized by the first polarizer (if there is no crystal, the light is blocked by the second polarizer). With no power, the orientation of the crystals molecules is given by the alignment with the surface of the polymer layer. With twisted nematic (helicoidal arrangement), the arrangement of the crystals at rest changes the polarization of the light of 90 (then the panel seems to be transparent). The change of polarization is due to the birefringence of liquid crystals. When some power is applied, it creates a magnetic field, which will modify the orientation of the molecules. In the case of twisted nematic, which will force the molecules to be aligned. if so, they do not change the polarization of the light, then no (less) quantity of light is in the good polarization state to pass through the second polarizer. Note that the use of polarized light induces a loss of energy while passing through the first polarizer since only the light in the right polarized state passes through.

Color and image The LCD panel is originally in gray level (let pass more or less the light). The color is reached applying color filters on sub pixels (spatial assimilation).

The color is limited by the spectral properties of the backlight and of the color filters used. Originally only 6^3 colors could be really reproduced instead of 8^3 for a 8 bits device because of a bad control of crystal' orientation. This problem is mostly overcome now.

When the monitor is not used in the native resolution, some aliasing effect may happen. Aliasing corresponds to the modifications a continuous signal can suffer when sampled and reconstructed with a too small number of sample (See Figure A.2)

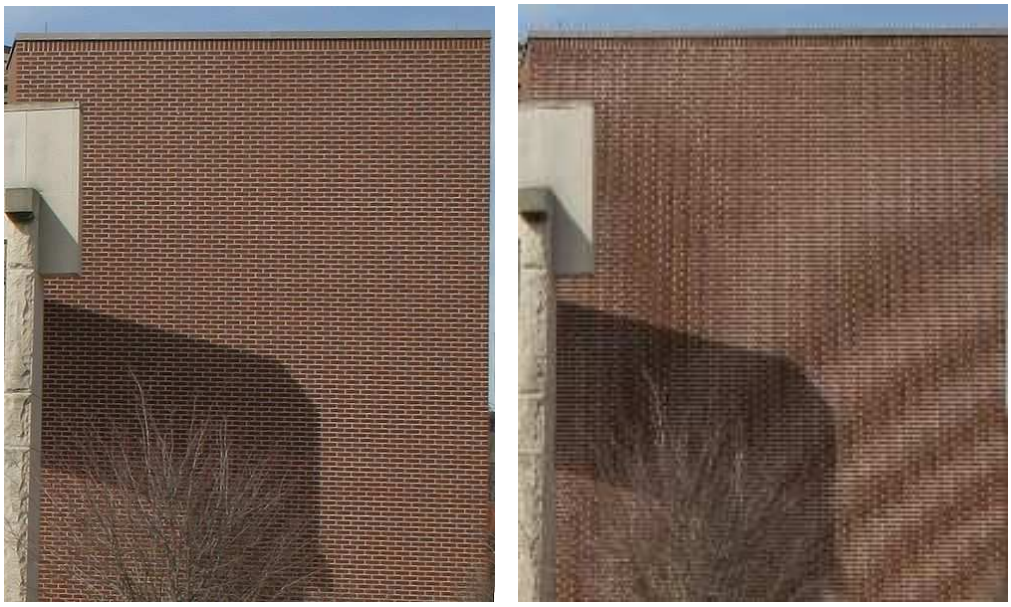

(a) Properly sampled image (b) Moiré effect due to aliasing

Figure A.2: *Visualizations of the aliasing effect. The first image (a) is properly sampled; The second one (b) shows some moiré effect due to a sampling badness. From http://en.wikipedia.org/wiki/File:Moire_pattern_of_bricks.jpg and http://en.wikipedia.org/wiki/File:Moire_pattern_of_bricks_small.jpg.*

Increasing the resolution of a LCD panel leads to a lack of brightness. On Figure A.3, one can see that the material used to fix the liquid crystal is filling more and more of the panel surface while increasing the resolution. Several solutions can be used to overcome this problem, such as using a reflective polarizing film to recycle existing light (increases efficiency of 20-30%), or adding bulbs or increasing the power of the existing bulb.

To enhance the color and image rendering capabilities of an LCD display, it is possible to use lumileds technology (using LEDs as backlight), to use wide color gamut cold cathode fluorescent lamp as backlight, instead of a normal cold cathode fluorescent (That increases the color space of about 28%, but is approximately 30% less efficient).

The in-plane switching and vertically aligned mode configurations improve the switching speeds, the contrast, and the viewing angle compared with twisted Nematic, but 50% less light

Figure A.3: *Illustration of the variation of luminance with the resolution. The surface covered by the material used to fix the liquid crystal fils more and more of the panel surface while increasing the resolution.*

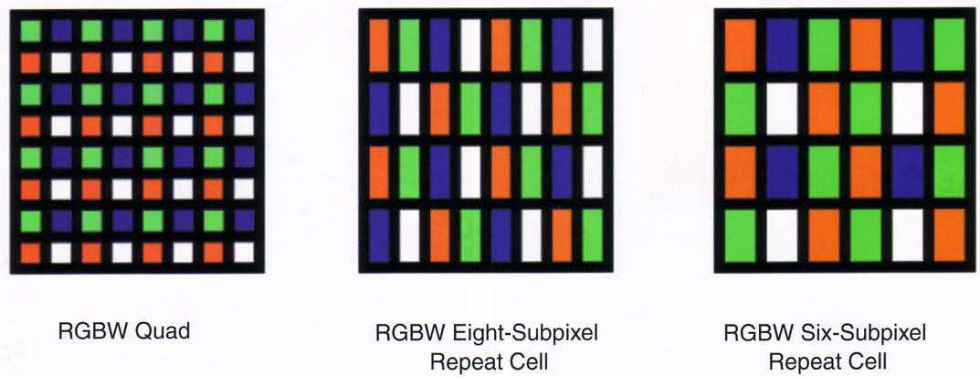

Figure A.4: *Example of arrangement of sub pixels in a RGBW based LC display. From (Elliott et al., 2005).*

is transmitted.

Considering that natural images are typically made up of rich saturated colors, which are hardly ever very bright, together with extremely bright unsaturated color, such as reflection from smooth objects, it is possible to augment the traditional RGB sub pixel with a white sub pixel (Elliott et al., 2005). Figure A.4 illustrates a way for the arrangement of such a pattern, Figure A.5 illustrates the comparison with a traditional RGB system. This solution has already been implemented in many mobile displays.

Main types of LCDs Following are the main arrangements:

- TN and DSTN (Dual Scan TN). TN is the basic technology, it has a bad response time (better with DSTN, which makes a double scan). It has a passive matrix, and it is transparent at rest state.
- TFT (Thin Film Transistor). The electrode is replaced by one electrode and a transistor layer at the back. That permits a better control of the tension, then improve the response time ($\leq 10ms$). It is an active matrix, and black at rest state (the layer of silicium for the transistors)

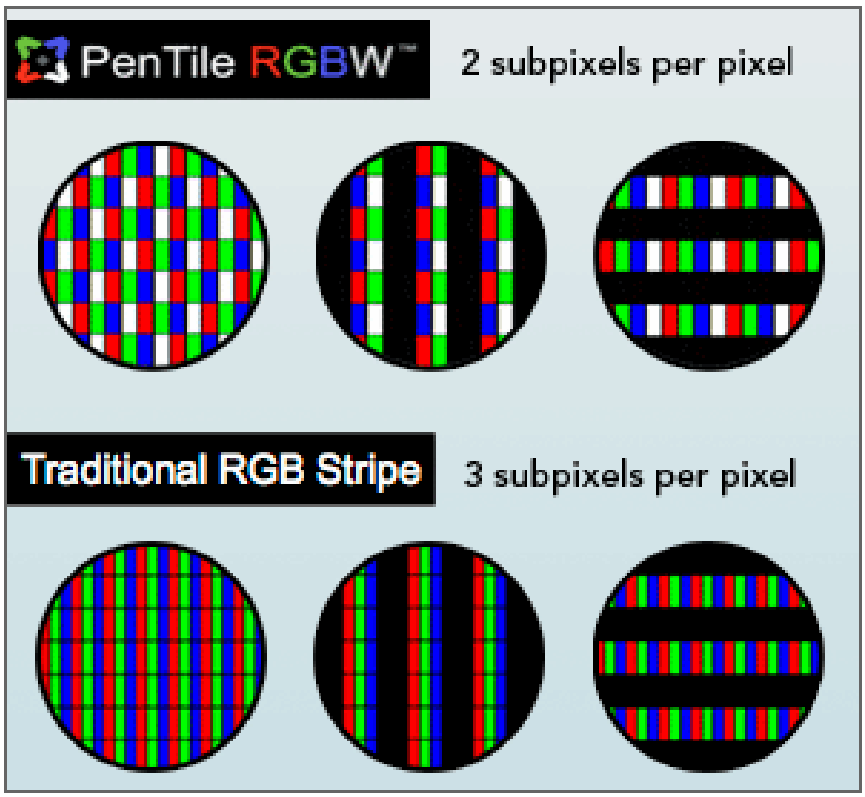

Figure A.5: *Example of arrangement of sub pixels in a RGBW based LC display compared with a traditional RGB pattern. Note that the structure shows the same modulation-transfer-function limit. From http://www.clairvoyante.com/images/rgb-v-rgbw-circle-chart.png.*

- IPS and S-IPS (In-Plane Switching) uses liquid crystals parallel to the screen (better vision angle, but double number of transistors).
- MVA (Multi-Domain Vertical Alignment) and PVA (Patterned Vertical Alignment). Several refraction domain by cells (better black level, then better contrast and angle view).

Latency time and motion blur The latency time or response time refers to the time for a pixel to change its state from the more complete black to the highest saturated white, and to come back to the black. Sometimes, the latency time is expressed as the time to go from a gray level to another. This is an important feature of LCDs since major drawbacks are resulting of a too slow response time. Between two frames, the pixels have not the time to reach the satisfactory level, and it results in a blurring (ghost effect or motion blur). Applying more voltage than required to the pixel at the beginning permits to reach faster the desired level. This was originally a problem for LCD technology, but now it is fast enough. However, this result is reach in decreasing the quality of the color rendering and the viewing angle.

Even if there is no latency, the motion blur will still happen since there is a hard transition between two images in a video. however, there is a solution that may be used to reach a *perfect*

motion. A black frame is intercalled between each frame. Images are combined with these black frames, and no more motion blur is perceivable since the visual system adapts for a short while to the black.

Advantages and drawbacks The design was clearly what made LCD to overcome CRT when it appeared on the market (weight, flat). Moreover, it provides less flickering effect, is energy efficient, and can provide high brightness.

However, there is a major leakage considering the contrast ratio (the crystal is not able to block all the light, then the black level is high). The angle-view dependence is large, and the color is limited by the backlight properties. Moreover, a major drawback is that it is defined for only an optimal resolution. Note as well that the cost of the backlight represents about 70% of the cost of the display. A major issue is that the spectral transmittance of a liquid crystal is varying with the arrangement of the crystals. The consequence is that the primaries spectral properties are not consistent with the increasing intensity.

Plasma Display Panel (PDP)

This technology exists since 1964.

Technology details It is based on the same principle as a fluorescent tube. Neon and Xenon (noble gases) are contained in several boxes, sandwiched between 2 plates of glass (Figure A.6). Electrodes are also present between the glass. Creating a voltage difference ionizes the gas (ionized gas : one or more free electrons present), and creates plasma, which is conductive. The gas ions can then rush and collide the electrodes. Their energy is transformed in photons. To create color primaries, phosphors cover the surface, and the UV photons emitted by the plasma excite the phosphor that emits light in the visible spectrum.

Advantages and drawbacks Using this technology, there are potentially no limit of size. It has a wide gamut considering the phosphors used as primaries. The angle of view is good, there is no black level, it is emissive.

However, it is expensive to build the system for very high resolution. The color control is difficult, especially because the displayed color (not only the perceived one) is dependent of the neighborhood, as the plasma is reacting with electro-magnetic fields, and as the luminance is limited for high luminance scene in order to save some energy (The power required varies a lot with the displayed content). Some ghost effects can appear when a cell stay excited even without intended input power. The life time is not that good, it looses its luminosity with the use.

LED based technology

Organic Light-Emitting Diode (OLED) (kodak, 1987), Light Emitting Polymer (LEP) (Cambridge, display tech), Organic Electro-Luminescence (OEL) are Light-Emitting Diode (LED) dis-

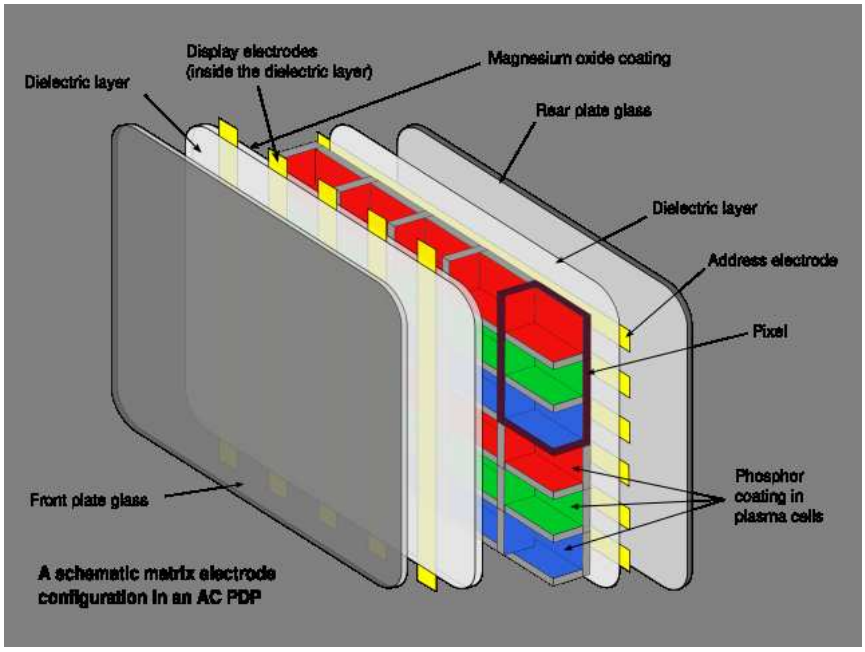

Figure A.6: *Plasma Display Panel technology. From http://en.wikipedia.org/wiki/File:Plasma-display-composition.svg.*

plays, which emissive electro-luminescence layer is composed of a film of organic components. The layer usually contains a polymer pixel, which can emit light of different colors

Technology details It is a solid state device, consisting in a series of organic thin films (semiconductors) sandwiched between two thin film conductive electrodes (See Figure A.7). When electricity is applied, charges are injected inside the organic semiconductor, the created color is dependent of the material used (red, green, orange, yellow, emerald green, blue, but as well ultra-violet or infra-red). The thin film can be of almost every material where you can depose the substrate. The technology to depose the substrate or to build the electrodes can be nanoimprint (electrodes), inkjet printing (organic sc) vacuum deposition, vacuum thermal evaporation or organic vapor phase deposition.

Semi-conductor A semi-conductor presents a conductivity between conductor and insulator. Electric current is possible because of holes or/and electrons. Propagation by electrons is normal (atoms exchange their extra electrons from one to the other from negative area to a less negative). Propagation by holes is different. Charges travel from positive area to a less positive because of the motion created by the miss of an electron in a quasi-full electrical structure. Controlling the number of holes or electrons permits to change the characteristic of the material (doping the material). A material with more holes is called N-type, one with more electrons is called P-type.

A P-N Junction is the juxtaposition of N and P material. When a positive tension is applied

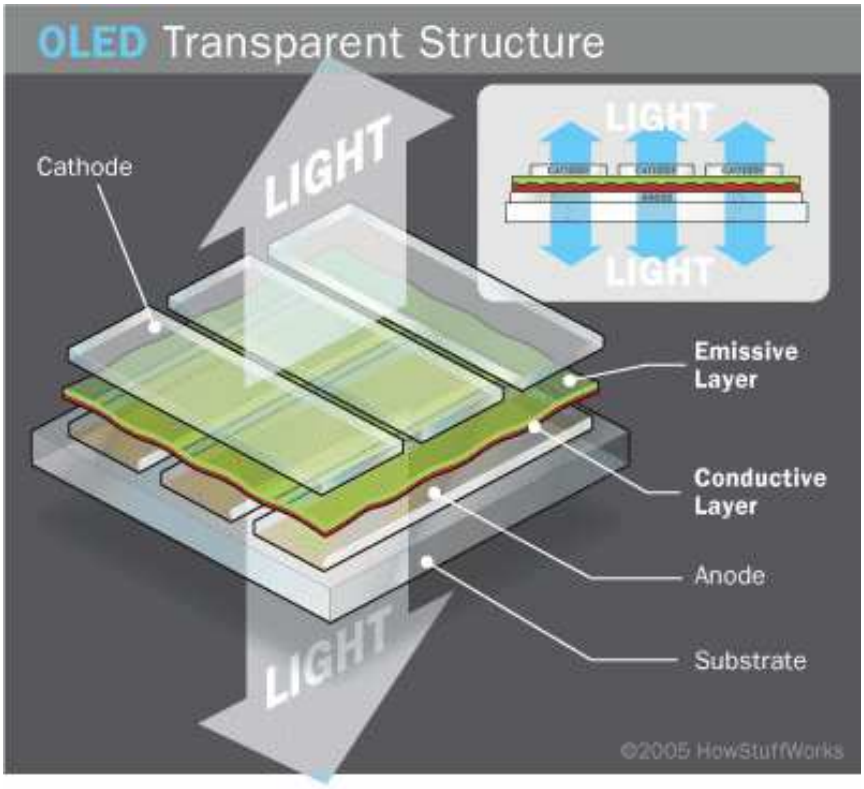

Figure A.7: *OLED principle. From http://static.howstuffworks.com/gif/oled-transparent.gif.*

to the P area, the holes are pushed to the junction. In the same time, in the N area, the electrons are pushed to the junction. When they meet in the border, they can combined (electron-hole) and emit a photon. See Figure A.8.

An organic semiconductor is the same process except that the material is different (crystal or polymer). Organic means carbon based.

Types of LED based displays Based on the OLED concept, several kinds of displays can be derived:

- FOLED (Flexible Organic Light-Emitting Diode) consists in printing the OLED on a flexible substrate (plastic or metal). A lot of applications can be imagined, but it is more breakable than glass substrates.
- PHOLED (Phosphorescent) A soluble phosphorescent material is used to create the OLED, instead of fluorescent material. That means that 100% of the power applied is converted into light.
- TOLED (Transparent) uses transparent electrodes and light emitting materials. Its then possible to emit light by the top surface, by the bottom surface or by both sides. It has 70%

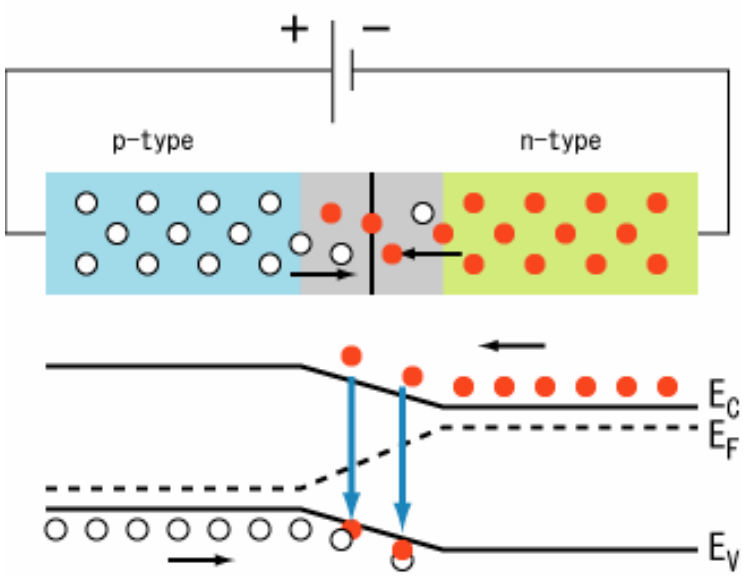

Figure A.8: *PN junction, illustration. From http://fr.wikipedia.org/wiki/Fichier:PnJunction-Diode-ForwardBias.PNG.*

transparency when not in use.

- SOLED (Stacked) improves color quality and resolution, stacking TOLEDs together. Stacking sub pixels together, each pixel have its color components at the same place.

Advantages and drawbacks This technology is low power consuming. It has a good color rendering (wide gamut), a good contrast because of a low black level, a good viewing angle. It is Thin and may be flexible. It is easy and cheap to build.

However its major drawback is its lifetime (PHOLEDs can improve it, using less energy leading to a longer life) and its sensibility to wetness during the fabrication process and the need for containment inside materials. Another brake to its expansion is that it is an owner technology (Eastman Kodak and others).

A.3.2 Projectors

We will review major projection system technologies, such as Cinema, CRT/Laser, LCD, DLP, LCoS and so on.

Cinema analogic projection displays

Although it is not a digital device, it is interesting to give a word about it. These displays are based on a printed film. Both subtractive and additive mixtures are present and the gamut of a film looks more like a printer one. There are more and more replaced in projection theater, but there are still present in the majority of the cinemas.

Figure A.9: *Pico projection display example. From http://www.macintom.com/wp/wp-content/gallery/2009-01/microvision-pico-projector.png.*

CRT projection displays

They use a small, high-brightness CRT to generate the image. This image is focused and enlarged using a lens in front on the CRT face. A typical configuration consists in 1 to 3 separate CRTs with 1 to 3 lenses. They have the same characteristics than the CRT monitors, augmented by the problem of moving these system, and by the low level of luminance that can be reached. Moreover they are expensive.

Laser projection displays

They are similar to CRTs, but the phosphors, emitting an incoherent and uncollimated light, are replaced by lasers emitting a coherent and collimated light. Usually each laser has its lens, but a one-lens solution can be performed without recombination (as in the CRT ones). the main advantages of these projectors is that they can be of real small size, and they can have a good intensity.

Note that pico projectors (See Figure A.9) are on the market for a couple of years now, and that they can be based as well on DLP principle, using Micro-Electro-Mechanical Systems (MEMS) or on LCoS and LED backlight. They have typically an output of about 10 lumens.

Light valve panels principle

The light is splitted in three (or more) components (RGB). Each color is modulated separately, then recombined and sent via a single lens to the user (via the screen). We can distinguish between single, two, or three panels:

- Single panel systems use only one light valve to modulate the three channels (color field

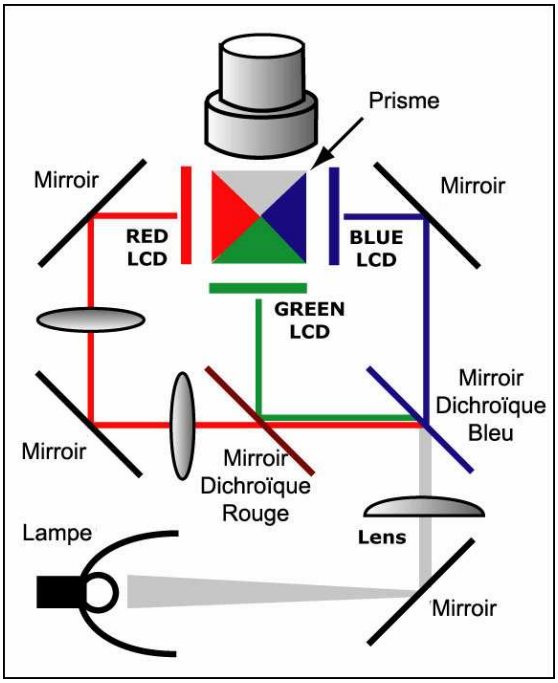

Figure A.10: *Tri-LCD projection system. From http://gp32.free.fr/projo/LCD.jpg.*

sequential systems -DLP-, color micro-filter designs, angular separation methods).

- In two panel systems, one light valve modulates one primary, and an other one modulates the 2 others. This configuration is useful if the panel can modulate 2 colors satisfactorily, but not 3. For instance if the projection lamp is deficient for one color, requiring a longer period of integration than for the 2 others to get enough light.
- Three panel systems consider one panel for each primary (many LCDs).

LCD projection systems

Technology details The light valve is a transmissive LCD Panel. The light is separated using dichroic mirrors. Information for each channel is modulated using LCD panel(s). The light is recombined within a dichroic prism and go through the lens to the screen, such as shown in Figure A.10.

Advantages and drawbacks LCD projectors have a good saturation compared with DLP when there is a white filter in the color wheel. it looks sharp at any resolutions.

However, the level of black offset is high (bad contrast). They suffer from the screen door effect (lines between pixels are visible), and from spatial non-uniformities due to the difficulty to align the LCD panels and the optics.

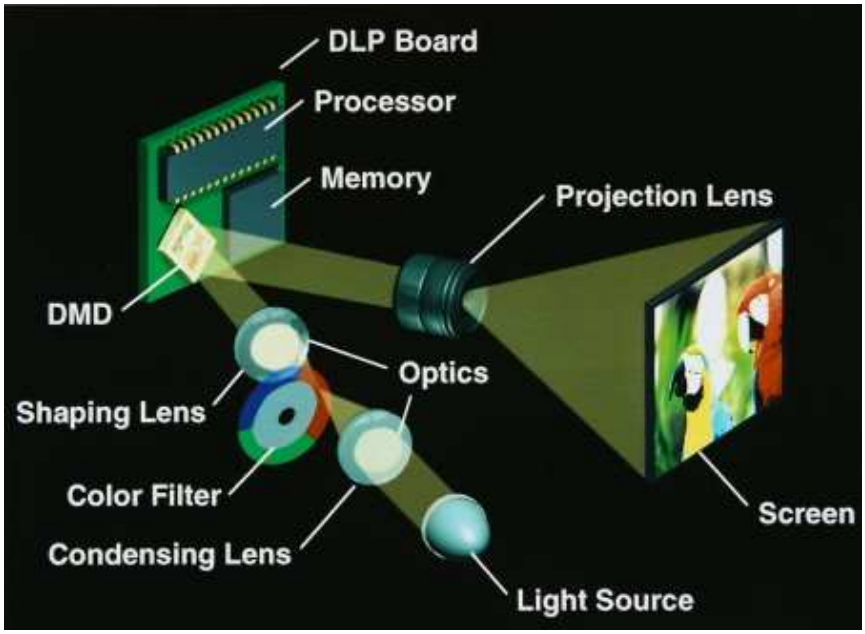

Figure A.11: *DLP principle. From http://www.pctechguide.com/images/57DLP_1chip.jpg.*

Digital Light Processing (DLP)

The light valve is a digital micro-mirror device (DMD) in this case. The light is separated temporally using a color wheel (Most part of the time, but a 3 DMDs system that uses dichroic mirrors can exist. The light is then recombined using a dichroic prism). The DMD contains one micro-mirror by pixel. The orientation of the mirrors determine the amount of light that will go through the lens. A typical configuration is shown on Figure A.11.

DMD DMD is a technology that has been created in the 70s. In 1987, TIs researchers have put the mirrors on a CMOS chipset matrix of 1280*1024 microscopic mirrors. Each mirror can pivot on 10-15 as a switcher (on-off). If its on, all the light is transmitted to the lens. In off case the light is not transmitted to the lamp, but to a black body, which absorbs it. The intensity levels are obtained combining these two states frequencies. The mirrors are controlled by electrostatic attraction.

Color wheel Although it is possible to use a dichroic mirror system to separate the light into several components, the use of 3 DMD is expensive. The most part of time the one DMD configuration appears. In this case, the light is separated temporally. To do that, a color wheel is used (Figure A.12):

- 3 colors color-wheel (RGB), some rainbow effect may appear.
- 3+1 color-wheel (RGBW), which desaturates the colors.

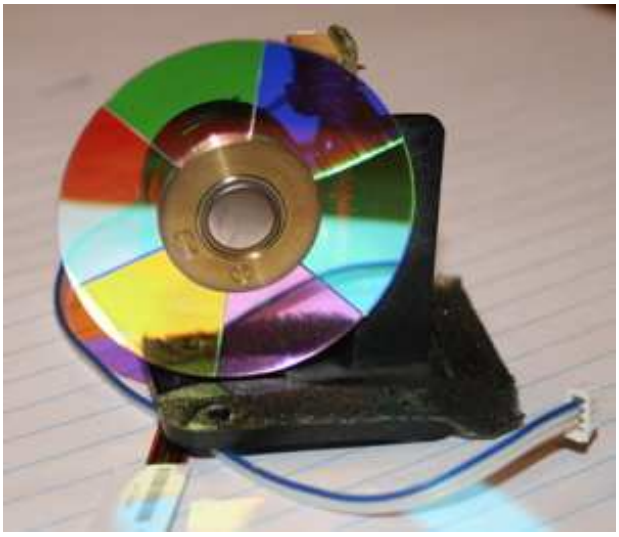

Figure A.12: *A color wheel with 6 primaries. Note that the size and the arrangement of each color is not the same to avoid some color breaking effect. From http://www.jangro.com/images/samsung-dlp/samsung-color-wheel.jpg.*

- 2*3 color-wheel (RGBRGB), helps to remove rainbow effect, in increasing the frequency.
- N primaries color-wheel (RGBCMY, RGBWCMY, RGBY, etc) are used to increase the size of the gamut.

Advantages and drawbacks Advantages include the low level of black offset. the good primaries constancy (the filter keeps on the same transmittance property), the *easy* way to increase the number of primaries and the small size in the case of a single DMD. Disadvantages include the color break-up (rainbow effect) and temporal stability that is less good than LCD but really acceptable.

Liquid Crystals on Silicon (LCoS)

The reflective light valve is based on liquid crystals deposed on a reflective silicon plate (Figure A.13). They can be based on a color wheel, on three chipsets or on a colored chipset.

Multi-projector systems

A way to increase the display's resolution is to tile several displays together. See Chapter 8.

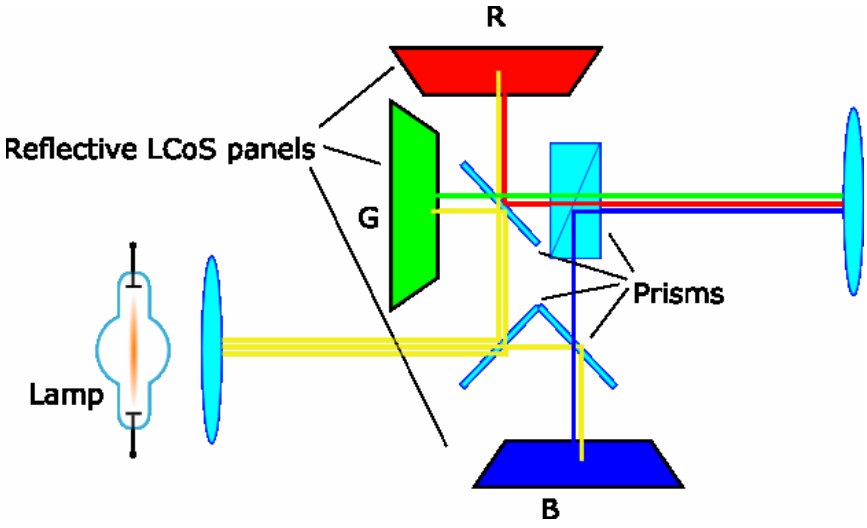

Figure A.13: *LCoS technology. From http://en.wikipedia.org/wiki/File:Lcos.svg.*

A.3.3 3D displays

Holography

The image captured is an image of interferences (not focused on a film). A coherent laser light is reflected by an object, and combined at a film with light from a reference beam : the two beams are interfering. The film records the interferences (keeping the information of phase) and, illuminating the film with the same light, one can see the object in 3D.

Stereoscopy

Two different images of the same scene are sent to each eyes. The brain understands the information as two perspectives of the same object, giving the illusion of 3D. The use of special glasses permits to separate both signals. Several ways may be used for this purpose, such as polarizing light, combined with different polarizers on the glasses for each eye. It is possible as well to use different spectral information to be sent, using different filters on the glasses for each eye.

Auto stereoscopy The monitor sends different information to each eye (without the need of special glasses). However, the head has to be well positioned.

Heliodisplay

The principle is to project images either on a compressed air flow or on a mist flow. Since there is no depth reference (such as a monitor border) that creates the effect of 3D. Considering a rear projection, the user has to have an oblique angle of view in order not to face the lamp.

A.4 A step further

Here is mixed some tomorrow's technologies that might be already yesterday's once since the market is evolving really fast.

- Photonic crystals improve the luminance of LEDs, maybe already in displays. They use a photonic crystal fixed on the LED, to improve the emission of light (Arsenault et al., 2007).
- TMOS (Time Multiplexed Optical Shutter) consists in temporal additivity in a solid state (Selbrede and Yost, 2006).
- SED (Surface-conduction Electron-emitter Display) and FED (Field Emission Display). The principle is the same than a CRT (so the same advantages), but with a kind of a cathode ray tube behind each pixel, and slim like a LCD. It was supposed to arrive on the market last year, but Canon and Toshiba, which were developing the project, stopped mid-2008. It seems now that Canon started again with SED at the beginning of 2009.
- Dual view concept makes two persons to watch the same screen and to see different scenes (See Figure A.14). These displays are based on the same approach than the stereoscopic displays, considering special glasses to isolate each signal, or considering geometry (each direction receives a different information).
- Real 3-D displays. On Figure A.15 is shown an attempt to create a real 3D display. The area contains ionized gas. Focusing a laser beam at a given position permits to produce plasma, which emits light. Currently there are many technical challenges with this approach.
- etc.

A.5 Color modification and black box effect on color characterization

When considering display accurate colorimetric rendering, a model has to be established between the input value and the color displayed. However, there are many effects, voluntarily done by the manufacturer to improve the image content, which affect the color rendering. For example:

- To improve the color content in using several primaries, there is a need of a transform between *RGB* and $P_1, P_2, P_3, ..., P_N$ primaries. As well, the color saturation of the original color can be increased to please more the user.

  These transforms are often kept secret by the manufacturer. However, if they are consistent, one can deal with them in using an empirical model for color control.

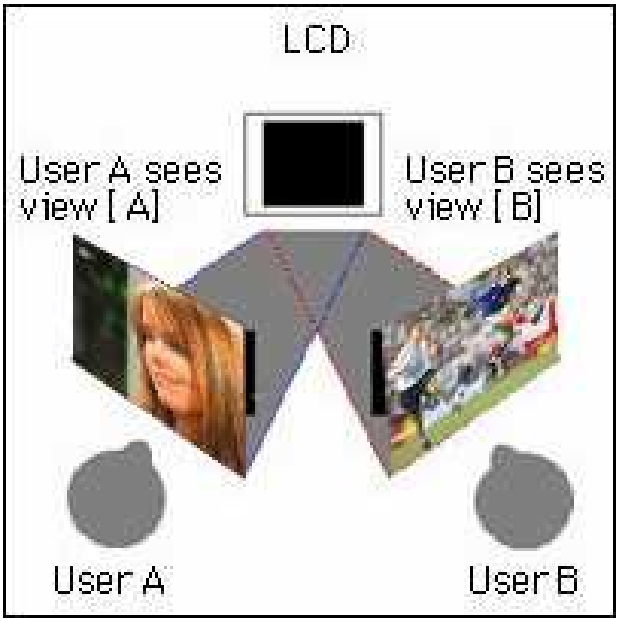

Figure A.14: *Dual view concept. From http://img1.lesnumeriques.com/news/712.jpg.*

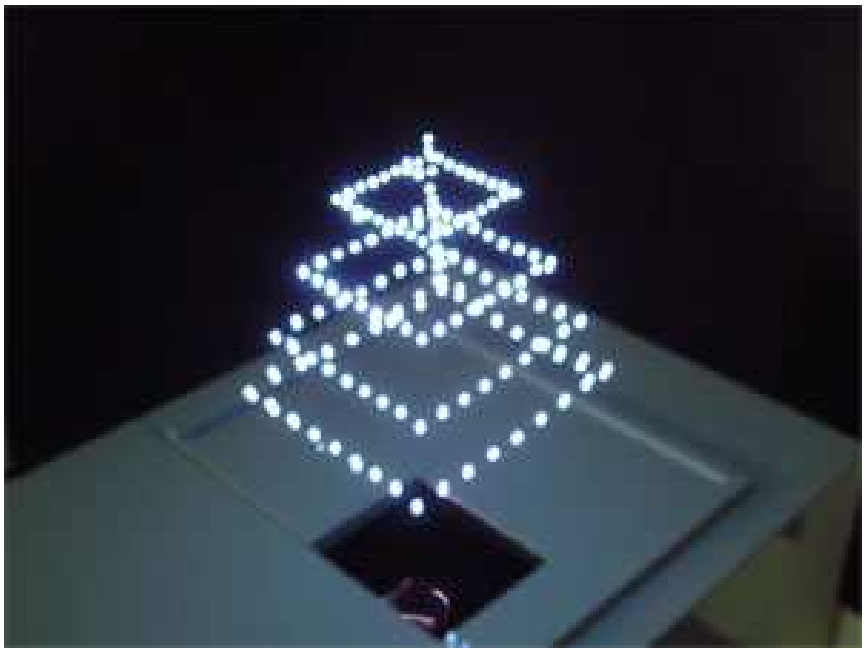

Figure A.15: *A real three dimensional display. From http://www.physorg.com/news11251.html.*

- When intercalling a black frame between each frame to reduce motion blur, or keeping the power consumption even in reducing the intensity of an image if it is very bright, the

modification is image dependent.

These transforms are more problematic. There are solutions to solve a given technical problem and in most cases can not be unactivated. The color rendering is then strongly modified depending on the image content (or depending on the problem to solve).

These effects are creating many problems for the calibration and color characterization of displays.

As a scientist or a designer, we want our display to be colorimetrically accurate, but as a common people we want to see a pleasant image. Until now, almost the same product was used by both communities. However, it seems that more and more the displays people are using are really different, depending on the purpose.

A.6 Conclusion

We hope this introduction to display technology, which is far beyond the purpose of the thesis, has enlarged your horizon, and has been of benefit for the understanding of the thesis and its context position.

Appendix B

Hexagonal regular sampling of *CIELAB* color space

Abstract

This appendix presents a method to distribute regularly spaced data in CIELAB. This method is based on sphere packing techniques. We used this distribution in order to perform a RBF interpolation for the forward display color characterization model proposed in Chapter 6. The first part of this annexe is mainly extracted from (Thomas, 2006). The algorithm details are mainly from (Stauder et al., 2006) and (Thomas and Trémeau, 2007).

B.1 Introduction

In 1611, Johannes Kepler proposed a mathematical conjecture concerning the densest way to arrange same sized spheres in a $3D$ euclidean space. Following that conjecture, a way to obtain the most compact arrangement is to arrange spheres in order to form a face-centered cubic distribution (Kepler, 1611). During the XIX^{th} century, Gauss demonstrated that the most compact way to arrange discs in a $2D$ plan, could be reached if they are arranged in an hexagonal way. His demonstration is based on the fact that the centers of the discs are at equal distance from each neighbor. He kept open the possibility that a random arrangement can be more compact (Gauss, 1801). Fejes proved that it is the only densest way in the XX^{th} century (Tóth, 1960/61).

In 1998, Thomas Hales demonstrated by exhaustion that spheres arranged in a face-centered cubic or in a hexagonal closed distribution show the more important density (Hales, 1998).

Based on these works and on the fact that the sphere centers are at equal distance from their direct neighbors, one can define a regular sampling of the *CIELAB* colorpace.

This *CIELAB* sampling has been already used in different works, such as (Colantoni and Thomas, 2009; Stauder et al., 2006, 2007; Thomas, 2006; Thomas, Chareyron and Trémeau, 2007; Thomas and Trémeau, 2007). We propose to detail this algorithm in this appendix.

B.2 Sampling strategy

We distribute the samples as if they were the center of the spheres in a close-packing of spheres problem. We sample a cube including the gamut of the display in *CIELAB* color space, using

a hexagonal closed packing. We do not use the face-centered cubic lattices for algorithmic simplicity. This last arrangement would not be of benefit for us since we do not use the properties of periodicity and symmetry of such a structure, while the sampling remains the same. We use then only the two layers alternative (see Figure B.1), creating a hexagonal closed lattice. It is enough to perform a translation to go from the first layer to the second, and so on. Then, each sphere center is at equal distance of its direct neighbors. Those neighbors form a Johnson polyhedron number 27 (J_{27}), i.e. a triangular orthobicupola.

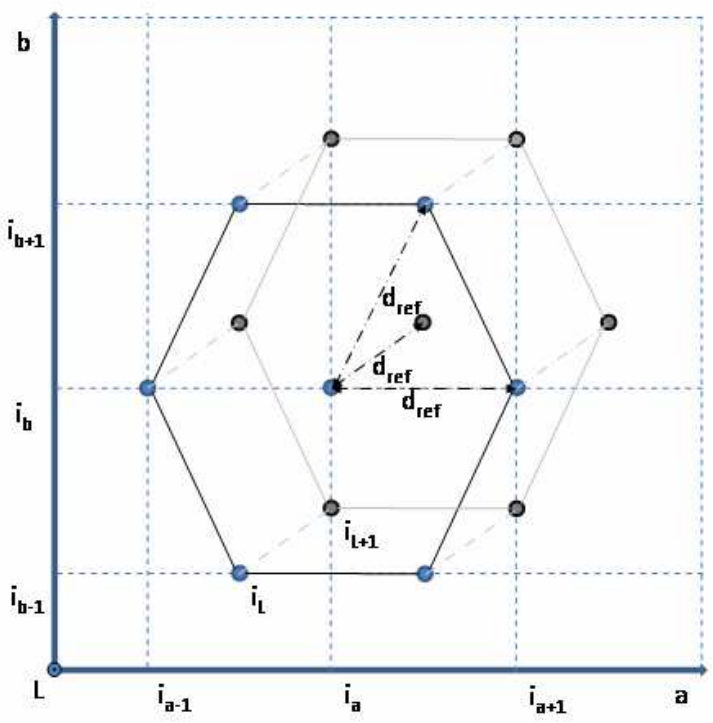

Figure B.1: *Sampling of the CIELAB color space.*

B.3 Sampling algorithm

In the following, we introduce the sampling algorithm, such as in (Stauder et al., 2006; Thomas and Trémeau, 2007).

Let us introduce the following notations:

Let us call L^*_x, a^*_x, b^*_x the coordinates of a given color in the *CIELAB* color space, and L^*_y,a^*_y,b^*_y the coordinates of a second color. The CIE ΔE^*_{76} color distance between these two colors is the euclidean distance, such as:

$$\Delta E^*_{76} = \sqrt{d_L^2 + d_a^2 + d_b^2} \tag{B.1}$$

with $|L^*_x - L^*_y| = d_L$, $|a^*_x - a^*_y| = d_a$, $|b^*_x - b^*_y| = d_b$.

Let d_{ref} be an arbitrary distance in *CIELAB* color space. If we consider $d_a = d_{ref}$, $d_b = 0$ and $d_L = 0$, then:

$$\sqrt{d_L^2 + d_a^2 + d_b^2} = d_{ref}.$$

Likewise, if we consider $d_a = \frac{1}{2} \times d_{ref}$, $d_b = \sqrt{\frac{3}{4}} \times d_{ref}$ and $d_L = 0$, then:

$$\sqrt{d_L^2 + d_a^2 + d_b^2} = d_{ref}$$

.

Finally, if we consider $d_a = \frac{1}{2} \times d_{ref}$, $d_b = \frac{1}{2\sqrt{3}} \times d_{ref}$ and $d_L = \sqrt{\frac{2}{3}} \times d_{ref}$, then:

$$\sqrt{d_L^2 + d_a^2 + d_b^2} = d_{ref}$$

.

Considering now the uniform color space sampling, let us give L_{min}, L_{max}, a_{min}, a_{max}, b_{min}, and b_{max} the lower and upper color values of the *CIELAB* color space along the L^*, a^* and b^* axis.

Considering the arrangement explained above, the 3D grid is defined such as:

- $|a^*_{i_a} - a^*_{i_{a+1}}| = d_{ref}$ the distance, which separates two consecutive samples along the a^* axis, such as the distance, which separates two samples along this axis is:

$$\sqrt{\left(a^*_{i_a} - a^*_{i_{a+1}}\right)^2} = d_{ref}.$$

- $|a^*_{i_a,i_b} - a^*_{i_a,i_{b+1}}| = \frac{1}{2} \times d_{ref}$ and $|b^*_{i_a,i_b} - b^*_{i_a,i_{b+1}}| = \sqrt{\frac{3}{4}} \times d_{ref}$ the distances, which separate two adjacent samples along the a* and b* axis, such as the distance, which separates two samples in the a*b* plane is

$$\sqrt{\left(a^*_{i_a,i_b} - a^*_{i_a,i_{b+1}}\right)^2 + \left(b^*_{i_a,i_b} - b^*_{i_a,i_{b+1}}\right)^2} = d_{ref}.$$

- $|a^*_{i_L,i_a,i_b} - a^*_{i_{L+1},i_a,i_b}| = \frac{1}{2} \times d_{ref}$, $|b^*_{i_L,i_a,i_b} - b^*_{i_{L+1},i_a,i_b}| = \frac{1}{2\sqrt{3}} \times d_{ref}$ and $|L^*_{i_L,i_a,i_b} - L^*_{i_{L+1},i_a,i_b}| = \sqrt{\frac{2}{3}} \times d_{ref}$ the distances, which separate two adjacent samples along the a^*, b^* and L^* axis such as the distance, which separates these two samples in *CIELAB* color space is:

$$\sqrt{\left(a^*_{i_L,i_a,i_b} - a^*_{i_{L+1},i_a,i_b}\right)^2 + \left(b^*_{i_L,i_a,i_b} - b^*_{i_{L+1},i_a,i_b}\right)^2 + \left(L^*_{i_L,i_a,i_b} - L^*_{i_{L+1},i_a,i_b}\right)^2} = d_{ref}$$

.

The smaller d_{ref} is, the finer the sampling of the color space is, then the number of samples increases inversely proportionally to the distance d_{ref}.

If we consider:

$$N_L = \frac{L_{max} - L_{min}}{d_{ref}\sqrt{\frac{2}{3}}}$$

$$N_a = \frac{a_{max} - a_{min}}{d_{ref}}$$

$$N_b = \frac{b_{max} - b_{min}}{d_{ref}\sqrt{\frac{3}{4}}}$$

with N_L, N_a and N_b the number of sample values for each axis. Then, $N = N_L \times N_a \times N_b$ is the number of samples, which is a function of $\frac{1}{\frac{1}{\sqrt{2}} \times d_{ref}^3}$.

The final number of patches is constituted of the intersection of the sampling and of the volume of the gamut computed with the temporary model.

Appendix C

Polyharmonic splines kernel and Radial Basis Function interpolation

Abstract

This appendix details the 3D polyharmonic splines interpolation/approximation we used in Chapter 6.

C.1 Introduction

Polyharmonic splines are a subset of RBF (Radial Basis Funtion) that can be used for interpolate or to approximate (Carr et al., 2001) arbitrarily distributed data.

In color imaging, beside of this method and its previous version, we only know the use of Thin Plate Splines (TPS) for printers colorimetric characterization (Sharma and Shaw, 2006). TPS are a subset of polyharmonic splines (bi-harmonic splines). Sharma and Shaw (2006) recalled the mathematical framework and presented some examples for printers characterization. They shown that using TPS, they achieved a better result than in using local polynomial regression. They shown that in using a smoothing factor, error in measurement impact can be avoided at the expense of the computational cost that optimize this parameter. However, they did not study data distribution influence (but they said that the data distribution can improve the accuracy in conclusion) neither the use of other kernels for interpolation.

C.2 Interpolation

The idea is to build a function f whose graph passes through the data and minimizes a bending energy function. For a general M-dimensional case, we want to interpolate a valued function $f(X) = Y$ given by the set of values $f = (f_1, ..., f_N)$ at the distinct points $X = x_1, ..., x_N \subset \Re^M$. We choose $f(X)$ to be a RBF of the shape:

$$f(x) = p(x) + \sum_{i=1}^{N} \lambda_i \phi(||x - x_i||) \quad x \in \Re^M$$

where p is a polynomial, λ_i is a real-valued weight, ϕ is a basis function, $\phi : \Re^M \rightarrow \Re$, and $||x - x_i||$ is the euclidean norm between x and x_i. Therefore, a RBF is a weighted sum of

translations of a radially symetric basis function augmented by a polynomial term. Different basis functions (kernel) $\phi(x)$ can be used.

Considering the color problem, we want to establish three three-dimensional functions $f_i(x, y, z)$. The idea is to build a function $f(x, y, z)$ whose graph passes through the tabulated data and minimizes the following bending energy function:

$$\iiint_{\Re^3} (f_{xxx}^3 + f_{yyy}^3 + f_{zzz}^3 + 3f_{xxy}^3 + 3f_{xxz}^3 + 3f_{xyy}^3 + 3f_{xzz}^3 + 3f_{yyz}^3 + 3f_{yzz}^3 + 6f_{xyz}^3)dxdydz \quad \text{(C.1)}$$

For a set of data $\{(x_i, y_i, z_i, w_i)\}_{i=1}^n$ (where $w_i = f(x_i, y_i, z_i)$) the minimizing function is such as:

$$f(x, y, z) = b_0 + b_1 x + b_2 y + b_3 z + \sum_{j=1}^{n} a_j \phi(||(x - x_j, y - y_j, z - z_j)||) \quad \text{(C.2)}$$

where the coefficients a_j and $b_{0,1,2,3}$ are determined by requiring exact interpolation using the following equation

$$w_i = \sum_{j=1}^{n} \phi_{ij} a_j + b_0 + b_1 x_i + b_2 y_i + b_3 z_i \quad \text{(C.3)}$$

for $1 \leq n$ where $\phi_{ij} = \phi(||(x_i - x_j, y_i - y_j, z_i - z_j)||)$. In matrix form this is

$$h = Aa + Bb \quad \text{(C.4)}$$

where $A = [\phi_{ij}]$ is an $n \times n$ matrix and B is an $n \times 4$ matrix whose rows are $[1 \quad x_i \quad y_i \quad z_i]$. To be solvable, an additional implication is that

$$B^T a = 0 \quad \text{(C.5)}$$

These two vector equations can then be solved to obtain

$$a = A^{-1}(h - Bb) \text{ and } b = (B^T A^{-1} B)^{-1} B^T A^{-1} h.$$

C.3 Approximation

It is possible to provide a smoothing term. In this case the interpolation is not exact and becomes an approximation. The modification is to use the equation

$$h = (A + \sigma I)a + Bb \quad \text{(C.6)}$$

$$a = (A + \sigma I)^{-1}(h - Bb) \text{ and } b = (B^T (A + \sigma I)^{-1} B)^{-1} B^T (A + \sigma I)^{-1} h.$$

where $\sigma > 0$ is a smoothing parameter and I is the $n \times n$ identity matrix.

C.4 Kernels

In our context we used a set of 4 real functions as possible kernels, the biharmonic ($\phi(x) = x$), triharmonic ($\phi(x) = x^3$), thin-plate spline 1 ($\phi(x) = x^2 log(x)$) and thin-plate spline 2 ($\phi(x) = x^2 log(x^2)$), with x the distance from the origin. The use of a given basis function depends on the display device, which is characterized, and gives some freedom to the model.

Appendix D

More results on PLVC

Abstract

The content of this appendix consists in more visualizations of the accuracy of the PLVC model compared with the PLCC model and in a non-additivity study of tested displays.*

D.1 Foreword

In this appendice are the materials we could not add to the content of the thesis or of the article for space and readability reasons.

D.2 Non-additivity evaluation

With regard to the non-additivity, we have performed a study of our tested devices. We present results for this criterion in table D.1 following (Kwak and MacDonald, 2000). It appears that at full intensity, the DLP shows good results considering this feature, the CRT is not really good, probably because of the insufficient power (this display has a really low white around $60cd/m^2$). For LCD projection, the results are good, it is believed that as they are 3-LCD, there is less interaction at subpixel level, and in displaying patches, the interaction is the same and is taken into account in the model globality. The two LCD monitors show really different results, but one has a really low brightness. It is strange to notice that MLCD1 with this high interaction between channel is giving such good results with the tested models (see Table 4.3), compared with MLCD2. But that does not influence the comparison of the models since all tested methods are supposing additivity.

D.3 More visualizations

Table D.1: *Basic additivity test for tested devices. The measured White is the full intensity of all primaries together. The R+G+B is the full intensity for each primary taken separately. The difference is expressed as a percentage. Note that MLCD1 has a very low brightness, less bright than the CRT, which could be seen as strange, but the settings were set for a dark surrounding work.*

additivity		X	Y	Z
ProjectorLCD1	White	115.00	128.60	155.40
	R+G+B	111.93	125.12	154.11
	Difference (%)	2.67	2.71	0.83
ProjectorLCD2	White	93.97	105.00	135.00
	R+G+B	94.81	105.96	136.9
	Difference (%)	0.89	0.91	1.41
ProjectorDLP	White	91.80	104.80	126.9
	R+G+B	92.69	105.726	127.974
	Difference (%)	0.97	0.88	0.85
MonitorCRT	White	61.36	63.21	83.61
	R+G+B	64.82	66.443	88.629
	Difference (%)	5.64	5.12	6.00
MonitorLCD1	White	53.33	55.76	71.62
	R+G+B	50.54	52.77	68.081
	Difference (%)	5.23	5.36	4.94
MonitorLCD2	White	188.10	191.10	209.90
	R+G+B	187.59	190.53	210.91
	Difference (%)	0.27	0.30	0.48

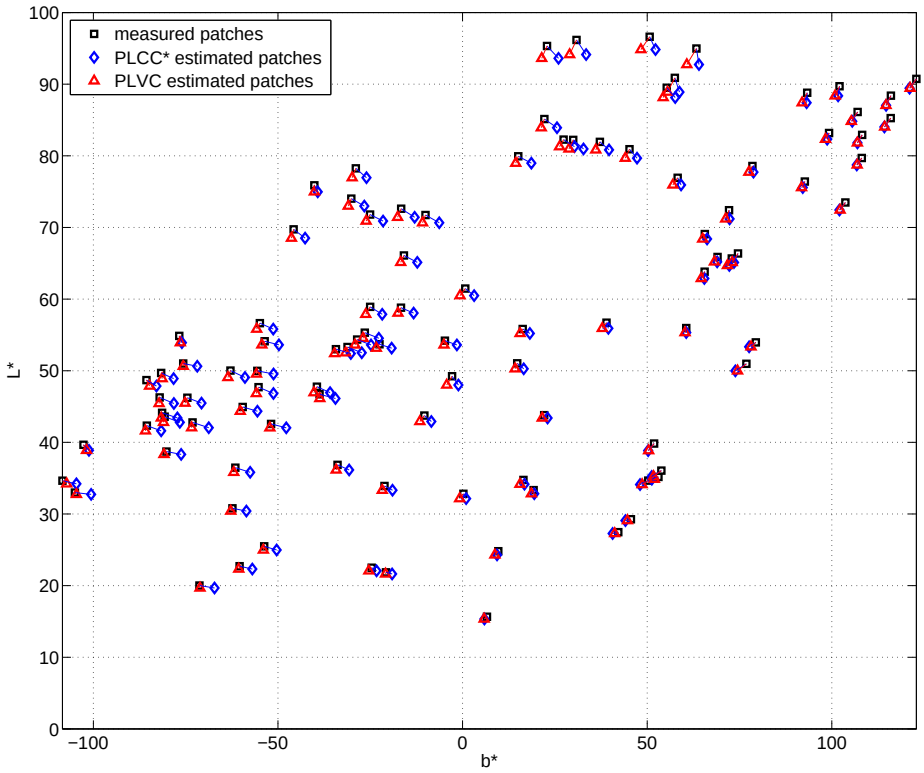

Figure D.1: *PLCD1: visualization of errors for the testing data set projected on the b^*L^* plane.*

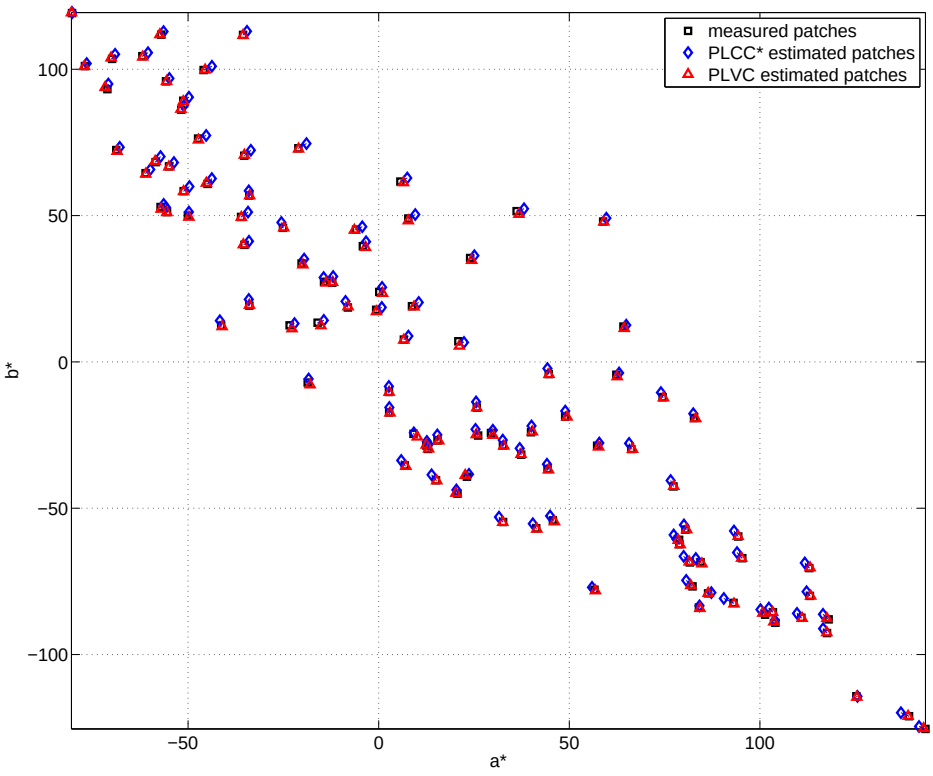

Figure D.2: *PLCD2: visualization of errors for the testing data set projected on the a^*b^* plane.*

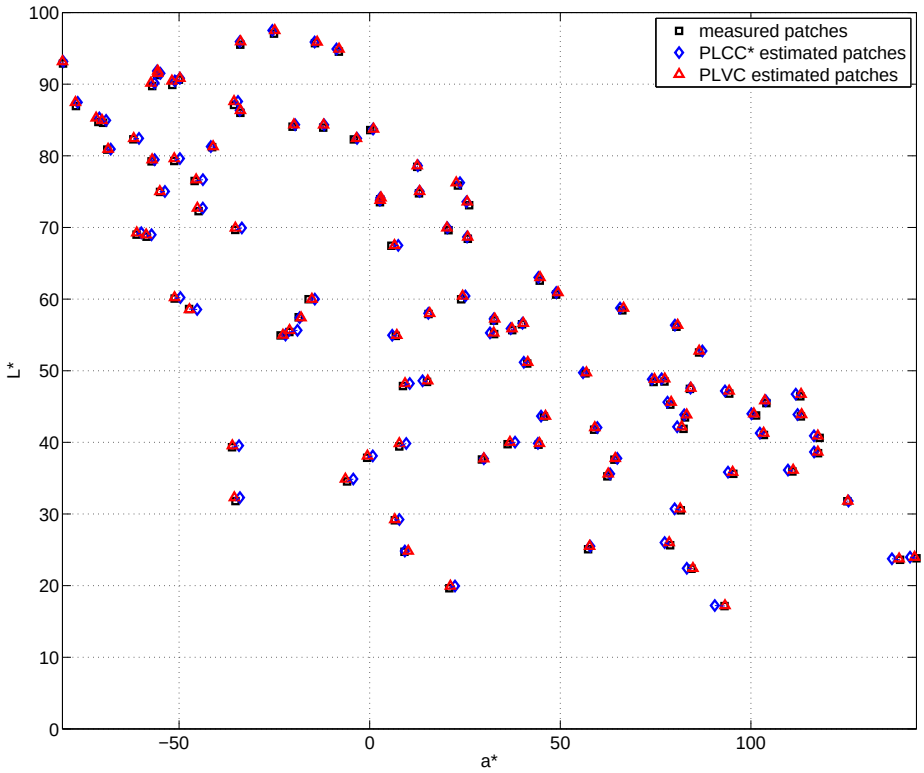

Figure D.3: *PLCD2: visualization of errors for the testing data set projected on the a^*L^* plane.*

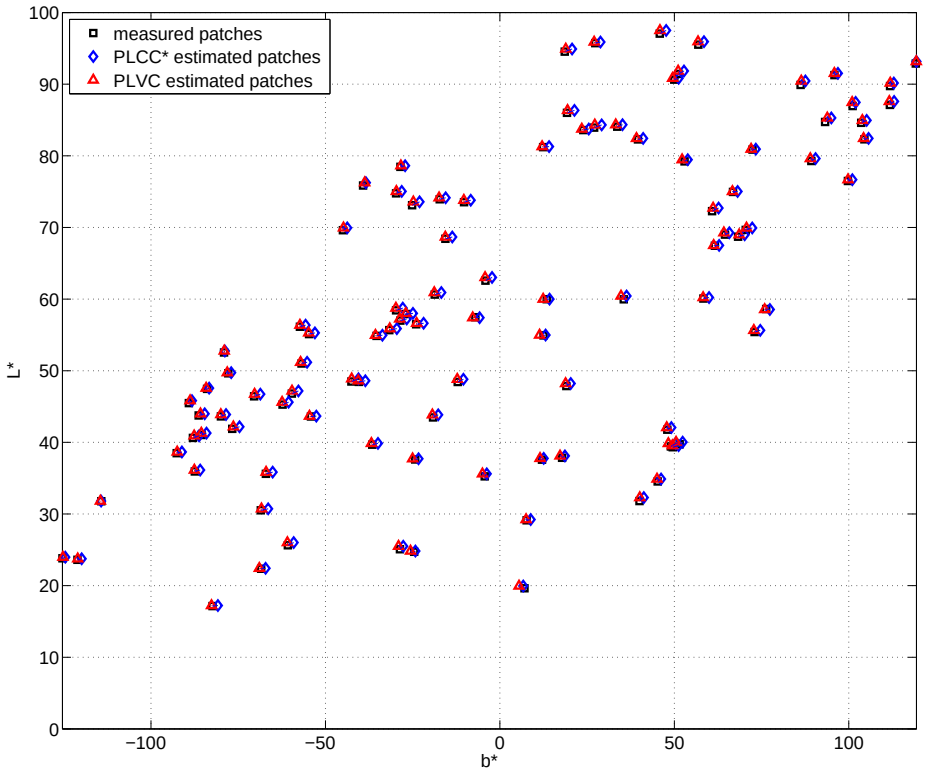

Figure D.4: *PLCD2: visualization of errors for the testing data set projected on the b^*L^* plane.*

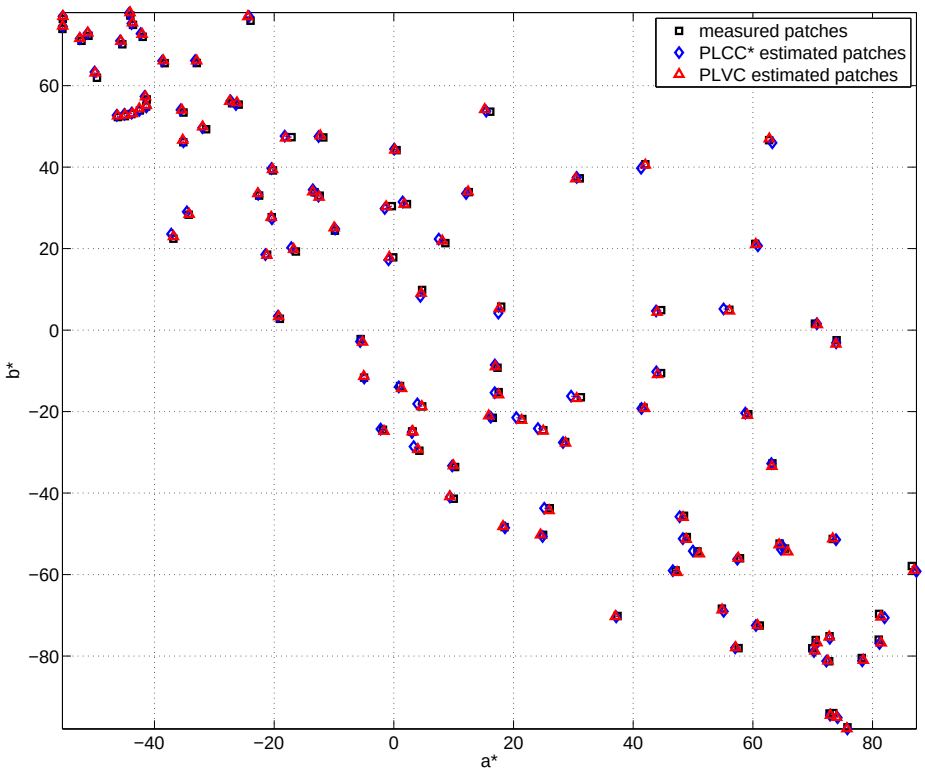

Figure D.5: *PDLP: visualization of errors for the testing data set projected on the a^*b^* plane.*

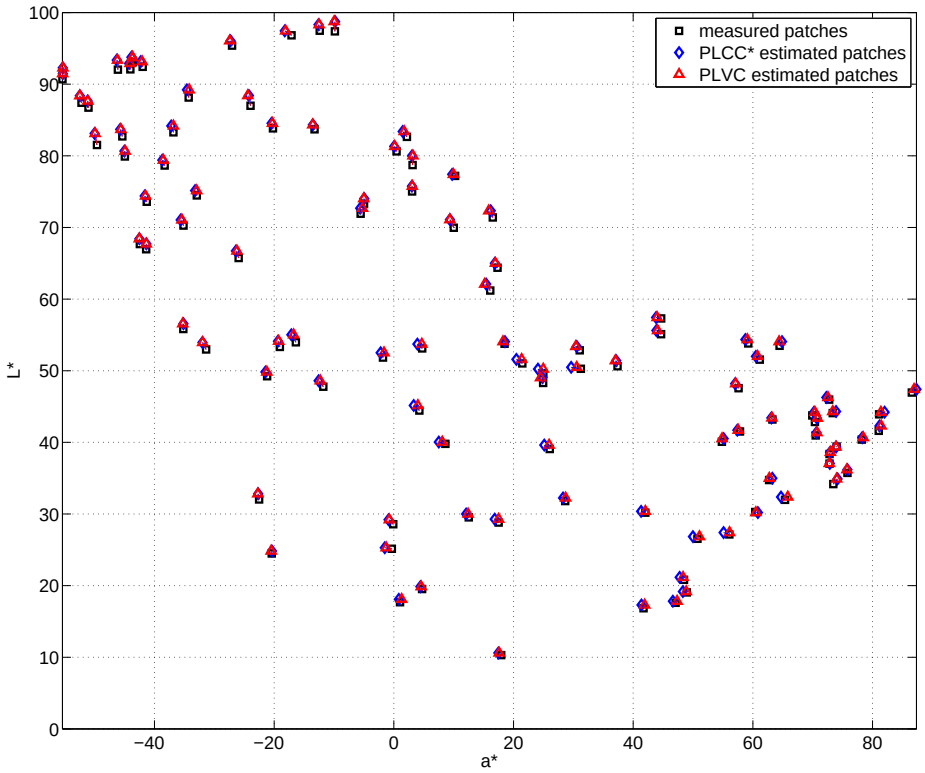

Figure D.6: *PDLP: visualization of errors for the testing data set projected on the a^*L^* plane.*

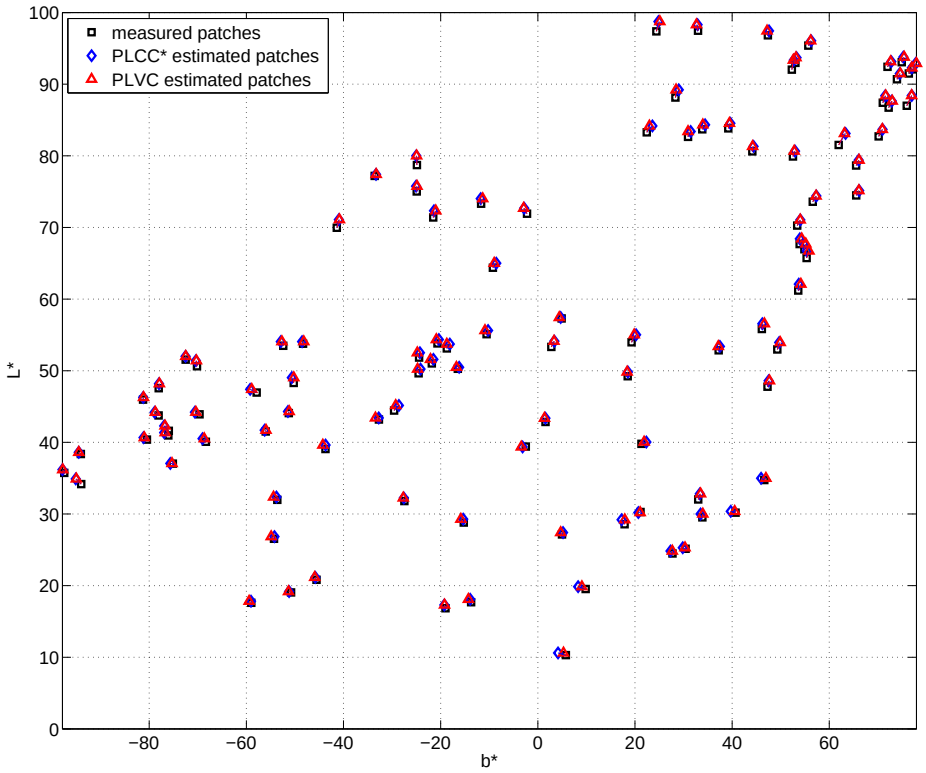

Figure D.7: *PDLP: visualization of errors for the testing data set projected on the b^*L^* plane.*

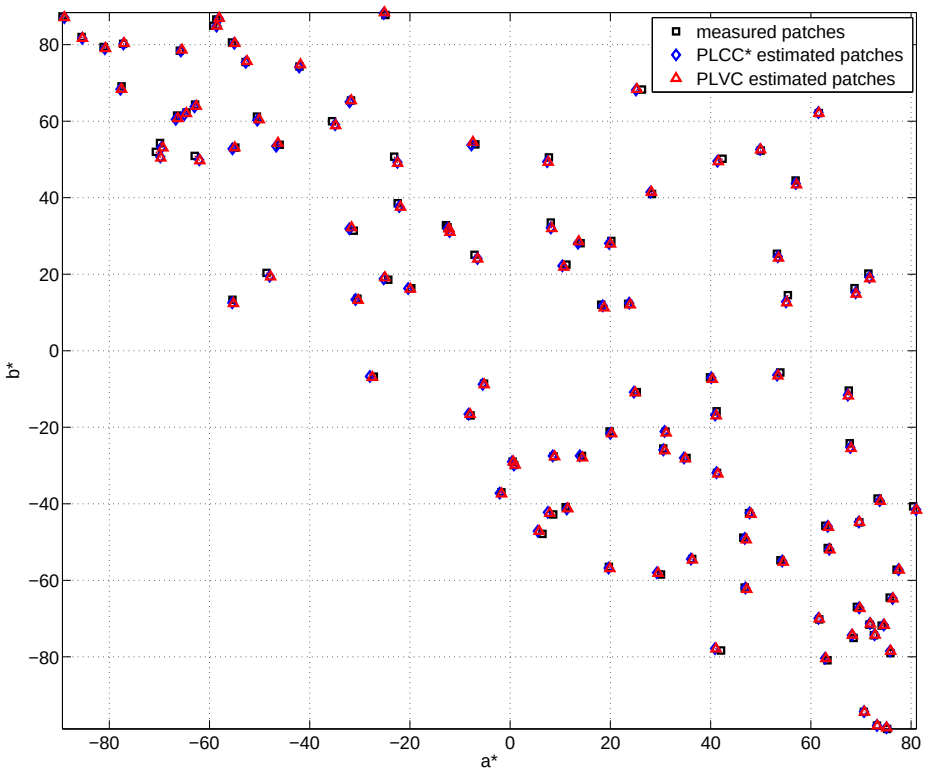

Figure D.8: *MCRT: visualization of errors for the testing data set projected on the a^*b^* plane.*

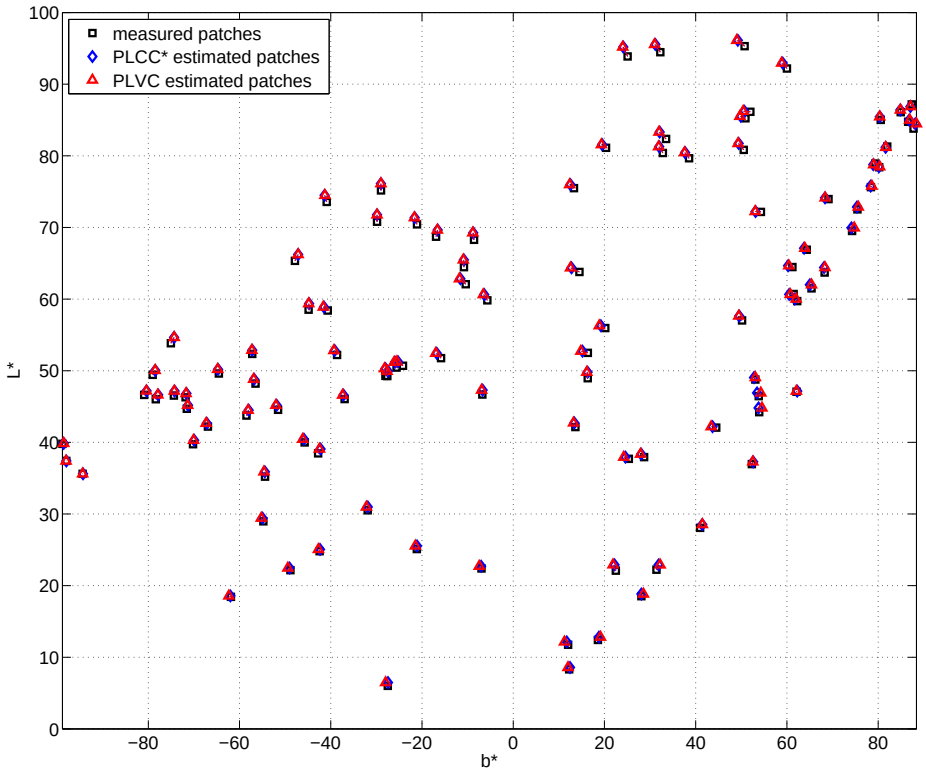

Figure D.9: *MCRT: visualization of errors for the testing data set projected on the b^*L^* plane.*

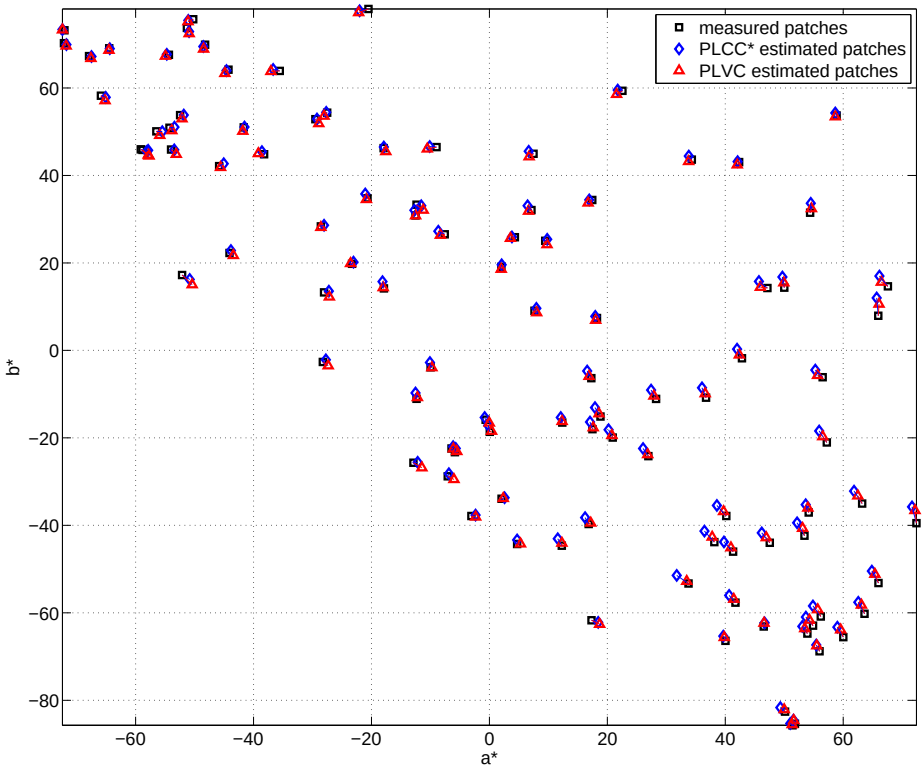

Figure D.10: *MLCD1: visualization of errors for the testing data set projected on the a^*b^* plane.*

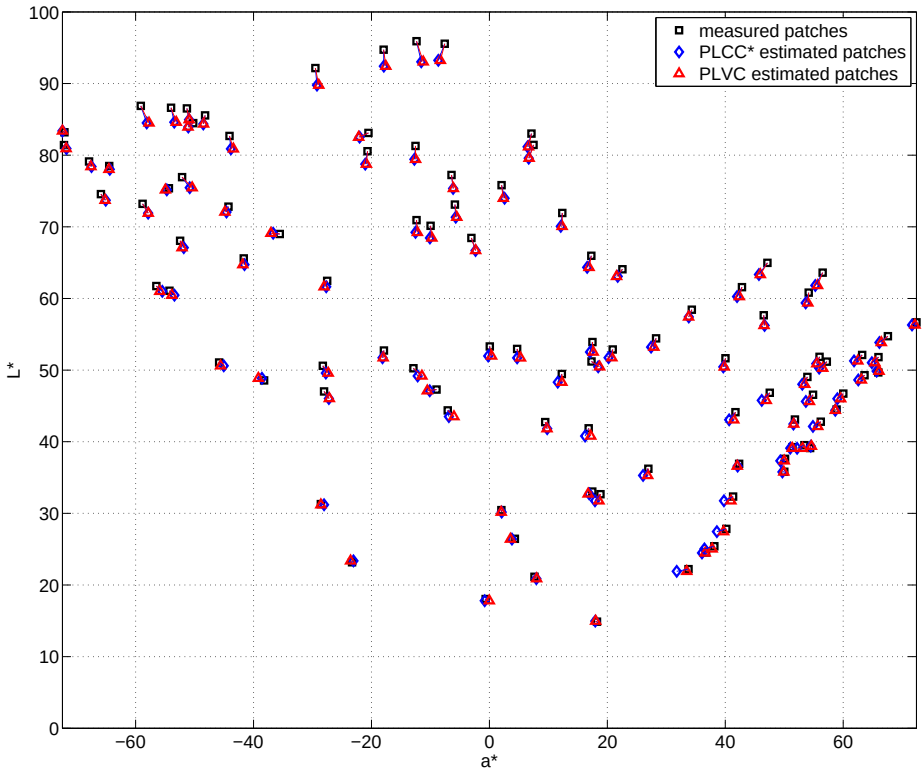

Figure D.11: *MLCD1: visualization of errors for the testing data set projected on the a^*L^* plane.*

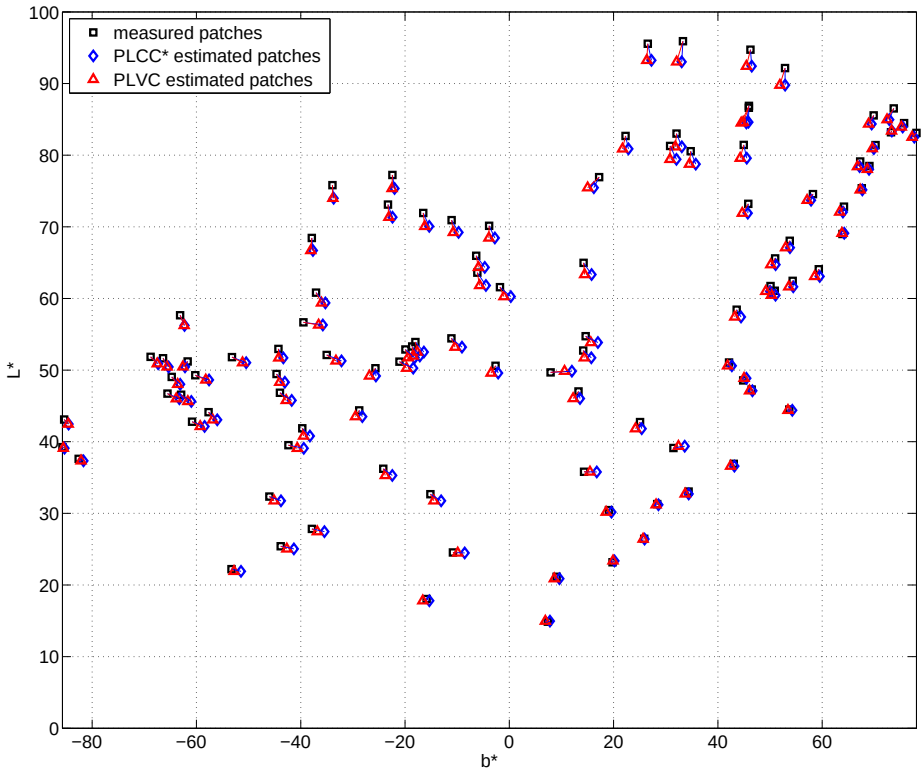

Figure D.12: *MLCD1: visualization of errors for the testing data set projected on the b^*L^* plane.*

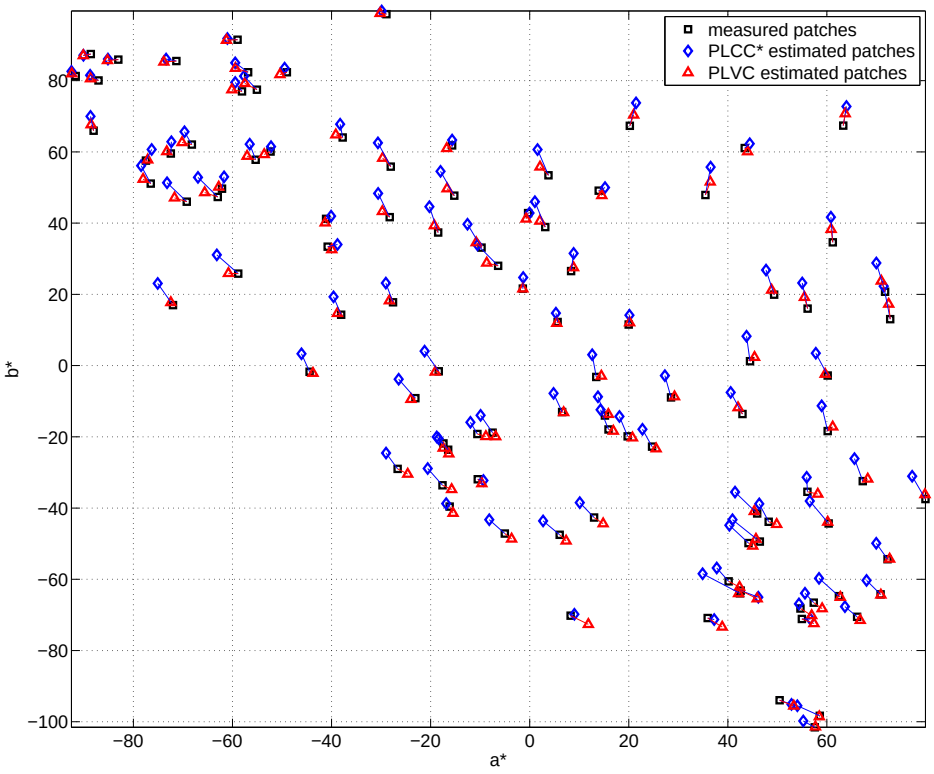

Figure D.13: *MLCD2: visualization of errors for the testing data set projected on the a^*b^* plane.*

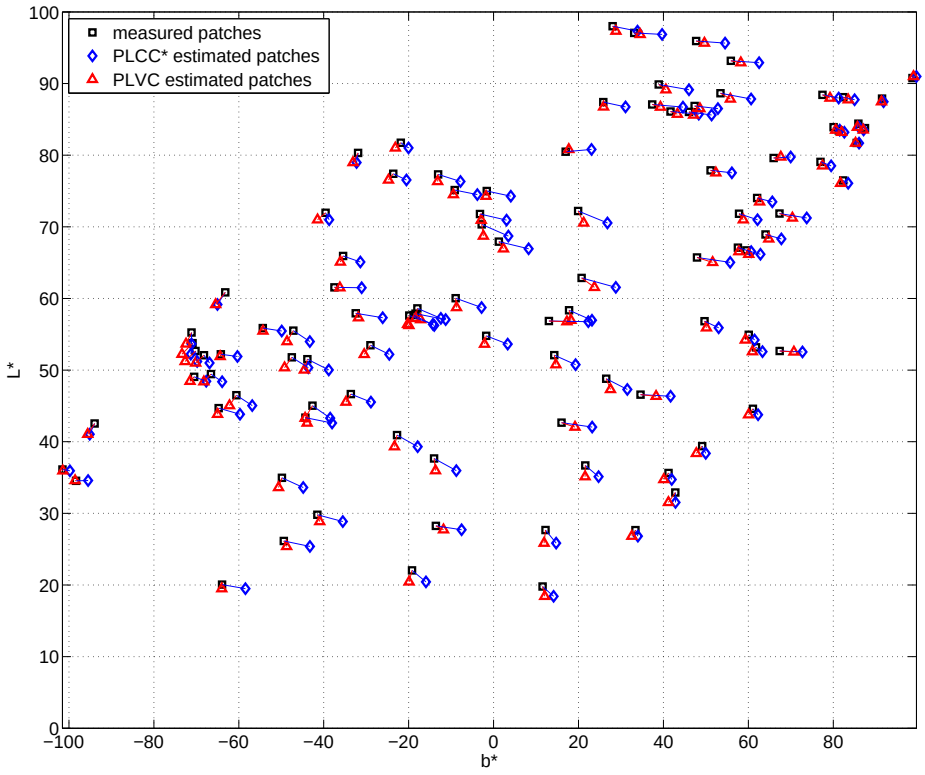

Figure D.14: *MLCD2: visualization of errors for the testing data set projected on the b^*L^* plane.*

Appendix E

List of Publications related with this thesis

E.1 Journal Publications

The work presented in this thesis has been published in two journals, and two more articles are in writing or submission process.

The PLVC display color characterization model revisited, Jean Baptiste THOMAS, Jon HARDEBERG, Irène FOUCHEROT, Pierre GOUTON, Color Research & Application., 33 (6), pp. 449-460, October 2008.

A geometrical approach for inverting display color-characterization models, Jean Baptiste THOMAS, Philippe COLANTONI, Jon HARDEBERG, Irène FOUCHEROT, Pierre GOUTON, Journal of the Society for Information Display, 16 (10), pp. 1021-1031, 2008.

Spatial non-uniformity of color features in projection displays: A quantitative analysis, Jean-Baptiste Thomas, Arne Magnus Bakke, Jérémie Gerhardt, submitted to Journal of Imaging Science and Technology, in review process.

E.2 Conference Publications

The work presented in this thesis has been presented in several conferences.

A color management process for real time color reconstruction of multispectral images, Philippe COLANTONI, Jean Baptiste THOMAS, 16th Scandinavian Conference on Image Analysis, Springer Verlag, Lecture Notes in Computer Science, 5575, Oslo, Norway, 2009.

Common assumptions in color characterization of projectors, Arne Magnus Bakke, Jean-Baptiste Thomas, Jérémie Gerhardt, GCIS09, Proc. of Gjøvik Color Imaging Symposium, 4, Gjøvik, Norway, pp. 45-53, 2009.

A colorimetric study of spatial uniformity in projection displays, Jean Baptiste THOMAS, Arne Magnus BAKKE, CCIW09, Springer Verlag, Lecture Notes in Computer Science, 5646, Saint-Etienne, France, pp. 160-169, 2009.

An inverse display color characterization model based on an optimized geometrical structure, Jean Baptiste THOMAS, Philippe COLANTONI, Jon HARDEBERG, Irène FOUCHEROT, Pierre GOUTON, Color Imaging XIII: Processing, Hardcopy, and Applications, 6807, Proc SPIE, San Jose, California, USA, 6807, pp. 68070A-1–12 , 2008.

Verification and extension of a camera-based end-user calibration method for projection displays, Espen MIKALSEN, Jon HARDEBERG, Jean Baptiste THOMAS, Proc. CGIV 2008,

IS&T, Terrassa, Spain, pp. 575-579, 2008.

Additivity based LC display color characterization, Jean Baptiste THOMAS, Jon HARDEBERG, Irène FOUCHEROT, Pierre GOUTON, Gjøvik Color Imaging Symposium, Gjøvik, Norway, June 2007.